

Научный рецензируемый журнал

ВАВИЛОВСКИЙ ЖУРНАЛ ГЕНЕТИКИ И СЕЛЕКЦИИ

Основан в 1997 г.

Периодичность 8 выпусков в год

DOI 10.18699/VJGB-22-14

Учредители

Сибирское отделение Российской академии наук

Федеральное государственное бюджетное научное учреждение «Федеральный исследовательский центр Институт цитологии и генетики Сибирского отделения Российской академии наук»

Межрегиональная общественная организация Вавиловское общество генетиков и селекционеров

Главный редактор

А.В. Кочетов – чл.-кор. РАН, д-р биол. наук (Россия)

Заместители главного редактора

Н.А. Колчанов – академик РАН, д-р биол. наук, профессор (Россия)

И.Н. Леонова – д-р биол. наук (Россия)

Н.Б. Рубцов – д-р биол. наук, профессор (Россия)

В.К. Шумный – академик РАН, д-р биол. наук, профессор (Россия)

Ответственный секретарь

Г.В. Орлова – канд. биол. наук (Россия)

Редакционная коллегия

Е.Е. Андронов – канд. биол. наук (Россия)

Ю.С. Аульченко – д-р биол. наук (Россия)

О.С. Афанасенко – академик РАН, д-р биол. наук (Россия)

Д.А. Афонников – канд. биол. наук, доцент (Россия)

Л.И. Афтанас – академик РАН, д-р мед. наук (Россия)

Л.А. Беспалова – академик РАН, д-р с.-х. наук (Россия)

А. Бёрнер – д-р наук (Германия)

Н.П. Бондарь – канд. биол. наук (Россия)

С.А. Боринская – д-р биол. наук (Россия)

П.М. Бородин – д-р биол. наук, проф. (Россия)

А.В. Васильев – чл.-кор. РАН, д-р биол. наук (Россия)

М.И. Воевода – академик РАН, д-р мед. наук (Россия)

Т.А. Гавриленко – д-р биол. наук (Россия)

И. Гроссе – д-р наук, проф. (Германия)

Н.Е. Грунтенко – д-р биол. наук (Россия)

С.А. Демаков – д-р биол. наук (Россия)

И.К. Захаров – д-р биол. наук, проф. (Россия)

И.А. Захаров-Гезехус – чл.-кор. РАН, д-р биол. наук (Россия)

С.Г. Инге-Вечтомов – академик РАН, д-р биол. наук (Россия)

А.В. Кильчевский – чл.-кор. НАНБ, д-р биол. наук (Беларусь)

С.В. Костров – чл.-кор. РАН, д-р хим. наук (Россия)

А.М. Кудрявцев – чл.-кор. РАН, д-р биол. наук (Россия)

И.Н. Лаврик – д-р биол. наук (Германия)

Д.М. Ларкин – канд. биол. наук (Великобритания)

Ж. Ле Гуи – д-р наук (Франция)

И.Н. Лебедев – д-р биол. наук, проф. (Россия)

Л.А. Лутова – д-р биол. наук, проф. (Россия)

Б. Люгтенберг – д-р наук, проф. (Нидерланды)

В.Ю. Макеев – чл.-кор. РАН, д-р физ.-мат. наук (Россия)

В.И. Молодин – академик РАН, д-р ист. наук (Россия)

М.П. Мошкин – д-р биол. наук, проф. (Россия)

С.Р. Мурсалимов – канд. биол. наук (Россия)

Л.Ю. Новикова – д-р с.-х. наук (Россия)

Е.К. Потокина – д-р биол. наук (Россия)

В.П. Пузырев – академик РАН, д-р мед. наук (Россия)

Д.В. Пышный – чл.-кор. РАН, д-р хим. наук (Россия)

И.Б. Розозин – канд. биол. наук (США)

А.О. Рувинский – д-р биол. наук, проф. (Австралия)

Е.Ю. Рыкова – д-р биол. наук (Россия)

Е.А. Салина – д-р биол. наук, проф. (Россия)

В.А. Степанов – чл.-кор. РАН, д-р биол. наук (Россия)

И.А. Тихонович – академик РАН, д-р биол. наук (Россия)

Е.К. Хлесткина – д-р биол. наук, проф. РАН (Россия)

Э.К. Хуснутдинова – д-р биол. наук, проф. (Россия)

М. Чен – д-р биол. наук (Китайская Народная Республика)

Ю.Н. Шавруков – д-р биол. наук (Австралия)

Р.И. Шейко – чл.-кор. НАНБ, д-р с.-х. наук (Беларусь)

С.В. Шестаков – академик РАН, д-р биол. наук (Россия)

Н.К. Янковский – академик РАН, д-р биол. наук (Россия)

Scientific Peer Reviewed Journal

VAVILOV JOURNAL OF GENETICS AND BREEDING

VAVILOVSKII ZHURNAL GENETIKI I SELEKTSII

*Founded in 1997**Published 8 times annually*

DOI 10.18699/VJGB-22-14

Founders

Siberian Branch of the Russian Academy of Sciences

Federal Research Center Institute of Cytology and Genetics of the Siberian Branch of the Russian Academy of Sciences

The Vavilov Society of Geneticists and Breeders

Editor-in-Chief*A.V. Kochetov*, Corr. Member of the RAS, Dr. Sci. (Biology), Russia**Deputy Editor-in-Chief***N.A. Kolchanov*, Full Member of the Russian Academy of Sciences, Dr. Sci. (Biology), Russia*I.N. Leonova*, Dr. Sci. (Biology), Russia*N.B. Rubtsov*, Professor, Dr. Sci. (Biology), Russia*V.K. Shumny*, Full Member of the Russian Academy of Sciences, Dr. Sci. (Biology), Russia**Executive Secretary***G.V. Orlova*, Cand. Sci. (Biology), Russia**Editorial board***O.S. Afanasenko*, Full Member of the RAS, Dr. Sci. (Biology), Russia*D.A. Afonnikov*, Associate Professor, Cand. Sci. (Biology), Russia*L.I. Aftanas*, Full Member of the RAS, Dr. Sci. (Medicine), Russia*E.E. Andronov*, Cand. Sci. (Biology), Russia*Yu.S. Aulchenko*, Dr. Sci. (Biology), Russia*L.A. Bespalova*, Full Member of the RAS, Dr. Sci. (Agricul.), Russia*N.P. Bondar*, Cand. Sci. (Biology), Russia*S.A. Borinskaya*, Dr. Sci. (Biology), Russia*P.M. Borodin*, Professor, Dr. Sci. (Biology), Russia*A. Börner*, Dr. Sci., Germany*M. Chen*, Dr. Sci. (Biology), People's Republic of China*S.A. Demakov*, Dr. Sci. (Biology), Russia*T.A. Gavrilenko*, Dr. Sci. (Biology), Russia*I. Grosse*, Professor, Dr. Sci., Germany*N.E. Gruntenko*, Dr. Sci. (Biology), Russia*S.G. Inge-Vechtomov*, Full Member of the RAS, Dr. Sci. (Biology), Russia*E.K. Khlestkina*, Professor of the RAS, Dr. Sci. (Biology), Russia*E.K. Khusnutdinova*, Professor, Dr. Sci. (Biology), Russia*A.V. Kilchevsky*, Corr. Member of the NAS of Belarus, Dr. Sci. (Biology),

Belarus

S.V. Kostrov, Corr. Member of the RAS, Dr. Sci. (Chemistry), Russia*A.M. Kudryavtsev*, Corr. Member of the RAS, Dr. Sci. (Biology), Russia*D.M. Larkin*, Cand. Sci. (Biology), Great Britain*I.N. Lavrik*, Dr. Sci. (Biology), Germany*J. Le Gouis*, Dr. Sci., France*I.N. Lebedev*, Professor, Dr. Sci. (Biology), Russia*B. Lugtenberg*, Professor, Dr. Sci., Netherlands*L.A. Lutova*, Professor, Dr. Sci. (Biology), Russia*V.Yu. Makeev*, Corr. Member of the RAS, Dr. Sci. (Physics and Mathem.),
Russia*V.I. Molodin*, Full Member of the RAS, Dr. Sci. (History), Russia*M.P. Moshkin*, Professor, Dr. Sci. (Biology), Russia*S.R. Mursalimov*, Cand. Sci. (Biology), Russia*L.Yu. Novikova*, Dr. Sci. (Agricul.), Russia*E.K. Potokina*, Dr. Sci. (Biology), Russia*V.P. Puzyrev*, Full Member of the RAS, Dr. Sci. (Medicine),
Russia*D.V. Pyshnyi*, Corr. Member of the RAS, Dr. Sci. (Chemistry),
Russia*I.B. Rogozin*, Cand. Sci. (Biology), United States*A.O. Ruvinsky*, Professor, Dr. Sci. (Biology), Australia*E.Y. Rykova*, Dr. Sci. (Biology), Russia*E.A. Salina*, Professor, Dr. Sci. (Biology), Russia*Y.N. Shavrukov*, Dr. Sci. (Biology), Australia*R.I. Sheiko*, Corr. Member of the NAS of Belarus,
Dr. Sci. (Agricul.), Belarus*S.V. Shestakov*, Full Member of the RAS, Dr. Sci. (Biology),
Russia*V.A. Stepanov*, Corr. Member of the RAS, Dr. Sci. (Biology),
Russia*I.A. Tikhonovich*, Full Member of the RAS, Dr. Sci. (Biology),
Russia*A.V. Vasiliev*, Corr. Member of the RAS, Dr. Sci. (Biology), Russia*M.I. Voevoda*, Full Member of the RAS, Dr. Sci. (Medicine),
Russia*N.K. Yankovsky*, Full Member of the RAS, Dr. Sci. (Biology),
Russia*I.K. Zakharov*, Professor, Dr. Sci. (Biology), Russia*I.A. Zakharov-Gezekhus*, Corr. Member of the RAS,
Dr. Sci. (Biology), Russia

Молекулярная и клеточная биология

- 121 **ОБЗОР**
Репликационно-транскрипционный комплекс коронавируса: функции индивидуальных вирусных неструктурных субъединиц, свойства и архитектура их комплексов.
Е.Л. Мищенко, В.А. Иванисенко

Генетика и биотехнология растений

- 128 **ОРИГИНАЛЬНОЕ ИССЛЕДОВАНИЕ**
Система молекулярных маркеров для идентификации аллелей генов короткостебельности *Rht-B1* и *Rht-D1* у мягкой пшеницы. *И.В. Поротников, О.П. Митрофанова, О.Ю. Антонова*
- 139 **ОРИГИНАЛЬНОЕ ИССЛЕДОВАНИЕ**
Андрогенетическая реакция амфидиплоидов *Triticum durum-Dasyurum villosum* и их родительских форм. *Х. Стоянов, И. Белчев (на англ. языке)*
- 146 **ОРИГИНАЛЬНОЕ ИССЛЕДОВАНИЕ**
Соответствие морфологии бутонных и пыльников стадиям развития мужского гаметофита дыни (*Cucumis melo* L.).
М.Л. Нгуен, Т.Н.Б.Т. Хуен, Д.М. Чинь, А.В. Воронина
- 153 **ОРИГИНАЛЬНОЕ ИССЛЕДОВАНИЕ**
Регуляция дельта-орнитинамино-трансферазы *Arabidopsis thaliana* в развитии и в ответ на гормоны.
А.А. Егорова, С.В. Герасимова, А.В. Кочетов (на англ. языке)

Физиологическая генетика

- 159 **ОРИГИНАЛЬНОЕ ИССЛЕДОВАНИЕ**
Зависимые и независимые от уровня эстрадиола эффекты FGF21 у самок мышей с ожирением. *Т.В. Яковлева, А.Ю. Казанцева, А.Д. Дубинина, Н.Ю. Балыбина, К.О. Баранов, Е.Н. Макарова, Н.М. Бажан*

169

ОРИГИНАЛЬНОЕ ИССЛЕДОВАНИЕ

Влияние продукта гена *Hsp67Bc* на продолжительность жизни, плодовитость и устойчивость *Drosophila melanogaster* к кратковременному тепловому стрессу. *Д.А. Малькева, С.А. Фёдорова, Е.В. Киселева (на англ. языке)*

Медицинская генетика

179

ОРИГИНАЛЬНОЕ ИССЛЕДОВАНИЕ

Роль генов воспалительного ответа организма в формировании индивидуальных различий в уровне невербального интеллекта. *Р.Ф. Еникеева, А.В. Казанцева, Ю.Д. Давыдова, Р.Н. Мустафин, З.Р. Тахирова, С.Б. Малых, Ю.В. Ковас, Э.К. Хуснутдинова*

188

ОРИГИНАЛЬНОЕ ИССЛЕДОВАНИЕ

Полиморфизм гена *TCF7L2* в популяциях пяти этносов Сибири.
Л.Э. Табиханова, Л.П. Осипова, Т.В. Чуркина, Е.Н. Воронина, М.Л. Филипенко

Актуальные технологии

196

ОБЗОР

Показатель снижения температуры растительного полога в селекции пшеницы на засухоустойчивость и жаростойкость. *С.Б. Ленехов*

202

ОБЗОР

Обзор современных методов обнаружения и идентификации болезней растений на основе анализа гиперспектральных изображений. *А.Ф. Чешкова*

214

ОБЗОР

Модельные системы вируса иммунодефицита человека (ВИЧ-1), используемые для оценки эффективности кандидатных вакцин и лекарственных препаратов против ВИЧ-1 *in vitro*.
Н.Б. Рудометова, Д.Н. Щербаков, А.П. Рудометов, А.А. Ильичев, Л.И. Карпенко

Molecular and cell biology

- 121 **REVIEW**
Replication-transcription complex of coronaviruses: functions of individual viral non-structural subunits, properties and architecture of their complexes.
E.L. Mishchenko, V.A. Ivanisenko

Plant genetics and biotechnology

- 128 **ORIGINAL ARTICLE**
A system of molecular markers to identify alleles of the *Rht-B1* and *Rht-D1* genes controlling reduced height in bread wheat.
I.V. Porotnikov, O.P. Mitrofanova, O.Yu. Antonova
- 139 **ORIGINAL ARTICLE**
Androgenic response of *Triticum durum-Dasypyrum villosum* amphidiploids and their parental forms. *H. Stoyanov, I. Belchev*
- 146 **ORIGINAL ARTICLE**
Association of bud and anther morphology with developmental stages of the male gametophyte of melon (*Cucumis melo* L.).
M.L. Nguyen, T.N.B.T. Huyen, D.M. Trinh, A.V. Voronina
- 153 **ORIGINAL ARTICLE**
Developmental and hormonal regulation of *Arabidopsis thaliana* ornithine-delta-aminotransferase. *A.A. Egorova, S.V. Gerasimova, A.V. Kochetov*

Physiological genetics

- 159 **ORIGINAL ARTICLE**
Estradiol-dependent and independent effects of FGF21 in obese female mice.
T.V. Jakovleva, A.Yu. Kazantseva, A.D. Dubinina, N.Yu. Balybina, K.O. Baranov, E.N. Makarova, N.M. Bazhan

- 169 **ORIGINAL ARTICLE**
The impact of the *Hsp67Bc* gene product on *Drosophila melanogaster* longevity, fecundity, and acute heat stress tolerance.
D. Malkeyeva, S.A. Fedorova, E. Kiseleva

Medical genetics

- 179 **ORIGINAL ARTICLE**
The role of inflammatory system genes in individual differences in nonverbal intelligence. *R.F. Enikeeva, A.V. Kazantseva, Yu.D. Davydova, R.N. Mustafin, Z.R. Takhirova, S.B. Malykh, Y.V. Kovas, E.K. Khusnutdinova*
- 188 **ORIGINAL ARTICLE**
TCF7L2 gene polymorphism in populations of five Siberian ethnic groups. *L.E. Tabikhanova, L.P. Osipova, T.V. Churkina, E.N. Voronina, M.L. Filipenko*

Mainstream technologies

- 196 **REVIEW**
Canopy temperature depression for drought- and heat stress tolerance in wheat breeding. *S.B. Lepekhov*
- 202 **REVIEW**
A review of hyperspectral image analysis techniques for plant disease detection and identification. *A.F. Cheshkova*
- 214 **REVIEW**
Model systems of human immunodeficiency virus (HIV-1) for *in vitro* efficacy assessment of candidate vaccines and drugs against HIV-1. *N.B. Rudometova, D.N. Shcherbakov, A.P. Rudometov, A.A. Ilyichev, L.I. Karpenko*

Original Russian text www.bionet.nsc.ru/vogis/

Replication-transcription complex of coronaviruses: functions of individual viral non-structural subunits, properties and architecture of their complexes

E.L. Mishchenko , V.A. Ivanisenko

Institute of Cytology and Genetics of the Siberian Branch of the Russian Academy of Sciences, Novosibirsk, Russia
 elmish@bionet.nsc.ru

Abstract. Coronaviruses (CoVs) belong to the subfamily Orthocoronavirinae of the family Coronaviridae. CoVs are enveloped (+) RNA viruses with unusually long genomes. Severe acute respiratory syndrome CoV (SARS-CoV), Middle East respiratory syndrome CoV (MERS-CoV), and the novel coronavirus (2019-nCoV, SARS-CoV-2) have been identified as causing global pandemics. Clinically tested vaccines are widely used to control rapidly spreading, acute, and often severe infections; however, effective drugs are still not available. The genomes of SARS-CoV-2 and SARS-CoV are approximately 80 % identical, while the genomes of SARS-CoV-2 and MERS-CoV are approximately 50 % identical. This indicates that there may be common mechanisms of coronavirus pathogenesis and, therefore, potential therapeutic targets for each virus may be the same. The enzymes and effector proteins that make up the replication-transcription complex (RTC) of coronaviruses are encoded by a large replicase gene. These enzymes and effector proteins represent promising targets for potential therapeutic drugs. The enzyme targets include papain- and 3C-like cysteine proteinases that process two large viral polyproteins, RNA-dependent RNA polymerase, RNA helicase, viral genome-modifying enzymes, and enzymes with 3'-5' exoribonuclease or uridylyte-specific endonuclease activity. Currently, there are many studies investigating the complex molecular mechanisms involved in the assembly and function of the RTC. This review will encompass current, modern studies on the properties and complexes of individual non-structural subunits of the RTC, the structures of individual coronavirus RTC subunits, domain organization and functions of subunits, protein-protein interactions, properties and architectures of subunit complexes, the effect of mutations, and the identification of mutations affecting the viability of the virus in cell culture.
Key words: non-structural proteins CoVs; subunits of replicase CoVs; replication-transcription complex of CoVs; architecture of non-structural protein complexes CoVs.

For citation: Mishchenko E.L., Ivanisenko V.A. Replication-transcription complex of coronaviruses: functions of individual viral non-structural subunits, properties and architecture of their complexes. *Vavilovskii Zhurnal Genetiki i Seleksii* = *Vavilov Journal of Genetics and Breeding*. 2022;26(2):121-127. DOI 10.18699/VJGB-22-15

Репликационно-транскрипционный комплекс коронавирусов: функции индивидуальных вирусных неструктурных субъединиц, свойства и архитектура их комплексов

Е.Л. Мищенко , В.А. Иванисенко

Федеральный исследовательский центр Институт цитологии и генетики Сибирского отделения Российской академии наук, Новосибирск, Россия
 elmish@bionet.nsc.ru

Аннотация. Коронавирусы относятся к семейству Coronaviridae подсемейства Orthocoronavirinae и представляют собой оболочечные (+) РНК-вирусы с необычно длинным геномом. В настоящее время часто идентифицируются, вызывая продолжающуюся пандемию во всем мире, коронавирусы Severe Acute respiratory syndrome CoV (SARS-CoV), Middle East respiratory syndrome CoV (MERS-CoV) и новый коронавирус (2019-nCoV, SARS-CoV-2). Для сдерживания быстро распространяющейся, острой и часто тяжело протекающей инфекции широко применяют прошедшие клинические испытания вакцины, однако эффективных лекарств по-прежнему нет. Геномы SARS-CoV-2 и SARS-CoV идентичны на ~80 %, а SARS-CoV-2 и MERS-CoV – на ~50 %. Это свидетельствует об общих механизмах патогенеза коронавирусов и одних и тех же потенциальных терапевтических мишенях. Ферменты и эффекторные белки, входящие в состав репликационно-транскрипционного комплекса (РТК) коронавирусов, кодируются весьма крупным геном репликазы и представляют собой перспективные мишени действия потенциальных эффективных лекарств. Эти мишени включают папаин- и 3С-подобные цистеиновые протеиназы, осуществляющие процессинг двух больших вирусных полипротеинов, РНК-зависимую РНК-полимеразу, РНК-хеликазу, ферменты, модифицирующие вирусный геном, ферменты, обладающие 3'-5'-экзорибонуклеазной и уридилат-специфичной эндонуклеазной активностью, а также важные эффекторные белки. В настоящее время изучение сложных молекулярных механизмов сборки и функционирования

РТК находится на пике изучения. Обзор посвящен актуальным и современным исследованиям свойств индивидуальных неструктурных субъединиц РТК и их комплексов и включает изучение структур индивидуальных субъединиц РТК коронавирусов, доменной организации субъединиц и их функций, белок-белковых взаимодействий, свойств и архитектуры комплексов субъединиц, влияния мутаций, а также выявления мутаций, влияющих на жизнеспособность вируса в клеточной культуре.

Ключевые слова: неструктурные белки коронавирусов (CoVs); субъединицы репликазы CoVs; репликационно-транскрипционный комплекс CoVs; архитектура комплексов неструктурных белков CoVs.

Introduction

The 2019 coronavirus infection has spread globally, often causing severe respiratory, intestinal, and systemic illnesses. Coronaviruses (CoVs) belong to the Orthocoronavirinae subfamily of the Coronaviridae family. The subfamily is further divided into α -, β -, γ -, and δ -coronaviruses. Severe acute respiratory syndrome CoV (SARS-CoV), Middle East respiratory syndrome CoV (MERS-CoV), novel coronavirus (2019-nCoV, SARS-CoV-2), mouse hepatitis virus (MHV), and bovine coronavirus (BCoV) are all β -coronaviruses (Malik et al., 2020). Coronaviruses are enveloped viruses with an unusually long, single-stranded (+) RNA genome (26–32 kb). The SARS-CoV-2 genome is similar to the SARS-CoV genome (sequence identity ~80 %), while the SARS-CoV-2 and MERS-CoV genomes are less similar (sequence identity ~50 %) (Lu et al., 2020). The structure and function of proteins are preserved at levels as low as 30 % of amino acid sequence identity (Rost, 1999). This indicates that there may be common mechanisms of pathogenesis among the CoVs and, therefore, the viruses may have the same potential therapeutic targets. The 5' proximal region of each CoV genome includes a cap, a 5' untranslated region (UTR) and a long replicase gene encoding 16 non-structural proteins (comprising two-thirds of the genome). The 3' regions encode structural proteins, including S (spike), E (surface), M (membrane), and N (nucleocapsid), auxiliary proteins (the number of these varies among CoVs), a 3' UTR, and a poly(A) tract.

The replication-transcription complex (RTC) of CoVs is a complex consisting of viral and, probably, cellular proteins. The RTC produces the (+) RNA genome and a set of subgenomic CoVs RNA in infected cells. The CoV replicase gene has two overlapping open reading frames, ORF1a and ORF1b, which encode the viral components of the RTC. Expression of the gene leads to the formation of the pp1a polyprotein, which is encoded by ORF1a. A ribosomal frameshift of –1 before the ORF1a translation termination codon and ORF1b are required for the formation of the pp1ab polyprotein, which is a continuation of pp1a. Polyproteins pp1a and pp1ab are processed by two viral cysteine proteinases, papain-like proteinase PLP^{pro} (PLP) and 3C-like proteinase 3CL^{pro} (M^{pro}), which results in the release of intermediate precursors and 16 mature highly conserved non-structural proteins (nsps) capable of associating with each other and being subunits of the RTC. The pp1a polyprotein includes nsp1–nsp11, while pp1ab includes all pp1a nsps, as well as nsp12–nsp16 (Nagvi et al., 2020).

Structural and functional properties of conserved non-structural RTC subunits and their complexes

The molecular mechanisms of the assembly and function of the RTC has not been studied. However, the structural and functional properties of conserved non-structural RTC sub-

units and their complexes have been extensively researched and are extremely important for the identification of key drug targets against CoVs:

nsp1 interacts with the 40S ribosome subunit and inhibits translation initiation of host proteins, including interferon response factors. Interaction of nsp1 with ribosomes also leads to the degradation of host RNA. Thus, nsp1 suppresses cellular defence antiviral mechanisms (Kamitani et al., 2006; Narayanan et al., 2008);

nsp2 is not part of the RTC in cell culture. However, the absence of nsp2 in cells infected with the MHV Δ nsp2 or SARS-CoV Δ nsp2 deletion mutants reduces the production of the virus and viral RNA (Graham et al., 2005);

nsp3 and **nsp5** are proteinases that process the pp1a and pp1ab polyproteins, resulting in the release of individual RTC components. The PLP nsp3 domain(s) process the N-proximal regions of pp1a and pp1ab. The MHV nsp3 has two domains, PL1^{pro} (PL1P) and PL2^{pro} (PL2P). The PL1P domain cleaves the nsp1/nsp2 and nsp2/nsp3 sites, while the PL2P domain cleaves the nsp3/nsp4 site (Hughes et al., 1995; Kanjanaluethai et al., 2000). The SARS-CoV nsp3 has a single PL2P domain that cleaves all three nsp sites (Thiel et al., 2003). The SARS-CoV PLP is an intracellular immune response antagonist. PLP blocks the activation of transcription factors IRF3 and NF- κ B, which induces the expression of IFN(I) and antiviral genes. It does this by indirectly inhibiting IKKi and TBK1 kinases that activate IRF3 and stabilizing I κ B α , an inhibitor of NF- κ B (Frieman et al., 2009). PLP also hydrolyzes elements of ubiquitin and the product of interferon-stimulating gene 15 of the ubiquitin-like protein, thereby blocking the cellular mechanism of post-translational ubiquitination and, in turn, enhancing viral replication (Daczkowski et al., 2017). However, nsp3 stabilizes the host E3 ubiquitin ligase RCHY1 through the interaction of its SUD and PLP domains with RCHY1. This activates the RCHY1-mediated degradation of p53, a cellular inhibitor of SARS-CoV replication (Ma-Lauer et al., 2016). SARS-CoV nsp3 interacts with nsp5, nsp6, nsp12, nsp13, nsp14, and nsp16 in the yeast two-hybrid (Y2H) system and is thought to serve as a scaffold for RTC assembly (Imbert et al., 2008);

nsp5 is a 3CL^{pro} (M^{pro}). M^{pro} plays a key role in the processing of pp1a and pp1ab polyproteins, cleaving the central and C-proximal regions of pp1ab at 11 highly conserved sites, which releases mature nsp4–nsp16 proteins (Ziebuhr et al., 2000; Thiel et al., 2003; Goyal B., Goyal D., 2020). M^{pro} is only active as a dimer. Self-elimination of MERS-CoV M^{pro} at the nsp4/nsp5 and nsp5/nsp6 sites occurs as a result of the ligand-induced formation of an “immature dimer” during the convergence of M^{pro} III domains within two polyproteins (Tomar et al., 2015). Structural analysis of the SARS-CoV-2 M^{pro} complexes with known antiviral inhibitors, Boceprevir (peptidomimetic NS3/4A protease of hepatitis C virus) and

GC376 (inhibitor of CoV replication), revealed atomic-level interactions between M^{pro} and these inhibitors. Such studies are important for the optimization and design of effective drugs against CoVs (Fu et al., 2020);

nsp6 interacts with nsp2, nsp8, and nsp9 in the Y2H system (Brunn et al., 2007). Six of the predicted hydrophobic domains of MHV nsp6 and SARS-CoV nsp6 are transmembrane domains (Oostra et al., 2008). MHV nsp6 and SARS-CoV nsp6 are localized in the membranes of the endoplasmic reticulum (ER) and induce the formation of autophagosomes from ER membranes and activate autophagy (Cottam et al., 2011). Co-transfection of nsp3, nsp4, and nsp6 induces a change in the internal membranes of the host cell through the formation of double-membrane vesicles (DMVs), similar to the DMVs induced by SARS-CoV (Angelini et al., 2013);

nsp7 and **nsp8** interact with each other. SARS-CoV nsp7 and nsp8 co-crystallize to form the nsp7/8 hexadecameric supercomplex. The assembly of the supercomplex involves the formation of two different nsp7/8 heterodimers, D1 and D2, which differ in nsp8 conformation. D1 and D2 each dimerize to form the heterotetramers T1 and T2. The interaction of two T1 with two T2, in the order T1–T2–T1'–T2' and with ring closure through the T1–T2' interaction, leads to the construction of the full supercomplex. The supercomplex has a unique architecture: 16 molecules (8 nsp7 molecules and 8 nsp8 molecules) interact tightly with each other, forming a hollow cylindrical structure in which two nsp8 conformations coexist. The positive charge of the inner channel of the cylinder and its diameter (30 Å) indicates the ability of the nsp7/8 supercomplex to surround and interact with double-stranded RNA (dsRNA) (Zhai et al., 2005). The SARS-CoV nsp7/8 hexadecameric supercomplex can be formed in solution at an equimolar nsp7: nsp8 ratio (Zhai et al., 2005; Velthuis et al., 2012).

In solution, hexadecameric SARS-CoV nsp7/8 associates with dsRNA ($K_d \sim 1.2 \mu M$). The association of nsp7/8 with dsRNA is mediated by nsp8 and enhanced by nsp7 (Velthuis et al., 2012). On its own, SARS-CoV nsp8 possesses primer-independent RNA-dependent RNA polymerase (RdRp) activity and initiates, with low fidelity, the *de novo* synthesis of short (less than 6 nucleotides) complementary oligomers (primers) on single-stranded RNA (ssRNA) templates (Imbert et al., 2006). SARS-CoV nsp8 and nsp7/8 complex also exhibit primer-dependent RdRp activity (Velthuis et al., 2012). The FCoV (feline coronavirus) nsp7/8 complex is a 2 : 1 heterotrimer formed by the association of two nsp7 molecules and one nsp8 molecule. This complex does not form a hollow structure, either in crystalline form or in solution. FCoV nsp7/8 has primer-independent RdRp activity (Xiao et al., 2012);

nsp9 is an ssRNA-binding protein (Egloff et al., 2004; Miknis et al., 2009). Both monomeric and dimeric forms of PDCoV (porcine δ coronavirus) nsp9 and PEDV (porcine epidemic diarrhoea virus related to α coronaviruses) nsp9 (Zeng et al., 2018), as well as the dimeric form of SARS-CoV nsp9 (Miknis et al., 2009), have been found in solution during *in vitro* experiments. Studies of the crystal structures of SARS-CoV nsp9 (Egloff et al., 2004; Miknis et al., 2009), PDCoV nsp9, and PEDV nsp9 (Zeng et al., 2018) have revealed dimeric forms of nsp9. The monomer SARS-CoV nsp9 is characterized by a different structure compared to

other proteins involved in the replicative complexes of RNA viruses, the features of which are similar to the structures of oligosaccharide/oligonucleotide-binding proteins (Egloff et al., 2004). Mutations affecting the dimerization of SARS-CoV nsp9 weaken its interaction with ssRNA, which is lethal for SARS-CoV replication in cell culture (Miknis et al., 2009);

nsp10 interacts with dsRNA, dsDNA, and ssRNA with micromolar affinity (Joseph et al., 2006). Crystal structure studies of SARS-CoV nsp10 showed that the monomer structure includes two zinc fingers, a new discovery among zinc finger protein structures. Motifs of zinc-binding nsp10 sequences have been identified. Twelve identical monomers form a unique spherical dodecameric architecture, which is hypothesized to be the functional form of nsp10 (Joseph et al., 2006; Su et al., 2006). Through two-hybrid analysis in mammalian cells, interactions of SARS-CoV nsp10 with nsp14 and nsp16 have been revealed (Pan et al., 2008);

nsp11 is a short peptide resulting from the cleavage of the pp1a polyprotein by the 3CL pro /M pro proteinase at the nsp10/nsp11 site. Nsp11 is encoded by the region of genomic RNA where the translational reading frame shift occurs (ORF1a to ORF1b). This shift results in the formation of nsp12–nsp16 proteins from the pp1ab polyprotein. SARS-CoV-2 nsp11 contains 13 amino acid residues and has a disordered conformation, the dynamics of which have been studied in the presence of lipid-membrane mimetics. In the presence of SDS micelles, the disordered conformation of nsp11 is transformed into an α -helix (Gadhavie et al., 2021);

nsp14 is bifunctional. The N-terminal domain of nsp14 has 3'–5' exoribonuclease activity (ExoN), and its C-terminal domain has (guanine-N7) methyltransferase activity (N7-MTase). ExoN corrects the low fidelity of synthesis of the complementary RNA strand by viral RdRp nsp12 and catalyzes the removal of 3'-terminal erroneous nucleotides in dsRNA. N7-MTase catalyzes the methylation of the viral RNA cap at the N7 guanine position in the presence of S-adenosylmethionine (methyl group donor). N7-MTase has an S-adenosylmethionine binding motif which recognizes the cap of viral GpppRNA and methylates guanine N7 GpppRNA to form $^{7Me}GpppRNA$ (cap-0). Cap-0 plays an important role in blocking the degradation of viral RNA by 5'–3' exoribonucleases, translation initiation, and immune system control escape (Chen et al., 2009; Tahir, 2021). Mutants of the catalytic motif MERS-CoV ExoN and SARS-CoV-2 ExoN are not viable in cell culture (Ogando et al., 2020). SARS-CoV nsp10 associates with the ExoN domain of SARS-CoV nsp14, increasing the ExoN activity of nsp14 by more than 35 times without affecting its N7-MTase activity (Bouvet et al., 2012). Structural studies of the SARS-CoV nsp10/14 complex showed that one nsp10 molecule associates with the ExoN domain of nsp14, stabilizing and enhancing the activity of the ExoN. The architecture of the nsp10/14 complex has been studied and has been found to include two regions of contact between the nsp10 molecule and the ExoN domain of nsp14 (Ma et al., 2015);

nsp16 has (nucleoside-2'O) methyltransferase activity (2'O-MTase). 2'O-MTase recognizes the cap-0 of viral RNA and catalyzes the transfer of the methyl group from S-adenosylmethionine to the 2'OH group of the first nucleotide's ribose after N7-methylated guanine, resulting in the

formation of $^{7\text{Me}}\text{GpppN}_{2'\text{OMe}}\text{-RNA}$ (conversion of cap-0 into cap-1). SARS-CoV nsp10 associates with nsp16 and stimulates the 2'O-MTase activity of nsp16 (Bouvet et al., 2010). Mutagenesis mapping of the surface amino acid residues of SARS-CoV nsp10 involved in nsp10–nsp14 interaction and structural analysis of the nsp10/16 complex revealed overlapping surfaces of nsp10 interacting with nsp14 and nsp16. Nsp10 can serve as a platform that recruits nsp14 or nsp16 to the RTC, stimulating the ExoN activity of nsp14 or the 2'O-MTase activity of nsp16. Therefore, nsp10 is an important regulator of the RTC. Mutations have been identified that disrupt the nsp10–nsp14 and nsp10–nsp16 interactions, some of which lead to a nonviable viral phenotype in cell culture (Bouvet et al., 2014);

nsp12, an RdRp, catalyzes the synthesis of complementary RNA strands on (+) and (–) viral RNA templates and is a key CoV RTC enzyme. CoVs nsp12 initiates *de novo* synthesis from the 3' end of the viral genome of the full-length (–) RNA strand, as well as for subgenomic (–) RNA transcripts, which have differing 3' end lengths. In turn, the full-length (–) RNA strands and subgenomic (–) RNA strands serve as templates for the synthesis of the new RNA genome and subgenomic (+) RNA transcripts. Subgenomic (+) RNA is important for the expression of structural and accessory proteins encoded by genes in the 3' proximal region of the viral genome, which is inaccessible to ribosomes that translate the viral genome (Pasternak et al., 2006). Full-length recombinant SARS-CoV nsp12 associates with short (20–30 nucleotides long) dsRNA and ssRNA (Kd 0.13 and 0.1 μM , respectively), and initiates primer-dependent RNA synthesis on both homo- and heteropolymeric RNA templates of the same length (Velthuis et al., 2010). However, the recombinant SARS-CoV nsp12 does not associate with a primer-template that mimics the 3'-terminal 40 nucleotides of the SARS-CoV UTR and does not exhibit RdRp activity on this primer-template (Subissi et al., 2014).

Cryo-electron microscopy determined the structure of the monomer SARS-CoV-2 nsp12, which includes the nidovirus-specific N-terminal domain of the RdRp-associated nucleotidyl transferase (NiRAN), the interface domain, and the C-terminal RdRp domain. The C-terminal RdRp domain has a conserved right-hand-like architecture, which includes three subdomains: fingers, palm, and thumb. The active centre is formed by conservative motifs of amino acid residues localized in the palm subdomain. The motifs of the channel of entry for nucleotide triphosphates and the primer-template and the exit of the resulting RNA strand converge in the central cavity, where these motifs carry out matrix-dependent RNA synthesis have been determined (Gao et al., 2020).

The association of the nsp7/8 complex with nsp12 leads to the formation of the nsp7/8/12 complex. This complex possesses high RNA-binding capacity, polymerase activity, and processivity. It is also capable of initiating *de novo* RNA synthesis on the 3' UTR template of the SARS-CoV genome, resulting in the elongation of the RNA product by over 300 nucleotides. For nsp7/8/12 complex-mediated initiation of processive RNA synthesis, three amino acid residues from nsp7 (K7, H36, N37) and one amino acid residue from nsp8 (K58) are required for the interaction of nsp7/8/12 with the RNA template, while four amino acid residues from nsp8 (D99, P116, P183, R190) interact with nsp12 (Subissi et al.,

2014). Moreover, nsp7/8/12 is able to associate with nsp14 to form the nsp7/8/12/14 multicomplex. This ensemble of non-structural proteins possesses high RNA polymerase activity and is involved in 5' RNA capping; however, it does not have ExoN activity (Subissi et al., 2014). The structure of the SARS-CoV-2 and SARS-CoV nsp7/8/12 complexes was determined by cryo-electron microscopy. These complexes, including the nsp12 monomer, nsp8 monomer, and nsp7/nsp8 heterodimer, have similar architecture: the nsp8-1 subunit interacts with the RdRp finger subdomain, while the nsp7 and nsp8-2 subunits interact with the RdRp thumb subdomain (Gao et al., 2020);

nsp13 possesses helicase and nucleoside-triphosphatase (NTPase) activities; nsp13 interacts with nsp7, nsp8, and nsp12 in the Y2H system (Brunn et al., 2007; Pan et al., 2008). The crystal structure of MERS-CoV nsp13 was determined. The structure includes an N-terminal zinc-binding domain (ZBD) rich in Cys/His residues that coordinate three zinc ions, as well as C-terminal helicase RecA1 and RecA2 domains which contain parallel β -chains (Hao et al., 2017). The nsp13 helicase separates dsRNA and dsDNA strands with overhanging (5–20 nucleotides long) 5' ends; nsp13 interacts with the single-stranded 5' end of the partial nucleic acid duplex of dsRNA and dsDNA and unwinds it in the 5'–3' direction, using the hydrolysis energy of the 5'-deoxy- and ribonucleotide triphosphates (Ivanov et al., 2004; Adedeji et al., 2012, 2016). The RNA 5'-triphosphatase activity of nsp13 catalyzes the cleavage of the γ phosphate from the 5'-terminal nucleotide of RNA and is thought to be involved in the capping of viral RNA (Ivanov et al., 2004). Studies of SARS-CoV nsp13 have shown that the unwinding of DNA duplexes occurs in discrete intervals of ~ 9.3 base pairs (bp) at a rate of 30 intervals per second. Therefore, the unwinding speed of DNA duplexes is approximately 280 bp/s.

The helicase activity of nsp13 increases approximately 2-fold when nsp13 interacts with nsp12, suggesting the interaction of these proteins is involved in the function of the RTC (Adedeji et al., 2012). When SARS-CoV-2 nsp13 interacts with the RTC, specifically with nsp7/2nsp8/nsp12: RNA, the stable complexes 2nsp13–RTC (67 %) and nsp13–RTC (20 %), as well as the dimer (2nsp13–RTC)₂ (13 %) are formed. Using cryo-electron microscopy, the architecture of the dominant 2nsp13–RTC complex has been determined. This involves the interaction of the ZBD on the first nsp13 molecule with the N-terminus of nsp8b and the nsp12 thumb subdomain, as well as the interaction of the ZBD of the second nsp13 molecule with the N-terminus of nsp8a. The catalytic RecA1 helicase domain of the first nsp13 molecule is fixed against nsp7 and the nsp8b head (Chen et al., 2020);

nsp15 is a nidovirus uridylyate-specific endoribonuclease (NendoU). It cleaves RNA at the 3' uridylyate in unpaired, single-stranded, and looped regions (Bhardwaj et al., 2006; Zang et al., 2018). The crystal structures of SARS-CoV-2, SARS-CoV, and MERS-CoV nsp15 are homologous, functionally active hexamers formed by the dimerization of trimers. Each of the hexamer protomers includes three domains: the N-terminal, middle, and C-terminal catalytic NendoU domains. During trimer assembly, the N-terminal domain of one protomer is packed into a gap between the central and C-terminal domains of the neighbouring protomer. During

assembly of the hexamer, the N-terminal domains of the protomers of the two trimers are packed back-to-back and are in the centre of the hexamer structure. The C-terminal domains containing active centres are located outward at the vertices of the cloverleaf. This architecture provides nsp15 with six functionally active centres (Zang et al., 2018; Kim et al., 2020).

The uridylylate content in RNA, Mn^{+2} and, to a lesser extent, Mg^{+2} increase the affinity of nsp15 for RNA. The hexameric structure of SARS-CoV and MERS-CoV nsp15 is critical for its substrate and catalytic activity. The study of a series of mono-, tri- and hexameric protein mutants revealed weak interactions with RNA (rU_{16-20}) and low catalytic activity in monomers and trimers compared to hexamers and wild-type nsp15 (Bhardwaj et al., 2006; Zang et al., 2018). Nsp8 and the nsp7/8 complex interact with MERS-CoV nsp15, enhancing the binding ability of the nsp15 hexamer for RNA and its catalytic activity (Zang et al., 2018). The NendoU activity of nsp15 is an antagonist of the IFN-induced cellular antiviral response and stimulates the initiation of viral RNA translation (Deng et al., 2018, 2019).

A large number of non-structural subunits and their respective complexes within the RTC is a defining feature of CoVs. An important feature is that some subunits have domains with different enzymatic activities. For example, nsp14 has both ExoN and N7-MTase activity, while nsp13 has helicase and nucleoside triphosphatase activity. Non-structural proteins have a set of activities universal for (+) RNA viruses: proteinases (nsp3, nsp5), RNA-dependent RNA polymerases (nsp12), RNA helicases (nsp13). There are also unique domains involved in mRNA capping, cap modification (nsp14, nsp16). Some proteins possess 3'-5' exoribonuclease activity (nsp14), which regulate the reliability of RNA genome replication, while some possess uridylylate-specific endonuclease activity (nsp15). Many proteins serve as cofactors for important enzymes (nsp7, nsp 8, nsp10) and affect cellular processes. In particular, some proteins suppress the antiviral cellular response (nsp1, nsp3, nsp6, nsp15). The nsp9 and nsp10 structures are unique among the protein structures of the replicative complexes of RNA viruses. Many CoVs subunits and their complexes have a complex architecture. For example, nsp7 and nsp8 form a functional and unique hexadecameric supercomplex, the nsp10 architecture includes 12 identical subunits, and the nsp15 architecture is a functionally active hexamer. The complex architecture of the RTC is defined by the 2 nsp13/2 nsp8/1 nsp7/1 nsp12 model.

Conclusion

The lack of effective drugs against the novel coronavirus infection is a current global challenge. The RTC of CoVs replicates (+) RNA and determines the production of the virus in infected cells; however, the molecular mechanisms of this remain unexplored. Currently, great efforts are being undertaken aimed at creating a structural or functional network of interactions within the CoV proteome, as well as its interactions with the host cell. This would identify a large-scale panel of therapeutic targets. The determination of the structures of individual non-structural RTC subunits and their complexes and the identification of key interacting amino acid residues and types of bonds between them will enable the design of selective and effective inhibitors. Investigations employing

biochemical methods and mutational analyses can identify factors that affect the efficiency of viral genomic RNA production and the virus in an infected cell, the multiple effects of viral proteins on the host cell, and potential key drug targets.

References

- Adedeji A.O., Lazarus H. Biochemical characterization of Middle East respiratory syndrome coronavirus helicase. *mSphere*. 2016;1(5): e00235-16. DOI 10.1128/mSphere.00235-16.
- Adedeji A.O., Marchand B., Velthuis A.J.W., Snijder E.J., Weiss S., Eoff R.L., Singh K., Sarafianos S.G. Mechanism of nucleic acid unwinding by SARS-CoV helicase. *PLoS One*. 2012;7(5):e36521. DOI 10.1371/journal.pone.0036521.
- Angelini M.M., Akhlaghpour M., Neuman B.W., Buchmeier M.J. Severe acute respiratory syndrome coronavirus nonstructural proteins 3, 4, and 6 induce double-membrane vesicles. *mBio*. 2013; 4(4):e00524-13. DOI 10.1128/mBio.00524-13.
- Bhardwaj K., Sun J., Holzenburg A., Guarino L.A., Kao C.C. RNA recognition and cleavage by the SARS coronavirus endoribonuclease. *J. Mol. Biol.* 2006;361(2):243-256. DOI 10.1016/j.jmb.2006.06.021.
- Bouvet M., Debarnot C., Imbert I., Selisko B., Snijder E.J., Canard B., Decroly E. *In vitro* reconstitution of SARS-coronavirus mRNA cap methylation. *PLoS Pathog.* 2010;6(4):e1000863. DOI 10.1371/journal.ppat.1000863.
- Bouvet M., Imbert I., Subissi L., Gluais L., Canard B., Decroly E. RNA 3'-end mismatch excision by the severe acute respiratory syndrome coronavirus nonstructural protein nsp10/nsp14 exoribonuclease complex. *Proc. Natl. Acad. Sci. USA*. 2012;109(24):9372-9377. DOI 10.1073/pnas.1201130109.
- Bouvet M., Lugari A., Posthuma C.C., Zevenhoven J.C., Bernard S., Betzi S., Imbert I., Canard B., Guillemot J.-C., Lécine P., Pfefferle S., Drosten C., Snijder E.J., Decroly E., Morelli X. Coronavirus Nsp10, a critical co-factor for activation of multiple replicative enzymes. *J. Biol. Chem.* 2014;289(37):25783-25796. DOI 10.1074/jbc.M114.577353.
- Brunn A., Teepe C., Simpson J.C., Pepperkok R., Friedel C.C., Zimmer R., Roberts R., Baric R., Haas J. Analysis of intraviral protein-protein interactions of the SARS coronavirus ORFome. *PLoS One*. 2007;2(5):e459. DOI 10.1371/journal.pone.0000459.
- Chen J., Malone B., Llewellyn E., Grasso M., Shelton P.M.M., Olinares P.D.B., Maruthi K., Eng E.T., Vatandaslar H., Chait B.T., Kapoor T.M., Darst S.A., Campbell E.A. Structural basis for helicase-polymerase coupling in the SARS-CoV-2 replication-transcription complex. *Cell*. 2020;182(6):1560-1573.e13. DOI 10.1016/j.cell.2020.07.033.
- Chen Y., Cai H., Pan J., Xiang N., Tien P., Ahola T., Guo D. Functional screen reveals SARS coronavirus nonstructural protein nsp14 as a novel cap N7 methyltransferase. *Proc. Natl. Acad. Sci. USA*. 2009;106(9):3484-3489. DOI 10.1073/pnas.0808790106.
- Cottam E.M., Maier H.J., Manifava M., Vaux L.C., Chandra-Schoenfelder P., Gerner W., Britton P., Ktistakis N.T., Wileman T. Coronavirus nsp6 proteins generate autophagosomes from the endoplasmic reticulum via an omegasome intermediate. *Autophagy*. 2011;7(11): 1335-1347. DOI 10.4161/auto.7.11.16642.
- Daczkowski C.M., Dzimianski J.V., Clasman J.R., Goodwin O., Mesezar A.D., Pegan S.D. Structural insights into the interaction of coronavirus papain-like proteases and interferon-stimulated gene product 15 from different species. *J. Mol. Biol.* 2017;429(11):1661-1683. DOI 10.1016/j.jmb.2017.04.011.
- Deng X., Baker S.C. An "Old" protein with a new story: Coronavirus endoribonuclease is important for evading host antiviral defenses. *Virology*. 2018;517:157-163. DOI 10.1016/j.virol.2017.12.024.
- Deng X., Geelen A., Buckley A.C., O'Brien A., Pillatzki A., Lager K.M., Faaborg K.S., Baker S.C. Coronavirus endoribonuclease

- activity in porcine epidemic diarrhea virus suppresses type I and type III interferon responses. *J. Virol.* 2019;93(8):e02000-18. DOI 10.1128/JVI.02000-18.
- Egloff M.-P., Ferron F., Campanacci V., Longhi S., Rancurel C., Dutartre H., Snijder E.J., Gorbalenya A.E., Cambillau C., Canard B. The severe acute respiratory syndrome-coronavirus replicative protein nsp9 is a single-stranded RNA-binding subunit unique in the RNA virus world. *Proc. Natl. Acad. Sci. USA.* 2004;101(11):3792-3796. DOI 10.1073/pnas.0307877101.
- Frieman M., Ratia K., Johnston R.E., Mesecar A.D., Baric R.S. Severe acute respiratory syndrome coronavirus papain-like protease ubiquitin-like domain and catalytic domain regulate antagonism of IRF3 and NF-kappaB signaling. *J. Virol.* 2009;83(13):6689-6705. DOI 10.1128/JVI.02220-08.
- Fu L., Ye F., Feng Y., Yu F., Wang Q., Wu Y., Zhao C., Sun H., Huang B., Niu P., Song H., Shi Y., Li X., Tan W., Qi J., Gao G.F. Both Bopreprevir and GC376 efficaciously inhibit SARS-CoV-2 by targeting its main protease. *Nat. Commun.* 2020;11(1):4417. DOI 10.1038/s41467-020-18233-x.
- Gadhve K., Kumar P., Kumar A., Bhardwaj T., Garg N., Giri R. Conformational dynamics of 13 amino acids long NSP11 of SARS-CoV-2 under membrane mimetics and different solvent conditions. *Microb. Pathog.* 2021;158:105041. DOI 10.1016/j.micpath.2021.105041.
- Gao Y., Yan L., Huang Y., Liu F., Zhao Y., Cao L., Wang T., Sun Q., Ming Z., Zhang L., Ge J., Zheng L., Zhang Y., Wang H., Zhu Y., Zhu C., Hu T., Hua T., Zhang B., Yang X., Li J., Yang H., Liu Z., Xu W., Guddat L.W., Wang Q., Lou Z., Rao Z. Structure of the RNA-dependent RNA polymerase from COVID-19 virus. *Science.* 2020;368(6492):779-782. DOI 10.1126/science.abb7498.
- Goyal B., Goyal D. Targeting the dimerization of the main protease of coronaviruses: a potential broad-spectrum therapeutic strategy. *ACS Comb. Sci.* 2020;22(6):297-305. DOI 10.1021/acscmbsci.0c00058.
- Graham R.L., Sims A.C., Brockway S.M., Baric R.S., Denison M.R. The nsp2 replicase proteins of murine hepatitis virus and severe acute respiratory syndrome coronavirus are dispensable for viral replication. *J. Virol.* 2005;79(21):13399-13411. DOI 10.1128/JVI.79.21.13399-13411.2005.
- Hao W., Wojdyla J.A., Zhao R., Han R., Das R., Zlatev I., Manoharan M., Wang M., Cui S. Crystal structure of Middle East respiratory syndrome coronavirus helicase. *PLoS Pathog.* 2017;13(6):e1006474. DOI 10.1371/journal.ppat.1006474.
- Hughes S.A., Bonilla P.J., Weiss S.R. Identification of the murine coronavirus p28 cleavage site. *J. Virol.* 1995;69(2):809-813. DOI 10.1128/JVI.69.2.809-813.1995.
- Imbert I., Guillemot J.-C., Bourhis J.-M., Bussetta C., Coutard B., Egloff M.-P., Ferron F., Gorbalenya A.E., Canard B. A second, non-canonical RNA-dependent RNA polymerase in SARS coronavirus. *EMBO J.* 2006;25(20):4933-4942. DOI 10.1038/sj.emboj.7601368.
- Imbert I., Snijder E.J., Dimitrova M., Guillemot J.-C., Lécine P., Canard B. The SARS-Coronavirus PLnc domain of nsp3 as a replication/transcription scaffolding protein. *Virus Res.* 2008;133(2):136-148. DOI 10.1016/j.virusres.2007.11.017.
- Ivanov K.A., Thiel V., Dobbe J.C., Meer Y., Snijder E.J., Ziebuhr J. Multiple enzymatic activities associated with severe acute respiratory syndrome coronavirus helicase. *J. Virol.* 2004;78(11):5619-5632. DOI 10.1128/JVI.78.11.5619-5632.2004.
- Joseph J.S., Saikatendu K.S., Subramanian V., Neuman B.W., Brooun A., Griffith M., Moy K., Yadav M.K., Velasquez J., Buchmeier M.J., Stevens R.C., Kuhn P. Crystal structure of nonstructural protein 10 from the severe acute respiratory syndrome coronavirus reveals a novel fold with two zinc-binding motifs. *J. Virol.* 2006;80(16):7894-7901. DOI 10.1128/JVI.00467-06.
- Kamitani W., Narayanan K., Huang C., Lokugamage K., Ikegami T., Ito N., Kubo H., Makino S. Severe acute respiratory syndrome coronavirus nsp1 protein suppresses host gene expression by promoting host mRNA degradation. *Proc. Natl. Acad. Sci. USA.* 2006;103(34):12885-12890. DOI 10.1073/pnas.0603144103.
- Kanjanahaluethai A., Baker S.C. Identification of mouse hepatitis virus papain-like proteinase 2 activity. *J. Virol.* 2000;74(17):7911-7921. DOI 10.1128/jvi.74.17.7911-7921.2000.
- Kim Y., Jedrzejczak R., Maltseva N.I., Wilamowski M., Endres M., Godzik A., Michalska K., Joachimiak A. Crystal structure of Nsp15 endoribonuclease NendoU from SARS-CoV-2. *Protein Sci.* 2020;29(7):1596-1605. DOI 10.1002/pro.3873.
- Lu R., Zhao X., Li J., Niu P., Yang B., Wu H., Wang W., Song H., Huang B., Zhu N., Bi Y., Ma X., Zhan F., Wang L., Hu T., Zhou H., Hu Z., Zhou W., Zhao L., Chen J., Meng Y., Wang J., Lin Y., Yuan J., Xie Z., Ma J., Liu W.J., Wang D., Xu W., Holmes E.C., Gao G.F., Wu G., Chen W., Shi W., Tan W. Genomic characterisation and epidemiology of 2019 novel coronavirus: implications for virus origins and receptor binding. *Lancet.* 2020;395(10224):565-574. DOI 10.1016/S0140-6736(20)30251-8.
- Ma Y., Wu L., Shaw N., Gao Y., Wang J., Sun Y., Lou Z., Yan L., Zhang R., Rao Z. Structural basis and functional analysis of the SARS coronavirus nsp14-nsp10 complex. *Proc. Natl. Acad. Sci. USA.* 2015;112(30):9436-9441. DOI 10.1073/pnas.1508686112.
- Ma-Lauer Y., Carbajo-Lozoya J., Hein M.Y., Müller M.A., Deng W., Lei J., Meyer B., Kusov Y., von Brunn B., Baird D.R., Hüntens S., Drosten C., Hermeking H., Leonhardt H., Mann M., Hilgenfeld R., von Brunn A. p53 down-regulates SARS coronavirus replication and is targeted by the SARS-unique domain and PLP^{ro} via E3 ubiquitin ligase RCHY1. *Proc. Natl. Acad. Sci. USA.* 2016;113(35):E5192-E5201. DOI 10.1073/pnas.1603435113.
- Malik Y.S., Sircar S., Bhat S., Sharun K., Dhama K., Dadar M., Tiwari R., Chaicumpa W. Emerging novel coronavirus (2019-nCoV) – current scenario, evolutionary perspective based on genome analysis and recent developments. *Vet. Q.* 2020;40(1):68-76. DOI 10.1080/01652176.2020.1727993.
- Miknis Z.J., Donaldson E.F., Umland T.C., Rimmer R.A., Baric R.S., Schultz L.W. Severe acute respiratory syndrome coronavirus nsp9 dimerization is essential for efficient viral growth. *J. Virol.* 2009;83(7):3007-3018. DOI 10.1128/JVI.01505-08.
- Naqvi A.A.T., Fatima K., Mohammad T., Fatima U., Singh I.K., Singh A., Atif S.M., Hariprasad G., Hasan G.M., Hassan M.I. Insights into SARS-CoV-2 genome, structure, evolution, pathogenesis and therapies: Structural genomics approach. *Biochim. Biophys. Acta Mol. Basis Dis.* 2020;1866(10):165878. DOI 10.1016/j.bbdis.2020.165878.
- Narayanan K., Huang C., Lokugamage K., Kamitani W., Ikegami T., Tseng C.-T.K., Makino S. Severe acute respiratory syndrome coronavirus nsp1 suppresses host gene expression, including that of type I interferon, in infected cells. *J. Virol.* 2008;82(9):4471-4479. DOI 10.1128/JVI.02472-07.
- Ogando N.S., Zevenhoven-Dobbe J.C., Meer Y., Bredenbeek P.J., Posthuma C.C., Snijder E.J. The enzymatic activity of the nsp14 exoribonuclease is critical for replication of MERS-CoV and SARS-CoV-2. *J. Virol.* 2020;94(23):e01246-20. DOI 10.1128/JVI.01246-20.
- Oostra M., Hagemeijer M.C., Gent M., Bekker C.P.J., Lintelo E.G., Rottier P.J.M., Haan C.A.M. Topology and membrane anchoring of the coronavirus replication complex: not all hydrophobic domains of nsp3 and nsp6 are membrane spanning. *J. Virol.* 2008;82(24):12392-12405. DOI 10.1128/JVI.01219-08.
- Pan J., Peng X., Gao Y., Li Z., Lu X., Chen Y., Ishaq M., Liu D., Dediego M.L., Enjuanes L., Guo D. Genome-wide analysis of protein-protein interactions and involvement of viral proteins in SARS-CoV replication. *PLoS One.* 2008;3(10):e3299. DOI 10.1371/journal.pone.0003299.
- Pasternak A.O., Spaan W.J.M., Snijder E.J. Nidovirus transcription: how to make sense...? *J. Gen. Virol.* 2006;87(6):1403-1421. DOI 10.1099/vir.0.81611-0.
- Rost B. Twilight zone of protein sequence alignments. *Protein Eng.* 1999;12(2):85-94. DOI 10.1093/protein/12.2.85.

- Su D., Lou Z., Sun F., Zhai Y., Yang H., Zhang R., Joachimiak A., Zhang X.C., Bartlam M., Rao Z. Dodecamer structure of severe acute respiratory syndrome coronavirus nonstructural protein nsp10. *J. Virol.* 2006;80(16):7902-7908. DOI 10.1128/JVI.00483-06.
- Subissi L., Posthuma C.C., Collet A., Zevenhoven-Dobbe J.C., Gorbalenya A.E., Decroly E., Snijder E.J., Canard B., Imbert I. One severe acute respiratory syndrome coronavirus protein complex integrates processive RNA polymerase and exonuclease activities. *Proc. Natl. Acad. Sci. USA.* 2014;111(37):E3900-E3909. DOI 10.1073/pnas.1323705111.
- Tahir M. Coronavirus genomic nsp14-ExoN, structure, role, mechanism, and potential application as a drug target. *J. Med. Virol.* 2021; 93(7):4258-4264. DOI 10.1002/jmv.27009.
- Thiel V., Ivanov K.A., Putics Á., Hertzog T., Schelle B., Bayer S., Weißbrich B., Snijder E.J., Rabenau H., Doerr H.W., Gorbalenya A.E., Ziebuhr J. Mechanisms and enzymes involved in SARS coronavirus genome expression. *J. Gen. Virol.* 2003;84(9):2305-2315. DOI 10.1099/vir.0.19424-0.
- Tomar S., Johnston M.L., John S.E.St., Osswald H.L., Nyalapatla P.R., Paul L.N., Ghosh A.K., Denison M.R., Mesecar A.D. Ligand-induced dimerization of Middle East respiratory syndrome (MERS) coronavirus nsp5 protease (3CLpro): implications for nsp5 regulation and the development of antivirals. *J. Biol. Chem.* 2015;290(32):19403-19422. DOI 10.1074/jbc.M115.651463.
- Velthuis A.J.W., Arnold J.J., Cameron C.E., Worm S.H.E., Snijder E.J. The RNA polymerase activity of SARS-coronavirus nsp12 is primer dependent. *Nucleic Acids Res.* 2010;38(1):203-214. DOI 10.1093/nar/gkp904.
- Velthuis A.J.W., Worm S.H.E., Snijder E.J. The SARS-coronavirus nsp7+nsp8 complex is a unique multimeric RNA polymerase capable of both *de novo* initiation and primer extension. *Nucleic Acids Res.* 2012;40(4):1737-1747. DOI 10.1093/nar/gkr893.
- Xiao Y., Ma Q., Restle T., Shang W., Svergun D.I., Ponnusamy R., Sczakiel G., Hilgenfeld R. Nonstructural proteins 7 and 8 of feline coronavirus form a 2:1 heterotrimer that exhibits primer-independent RNA polymerase activity. *J. Virol.* 2012;86(8):4444-4454. DOI 10.1128/JVI.06635-11.
- Zeng Z., Deng F., Shi K., Ye G., Wang G., Fang L., Xiao S., Fu Z., Peng G. Dimerization of coronavirus nsp9 with diverse modes enhances its nucleic acid binding affinity. *J. Virol.* 2018;92(17):e00692-18. DOI 10.1128/JVI.00692-18.
- Zhai Y., Sun F., Li X., Pang H., Xu X., Bartlam M., Rao Z. Insights into SARS-CoV transcription and replication from the structure of the nsp7–nsp8 hexadecamer. *Nat. Struct. Mol. Biol.* 2005;12(11):980-986. DOI 10.1038/nsmb999.
- Zhang L., Li L., Yan L., Ming Z., Jia Z., Lou Z., Rao Z. Structural and biochemical characterization of endoribonuclease nsp15 encoded by Middle East respiratory syndrome coronavirus. *J. Virol.* 2018; 92(22):e00893-18. DOI 10.1128/JVI.00893-18.
- Ziebuhr J., Snijder E.J., Gorbalenya A.E. Virus-encoded proteinases and proteolytic processing in the Nidovirales. *J. Gen. Virol.* 2000; 81(4):853-879. DOI 10.1099/0022-1317-81-4-853.

Acknowledgements. The work was carried out with the support of budget project No. FWNR-2022-0020.

Conflict of interest. The authors declare no conflict of interest.

Received October 7, 2021. Revised November 24, 2021. Accepted November 25, 2021.

Original Russian text www.bionet.nsc.ru/vogis/

A system of molecular markers to identify alleles of the *Rht-B1* and *Rht-D1* genes controlling reduced height in bread wheat

I.V. Porotnikov , O.P. Mitrofanova, O.Yu. Antonova

Federal Research Center the N.I. Vavilov All-Russian Institute of Plant Genetic Resources (VIR), St. Petersburg, Russia
 i.v.porotnikov@gmail.com

Abstract. Mutant alleles of the *Rht-B1* and *Rht-D1* (*Reduced height*) genes are widely used in bread wheat breeding for the development of intensive-type cultivars. These genes and their flanking regions have been sequenced and the point mutations leading to the nonsense codons (*Rht-B1b*, *Rht-B1e*, *Rht-B1p* and *Rht-D1b* alleles) and various insertions (*Rht-B1c*, *Rht-B1h* and *Rht-B1i-1*) associated with a change in plant height have been described. DNA-markers based on the allele-specific PCR have been developed to identify single-nucleotide changes. However, the use of such technique imposes stringent PCR conditions, and the resulting data are not always unambiguous. An alternative can be found in the CAPS technology: it detects differences in sequences by digesting PCR products. In the absence of restrictases capable of digesting DNA at the point mutation site, restriction sites can be introduced into the primer sequence (derived CAPS). The aim of this study was to propose a system of CAPS-, dCAPS- and STS-markers for identifying alleles of the reduced height genes frequently used in breeding programs. Three CAPS have been developed to identify the *Rht-B1b*, *Rht-D1b*, *Rht-B1p* alleles, as well as two dCAPS for *Rht-B1b*, *Rht-B1e*. STS-markers for the insertion-containing alleles *Rht-B1c*, *Rht-B1h* and *Rht-B1i-1* have been selected from publications. The proposed markers were tested during the genotyping of 11 bread wheat accessions from the VIR collection with the abovementioned mutant alleles and the wild-type *Rht-B1a* and *Rht-D1a*. The presence of nonsense mutations was also confirmed by the results of allele-specific PCR. This marker system, along with the existing ones, can be used to identify dwarfing alleles of the *Rht-B1* and *Rht-D1* genes in bread wheat for genetic screening of accessions from *ex situ* collections and/or for marker-assisted selection.

Key words: *Triticum aestivum*; alleles of *Rht*-genes; AS-PCR; CAPS; dCAPS; genotyping.

For citation: Porotnikov I.V., Mitrofanova O.P., Antonova O.Yu. A system of molecular markers to identify alleles of the *Rht-B1* and *Rht-D1* genes controlling reduced height in bread wheat. *Vavilovskii Zhurnal Genetiki i Seleksii = Vavilov Journal of Genetics and Breeding*. 2022;26(2):128-138. DOI 10.18699/VJGB-22-16

Система молекулярных маркеров для идентификации аллелей генов короткостебельности *Rht-B1* и *Rht-D1* у мягкой пшеницы

И.В. Поротников , О.П. Митрофанова, О.Ю. Антонова

Федеральный исследовательский центр Всероссийский институт генетических ресурсов растений им. Н.И. Вавилова (ВИР), Санкт-Петербург, Россия
 i.v.porotnikov@gmail.com

Аннотация. Мутантные аллели генов *Rht-B1* и *Rht-D1* (*Reduced height*) широко используют для создания короткостебельных сортов мягкой пшеницы интенсивного типа. Эти гены и фланкирующие их области секвенированы, в последовательностях описаны ассоциированные с изменением высоты растения однонуклеотидные замены, приводящие к образованию нонсенс-кодонов (аллели *Rht-B1b*, *Rht-B1e*, *Rht-B1p* и *Rht-D1b*), и различные инсерции (аллели *Rht-B1c*, *Rht-B1h* и *Rht-B1i-1*). Для идентификации такого типа однонуклеотидных мутаций разработаны ДНК-маркеры, основанные на принципе аллель-специфичной полимеразной цепной реакции (ПЦР). Однако идентификация аллелей этим методом предъявляет повышенные требования к соблюдению условий реакции, а получаемые результаты не всегда однозначны. Альтернативой может быть CAPS-технология, детектирующая различия в последовательностях путем рестрикции ПЦР-продуктов. В случае отсутствия рестриктаз, способных расщеплять ДНК в месте локализации точечной мутации, рестрикционные сайты могут быть искусственно внесены в последовательность праймера (derived CAPS). Цель настоящей работы – разработать CAPS- и dCAPS-маркеры для выявления замен оснований, подобрать по литературным источникам STS-маркеры для детекции инсерций и тем самым предложить систему молекулярных маркеров для идентификации аллелей генов короткостебельности, часто используемых и перспективных для селекции. Разработано три CAPS-маркера для выявления аллелей *Rht-B1b*, *Rht-D1b*, *Rht-B1p* и два dCAPS-маркера для *Rht-B1b* и *Rht-B1e*, предложены про-

граммы для их амплификации. По литературным источникам подобраны STS-маркеры аллелей *Rht-B1c*, *Rht-B1h*, *Rht-B1i-1*, содержащих инсерции. Предложенная система маркеров апробирована при генотипировании 11 образцов мягкой пшеницы из коллекции ВИР, несущих вышеуказанные мутантные аллели генов короткостебельности и аллели дикого типа *Rht-B1a* и *Rht-D1a*. Наличие нонсенс-мутаций подтверждено также при помощи аллель-специфичной ПЦР. Эта система маркеров наряду с уже существующими может быть использована для идентификации аллелей генов короткостебельности *Rht-B1* и *Rht-D1* у мягкой пшеницы с целью генетического скрининга образцов *ex situ* коллекций и/или в маркер-ориентированной селекции.

Ключевые слова: *Triticum aestivum*; аллели *Rht*-генов; AS-PCR; CAPS; dCAPS; генотипирование.

Introduction

The development of intensive-type short-stemmed wheat cultivars is considered one of the key success factors in bread wheat breeding, primarily in implementing the Green Revolution initiative in the world's developing countries (Hedden, 2003; Sukhikh et al., 2021). The decrease in plant height not only entailed higher resistance to lodging, with its favorable effect on the efficiency of mechanized harvesting, but also increased the number of grains per ear and their number per 1 m², which aggregately led to higher yields (Gale et al., 1985; Youssefian et al., 1992; Evans, 1998).

At least 25 genes controlling plant height in bread wheat (*Triticum aestivum* L.) and related species were described: they are known as *Reduced height – Rht1–Rht25*. All these genes are in one way or another associated with the growth hormone gibberellin (McIntosh et al., 2013, 2016, 2018). Some of them, the so-called GA-sensitive genes *Rht4–Rht9*, *Rht12–Rht20* and *Rht25*, are apparently involved in the synthesis or degradation of gibberellic acid (GA). Other genes, GA-insensitive ones, such as *Rht-A1*, *Rht-B1*, and *Rht-D1*, determine the response to this acid. For some genes (*Rht22*, *Rht23* and *Rht24*), the nature of their response has not yet been clarified (Sukhikh et al., 2021).

The most widespread among GA-sensitive genes is *Rht8*, transferred in the early 20th century, together with the closely linked photoperiod insensitivity allele *Ppd-D1a* of the *Ppd* gene (response to photoperiod), from the Japanese cultivar Akakomugi first to Italian and later to many East and South European cultivars (Borojevic K., Borojevic Ks., 2005). This gene does not exert any significant reducing effect on the coleoptile length and, as a consequence, makes it possible to sow seeds to a greater depth, which plays a decisive role in maintaining the viability of seedlings under water deficits or high temperatures (Korzun et al., 1998; Ellis et al., 2004; Divashuk et al., 2013; Grover et al., 2018).

GA-insensitive genes were studied in more detail; they are located on the short arms of chromosomes of homeologous group 4 (Gale, Marshall, 1976; Börner et al., 1996). Dominant alleles of these genes (wild-type) encode DELLA proteins, belonging to the family of GRAS proteins (transcription regulators); at their C-terminus, there is a conservative domain that can bind to other transcription factors and thereby block their function. That is why large amounts of DELLA proteins in cells decelerate plant growth. There is a DELLA domain at the variable N-terminus: it is capable of forming the GA–GID1 complex (gibberellin insensitive dwarf 1, GA receptor). This complex undergoes polyubiquitination and degradation induced by proteasomes. Accordingly, a decrease in the amount of DELLA proteins in cells in the presence of GA reduces their negative effect on plant growth (Peng et al., 1999; Bazhenov et al., 2015; Thomas, 2017; Sukhikh et al., 2021).

A fairly large number of recessive and semi-dominant mutant alleles altering the stem length in different ways have been described for the *Rht-B1* and *Rht-D1* genes. These alleles have been sequenced; the most thoroughly studied sequences are presented by us in Supplementary material 1¹. The alleles *Rht-B1b* (= *Rht1*), *Rht-B1e* (= *Rht11*, = *Rht Krasnodari 1*), *Rht-B1p* (= *Rht17*) and *Rht-D1b* (= *Rht2*) were shown to be associated with single-nucleotide substitutions that lead to the formation of premature stop codons (Peng et al., 1999; Ellis et al., 2002; Pearce et al., 2011; Divashuk et al., 2012; Li et al., 2012; Bazhenov et al., 2015). The phenotypic effect of such nonsense mutations varies from moderate (a decrease in plant height by 20–24 % in the presence of *Rht-B1b* and *Rht-D1b* alleles) to strong (by 33 and 40 % in the presence of *Rht-B1p* and *Rht-B1e*, respectively) (Gale et al., 1985; Sukhikh et al., 2021).

The alleles *Rht-B1h* and *Rht-B1i-1* have large (over 100 bp) insertions in the 5' flanking region, while *Rht-B1c* (= *Rht3*) is characterized by the presence of an insertion in the 5' untranslated region identical to that in *Rht-B1h* and, at the same time, the presence of the *Veju* retrotransposon in the coding region (Wu et al., 2011; Li et al., 2013; Wen et al., 2013; Lou et al., 2016). Such insertions can lead to the formation of nondegradable proteins, so the growth of mutant plants is constitutively repressed, more significantly than in the case of nonsense mutations in the N-terminal coding region (Wu et al., 2011; Wen et al., 2013). For example, the *Rht-B1c* allele reduces plant height approximately by 60 % (Flintham, Gale, 1983; Sukhikh et al., 2021). However, insertions can not only reduce but also increase the height of plants (by 10–15 %, compared to the wild type) as, for example, in the case of *Rht-B1i-1* (Lou et al., 2016). Besides, the alleles of “strong dwarfing”, *Rht-D1c* (*Rht10*) and *Rht-D1d* (*Rht Ai-bian 1a*), reducing the height by 60–70 %, were identified in the *Rht-D1* gene; they turned out to be multiple copies of the mutant allele *Rht-D1b* (Pearce et al., 2011). There are also other known alleles of the *Rht-B1h-o* and *Rht-D1e-j* genes, associated with either nucleotide changes (missense mutations) or indels. They are identified in a large number of Chinese cultivars using the EcoTILLING method; however, their phenotypic effect has not yet been described. Mutant alleles of the *Rht-A1* gene were also identified for the first time in Chinese cultivars (Li et al., 2013).

The alleles most frequently used in breeding programs are *Rht-B1b* and *Rht-D1b*. Their source was the Japanese cultivar Norin 10. At the end of the 20th century, more than 70 % of the world's bread wheat cultivars contained these alleles (Gale et al., 1985; Evans, 1998). Later, however, it was shown that their occurrence depended on the region of the world. *Rht-B1b*

¹ Supplementary materials 1 and 2 are available in the online version of the paper: http://vavilov.elpub.ru/jour/manager/files/Suppl_Porotnikov_Engl.pdf

was detected in 36.2 % of bread wheat cultivars from China, and *Rht-D1b* in 53.4 % (Zhang et al., 2006). Meanwhile, the genotyping of 247 cultivars from the United States and Canada helped to identify these alleles in more than 90 % of them (Guedira et al., 2010). *Rht-D1b* predominates in the genotypes of European cultivars, while its occurrence in the cultivars registered after 1990 is 49 % (Würschum et al., 2017).

Widespread in Russia are cultivars with the *Rht-B1e* allele, obtained by mutagenesis in cv. Bezostaya 1; the mutant form is Krasnodarsky Karlik 1 (Lukyanenko, Zhogin, 1974; Rabinovich, 1986). At present, semi-dwarf cultivars (Kroshka, Pobeda 50, Fisht, Palpich, Vostorg, Doka, Tanya, Yesaul, Kalym, Pervitsa, and Grom), homozygous for *Rht-B1e* alleles, are cultivated both in Russia and the ex-USSR countries on an area of more than 4 million hectares (Divashuk et al., 2012, 2013).

The allele *Rht-B1p* is also promising for breeding: a stop codon emerges in its DELLA domain due to the substitution of cytosine for thymine at position 178 from the start codon. This mutation causes an up to 30 cm decrease in the height of bread wheat plants, especially as far as the lower internode is concerned, but it does not reduce the length of the ear (Bazhenov et al., 2015).

The sequencing of *Rht-B1* and *Rht-D1* alleles in various bread wheat cultivars have led to the development of molecular markers for their identification. For example, STS markers were obtained to identify the insertion-containing alleles *Rht-B1c*, *Rht-B1h* and *Rht-B1i-1* (Pearce et al., 2011; Li et al., 2013; Lou et al., 2016). Markers based on allele-specific PCR (AS-PCR), including real-time AS-PCR, are used to identify the alleles *Rht-B1b*, *Rht-B1e*, *Rht-B1p* and *Rht-D1b*, carrying single-nucleotide substitutions (Ellis et al., 2002; Pearce et al., 2011; Li et al., 2012; Bazhenov et al., 2015, 2019).

The widespread alleles *Rht-B1b* and *Rht-D1b* as well as those of the *Rht24* gene are identified on the basis of competitive allele-specific PCR (KASP-markers), offering a possibility to evaluate large numbers of bread wheat accessions at low time costs (Rasheed et al., 2016; Würschum et al., 2017). It should also be mentioned that AS-PCR results strongly depend on the reaction conditions, require several replications of the analysis, and call for strict observance of the author's protocol, which is not always possible. The KASP analysis, in its turn, requires sophisticated equipment and expensive reagents, which are often unaffordable to small practice-oriented laboratories.

The use of CAPS (cleaved amplified polymorphic sequence) markers can be an alternative to AS-PCR: they are based on the presence of a restriction site in the region with a single-nucleotide mutation (the site is absent in the wild type) or, contrariwise, on the disappearance of the site typical of the wild type in the mutant version (Shavrukov, 2015). If restriction sites are absent at the locations of the analyzed mutations, they can be produced purposefully through designing modified primers, i. e., by the derived CAPS method, or dCAPS (Neff et al., 1998, 2002).

Unlike AS-PCR, the CAPS and dCAPS marker techniques are effortlessly reproducible and do not require stringent PCR conditions, while the results of such analysis are easily interpreted in agarose gels. It is possible to generate markers

using the basic PCR equipment. Previously, such markers were developed for the *Rht24* dwarfing gene (Tian et al., 2017).

The objective of the present study was to develop CAPS and dCAPS markers for the analysis of single-nucleotide changes in *Rht-B1* and *Rht-D1*, test STS markers for identification of insertions in these genes and, as a result, propose a marker system for identifying the alleles most frequently used in bread wheat breeding.

Materials and methods

Plant material. Eleven bread wheat accessions from the VIR collection with known alleles of the *Rht-B1* and *Rht-D1* dwarfing genes (Table 1) served as the material for this study. The cultivars Chinese Spring and Hongdongmai with wild-type alleles *Rht-B1a* and *Rht-D1a* were used as controls. Each of the studied accessions was represented in the genotyping process by two or three individual plants as well as by bulk DNA sample, which was isolated from a total of 10–20 genotypes (seedlings).

DNA extraction. DNA was extracted from 10-day-old seedlings using a modified CTAB extraction technique (Antonova et al., 2020).

Sequences alignment. The sequences of different alleles of the *Rht-B1* and *Rht-D1* genes were aligned using MEGA X (<https://www.megasoftware.net/>), Unipro UGENE (Okonechnikov et al., 2012), and BioEdit Sequence Alignment Editor (Hall, 1999). Restriction sites were searched for using the GenScript Restriction Enzyme Map Analysis Tools (<https://www.genscript.com/tools/restriction-enzyme-map-analysis>).

Primers development. Primers for the nested PCR and CAPS analysis were developed with the Primer3Plus software (Untergasser et al., 2007). Primer quality (number of hairpins, homo- and heterodimers) was monitored using OligoAnalyzer Tool, a web resource from Integrated DNA Technologies, Inc. (<https://eu.idtdna.com/calc/analyzer>). Primers for dCAPS markers were generated using the dCAPS Finder 2.0 software (Neff et al., 2002). The primers developed in the course of this study and those supplied from published sources are presented in Tables 2 and 3, and their locations are shown in Fig. 1, a, b.

PCR procedure: a) **nested PCR.** The nested PCR method was applied to enhance the specificity of the dCAPS analysis: the first PCR was performed with primers BF/VIR.B1R flanking the region of point mutations in the *Rht-B1* gene; after that, the resulting PCR product was used as a template for the second PCR with dCAPS (B1bF/R, B1epF/B1eR) and CAPS (B1epF/B1pR) primers. The first round of nested PCR was carried out in 25 µl of the reaction mixture containing 40 ng of total wheat DNA; 1× reaction buffer; 1.5 mM of MgCl₂; 0.6 mM of each dNTP; 0.25 µM of both forward and reverse primer, and 1 unit of Taq DNA polymerase (Dialat, Russia, <http://dialat.ru/>). For higher specificity, the PCR program contained the Touchdown function: the initial annealing temperature was 4 degrees higher than the design temperature and decreased by 0.5 degrees per cycle for 8 cycles (see Table 3).

Samples of the resulting amplification products (2 µl of each) were transferred into clean tubes, diluted 50 times with water, and used as a template in the second stage of PCR. Another 10 µL of each PCR product was taken to control the

Table 1. Bread wheat accessions with the known alleles of the *Rht-B1* and *Rht-D1* dwarfing genes used in the study

Alleles of genes	VIR catalogue number "k-"	Accession	Origin	References
<i>Rht-B1a, Rht-D1a</i>	44435	Chinese Spring	China	Peng et al., 1999
	61292	Hongdongmai	»	Li et al., 2013
<i>Rht-B1b, Rht-D1a</i>	63045	Knyazhna	Russia, Krasnodar krai	Divashuk et al., 2013
	64312	Krasota	»	»
<i>Rht-B1c, Rht-D1a</i>	40699	Tom Thumb	Китай	Pearce et al., 2011
<i>Rht-B1e, Rht-D1a</i>	64583	Veda	Russia, Krasnodar krai	Divashuk et al., 2013
	65223	Grom	»	»
<i>Rht-B1h, Rht-D1a</i>	44977	Atlas 66	USA	Li et al., 2013
<i>Rht-B1h, Rht-D1b</i>	65711	Zheng 9023	China	»
<i>Rht-B1i-1, Rht-D1a</i>	10152	Triumph	USSR, Ukrainian SSR	»
<i>Rht-B1p, Rht-D1a</i>	54848	Chris Mutant	Russia, Krasnodar krai	Bazhenov et al., 2015

success of PCR by agarose gel electrophoresis (Fig. 2, a). The remainder (approximately 12 µl) was treated with the restriction enzyme *BstVII* (SibEnzyme, Russia, <http://russia.sibenzyme.com/>) to generate the CAPS marker for the *Rht-B1b* allele.

The second round of nested PCR was performed in 20 µl of the reaction mixture containing 4 µl of the template; 1× reaction buffer; 2.5 mM of MgCl₂; 0.3 mM of each dNTP; 0.25 µM of both forward and reverse primer, and 1 unit of Taq DNA polymerase (Dialat). The programs for each pair of primers are also presented in Table 3. Approximately 12 µl of the amplification mixture were taken for restriction analysis, and the remainder was used for PCR control by electrophoresis;

b) **standard PCR.** In the cases of CAPS markers for the *Rht-D1b* allele and the markers detecting retrotransposon in the gene's coding region and insertions in the 5' flanking region, PCR was performed under standard conditions. The reaction mixture (20 µl) contained 40 ng of DNA; 1× reaction buffer; 2.5 mM of MgCl₂; 0.3 mM of each dNTP; 0.25 µM of each primer, and 1 unit of Taq DNA polymerase (Dialat); the programs are presented in Tables 2 and 3;

c) **allele-specific PCR.** The conditions and the programs for AS-PCR corresponded to those recommended by the authors of the primers (Ellis et al., 2002; Bazhenov et al., 2015).

Restriction analysis. PCR products were treated with restriction enzymes produced by SibEnzyme, using the manufacturer's protocol (<http://russia.sibenzyme.com/>).

Fragment separation was done in horizontal agarose gels in the 1× TBE buffer under the voltage of 5 V/cm. The gels were stained with ethidium bromide and visualized in UV light.

Results and discussion

For the development of CAPS and dCAPS markers, the sequences from the NSBI databases were analyzed (<https://www.ncbi.nlm.nih.gov/>) for the following alleles of the dwarfing genes: *Rht-B1b*, *Rht-B1e*, *Rht-B1p* and *Rht-D1b*. Also,

the sequences of the wild-type alleles *Rht-A1a*, *Rht-B1a* and *Rht-D1a* were retrieved as controls. The Genbank accession numbers for used sequences are given in Supplementary material 1. Sequence alignment confirmed the presence of nonsense mutations in these allelic forms, which made it possible to start the development of CAPS and dCAPS markers (see Fig. 1).

A search was made for each nonsense mutation to identify restriction sites that would distinguish the target allele from all others, including wild-type ones. The *BstVII* (GCAGC) restriction enzyme, unable to digest the mutant GTAGC site, was selected for *Rht-B1b*. Similarly, *BstHHI* (GCGC) became the restriction enzyme for the *Rht-B1p* detection (mutant site GCGT). On the contrary, the *BstSFI* restriction enzyme (CTRYAG) exclusively digested the mutant site (CTGTAG) contained in *Rht-D1b*. Thus, it was possible to develop such CAPS markers as CB1b/*BstVII*, CB1p/*BstHHI* and CD1b/*BstSFI* to identify the alleles *Rht-B1b*, *Rht-B1p* and *Rht-D1b*, respectively.

We failed to identify restriction sites at the location of the nonsense mutation in the *Rht-B1e* allele. Hence, the dCAPS marker dCB1e/*HinfI* was developed for it: the sequence of the reverse primer was modified so that the analyzed nucleotide, together with the 3' end of the primer, formed a GATTC restriction site, providing an opportunity to distinguish this mutation from all other alleles by means of the *HinfI* restriction. The dCAPS marker dCB1b/*Acc36I* was additionally constructed to identify *Rht-B1b* (see Fig. 1).

When performing PCR under standard conditions, with the genomic DNA of bread wheat used as a template, we were unable to obtain specific fragments for the dCAPS markers and the CAPS marker CB1p/*BstHHI* (the data are not presented). We therefore applied the nested PCR method: the amplification products of the BF/VIR.B1R primers, flanking the region of localization of all analyzed point mutations in the *Rht-B1* gene, were used as a template for the second round (see Fig. 1).

The developed markers were tested on a set of bread wheat accessions with known alleles of the dwarfing genes, and all

Table 2. Primers used in this study to identify alleles of the *Rht-B1* gene

Primer	Sequence 5'→3'	Marker	Primer combination	Target area	Method of target allele identification	References
Nested-PCR						
BF	ggtagggaggcgagaggcgag	–	BF/VIR.B1R	–	338 bp – all alleles; <i>Rht-B1c</i> – no fragment	Ellis et al., 2002
VIR.B1R	tcgaccaggaggagaggtcg					This study
Program: 94 °C – 3 min 30 s; 8 cycles (94 °C – 45 s, 69 °C with a 0.5 °C drop in annealing temperature at each cycle – 150 s, 72 °C – 60 s); 30 cycles (94 °C – 45 s, 65 °C – 45 s, 72 °C – 45 s); 72 °C – 7 min						
Identification of <i>Rht-B1b</i>						
BF	ggtagggaggcgagaggcgag	–	BF/MR1	190 C→T	237 bp	Ellis et al., 2002
MR1	catcccatggccatctcgagcta					
WR1	catcccatggccatctcgagctg	–	BF/WR1	190 C→T	No fragment	
VIR.B1R	tcgaccaggaggagaggtcg	CB1b	BF/VIR.B1R	<i>Bst</i> V11 ¹ : GCAGC ²	No restriction site	This study
B1bF	caagatgatggtgtcggggtcgg	dCB1b	B1bF/R ³	<i>Acc</i> 361 ¹ : <i>ACCTGC</i> ²	No restriction site	
B1bR	ccatcccatggccatctccagct ⁴					
Program (for dCB1b/ <i>Acc</i> 361 marker): 94 °C – 3 min 30 s; 37 cycles (94 °C – 45 s, 68 °C – 45 s, 72 °C – 45 s); 72 °C – 7 min						
Identification of <i>Rht-B1e</i>						
MR3	ggccatctccagctgtccagcta	–	BF/MR3	181 A→T	228 bp	Pearce et al., 2011
WR3	ggccatctccagctgtccagctt		BF/WR3		No fragment	
B1epF	acaagatgatggtgtcggggtc	dCB1e	B1epF/B1eR ³	<i>Hinf</i> I – GANTC ²	No restriction site	This study
B1eR	ggccatctccagctgtccagat ⁴					
Program (for dCB1e/ <i>Hinf</i> I marker): 94 °C – 3 min 30 s; 37 cycles (94 °C – 45 s, 61 °C – 45 s, 72 °C – 45 s); 72 °C – 7 min						
Identification of <i>Rht-B1p</i>						
Rht-B1p-F	acatggcggagctggtgt	–	Rht-B1p-F/Rht-B1-R1	178 C→T	425 bp	Bazhenov et al., 2015
Rht-B1-R1	gccgagagaggacgat					
B1pR	catctccagctgtccagcttc	CB1p	B1epF/B1pR ³	<i>Bst</i> HHI ¹ : GCGC ²	No restriction site	This study
Program (for CB1p/ <i>Bst</i> HHI marker): 94 °C – 3 min 30 s; 30 cycles (94 °C – 45 s, 62 °C – 45 s, 72 °C – 45 s); 72 °C – 7 min						
Identification of <i>Rht-B1c</i>						
Rht-B1c-F1	ggcaactccaccggagcg	–	Rht-B1c-F1/Rht-B1c-R1	150 G ¹²⁰²⁶ bpC	256 bp	Pearce et al., 2011
Rht-B1c-R1	gctctcgaccaggaggag					
Program: 94 °C – 3 min 30 s; 8 cycles (94 °C – 45 s, 61 °C with a 0.5 °C drop in annealing temperature at each cycle – 1 min 30 s, 72 °C – 1 min); 30 cycles (94 °C – 45 s, 57 °C – 45 s, 72 °C – 45 s); 72 °C – 7 min						
Identification of <i>Rht-B1h</i>						
Rht-B1h.F	gaggcaaaatcacgcaagtact	–	Rht-B1h.F/Rht-B1h.1R	–592 T ¹⁹⁷ bpC	247 bp	Li et al., 2013
Rht-B1h.1R	taccaaggatattcattccgtagga					
Rht-B1h.2R	cttatggcaaaatggattccaaga	–	Rht-B1h.F/Rht-B1h.2R		331 (another alleles – 134 bp)	
Program: 94 °C – 3 min 30 s; 8 cycles (94 °C – 45 s, 63 °C with a 0.5 °C drop in annealing temperature at each cycle – 1 min 30 s, 72 °C – 1 min); 30 cycles (94 °C – 45 s, 59 °C – 45 s, 72 °C – 45 s); 72 °C – 7 min						
Identification of <i>Rht-B1i-1</i>						
B1i-MF1	cagacgatattaactggccgattga	–	B1i-MF1/B1i-MR1	–366 A ¹⁶⁰ bpT	330 bp	Lou et al., 2016
B1i-MR1	gggagcggcagcgtagtagttga					
Program: 94 °C – 3 min 30 s; 37 cycles (94 °C – 45 s, 56 °C – 45 s, 72 °C – 45 s); 72 °C – 7 min						
B1i-MF2	ctctaattgctgggatttc	–	B1i-MF2/B1i-MR2	–366 A ¹⁶⁰ bpT	586 bp (another alleles – 426 bp)	Lou et al., 2016
B1i-MR2	cgctcgtgactcgcttcat					
Program: 94 °C – 3 min 30 s; 8 cycles (94 °C – 45 s, 66 °C with a 0.5 °C drop in annealing temperature at each cycle – 1 min 30 s, 72 °C – 1 min); 30 cycles (94 °C – 60 s, 62 °C – 60 s, 72 °C – 45 s); 72 °C – 7 min						

¹ The listed restriction enzymes may be replaced with their isoschizomers: *Bst*V11 (*Bse*XI, *Bbv*I), *Acc*361 (*Bve*I, *Bsp*MI), *Bst*HHI (*Asp*LEI, *Cfo*I, *Hin*6I, *Hin*P11, *Hsp*AI).

² Boldfaced in the selective area are the nucleotides at restriction sites, variation of which enables the researcher to identify the required alleles.

³ The nested PCR products of the first round were used as a template for these combinations of primers (50 times dilution).

⁴ Boldfaced and underlined are the modified nucleotides in primers for dCAPS markers.

Table 3. Primers used in this study to identify alleles of the *Rht-D1* genes

Primer	Sequence 5'→3'	Marker	Primer combination	Target area	Method of target allele identification	References
Identification of <i>Rht-D1b</i>						
DF	cgcgcaattattggccagagatag	–	DF/MR2	181 G→T	254	Ellis et al., 2002
MR2	ccccatggccatctcgagctgcta					
DF2	ggcaagcaaaagcttcgcg	–	DF2/WR2		No fragment	
WR2	ggccatctcgagctgcac					
VIR.D1R	tgctctgaccaagacgacag	CD1b	DF/VIR.D1b	<i>BstSFI</i> ¹ : CTRYAG ²	Restriction site is present	This study

Program (for CD1b/*BstSFI* marker): 94 °C – 3 min 30 s; 8 cycles (94 °C – 45 s, 68 °C with a 0.5 °C drop in annealing temperature at each cycle – 1 min 30 s, 72 °C – 1 min); 30 cycles (94 °C – 45 s, 64 °C – 45 s, 72 °C – 45 s); 72 °C – 7 min

¹ Isoschizomers for the *BstSFI* restriction enzyme: *BfmI*, and *SfcI*.

² Boldfaced in the selective area are the nucleotides at restriction sites, variation of which enables the researcher to identify the required alleles.

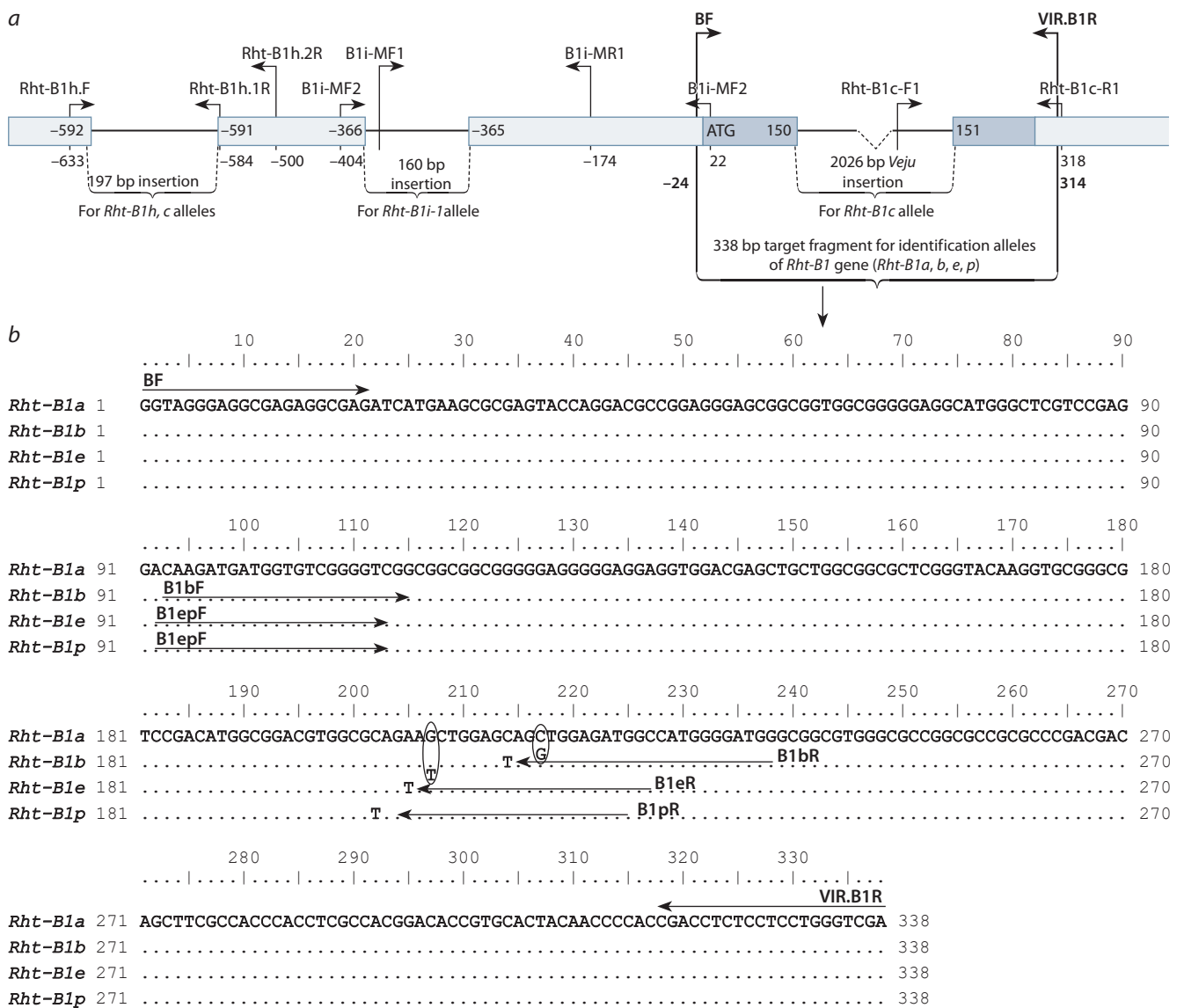


Fig. 1. Localization of primers for identifying the main alleles of the *Rht-B1* gene.

a – scheme of the gene and adjacent regions with the marked primer localizations for the first round of nested PCR and for identification of insertions in the *Rht-B1c*, *Rht-B1h* and *Rht-B1i-1* alleles; *b* – alignment results for the sequences flanked by the BF/VIR.B1R primers (first round of nested PCR), and primers for identification of point mutations in the *Rht-B1b*, *Rht-B1e* and *Rht-B1p* alleles using CAPS/dCAPS analysis.

Borders of the 197 bp insertion and *Veju* retrotransposon are taken from the publication by W. Wen et al. (2013); borders of the 160 bp insertion are taken from the publication by X. Lou et al. (2016). The gene's coding region is filled with dark color, and the *Veju* retrotransposon and insertions in the 5' flanking region are marked with thin lines. Ovals in Fig. 1, *b* indicate nucleotide changes in dCAPS primers.

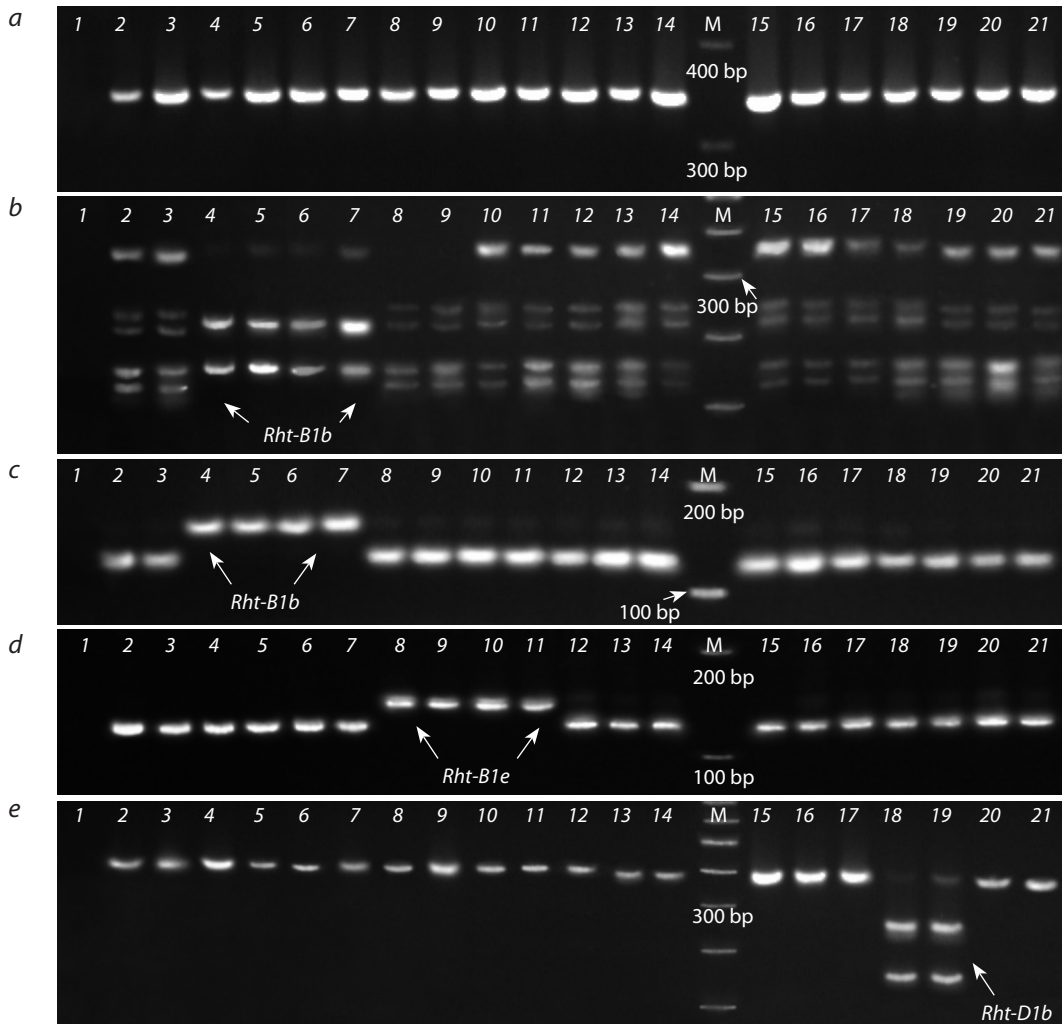


Fig. 2. Identification of nonsense mutations in the *Rht-B1* and *Rht-D1* genes using the developed CAPS and dCAPS markers. *a* – amplification products obtained with the BF/VIR.B1R primers, serving as a template for the second round of nested PCR; *b* – identification of the *Rht-B1b* allele: CAPS marker CB1b/BstV11; *c* – identification of the *Rht-B1b* allele: dCAPS marker dCB1b/Acc361; *d* – identification of the *Rht-B1e* allele: dCAPS marker dCB1e/Hinfl; *e* – identification of the *Rht-D1b* allele: CAPS marker CD1b/BstSFL.

Numbers designate accessions with different alleles of the *Rht-B1* and *Rht-D1* genes: 1 – negative control (H₂O); 2, 3 – Hongdongmai (wild-type); 4, 5 – Krasota (*Rht-B1b*, *Rht-D1a*); 6, 7 – Knyazhna (*Rht-B1b*, *Rht-D1a*); 8, 9 – Grom (*Rht-B1e*, *Rht-D1a*); 10, 11 – Veda (*Rht-B1e*, *Rht-D1a*); 12, 13 – Chris Mutant (*Rht-B1p*, *Rht-D1a*); 14, 15 – Triumph (*Rht-B1i-1*, *Rht-D1a*); 16, 17 – Chinese Spring (wild-type); 18, 19 – Zheng 9023 (*Rht-B1h*, *Rht-D1b*); 20, 21 – Atlas 66 (*Rht-B1h*, *Rht-D1a*). M – molecular marker 100 bp DNA Ladder (SibEnzyme).

of them demonstrated high efficiency in differentiating the wild-type *Rht-B1a*, *Rht-D1a* and mutant versions *Rht-B1b*, *Rht-B1e*, *Rht-B1p* and *Rht-D1b* (see Fig. 2 and 3).

Concurrently, allele-specific primers retrieved from published sources were used to identify nonsense mutations in *Rht-B1b*, *Rht-B1e*, *Rht-B1p* and *Rht-D1b* compared to the wild type (Ellis et al., 2002; Pearce et al., 2011; Bazhenov et al., 2015). For this purpose, two pairs of primers were used for identification of each mutation: one of them detected the mutant version, while the other spotted the wild type and all other alleles. It was shown for *Rht-B1b*, *Rht-B1e* and *Rht-D1b* that the results of allele-specific PCR on the whole agreed with the data of CAPS and dCAPS analyses. However, identification of the wild-type *Rht-B1a* and *Rht-D1a* alleles with the primers BF/WR and DF2/WR2, respectively (Ellis et al., 2002), involved certain difficulties: poor reproducibility

of results, and generation of weakly expressed fragments in forms with *Rht-B1b* and/or *Rht-D1b* (Supplementary material 2). In the case of *Rht-B1p*, allele-specific PCR under the conditions of this study turned out to be ineffective: after amplification with the *Rht-B1p*-F/R1 primers (Bazhenov et al., 2015), a specific product was generated both in the forms with mutant alleles and in those with the wild-type ones (see Supplementary material 2).

The study also employed five pairs of STS primers (Pearce et al., 2011; Li et al., 2013; Lou et al., 2016) as a tool for identifying mutations associated with the presence of a retrotransposon in the coding region (*Rht-B1c*) as well as with insertions in the promoter region (*Rht-B1i-1*) and the 5' flanking region (*Rht-B1h*). The locations of these insertions are marked in the scheme of the *Rht-B1* gene; it also shows primers for their detection (see Fig. 1, a).

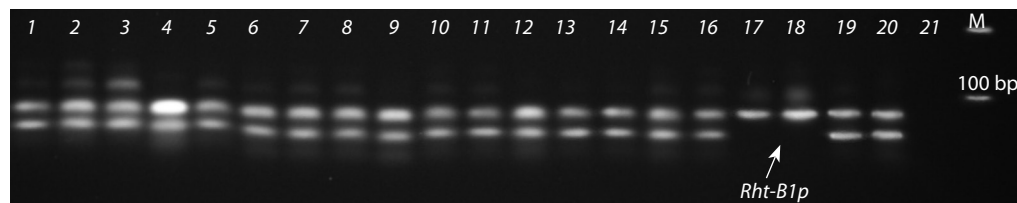


Fig. 3. Identification of the *Rht-B1p* allele with the CAPS marker CB1p/BstHHI.

The arrow points at genotypes with *Rht-B1p*, the PCR products of which were not restricted. Numbers designate accessions with different alleles of the *Rht-B1* and *Rht-D1* genes: 1, 2 – Hongdongmai (wild-type); 3, 4 – Krasota (*Rht-B1b*, *Rht-D1a*); 5, 6 – Knyazhna (*Rht-B1b*, *Rht-D1a*); 7, 8 – Grom (*Rht-B1e*, *Rht-D1a*); 9, 10 – Veda (*Rht-B1e*, *Rht-D1a*); 11, 12 – Triumph (*Rht-B1i-1*, *Rht-D1a*); 13, 14 – Chinese Spring (wild-type); 15, 16 – Zheng 9023 (*Rht-B1h*, *Rht-D1b*); 17, 18 – Chris Mutant (*Rht-B1p*, *Rht-D1a*); 19, 20 – Atlas 66 (*Rht-B1h*, *Rht-D1a*); 21 – negative control (H₂O). M – molecular marker 100 bp DNA Ladder (SibEnzyme).

Table 4. Marker profiles for identifying alleles of the *Rht-B1* and *Rht-D1* dwarfing genes using the system proposed in the present study

Allele (old gene name)	Target mutation	CAPS/dCAPS-markers for detection of nonsense mutations (0 – no restriction site, 1 – restriction site is present)					STS-primers combination for detection of insertion (size of amplification products is given in bp)				
		CB1b /BstV11	dCB1b /Acc361 ¹	dCB1e /HinfI ¹	CB1p /BstHHI ¹	CD1b /BstSFI	B1i-MF1 /MR1	B1i-MF2 /MR2	Rht-B1c-F1 /R1	Rht-B1h.F /1R	Rht-B1h.F /2R
<i>Rht-B1a</i>	Wild type	1	1	1	1	–	No PCR	426	No PCR	No PCR	134
<i>Rht-B1b</i> (<i>Rht1</i>)	190 C→T	0 ²	0 ²	1	1	–	No PCR	426	No PCR	No PCR	134
<i>Rht-B1e</i> (<i>Rht11</i>)	181 A→T	1	1	0 ²	1	–	No PCR	426	No PCR	No PCR	134
<i>Rht-B1p</i> (<i>Rht17</i>)	178 C→T	1	1	1	0 ²	–	No PCR	426	No PCR	No PCR	134
<i>Rht-B1c</i> (<i>Rht3</i>)	Insertion 150 G ^{↓2026} bpC	No PCR	No PCR	No PCR	No PCR	–	No PCR	426	256 ²	247 ²	331 ²
<i>Rht-B1h</i>	Insertion –592 T ^{↓197} bpC	1	1	1	1	–	No PCR	426	No PCR	247 ²	331 ²
<i>Rht-B1i-1</i>	Insertion –366 A ^{↓160} bpC	1	1	1	1	–	330 ²	586 ²	No PCR	No PCR	134
<i>Rht-D1a</i>	Wild type	–	–	–	–	0	–	–	–	–	–
<i>Rht-D1b</i> (<i>Rht2</i>)	181 G→T	–	–	–	–	1 ²	–	–	–	–	–

¹ The products of the first round of nested PCR (50 times dilution) were used as a template for these markers.

² Boldfaced and underlined are the amplification products, the presence/absence of which makes it possible to pinpoint the target alleles of the *Rht-B1* and *Rht-D1* genes.

Two pairs of primers were used for the *Rht-B1i-1* allele (Lou et al., 2016): one of them (B1i-MF1/MR1) in the presence of an insertion produced a specific 330 bp fragment, while the other (B1i-MF2/MR2) amplified fragments of different sizes in genotypes with or without an insertion (see Tables 2 and 4, Fig. 4, c). Similarly, to detect the *Rht-B1h* allele, the Rht-B1h.F/R1 primers were used, resulting in a specific product of 247 bp, as well as the Rht-B1h.F/R2 primers, generating fragments of different sizes (see Tables 2 and 4; Fig. 4, b) (Li et al., 2013). Since *Rht-B1h* has a common insertion in the 5' flanking region with *Rht-B1c*, the Rht-B1c-F1/R1 primer, specific for the retrotransposon sequence, was also used for

their differentiation (see Tables 2 and 4, Fig. 4, a) (Pearce et al., 2011). Additional evidence of the presence of a retrotransposon may be found in the fact that no PCR products are generated in genotypes with this insertion during the first round of nested PCR with the BF/VIR.B1R primers: it can be explained by a big distance between the primers (see Fig. 4, d).

Our testing of STS markers showed a complete concordance between the presence of their diagnostic fragments and the composition of alleles present in the studied genotypes (see Fig. 4). The accessions Atlas 66 and Zheng 9023 containing *Rht-B1h* yielded amplification products pointing to the presence of an insertion in the 5' flanking region. In the acces-

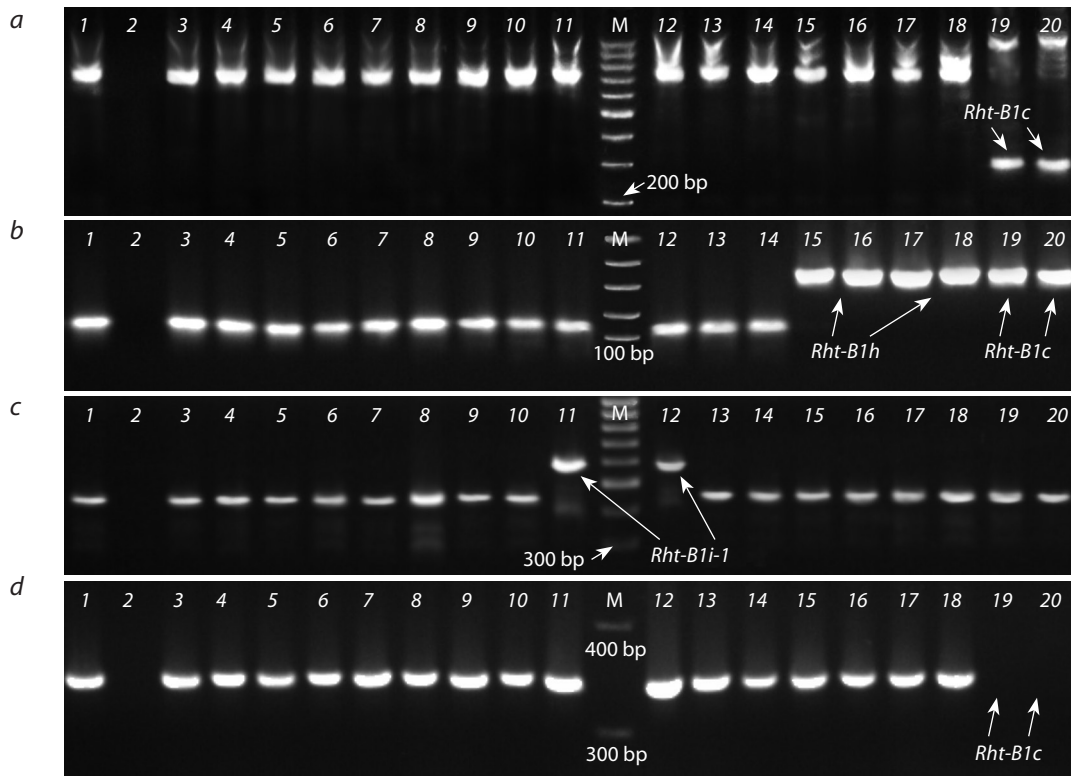


Fig. 4. Identification of insertion-carrying alleles for the *Rht-B1* gene using STS primers.

a – PCR products of the *Rht-B1c*-F1/R1 primers specific to *Rht-B1c*; *b* – PCR products of the *Rht-B1h*-MF1/MR2 primers specific to *Rht-B1h* and *Rht-B1c*; *c* – PCR products of the B1i-MF2/MR2 primers specific to *Rht-B1i-1*; *d* – absence of PCR products of the BF/VIR.B1R primers in genotypes with the *Rht-B1c* allele carrying a 2026 bp insertion.

Numbers designate accessions with different alleles of the *Rht-B1* and *Rht-D1* genes: 1 – Krasota (*Rht-B1b*, *Rht-D1a*); 2 – negative control (H₂O); 3, 4 – Knyazhna (*Rht-B1b*, *Rht-D1a*); 5, 6 – Grom (*Rht-B1e*, *Rht-D1a*); 7, 8 – Veda (*Rht-B1e*, *Rht-D1a*); 9, 10 – Chris Mutant (*Rht-B1p*, *Rht-D1a*); 11, 12 – Triumph (*Rht-B1i-1*, *Rht-D1a*); 13, 14 – Chinese Spring (wild-type); 15, 16 – Zheng 9023 (*Rht-B1h*, *Rht-D1b*); 17, 18 – Atlas 66 (*Rht-B1h*, *Rht-D1a*); 19, 20 – Tom Thumb (*Rht-B1c*, *Rht-D1a*). M – molecular marker 100 bp DNA Ladder (SibEnzyme).

sion Triumph carrying the *Rht-B1i-1* allele, which increases plant height, an insertion in the promoter region was detected using molecular markers, and in Tom Thumb (*Rht-B1c*), a retrotransposon in the coding sequence and an insertion in the 5' flanking region were found. It should be mentioned that when a retrotransposon was identified using the *Rht-B1c*-F1/R1 primers, in addition to the formation of a fragment of the expected size, the emergence of nonspecific products of a larger size was observed in Tom Thumb (*Rht-B1c*) and in all other genotypes (see Fig. 4, *a*).

Assessing the system of the proposed molecular markers in its entirety, it should be kept in mind that it can be used to generate a marker profile for each of the studied alleles of the *Rht-B1* and *Rht-D1* genes, i. e., to get an unambiguous answer whether one of the abovementioned alleles of the *Rht-B1* and *Rht-D1* dwarfing genes is present in one or another genotype. Marker profiles for the alleles are presented in Table 4.

Conclusion

As a result of this study, a system of molecular markers was proposed for the *Rht-B1* and *Rht-D1* dwarfing genes to identify the alleles most often used in bread wheat breeding. The system is based on the developed CAPS and dCAPS markers of nonsense mutations in these genes, which were previously detected by allele-specific PCR (Ellis et al., 2002; Pearce et

al., 2011; Bazhenov et al., 2015, 2019). Five STS markers retrieved from published sources were used to identify insertions (Pearce et al., 2011; Li et al., 2013; Lou et al., 2016).

The CAPS and dCAPS markers were tested during the genotyping of bread wheat accessions from the VIR collection, containing the mutant *Rht-B1b*, *Rht-B1c*, *Rht-B1e*, *Rht-B1h*, *Rht-B1i-1*, *Rht-B1p* and *Rht-D1b* alleles as well as those of the wild-type. The tests showed complete concordance of the obtained results with the expected ones. The presence of *Rht-B1b*, *Rht-B1e*, *Rht-B1p* and *Rht-D1b* was also confirmed by allele-specific PCR with the primers widely used in research and breeding programs (Kurkiev et al., 2008; Pestsova et al., 2008; Divashuk et al., 2013; Li et al., 2013; Lou et al., 2016).

The main advantage of our molecular marker system lies in good reproducibility of results and their unambiguous interpretation. The CASP/dCAPS analysis faces no problems with controlling the PCR reaction success, because amplification products are formed in all genotypes, and differences between alleles are pinpointed after treatment with restriction enzymes. Besides, notwithstanding the high cost of restriction enzymes, CASP/dCAPS analysis is less expensive, since there is no need to perform two independent PCRs in several replications to detect each allele. The procedure is conducted employing standard PCR equipment and using agarose gel

electrophoresis, so it can be carried out by small practice-oriented laboratories. When any new point mutations in the *Rht-B1* and *Rht-D1* dwarfing genes become known, a similar approach to the development of CAPS/dCAPS markers can be applied to identify them.

References

- Antonova O.Yu., Klimentko N.S., Rybakov D.A., Fomina N.A., Zheltova V.V., Novikova L.Yu., Gavrilenko T.A. SSR analysis of modern russian potato varieties using DNA samples of nomenclatural standards. *Biotechnologiya i Seleksiya Rasteniy = Plant Biotechnology and Breeding*. 2020;3(4):77-96. DOI 10.30901/2658-6266-2020-4-o2. (in Russian)
- Bazhenov M.S., Divashuk M.G., Amagai Y., Watanabe N., Karlov G.I. Isolation of the dwarfing *Rht-B1p* (*Rht17*) gene from wheat and the development of an allele-specific PCR marker. *Mol. Breed.* 2015; 35(11):1-8. DOI 10.1007/s11032-015-0407-1.
- Bazhenov M.S., Nazarova L.A., Chernook A.G., Divashuk M.G. Improved marker for the *Rht-B1p* dwarfing allele in wheat. In: Current Challenges in Plant Genetics, Genomics, Bioinformatics, and Biotechnology: Proc. of the Fifth International Scientific Conference PlantGen2019 June 24–29, 2019. Novosibirsk, Russia. Novosibirsk: ICG SB RAS. 2019;190-192. DOI 10.18699/ICG-PlantGen2019-61.
- Borojevic K., Borojevic Ks. The transfer and history of “reduced height genes” (*Rht*) in wheat from Japan to Europe. *J. Hered.* 2005;96(4): 455-459. DOI 10.1093/jhered/esi060.
- Börner A., Plaschke J., Korzun V., Worland A.J. The relationships between the dwarfing genes of wheat and rye. *Euphytica*. 1996;89(1): 69-75. DOI 10.1007/BF00015721.
- Divashuk M.G., Bespalova L.A., Vasilyev A.V., Fesenko I.A., Puzyrnaya O.Y., Karlov G.I. Reduced height genes and their importance in winter wheat cultivars grown in southern Russia. *Euphytica*. 2013; 190(1):137-144. DOI 10.1007/s10681-012-0789-7.
- Divashuk M.G., Vasilyev A.V., Bespalova L.A., Karlov G.I. Identity of the *Rht-11* and *Rht-B1e* reduced plant height genes. *Russ. J. Genet.* 2012;48(7):761-763. DOI 10.1134/S1022795412050055.
- Ellis M.H., Rebetzke G.J., Chandler P., Bonnett D., Spielmeier W., Richards R.A. The effect of different height reducing genes on the early growth of wheat. *Funct. Plant Biol.* 2004;31(6):583-589. DOI 10.1071/FP03207.
- Ellis M.H., Spielmeier W., Gale K., Rebetzke G., Richards R. “Perfect” markers for the *Rht-B1b* and *Rht-D1b* dwarfing genes in wheat. *Theor. Appl. Genet.* 2002;105(6-7):1038-1042. DOI 10.1007/s00122-002-1048-4.
- Evans L.T. Feeding the Ten Billion: Plants and Population Growth. Cambridge: Cambridge University Press, 1998.
- Flintham J.E., Gale M.D. The Tom Thumb dwarfing gene *Rht3* in wheat. *Theor. Appl. Genet.* 1983;66(3-4):249-256. DOI 10.1007/BF00251155.
- Gale M.D., Marshall G.A. The chromosomal location of *Gai 1* and *Rht 1*, genes for gibberellin insensitivity and semi-dwarfism, in a derivative of Norin 10 wheat. *Heredity*. 1976;37(2):283-289. DOI 10.1038/hdy.1976.88.
- Gale M.D., Youssefian S., Russell G.E. Dwarfing genes in wheat. In: Russel G.E. (Ed.). Progress in Plant Breeding. London: Butterworths-Heinemann, 1985;1-35.
- Grover G., Sharma A., Gill H.S., Srivastava P., Bains N.S. *Rht8* gene as an alternate dwarfing gene in elite Indian spring wheat cultivars. *PLoS One*. 2018;13(6):e0199330. DOI 10.1371/journal.pone.0199330.
- Guedira M., Brown-Guedira G., Van Sanford D., Sneller C., Souza E., Marshall D. Distribution of *Rht* genes in modern and historic winter wheat cultivars from the Eastern and Central USA. *Crop Sci.* 2010; 50(5):1811-1822. DOI 10.2135/cropsci2009.10.0626.
- Hall T. BioEdit: a user-friendly biological sequence alignment editor and analysis program for Windows 95/98/NT. *Nucleic Acids Symp. Ser.* 1999;41:95-98.
- Hedden P. The genes of the green revolution. *Trends Genet.* 2003; 19(1):5-9. DOI 10.1016/S0168-9525(02)00009-4.
- Korzun V., Röder M.S., Ganai M.W., Worland A.J., Law C.N. Genetic analysis of the dwarfing gene (*Rht8*) in wheat. Part I. Molecular mapping of *Rht8* on the short arm of chromosome 2D of bread wheat (*Triticum aestivum* L.). *Theor. Appl. Genet.* 1998;96(8):1104-1109. DOI 10.1007/s001220050845.
- Kurkiv K.U., Tyryshkin L.G., Kolesova M.A., Kurkiv U.K. Identification of *Rht2* and *Rht8* genes for semidwarfness in hexaploid triticale with use of DNA markers. *Vavilovskii Zhurnal Genetiki i Seleksii = Vavilov Journal of Genetics and Breeding*. 2008; 12(3):372-377. (in Russian)
- Li A., Yang W., Guo X., Liu D., Sun J., Zhang A. Isolation of a gibberellin-insensitive dwarfing gene, *Rht-B1e*, and development of an allele-specific PCR marker. *Mol. Breed.* 2012;30(3):1443-1451. DOI 10.1007/s11032-012-9730-y.
- Li A., Yang W., Lou X., Liu D., Sun J., Guo X., Wang J., Li Y., Zhan K., Ling H.Q., Zhang A. Novel natural allelic variations at the *Rht-1* loci in wheat. *J. Integr. Plant Biol.* 2013;55(11):1026-1037. DOI 10.1111/jipb.12103.
- Lou X., Li X., Li A., Pu M., Shoaib M., Liu D., Sun J., Zhang A., Yang W. The 160 bp insertion in the promoter of *Rht-B1i* plays a vital role in increasing wheat height. *Front. Plant Sci.* 2016;7(307): 1-13. DOI 10.3389/fpls.2016.00307.
- Lukyanenko P.P., Zhogin A.F. Use of induced dwarf mutants in winter wheat breeding. *Seleksiya i Semenovodstvo = Breeding and Seed Industry*. 1974;1:13-17. (in Russian)
- McIntosh R.A., Dubcovsky J., Rogers W.J., Morris C., Appels R., Xia X.C. Catalogue of gene symbols for wheat: 2015–2016 supplement. 2016. Available at: <https://shigen.nig.ac.jp/wheat/komugi/genes/macgene/supplement2015.pdf>.
- McIntosh R.A., Dubcovsky J., Rogers W.J., Xia X.C., Raupp W.J. Catalogue of gene symbols for wheat: 2018 supplement. 2018. Available at: [https://wheat.pw.usda.gov/GG3/sites/default/files/Catalogue %20of %20Gene %20Symbols %20for %20Wheat %20- %20supplement2018-2019.pdf](https://wheat.pw.usda.gov/GG3/sites/default/files/Catalogue%20of%20Gene%20Symbols%20for%20Wheat%20-%20supplement2018-2019.pdf).
- McIntosh R.A., Yamazaki Y., Dubcovsky J., Rogers J., Morris C., Appels R., Xia X.C. Catalogue of gene symbols for wheat. 2013. Available at: <https://shigen.nig.ac.jp/wheat/komugi/genes/download.jsp>.
- Neff M.M., Neff J.D., Chory J., Pepper A.E. dCAPS, a simple technique for the genetic analysis of single nucleotide polymorphisms: experimental applications in *Arabidopsis thaliana* genetics. *Plant J.* 1998;14(3):387-392. DOI 10.1046/j.1365-313X.1998.00124.x.
- Neff M.M., Turk E., Kalishman M. Web-based primer design for single nucleotide polymorphism analysis. *Trends Genet.* 2002;18(12):613-615. DOI 10.1016/s0168-9525(02)02820-2.
- Okonechnikov K., Golosova O., Fursov M. Unipro UGENE: a unified bioinformatics toolkit. *Bioinformatics*. 2012;28(8):1166-1167. DOI 10.1093/bioinformatics/bts091.
- Pearce S., Saville R., Vaughan S.P., Chandler P.M., Wilhelm E.P., Sparks C.A., Al-Kaff N., Korolev A., Boulton M.I., Phillips A.L., Hedden P., Nicholson P., Thomas S.G. Molecular characterization of *Rht-1* dwarfing genes in hexaploid wheat. *Plant Physiol.* 2011; 157(4):1820-1831. DOI 10.1104/pp.111.183657.
- Peng J., Richards D.E., Hartley N.M., Murphy G.P., Devos K.M., Flintham J.E., Beales J., Fish L.J., Worland A.J., Pelica F., Sadhakar D., Christou P., Snape J.W., Gale M.D., Harberd N.P. ‘Green revolution’ genes encode mutant gibberellin response modulators. *Nature*. 1999;400(6741):256-261. DOI 10.1038/22307.
- Pestsova E., Korzun V., Börner A. Validation and utilisation of *Rht* dwarfing gene specific. *Cereal Res. Commun.* 2008;36(2):235-246. DOI 10.1556/CRC.36.2008.2.4.
- Rabinovich S.V. The breeding value of the Krasnodarskiy karlik 1 mutant. In: Chemical Mutagenesis in the Creation of Varieties with New Properties. Moscow: Nauka Publ., 1986;88-92. (in Russian)
- Rasheed A., Wen W., Gao F., Zhai S., Jin H., Liu J., Guo Q., Zhang Y., Dreisigacker S., Xia X., He Z. Development and validation of

- KASP assays for genes underpinning key economic traits in bread wheat. *Theor. Appl. Genet.* 2016;129(10):1843-1860. DOI 10.1007/s00122-016-2743-x.
- Shavrukov Y.N. CAPS markers in plant biology. *Russ. J. Genet. Appl. Res.* 2016;6(3):279-287. DOI 10.1134/S2079059716030114.
- Sukhikh I.S., Vavilova V.Y., Blinov A.G., Goncharov N.P. Diversity and phenotypical effect of the allele variants of dwarfing *Rht* genes in wheat. *Russ. J. Genet.* 2021;57(2):127-138. DOI 10.1134/S1022795421020101.
- Thomas S.G. Novel *Rht-1* dwarfing genes: tools for wheat breeding and dissecting the function of DELLA proteins. *J. Exp. Bot.* 2017;68(3):354-358. DOI 10.1093/jxb/erw509.
- Tian X., Wen W., Xie L., Fu L., Xu D., Fu C., Wang D., Chen X., Xia X., Chen Q., He Z., Cao S. Molecular mapping of reduced plant height gene *Rht24* in bread wheat. *Front. Plant Sci.* 2017;8:1-9. DOI 10.3389/fpls.2017.01379.
- Untergasser A., Nijveen H., Rao X., Bisseling T., Geurts R., Leunissen J.A. Primer3Plus, an enhanced web interface to Primer3. *Nucleic Acids Res.* 2007;35(2):71-74. DOI 10.1093/nar/gkm306.
- Wen W., Deng Q., Jia H., Wei L., Wei J., Wan H., Yang L., Cao W., Ma Z. Sequence variations of the partially dominant DELLA gene *Rht-B1c* in wheat and their functional impacts. *J. Exp. Bot.* 2013;64(11):3299-3312. DOI 10.1093/jxb/ert183.
- Wilhelm E.P., Mackay I.J., Saville R.J., Korolev A.V., Balfourier F., Greenland A.J., Boulton M.I., Powell W. Haplotype dictionary for the *Rht-1* loci in wheat. *Theor. Appl. Genet.* 2013;126(7):1733-1747. DOI 10.1007/s00122-013-2088-7.
- Wu J., Kong X., Wan J., Liu X., Zhang X., Guo X., Zhou R., Zhao G., Jing R., Fu X., Jia J. Dominant and pleiotropic effects of a *GAI* gene in wheat results from a lack of interaction between DELLA and GID1. *Plant Physiol.* 2011;157(4):2120-2130. DOI 10.1104/pp.111.185272.
- Würschum T., Langer S.M., Longin C.F.H., Tucker M.R., Leiser W.L. A modern Green Revolution gene for reduced height in wheat. *Plant J.* 2017;92(5):892-903. DOI 10.1111/tpj.13726.
- Youssefian S., Kirby E.J.M., Gale M.D. Pleiotropic effects of the GA-insensitive *Rht* dwarfing genes in wheat. 2. Effects on leaf, stem, ear and floret growth. *Field Crops Res.* 1992;28(3):191-210. DOI 10.1016/0378-4290(92)90040-G.
- Zhang X., Yang S., Zhou Y., He Z., Xia X. Distribution of the *Rht-B1b*, *Rht-D1b* and *Rht8* reduced height genes in autumn-sown Chinese wheats detected by molecular markers. *Euphytica.* 2006;152(1):109-116. DOI 10.1007/s10681-006-9184-6.

ORCID ID

I.V. Porotnikov orcid.org/0000-0001-5841-8803
O.P. Mitrofanova orcid.org/0000-0002-9171-2964
O.Yu. Antonova orcid.org/0000-0001-8334-8069

Acknowledgements. The study was implemented within the framework of the state mission delegated to VIR under Projects No. 0481-2019-0002 and No. 0662-2019-0006.

Conflict of interest. The authors declare no conflict of interest.

Received October 1, 2021. Revised October 31, 2021. Accepted November 3, 2021.

Androgenic response of *Triticum durum*-*Dasypyrum villosum* amphidiploids and their parental forms

H. Stoyanov , I. Belchev

Dobrudzha Agricultural Institute, General Toshevo, Bulgaria
 hpstoyanov@abv.bg

Abstract. Wide hybridization in cereal crops is one of the most efficient tools for the enrichment of genetic variability and addressing a number of breeding problems related to resistance and tolerance to biotic and abiotic stresses. Therefore, a large number of amphidiploids between species possessing different morphological, genetic and physiological properties have been developed. One of the most valuable species with regard to the possibilities for introducing valuable traits and properties into wheat species is the wild *Dasypyrum villosum*. With the aim to study the androgenic response of the *Triticum durum*-*D. villosum* amphidiploids, two accessions and their parental forms – the durum wheat cultivars Gergana and Argonavt and a landrace of the *D. villosum* – were studied. The following parameters were determined: callus induction, plant regeneration, yield of albino and green regenerants. It was found that the callus induction of the two studied amphidiploids differed significantly from that of the parental forms (2.1–7.2 %), being significantly higher, 30.7 and 16.5 %, respectively. Regardless of the difference in callus induction, the amphidiploids did not significantly differ from the parental forms in their regeneration ability. The yield of albino plants exceeded the yield of green regenerants and followed the tendency observed in callus induction. Green plants were found only in the amphidiploid Gergana-*D. villosum* and in the parental form durum wheat Gergana. Plants were regenerated from the species *D. villosum*, although they were only albinos, showing its good responsiveness to anther culture. The established characteristics of the amphidiploids and their parental forms make their practical use highly valuable for the improvement of different types of cereal crops.

Key words: anther culture; androgenic response; amphidiploid; *Dasypyrum villosum*; parental forms.

For citation: Stoyanov H., Belchev I. Androgenic response of *Triticum durum*-*Dasypyrum villosum* amphidiploids and their parental forms. *Vavilovskii Zhurnal Genetiki i Seleksii* = *Vavilov Journal of Genetics and Breeding*. 2022;26(2): 139-145. DOI 10.18699/VJGB-22-17

Андрогенетическая реакция амфидиплоидов *Triticum durum*-*Dasypyrum villosum* и их родительских форм

Х. Стоянов , И. Белчев

Добруджанский сельскохозяйственный институт, г. Генерал Тошево, Болгария
 hpstoyanov@abv.bg

Аннотация. Отдаленная гибридизация злаков является одним из самых эффективных способов обогащения генетического разнообразия и решения множества селекционных задач в отношении устойчивости и толерантности к биотическому и абиотическому стрессу. Поэтому создано большое количество амфидиплоидов между отдельными видами, которые наделены разными морфологическими, генетическими и физиологическими характеристиками. Дикий вид *Dasypyrum villosum* – один из самых ценных видов с точки зрения возможности интродуцирования ценных качеств и свойств в разные сорта пшеницы. Для изучения реакции амфидиплоидов *Triticum durum*-*D. villosum* исследованы два образца, их родительские формы – сорта твердой пшеницы Гергана и Аргонавт, а также местная популяция вида *D. villosum*. Установлены следующие параметры: индукция каллусов, частота всех проростков к 100 эмбриоподобным структурам, частота альбиносных проростков и частота зеленых проростков. По полученным результатам выявлено, что индукция каллусов двух амфидиплоидов статистически достоверно отличается от родительских форм (2.1–7.2 %), будучи значительно выше, 30.7 и 16.5 % соответственно. Несмотря на разницу в индукции каллусов, амфидиплоиды практически не отличаются от родительских форм своей регенерирующей способностью. Частота альбиносных проростков значительно превышает частоту зеленых проростков, следуя тенденции, наблюдаемой в индукции каллусов. Зеленые проростки зарегистрированы только у амфидиплоида Гергана-*D. villosum* и у родительской формы твердой пшеницы Гергана. Растения вида *D. villosum* были регенерированы, и то, что были только альбиносные проростки, показывает хорошую отзывчивость вида на культивирование пыльников. Установленные характеристики испытанных амфидиплоидов и их родительских форм делают практическое использование этих амфидиплоидов особенно ценным для селекции различных видов злаков.

Ключевые слова: пыльниковая культура; андрогенетическая реакция; амфидиплоид; *Dasypyrum villosum*; родительские формы.

Introduction

The development of highly productive varieties of cultivated plants, which at the same time are characterized with stable yields and are resistant to different biotic and abiotic stress factors, is a primary task in plant breeding (Chahal, Gosal, 2000). However, the increase of yield within the genome of a given species is not limitless (Grassini et al., 2013). In this respect, there are different approaches to enrich the genome of the cultivated plants – wide hybridization, genetic engineering, genome editing technologies, etc. (Chahal, Gosal, 2000; Liu et al., 2014; Okada et al., 2019; Li, 2020; Wang et al., 2020).

Although contemporary science has reached high levels of use of the latter two technologies, wide hybridization remains a main conventional tool for achieving high genetic variability. There is a large amount of research on amphidiploids developed through wide hybridization among the cereal crops (Zhang et al., 2010; Ming et al., 2011; Babaiants et al., 2012; Stoyanov, 2013, 2014; Dai et al., 2015; Nemeth et al., 2015; Song et al., 2019; Klimushina et al., 2020; Zuo et al., 2020; Kiani et al., 2021). One of the most promising species for enrichment of the genome of common and durum wheat, however, is *Dasyphyrum villosum*. This species has been described in detail with regard to the possibility of being used in the improvement work on the wheat species in the researches of A. Grądzielewska (2006a) and C. De Pace et al. (2011). In another research, A. Grądzielewska (2006b) described in detail a large number of studies on the production of hybrids, natural hybrids, substitution and addition lines with wheat and other species. There are a number of studies on the possibility of using the hybrids and amphidiploids of the wheat species with *D. villosum* in practical breeding (De Pace et al., 2001; Vaccino et al., 2010; De Pace et al., 2011; Zhang et al., 2015, 2016a, b, 2018; Ando et al., 2019). A. Stefani et al. (1987) reported rather detailed morphological characteristics of the amphidiploid *Triticum durum*-*D. villosum*.

Since plant breeding is a rather dynamic process, when developing lines from the cereal species, the biotechnological method of anther culture is often used to accelerate the breeding process (Belchev, 2003; Lantos, 2009). Different researchers report that the efficiency of the process and the production of a high number of green plants is related to the response to anther culture of the parental forms involved in the cross (Zamani et al., 2003; Dagüstü, 2008; Yildirim et al., 2008; El-Hennawy et al., 2011). In this respect, the developed amphidiploids, substitution and addition lines with *D. villosum*, are specific parental forms, the reaction to anther culture of which has not been studied up to now. The possibility to apply anther culture to amphidiploids in principle has been little investigated. The response to anther culture in the amphidiploids has been studied in the amphidiploid *Aegilops variabilis*-*Secale cereale* (Ponitka et al., 2002), and the authors determined 0.1–13.4 % of regenerants obtained from 100 androgenic embryoids. D. Plamenov et al. (2009) determined 1.9–3.2 % of green regenerants from 100 cultured anthers in the amphidiploid *T. durum*-*T. monococcum* ssp. *aegilopoides*. In tritordeum (Barcelo et al., 1994), it was also found out that anther culture is an efficient process. The results from these researches showed that different amphidiploids are able to give positive response to anther culture.

The aim of this study was to determine the reaction of the amphidiploid *T. durum*-*D. villosum* to anther cultivation in comparison to its parental forms.

Materials and methods

Plant material. Two accessions of the amphidiploid *T. durum*-*D. villosum* (1dv (Gergana-*D. villosum*) and 2dv (Argonavt-*D. villosum*)), a part of the collection of Dobrudzha Agricultural Institute were used, as well the durum wheat parental forms (*T. durum* cv. Gergana and cv. Argonavt) and the wild species *D. villosum*.

The accession of *D. villosum* ($2n = 2x = 14$ (VV); family Poaceae, tribe Triticeae, subtribe Triticineae, genus *Dasyphyrum*) was collected in Dobrich region in 2011.

Crosses Gergana \times *D. villosum* and Argonavt \times *D. villosum* were made conventionally, without embryo rescue in 2012; the obtained seeds (Gergana \times *D. villosum* – 3 seeds and Argonavt \times *D. villosum* – 8 seeds) were germinated and at tillering stage the plants (Gergana \times *D. villosum* – 1 plant and Argonavt \times *D. villosum* – 3 plants) were treated with colchicine in 2013. The seeds from the two obtained primary amphidiploids were multiplied several times.

Anther culture. The experiment was carried out during 2016/2017. Anther donor plants were grown under greenhouse conditions. The seeds from the accessions were germinated in Petri dishes and then planted in plastic pots. Fifteen plants from each accession were grown in three pots, using 10 plants per genotype. Primary, seedling were vernalized at 4 °C (3000 lx, 16 h day/8 h night) for 45 days. After this period, the plants were transferred to a cold greenhouse (5–15 °C) for about three months, and the temperature was later increased to 15–20 (25) °C. Tillers bearing spikes containing anthers with microspores at mid- to late uninucleate stage were cut, put in a vessel with water and pretreated at 4 °C for 8–9 days. Ten spikes from each genotype were collected. Cold pretreated spikes were surface sterilized with 70 % ethanol under aseptic conditions. Sixty anthers from each spike were placed in test tubes with 20 ml P2 induction medium (Chuang et al., 1978). The anthers were cultured at 28 °C in darkness for about 60 days. After the 30th day, they were periodically checked for induction of embryogenic structures (calli and embryoids), which were transferred to test tubes with 10 ml regeneration medium (Zhuang, Jia, 1983) and cultured at 25 °C (3000 lx, 16 h day/8 h night). Green and albino regenerants were counted after 30 days.

The androgenic response was estimated by the following traits: callus induction (CI) (number of embryogenic structures induced per 100 cultured anthers, %), plant regeneration (PR) (number of regenerated green and albino plants per 100 embryogenic structures, %), frequency (yield) of green plants (YGR) (number of regenerated green plants per 100 cultured anthers, %) and frequency (yield) of albino plants (YAR) (number of regenerated albino plants per 100 cultured anthers, %).

Statistics. The obtained results were summarized over genotypes and parameters. One way ANOVA was carried out with the aim of determining the effect of the genotype on the studied parameters to estimate their androgenic response. Significant differences between the amphidiploids and their

parental forms were calculated based on the Duncan test. To process the data, software MS Office Excel 2003 was used, and to perform ANOVA and the Duncan test – IBM SPSS Statistics v.19.

Results

The results on the androgenic potential of the investigated amphidiploids and their parental forms (Table 1) showed that accession 1dv had the highest callus induction (30.7 %), and durum wheat Argonavt – the lowest (2.1 %). Between the parental forms, there were no significant differences (both between the durum wheat cultivars and between the species durum wheat and *D. villosum*). The two amphidiploids differed significantly by their callus induction, which was probably related to the effect of the maternal component.

The yield of green plants, averaged for the entire investigated set, was extremely low. In the entire experiment, only 5 green regenerants were produced, one of them being from the durum wheat cultivar Gergana, and the other 4 – from the amphidiploid 1dv (Gergana-*D. villosum*). No green regenerants were obtained from cultivar Argonavt and from the amphidiploid 2dv. Also, no green plants were produced from the wild species *D. villosum*. Although there was a rather small number of the obtained plants for formulating a general tendency for the effect of the parental forms, the presence of green plants in cultivar Gergana and the amphidiploid, in which it was involved, was probably due to genotypic specificity.

The albino plants considerably exceeded the green regenerants. In practice, they were predominant with regard to the total number of regenerants. The amphidiploid 1dv again had the highest yield of albino plants (10.3 %), and the lowest values were observed in cultivar Argonavt (0.4 %). The tendency in yield of obtained albinos largely followed the tendency of callus induction. The two amphidiploids significantly differed from the parental forms by their values, as well as between themselves (10.3 and 5.8 %, respectively). Meanwhile, significant differences between the two durum wheat cultivars and between the durum wheat and the wild species were not registered. The higher yield values of the albino plants in the amphidiploid 1dv may be related to the higher responsiveness of cultivar Gergana, which was the maternal component of this amphidiploid, although the difference between Gergana and Argonavt was not significant.

On the whole, plant regeneration, expressed as a number of regenerants per 100 embryogenic structures, was compara-

tively low. The highest values were read in the two investigated amphidiploids (35.9 and 35.4 %, respectively), and the lowest – in the wild species *D. villosum* (13.0 %). This parameter did not follow the tendency observed in the values of callus induction and yield of green and albino regenerants. There were no significant differences between any of the studied accessions. However, higher plant regeneration was registered in the amphidiploids, in comparison to cultivar Argonavt and the wild species, and the difference with cultivar Gergana was considerably lower. The differences not being significant was an indication that the regeneration potential of all studied accessions was practically identical, and the differences formed were entirely random. The total number of regenerants, however, expressly followed the tendency of callus induction and yield of albino plants. The higher responsiveness to anther culture of the two investigated amphidiploids in comparison to either of the parental forms could be clearly observed in this parameter.

The results from the analysis of the variance of the studied parameters (Table 2) showed that the genotype had a significant effect on the parameters callus induction and yield of albino regenerants. This allows supposing that the separate accessions gave specific responses and that there are significant differences between them, as determined by the Duncan test that was carried out. At the same time, the effect of the separate accessions on the plant regeneration and the yield of green plants was not significant. Worth mentioning are accessions Gergana and Gergana-*D. villosum*, in which higher responsiveness to anther culture was observed, in general. Nevertheless, these results do not give a definite answer to the question of whether the amphidiploids are different as a biologically distinct organism from the two parental forms with regard to their androgenic response.

When summarizing the results at the level of the species, a clear tendency of the amphidiploid *T. durum-D. villosum* having significantly higher callus induction and yield of albino regenerants was evident (Table 3).

Simultaneously, significant differences between the two parental forms were not observed, the values of both parameters being significantly lower in them. The yield of green plants from the parental forms and from the amphidiploid was extremely low and did not allow forming a clear tendency. In this case, the production of green regenerants was rather random, without observing significant differences between the investigated species. Plant regeneration, at the levels of

Table 1. Androgenic response of parental forms and durum wheat-*D. villosum* amphidiploids

Genotype	NCA	NOC	CI, %	NRC	PR, %	NAR	YAR, %	NGR	YGR, %
Gergana	600	43	7.2ab	13	30.2a	12	2ab	1	0.2ab
Argonavt	480	10	2.1a	2	20.0a	2	0.4a	0	0.0a
<i>D. villosum</i> (Dv)	540	23	4.3ab	3	13.0a	3	0.6a	0	0.0a
1dv (Gergana-Dv)	600	184	30.7c	66	35.9a	62	10.3c	4	0.7b
2dv (Argonavt-Dv)	480	79	16.5b	28	35.4a	28	5.8b	0	0.0a

Note. NCA – number of cultivated anthers; NOC – number of obtained calli; CI – callus induction; NRC – number of regenerative calli; PR – plant regeneration; NAR – number of albino regenerants; YAR – yield of albino regenerants; NGR – number of green regenerants; YGR – yield of green regenerants.

Table 2. ANOVA according to factor “accession” of the studied accessions

Parameters		Sum of squares	df	Mean square	F	Significance
CI	Between groups	0.51892	4	0.12973	8.693	0.000
	Within groups	0.59697	40	0.01492		
	Total	1.11589	44			
YAR	Between groups	0.06774	4	0.01694	7.799	0.000
	Within groups	0.08686	40	0.00217		
	Total	0.15460	44			
YGR	Between groups	0.00032	4	0.00008	2.159	0.091
	Within groups	0.00147	40	0.00004		
	Total	0.00179	44			
PR	Between groups	0.36055	4	0.09014	0.899	0.474
	Within groups	4.01134	40	0.10028		
	Total	4.37188	44			

Note. CI – callus induction; YAR – yield of albino regenerants; YGR – yield of green regenerants; PR – plant regeneration.

Table 3. Androgenic response of parental forms and durum wheat-*D. villosum* amphidiploid

Species	NCA	NOC	CI, %	NRC	PR, %	NAR	YAR, %	NGR	YGR, %
<i>T. durum</i> (Td)	1080	53	4.9a	15	28.3a	14	1.3a	1	0.1a
<i>D. villosum</i> (Dv)	540	23	4.3a	3	13.0a	3	0.6a	0	0.0a
Td-Dv	1080	263	24.4b	94	35.7a	90	8.3b	4	0.4a

Note. NCA – number of cultivated anthers; NOC – number of obtained calli; CI – callus induction; NRC – number of regenerative calli; PR – plant regeneration; NAR – number of albino regenerants; YAR – yield of albino regenerants; NGR – number of green regenerants; YGR – yield of green regenerants.

Table 4. ANOVA according to factor “species” of the studied accessions

Parameters		Sum of squares	df	Mean square	F	Significance
CI	Between groups	0.41771	2	0.20885	12.564	0.000
	Within groups	0.69818	42	0.01662		
	Total	1.11589	44			
YAR	Between groups	0.05763	2	0.02881	12.480	0.000
	Within groups	0.09698	42	0.00231		
	Total	0.15460	44			
YGR	Between groups	0.00011	2	0.00005	1.349	0.271
	Within groups	0.00168	42	0.00004		
	Total	0.00179	44			
PR	Between groups	0.31393	2	0.15696	1.625	0.209
	Within groups	4.05795	42	0.09662		
	Total	4.37188	44			

Note. CI – callus induction; YAR – yield of albino regenerants; YGR – yield of green regenerants; PR – plant regeneration.

both genotype and species, did not differ as a tendency. The observed differences were not significant (see Tables 3 and 4), which indicated that the studied amphidiploid did not differ from the parental forms by its regeneration capacity.

Discussion

Concerning the results obtained on the androgenic response of the used accessions, it should be emphasized, that no source

was found in world literature that would present data on the amphidiploid *T. durum*-*D. villosum* or the species *D. villosum*. An exception was the research of X. Chen et al. (1996), who suggested applying the anther culture method on hybrids (not amphidiploids) of the F₁ (*T. durum* × *D. villosum*). These authors reported successful production of amphidiploids, regenerated from colchicine-treated calli. At the same time, there are researches on the use of tissue cultures on three-

component hybrids *T. aestivum* × (*T. durum*-*D. villosum*). H. Li et al. (2005) reported lines with high powdery mildew resistance obtained from such hybrids through the method of embryo rescue and subsequent anther culture.

D. Plamenov et al. (2009), when investigating the androgenic response of accessions from the amphidiploid *T. durum*-*T. monococcum* ssp. *aegilopoides*, came up with results different from ours. The reported callus induction was 3.3–11.7 % for the two studied accessions, the plant regeneration was considerably higher, 33.8–68.4 %, respectively, and the albino regenerants yield was 1.9–3.2 %. At the same time, the yield of green plants (0.4–0.8 %) was a little higher than the data we obtained in our experiment (0.0–0.7 %). These authors reported a total of seven regenerated plants from both accessions, this parameter being significant, unlike the results we obtained. Using anther culture in the amphidiploid *Ae. variabilis*-*S. cereale*, and P2 medium, A. Ponitka et al. (2002) observed 1.4–15.7 % of callus induction, and on C17 medium – 20.0–65.2 %. Subsequently, the authors reported 0.1–13.4 % yield of green regenerants using 190-2 regeneration medium. It was found out that the androgenic response was strongly dependent on the genotype, similar to the results of the experiment we conducted. Successful regeneration of green plants through the method of anther culture has also been reported for an aneupolyhaploid of *Thynopyrum ponticum* (Wang et al., 1991), for the amphidiploid *Festuca pratensis*-*Lolium multiflorum* (Lesniewska et al., 2001; Zwierzykowski et al., 2001; Rapacz et al., 2005) and the amphidiploid *Cyclamen persicum*-*C. purpurascens* (Ishizaka, 1998).

In contrast to these results, the parental forms were characterized with much lower androgenic response. This was confirmed by the absence of callus induction in *Ae. variabilis* and rye, reported by A. Ponitka et al. (2002), and also in the species *T. monococcum* ssp. *aegilopoides* in the research of D. Plamenov et al. (2009). Durum wheat is also characterized by weak androgenic response, in general. M. Doğramacı-Altuntepe et al. (2001), using 10 durum wheat genotypes, obtained only 248 green regenerants from 86,400 anthers (0.29 %). F. J'Aiti et al. (1999), investigating 15 durum wheat genotypes and 7500 cultivated anthers, obtained just three albino regenerants and one green plant.

L. Cistúe et al. (2006), on the other hand, reported significantly higher production of green plants, but including 6-benzylaminopurine or 6-furfurilaminopurine in the induction medium (C17). In more recent researches, the production of haploids, even by the method of isolated microspores, has been of extremely low efficiency in durum wheat (Slama-Ayed et al., 2019). These results entirely corresponded to the data we obtained with regard to the two cultivars Argonavt and Gergana. Clear genotypic specificity was observed in the better response of Gergana to anther culture as compared to Argonavt, although the difference was not statistically significant. It is probable that this tendency is the reason for the amphidiploid Gergana-*D. villosum* having better responsiveness to anther culture. In this respect, the amphidiploid *T. durum*-*D. villosum* we investigated, and the amphidiploids reported by A. Ponitka et al. (2002) and D. Plamenov et al. (2009) were closer by their androgenic response to the response of triticale (which is a typical amphidiploid crop) than to the response of the parental forms. J. Pauk et al. (2000), K. Marciniak et al.

(2003), C. Lantos et al. (2014) and H. Stoyanov et al. (2019) demonstrated that in triticale the albino regenerants are often predominant, similar to the amphidiploid we studied. The values of the green regenerants in triticale also varied (from 0.9 to 27.9 %, but more often within 3–6 %), according to data from various researches (Gonzales, Jouve, 2000; Marciniak et al., 2003; Banaszak, 2011; Lantos et al., 2014).

In contrast to the above responses of the parental forms *Ae. variabilis*, *S. cereale* and *T. monococcum* ssp. *aegilopoides*, our study, although limited in volume, demonstrated the comparatively good responsiveness of the species *D. villosum* to anther culture. This is the first time when results on regenerants from this species (although only albinos) are being reported. At the same time, it should be emphasized that until this moment results from testing of the reaction of *D. villosum* to the anther culture method have never been reported. This is highly significant for the breeding of the wheat species since it would allow transferring genes from the wild species through the methods of wide hybridization and anther culture more easily, quickly and efficiently. X. Chen et al. (1996) and C. Li et al. (2000) reported common wheat lines resistant to powdery mildew, which were obtained by crossing common wheat to the amphidiploid *T. durum*-*D. villosum*, followed by embryo rescue and anther culture. Such results showed that the combination of wide hybridization with the method of anther culture is an efficient tool that can be used in the breeding of different cereal crops.

Conclusion

Based on the presented results, the following conclusions could be made:

1. For the first time, results on the androgenic response (callus induction, plant regeneration, yield of albino plants, yield of green plants) of the amphidiploid *T. durum*-*D. villosum* and of the parental component *D. villosum* are being reported.
2. The callus induction of the two studied amphidiploids differed significantly from that of the parental forms (2.1–7.2 %), being considerably higher – 30.7 and 16.5 %, respectively.
3. The plant regeneration of the investigated accessions varied within a certain range (13.0–35.9 %), the differences not being statistically significant. This indicated that in spite of the differences in the callus induction, the amphidiploids did not practically differ from the parental forms by their regeneration capacity.
4. Although plant regeneration was observed in all studied accessions, the yield of albino plants considerably exceeded the yield of green regenerants and followed the tendency observed in callus induction – the two amphidiploids had significantly higher values. At the same time, green plants were registered only in the amphidiploid Gergana-*D. villosum* and in the parental form durum wheat Gergana. Such results emphasized the genotypic specificity of the response to anther culture.
5. Plants were regenerated from the species *D. villosum*, although only albinos, which indicated its good responsiveness to anther culture. This, together with the good response of the amphidiploids with the participation of this species, makes their practical use, in combination with the anther culture method, highly valuable for improving the cereals.

References

- Ando K., Krishnan V., Rynearson S., Rouse M.N., Danilova T., Friebe B., See D., Pumphrey M.O. Introgression of a novel Ug99-effective stem rust resistance gene into wheat and development of *Dasypyrum villosum* chromosome-specific markers via genotyping-by-sequencing (GBS). *Plant Dis.* 2019;103:1068-1074. DOI 10.1094/PI-S-05-18-0831-RE.
- Babaiaants O.V., Babaiaants L.T., Horash A.F., Vasil'ev A.A., Trackovetskaia V.A., Paliasn'iĭ V.A. Genetics determination of wheat resistance to *Puccinia graminis* f. sp. *tritici* deriving from *Aegilops cylindrica*, *Triticum erebuni* and amphidiploid 4. *Isitol. Genet.* 2012; 46(1):10-17. (in Ukrainian)
- Banaszak Z. Breeding of triticale in DANKO. In: Tagungsband der 61. Jahrestagung der Vereinigung der Pflanzenzüchter und Saatgutkaufleute Österreichs 23–25 November 2010. Raumberg-Gumpenstein. Irnding, 2011;65-68.
- Barceló P., Cabrera A., Hagel C., Lörz H. Production of doubled-haploid plants from tritordeum anther culture. *Theor. Appl. Genet.* 1994; 87:741-745.
- Belchev I. Studies on Anther Culture of Common Winter Wheat (*Triticum aestivum* L.) and Application of Double Haploid Lines in Breeding. General Toshevo, 2003. (in Bulgarian)
- Chahal G.S., Gosal S.S. Principles and Procedures of Plant Breeding: Biotechnological and Conventional Approaches. New York: CRC Press, 2000.
- Chen X., Xu H.J., Du L.P., Shang L.M., Han B., Shi A., Xiao S. Transfer of gene resistant to powdery mildew from *H. villosa* to common wheat by tissue culture. *Sci. Agric. Sin.* 1996;29:1-8.
- Chuang C.C., Ouyang T.W., Chia H., Chou S.M., Ching C.K. A set of potato media for wheat anther culture. In: Proc. of Symposium on Plant Tissue Culture 1978. Peking: Science Press, 1978;51-56.
- Cistué L., Soriano M., Castillo A.M., Vallés M.P., Sanz J.M., Echávarri B. Production of doubled haploids in durum wheat (*Triticum turgidum* L.) through isolated microspore culture. *Plant Cell Rep.* 2006;25(4):257-264. DOI 10.1007/s00299-005-0047-8.
- Dagüstü N. Diallel analysis of anther culture response in wheat (*Triticum aestivum* L.). *Afr. J. Adv. Biotechnol.* 2008;7(19):3419-3423.
- Dai S., Li Z., Xue X., Jia Y., Liu D., Pu Z., Zheng Y., Yan Z. Analysis of high-molecular-weight glutenin subunits in five amphidiploids and their parental diploid species *Aegilops umbellulata* and *Aegilops uniaristata*. *Plant Genet. Resour.* 2015;13(2):186-189. DOI 10.1017/S1479262114000719.
- De Pace C., Snidaro D., Ciaffi M., Vittori D., Ciofo A., Cenci A., Tanzarella O.A., Qualset C.O., Mugnozza G.T.S. Introgression of *Dasypyrum villosum* chromatin into common wheat improves grain protein quality. *Euphytica.* 2001;117(1):67-75. DOI 10.1023 A:1004095705460.
- De Pace C., Vaccino P., Cionini P.G., Pasquini M., Bizzarri M., Qualset C.O. *Dasypyrum*. Chapter 4. In: Kole C. (Ed.). *Wild Crop Relatives: Genomic and Breeding Resources*. Cereals. Berlin; Heidelberg: Springer-Verlag, 2011;185-292. DOI 10.1007/978-3-642-14228-4_4.
- Doğramacı-Altuntepe M., Peterson T.S., Jauha P.P. Anther culture-derived regenerants of durum wheat and their cytological characterization. *J. Hered.* 2001;92(1):56-64.
- El-Hennawy M.A., Abdalla A.F., Shafey S.A., Al-Ashkar I.M. Production of doubled haploid wheat lines (*Triticum aestivum* L.) using anther culture technique. *Ann. Agric. Sci.* 2012;56(2):63-72. DOI 10.1016/j.aos.2011.05.008.
- Gonzales J.M., Jouve N. Improvement of anther culture media for haploid production in triticale. *Cereal Res. Commun.* 2000;28(1-2): 65-72.
- Grądzielewska A. The genus *Dasypyrum* – part 2. *Dasypyrum villosum* – a wild species used in wheat improvement. *Euphytica.* 2006a; 152:441-454.
- Grądzielewska A. The genus *Dasypyrum* – part 1. The taxonomy and relationships within *Dasypyrum* and with *Triticeae* species. *Euphytica.* 2006b;152:429-440.
- Grassini P., Eskridge K., Cassman K. Distinguishing between yield advances and yield plateaus in historical crop production trends. *Nat. Commun.* 2013;4:2918. DOI 10.1038/ncomms3918.
- Ishizaka H. Production of microspore-derived plants by anther culture of an interspecific F1 hybrid between *Cyclamen persicum* and *C. purpurascens*. *Plant Cell Tissue Organ Cult.* 1998;54:21-28.
- J'Aiti F., Benlhabib O., Sharma H.C., El Jaafari S., El Hadrami I. Genotypic variation in anther culture and effect of ovary coculture in durum wheat. *Plant Cell Tissue Organ Cult.* 1999;59:71-76.
- Kiani R., Arzani A., Meibody S.A.M.M., Rahimmalek M., Razavi K. Morpho-physiological and gene expression responses of wheat by *Aegilops cylindrica* amphidiploids to salt stress. *bioRxiv.* 2021. DOI 10.1101/2020.06.07.139220.
- Klimushina M.V., Kroupin P.Y., Bazhenov M.S., Karlov G.I., Divashuk M.G. Waxy gene-orthologs in wheat × *Thinopyrum* amphidiploids. *Agronomy.* 2020;10(7):963. DOI 10.3390/agronomy10070963.
- Lantos C. *In vitro* androgenesis induction in wheat (*Triticum aestivum* L.), Triticale (×*Triticosecale* Wittmack), spice pepper (*Capsicum annum* L.) and integration of the results into breeding: Thesis of the Ph.D. dissertation. Szent Istvan University, 2009.
- Lantos C., Bona L., Boda K., Pauk J. Comparative analysis of *in vitro* anther- and isolated microspore culture in hexaploid Triticale (×*Triticosecale* Wittmack) for androgenic parameters. *Euphytica.* 2014; 197(1):27-37.
- Lesniewska A., Ponitka A., Slusarkiewicz-Jarżina A., Zwierzykowska E., Zwierzykowski Z., James A.R., Thomas H., Humphreys M.W. Androgenesis from *Festuca pratensis* × *Lolium multiflorum* amphidiploid cultivars in order to select and stabilize rare gene combinations for grass breeding. *Heredity.* 2001;86:167-176.
- Li C. Breeding crops by design for future agriculture. *J. Zhejiang Univ. Sci. B.* 2020;21(6):423-425. DOI 10.1631/jzus.B2010001.
- Li H., Chen X., Xin Z.Y., Ma Y.Z., Xu H.J., Chen X.Y., Jia X. Development and identification of wheat–*Haynaldia villosa* T6DL.6VS chromosome translocation lines conferring resistance to powdery mildew. *Plant Breed.* 2005;124:203-205. DOI 10.1111/j.1439-0523.2004.01062.x.
- Li H.J., Li Y.W., Zhang Y.M., Li H., Guo B.H., Wang Z.N., Wen Z.Y., Liu Z.Y., Zhu Z.Q., Jia X. Tissue culture induced translocation conferring powdery mildew resistance between wheat and *Dasypyrum villosum* and its marker-assisted selection. *Yi Chuan Xue Bao.* 2000;27(7):608-613.
- Liu D., Zhang H., Zhang L., Yuan Z., Hao M., Zheng Y. Distant hybridization: a tool for interspecific manipulation of chromosomes. In: Pratap A., Kumar J. (Eds.). *Alien Gene Transfer in Crop Plants*. Vol. 1. New York: Springer, 2014. DOI 10.1007/978-1-4614-8585-8_2.
- Marciniak K., Kaczmarek Z., Adamski T., Surma M. The anther-culture response of triticale line × tester progenies. *Cell. Mol. Biol. Lett.* 2003;8:343-351.
- Ming D., Xiuqin W., Fu Q., Zhao Q., Zhao F., Wang Y. Cytogenetical analysis of hybrid F1 from common wheat and *Aegilops ventricosa* × *Aegilops cylindrica* amphidiploid. *Agric. Sci. Technol. Hunan.* 2011;12(9):1298-1302.
- Nemeth C., Yang C.-y., Kasprzak P., Hubbart S., Scholefield D., Mehra S., Skipper E., King I., King J. Generation of amphidiploids from hybrids of wheat and related species from the genera *Aegilops*, *Secale*, *Thinopyrum*, and *Triticum* as a source of genetic variation for wheat improvement. *Genome.* 2015;58(2):71-79. DOI 10.1139/gen-2015-0002.
- Okada A., Arndell T., Borisjuk N., Sharma N., Watson-Haigh N.S., Tucker E.J., Baumann U., Langridge P., Whitford R. CRISPR/Cas9-mediated knockout of Ms1 enables the rapid generation of male-sterile hexaploid wheat lines for use in hybrid seed production. *Plant Biotechnol. J.* 2019;17:1905-1913. DOI 10.1111/pbi.13106.
- Pauk J., Poulimatka M., Toth K.L., Monostori T. *In vitro* androgenesis of triticale in isolated microspore culture. *Plant Cell Tissue Organ Cult.* 2000;61(3):221-229. DOI 10.1023/A:1006416116366.

- Plamenov D., Belchev I., Spetsov P. Anther culture response of *Triticum durum* × *T. monococcum* ssp. *aegilopoides* amphiploid. *Cereal Res. Commun.* 2009;37(2):255-259. DOI 10.1556/CRC.37.2009.2.13.
- Ponitka A., Slusarkiewicz-Jarzina A., Wojciechowska B. Production of haploids and doubled haploids of the amphiploids *Aegilops variabilis* × *Secale cereale*. *Cereal Res. Commun.* 2002;30(1):39-45. DOI 10.1007/BF03543387.
- Rapacz M., Gašior D., Humphreys M.W., Zwierzykowski Z., Płażek A., Lésniewska-Bocianowska A. Variation for winter hardiness generated by androgenesis from *Festuca pratensis* × *Lolium multiflorum* amphidiploid cultivars with different winter susceptibility. *Euphytica*. 2005;142:65-73.
- Slama-Ayed O., Bouhaouel I., Ayed S., De Buyser J., Picard E., Amara H.S. Efficiency of three haplomehtods in durum wheat (*Triticum turgidum* subsp. *durum* Desf.): isolated microspore culture, gynogenesis and wheat × maize crosses. *Czech J. Genet. Plant Breed.* 2019;55(3):101-109. DOI 10.17221/188/2017-CJGPB.
- Song Z., Dai S., Jia Y., Zhao L., Kang L., Liu D., Wei Y., Zheng Y., Yan Z. Development and characterization of *Triticum turgidum*-*Aegilops umbellulata* amphidiploids. *Plant Genet. Resour.* 2019;17(1):24-32. DOI 10.1017/S1479262118000254.
- Stefani A., Meletti P., Onnis A. Morphological characteristics of the experimental allopolyploid *Triticum durum* × *Haynaldia villosa* (2n = 42). *Can. J. Bot.* 1987;65:1948-1951.
- Stoyanov H. Status of remote hybrids in the Poaceae: problems and prospects. *Agric. Sci. Technol.* 2013;5(1):3-12.
- Stoyanov H. Analysis and assessment of amphidiploids of *Triticum-Aegilops* group as a source of genetic diversity. *Bulg. J. Agric. Sci.* 2014;20(Suppl. 1):173-178.
- Stoyanov H., Belchev I., Baychev V. Changes in the androgenic response of triticale (×*Triticosecale* Wittm.) as a result of the inclusion of sweet potato extract in the induction media. *Rastenievadni Nauki.* 2019;56(5):92-98. (in Bulgarian)
- Vaccino P., Banfi R., Corbellini M., De Pace C. Improving the wheat genetic diversity for end-use grain quality by chromatin introgression from the wheat wild relative *Dasypyrum villosum*. *Crop Sci.* 2010;50(2):528-540.
- Wang H., Sun S., Ge W., Zhao L., Hou B., Wang K., Lyu Z., Chen L., Xu S., Guo J., Li M., Su P., Li X., Wang G., Bo C., Fang X., Zhuang W., Cheng X., Wu J., Dong L., Chen W., Li W., Xiao G., Zhao J., Hao Y., Xu Y., Gao Y., Liu W., Liu Y., Yin H., Li J., Li X., Zhao Y., Wang X., Ni F., Ma X., Li A., Xu S.S., Bai G., Nevo E., Gao C., Ohm H., Kong L. Horizontal gene transfer of *Fhb7* from fungus underlies *Fusarium* head blight resistance in wheat. *Science.* 2020;368(6493):eaba5435. DOI 10.1126/science.aba5435.
- Wang R.R.C., Marburger J.E., Hu C.J. Tissue-culture-facilitated production of aneupolyhaploid *Thinopyrum ponticum* and amphidiploid *Hordeum violaceum* × *H. bogdanii* and their uses in phylogenetic studies. *Theor. Appl. Genet.* 1991;81:151-156. DOI 10.1007/BF00215716.
- Yildirim M., Bahar B., Genç İ., Hatipoğlu R., Altıntaş S. Reciprocal effects in anther cultures of wheat hybrids. *Biol. Plant.* 2008;52:779-782. DOI 10.1007/s10535-008-0152-y.
- Zamani I., Gouli-Vavdinoudi E., Kovacs G., Xynias I., Roupakias D., Barnabas B. Effect of parental genotypes and colchicine treatment on the androgenic response of wheat F1 hybrids. *Plant Breed.* 2008;122(4):314-317. DOI 10.1046/j.1439-0523.2003.00866.x.
- Zhang L.Q., Liu D.C., Zheng Y.L., Yan Z.H., Dai S.F., Li Y.F., Jiang Q., Ye Y.Q., Yen Y. Frequent occurrence of unreduced gametes in *Triticum turgidum*-*Aegilops tauschii* hybrids. *Euphytica.* 2010;172:285-294. DOI 10.1007/s10681-009-0081-7.
- Zhang R., Fan Y., Kong L., Wang Z., Wu J., Xing L., Cao A., Feng Y. Pm62, an adult-plant powdery mildew resistance gene introgressed from *Dasypyrum villosum* chromosome arm 2VL into wheat. *Theor. Appl. Genet.* 2018;131(12):2613-2620. DOI 10.1007/s00122-018-3176-5.
- Zhang R., Feng Y., Li H., Yuan H., Dai J., Cao A., Xing L., Li H. Cereal cyst nematode resistance gene *CreV* effective against *Heterodera filipjevi* transferred from chromosome 6VL of *Dasypyrum villosum* to bread wheat. *Mol. Breed.* 2016a;36:122. DOI 10.1007/s11032-016-0549-9.
- Zhang R., Sun B., Chen J., Cao A., Xing L., Feng Y., Lan C., Chen P. Pm55, a developmental-stage and tissue-specific powdery mildew resistance gene introgressed from *Dasypyrum villosum* into common wheat. *Theor. Appl. Genet.* 2016b;129:1975-1984. DOI 10.1007/s00122-016-2753-8.
- Zhang R.Q., Hou F., Feng Y.G., Zhang W., Zhang M.Y., Chen P.D. Characterization of a *Triticum aestivum*-*Dasypyrum villosum* T2VS-2DL translocation line expressing a longer spike and more kernels traits. *Theor. Appl. Genet.* 2015;128(12):2415-2425. DOI 10.1007/s00122-015-2596-8.
- Zhuang J.J., Jia X. Increasing differentiation frequencies in wheat pollen callus. In: Cell and Tissue Culture Techniques for Cereal Crop Improvement. Beijing: Science Press, 1983.
- Zuo Y., Xiang Q., Dai S., Song Z., Bao T., Hao M., Zhang L., Liu G., Li J., Liu D., Wei Y., Zheng Y., Yan Z. Development and characterization of *Triticum turgidum*-*Aegilops comosa* and *T. turgidum*-*Ae. markgrafii* amphidiploids. *Genome.* 2020;63(5):263-273. DOI 10.1139/gen-2019-0215.
- Zwierzykowski Z., Ponitka A., Slusarkiewicz-Jarzina A., Zwierzykowska E., Lesniewska-Bocianowska A. Androgenesis in amphidiploid F1 hybrids and cultivars of *Festulolium*. *Zeszyty Problemowe Postepow Nauk Rolniczych (Poland).* 2001;474:47-54. (in Polish)

ORCID ID

H. Stoyanov orcid.org/0000-0003-0733-9077

Conflict of interest. The authors declare no conflict of interest.

Received August 2, 2021. Revised November 27, 2021. Accepted December 30, 2021.

Original Russian text www.bionet.nsc.ru/vogis/

Association of bud and anther morphology with developmental stages of the male gametophyte of melon (*Cucumis melo* L.)

M.L. Nguyen¹ , T.N.B.T. Huyen¹, D.M. Trinh¹, A.V. Voronina²

¹ Da Nang University – University of Education and Science, Da Nang City, Vietnam

² Russian State Agrarian University – Moscow Timiryazev Agricultural Academy, Moscow, Russia

 nmly@ued.udn.vn

Abstract. Correlations between the morphological features of flower buds and the developmental stages of the male gametophyte are of great practical interest as a reliable marker that accelerates and simplifies the selection of appropriate plant material for isolated microspore culture. Microspore culture enables one to quickly obtain many pure lines of different vegetable crops, but it has not yet been widely applied in the melon (*Cucumis melo* L.). To successfully apply this technique in a new culture, one has to optimize many of its elements: first, find the biological markers for selecting the flower buds containing the microspores of certain development stages. The paper presents the results of research estimating the correlations between the length and diameter of the flower buds, the length of the visual part of the corolla, the length of the anthers and the development stages of the male gametophyte in the F₁ hybrid of the Kim Hong Ngoc melon. The strongest correlation (CC = 0.885) was found for the flower bed diameter and a strong correlation (CC = 0.880), for the bud length. The corolla's visual part was a less reliable morphological feature, and the anther's length should not be used as a parameter to predict the developmental stages of the melon's male gametophyte. It was also found that one anther could contain the microspores and pollen grains of different developmental stages. In the flower buds less than 4 mm in length and 1.51 ± 0.02 mm in diameter prevailed tetrads, and in the buds 4.0–4.9 mm in length and 2.30 ± 0.02 mm in diameter, early microspores. The microspores of a middle stage of development prevailed in the flower buds 5.0–5.9 mm in length and 2.32 ± 0.00 mm in diameter; mid and late vacuolated microspores, in the buds 6.0–8.9 mm in length and 2.96 ± 0.37 mm in diameter; and two-celled pollen, in the buds more than 9 mm in length and more than 3.97 ± 0.34 mm in diameter. Key words: male gametophyte; stages of microspore development; tetrad; pollen; flower bud; anther; *Cucumis melo* L.; melon.

For citation: Nguyen M.L., Huyen T.N.B.T., Trinh D.M., Voronina A.V. Association of bud and anther morphology with developmental stages of the male gametophyte of melon (*Cucumis melo* L.). *Vavilovskii Zhurnal Genetiki i Selekcii* = *Vavilov Journal of Genetics and Breeding*. 2022;26(2):146-152. DOI 10.18699/VJGB-22-18

Соответствие морфологии бутонов и пыльников стадиям развития мужского гаметофита дыни (*Cucumis melo* L.)

M.A. Нгуен¹ , T.H.B.T. Хуен¹, Д.М. Чинь¹, А.В. Воронина²

¹ Университет Дананг – Университет образования и науки, Дананг, Вьетнам

² Российский государственный аграрный университет – МСХА им. К.А. Тимирязева, Москва, Россия

 nmly@ued.udn.vn

Аннотация. Выявление корреляций между морфологическими признаками бутонов и стадиями развития мужского гаметофита представляет большой практический интерес, так как наличие надежного маркера ускоряет и упрощает отбор подходящего растительного материала для культуры изолированных микроспор. Культура изолированных микроспор позволяет в короткие сроки получать чистые линии многих овощных культур, однако для дыни (*Cucumis melo* L.) эта технология пока не получила распространения. Чтобы успешно применить данную технологию для новой культуры, необходимо оптимизировать множество ее элементов, прежде всего подобрать морфологические маркеры, позволяющие отбирать бутоны, которые содержат микроспоры определенных стадий развития. В нашей работе приведена оценка корреляции между длиной бутонов, диаметром бутонов, длиной видимой части венчика, длиной пыльников и стадиями развития мужского гаметофита дыни F₁ гибрида Kim Hong Ngoc. Наиболее сильная корреляция установлена для диаметра бутонов, коэффициент корреляции составил 0.885. Сильная корреляция выявлена также для длины бутона, коэффициент корреляции 0.880. Длина видимой части венчика являлась менее надежным признаком, а длина пыльников не следует использовать в качестве параметра для прогнозирования стадий развития мужского гаметофита дыни. Отмечено, что в одном пыльнике одновременно находились микроспоры и пыльцевые

зерна разных стадий развития. В бутонках длиной менее 4.00 мм и диаметром до 1.51 ± 0.02 мм преобладали тетрады; в бутонках длиной 4.0–4.9 мм и диаметром 2.30 ± 0.02 мм обнаружена наибольшая доля ранних микроспор, при этом преобладали микроспоры средней стадии развития; в бутонках длиной 5.0–5.9 мм и диаметром 2.32 ± 0.00 мм преобладали средние и поздние вакуолизованные микроспоры; в бутонках длиной 6.0–8.9 мм и диаметром 2.96 ± 0.37 мм – поздние вакуолизованные микроспоры; в бутонках длиной 9.0 мм и более, диаметром 3.97 ± 0.34 мм и более – двухклеточная пыльца.

Ключевые слова: мужской гаметофит; стадии развития микроспор; тетрада; пыльца; бутон; пыльник; *Cucumis melo* L.; дыня.

Introduction

The melon (*Cucumis melo* L.) is an economically important cultivated plant (Sebastian et al., 2010) grown in more than 1 mln ha of agricultural lands (FAOSTAT, 2019)¹. For the time being, the most common melon has been F₁ hybrids praised for their uniformity and high yield and providing proper biological protection of originator's ownership.

Double haploids (DHs) are a valuable material of genetic research and selection, especially for F₁ hybrids of agricultural plants (Shmykova et al., 2015b; Abdollahi et al., 2016). As of today, the technologies to obtain DHs have been developed for more than 250 species (Maluszynski et al., 2003) and many of them have been used to produce homozygous plants (Ferrie, Caswell, 2011).

Several publications describe successful melon DH production via pollination with irradiated pollen (Sauton, 1988; Hooghvorst et al., 2020) or via remote hybridization followed by embryo growing *in vitro* (Lotfi et al., 2003). There are also papers, whose authors cultivated the anthers (Abdollahi et al., 2016), unfertilized seedbuds (Shmykova et al., 2015a) and isolated microspores (Zhan et al., 2009; Chen et al., 2017) of members of the cucumber family.

The isolated microspore culture technique produces more regenerates compared to those of unfertilized seedbuds and anthers and is widely applied, especially in the cabbage family (Djatchouk et al., 2019; Kozar et al., 2020). Moreover, this technique excludes the somatic cells of a donor plant from the growing medium, leaving no doubt about the regenerates' origin. However, it has never been applied to produce the DHs of members of the cucumber family.

DH production in isolated microspore culture can be affected by multiple factors such as microspore development stage; their genotype; growing medium composition; cell-rich fluid density; culture introduction technique; the effect of temperature and other cultivation conditions (Dunwell, 2010; Niaziyan, Shariatpanahi, 2020). The microspore development stage is the first factor to be accounted for when applying the isolated microspore culture technique to a new culture, because the development from tetrads to two-celled pollen may involve different stages (Touraev et al., 1991; Germanà, 2011). For example, to produce carrot DHs, it is recommended to cultivate tetrads and early microspores (Gorecka et al., 2010), while cultivation of middle and late microspores is most effective for callus induction in the balsam apple anther culture (Nguyen et al., 2019). And in the cabbage family, vacuolated microspores and two-celled pollen have the highest ability for embryogenesis (Telmer et al., 1992; Binarova et

al., 1997; Custers et al., 2001; Babbar et al., 2004; Winarto, Teixeira da Silva, 2011).

Direct selection of separate microspores corresponding to a certain development stage to be cultivated *in vitro* seems to be an unresolvable problem. As a rule, plant material is selected based on such markers as the morphological characteristics of the flower buds and anthers (Takahata, Keller, 1991; Parra-Vega et al., 2013). In rape, soya, reddish, tomato, balsam apple, these markers include the length and widths of their flower buds (Weber et al., 2005; Han et al., 2014; Sumarmi et al., 2014; Adhikari, Kang, 2017; Nguyen et al., 2019). Several studies have proved that such parameters as the size and color of the flower cup as well as the cup/corolla length ratio and anther size can do the trick (De Moraes et al., 2008; Parra-Vega et al., 2013; Zhang et al., 2013). Since these parameters are species-specific, it is necessary to work out a specific protocol for the melon.

This paper presents the results of investigation into the morphological characteristics of the melon's flower buds and anthers and the way they correlate with the plant's microspore development stages.

Materials and methods

The flower buds of the F₁ hybrid plants of the Kim Hong Ngoc melon produced by the Chia Tai Seed company (Thailand) were collected at 5:30–6:30 a. m. The buds of 3.6 to 15.6 mm in length (with 1-mm interval) were transported in ice and then stored for 24 hours at 4 °C. At least 10 buds were accounted for each of the intervals.

The buds' morphological characteristics were assessed using a Zeiss Stemi 2000-C stereomicroscope (Suzhou Co., Ltd). Microspores were obtained from the anthers of each flower bud to be put on a glass slide into a drop of glycerin mixed with distilled water in proportion 1:1. Then the 15 µl of 2 % acetocarmine solution drop was added, covered with a cover slide and microscopied. For the purpose of fluorescent staining, the microspores extracted from the anthers were washed three times in PBS (8.0 g/l of NaCl, 0.20 g/l of KCl, 1.44 g/l of Na₂HPO₄ and 0.24 g/l of KH₂PO₄ were dissolved in the 3/4 of the required volume of distilled water; HCl and KOH were added to bring the pH value to 7.4, and distilled water was added to reach the finite volume), DAPI (4',6-diamidino-2-phenylindole) was added and then the microspores were studied using a Zeiss Axio Lab1 fluorescent microscope (Suzhou Co., Ltd).

The microspore development stages were determined from the size and shape of the cells, the number of cell nuclei and their interposition (Vergne et al., 1987; Maluszynski et al.,

¹ <http://www.fao.org/faostat/en/#data/QC> (Accessed 01.06.2021).

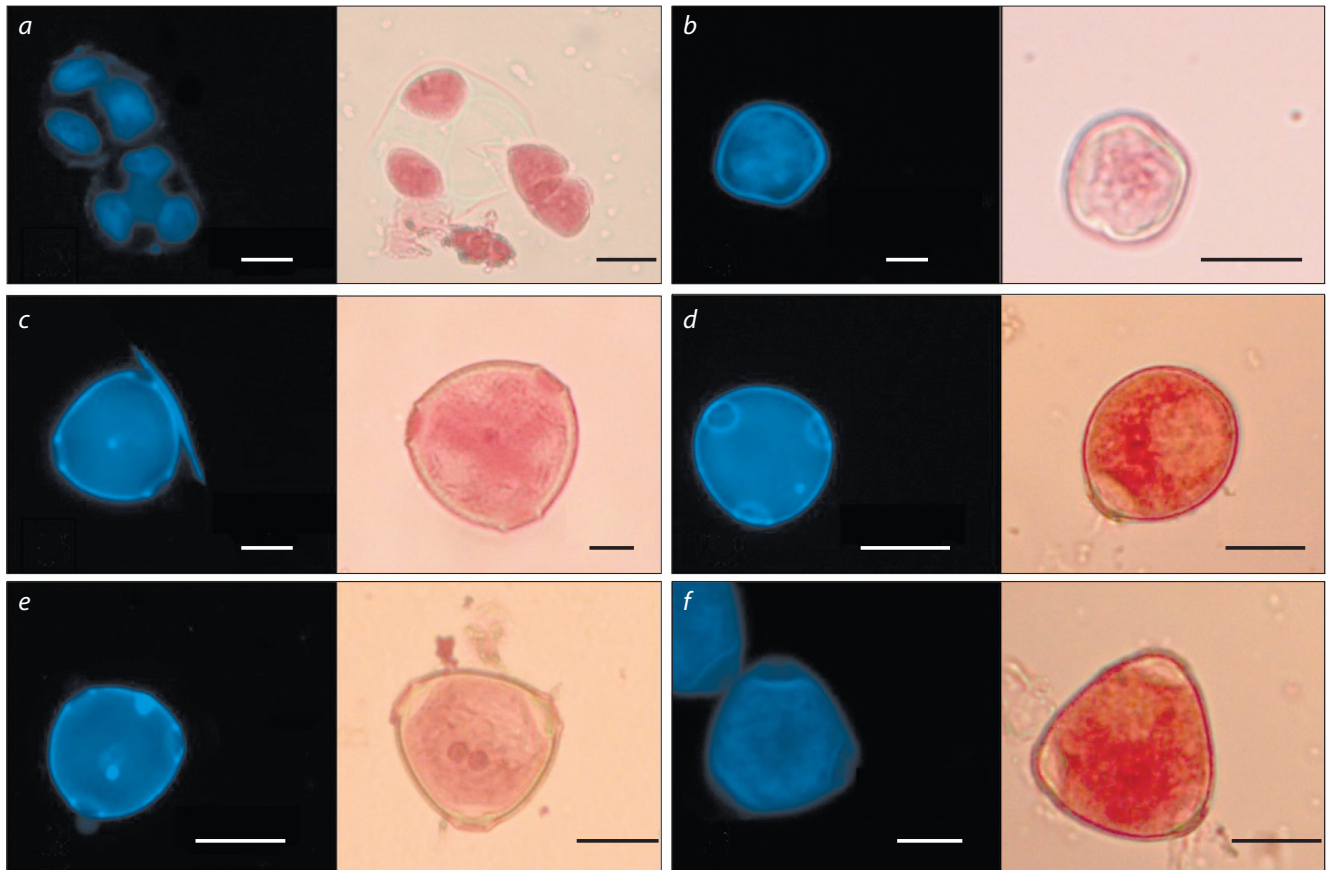


Fig. 1. DAPI- and acetocarmine-dyed microspore development stages of *Cucumis melo* L.: a – tetrads, b – early microspores, c – mid microspores, d – late vacuolated microspores, e – early two-celled pollen, f – late two-celled pollen. Bar = 20 μm .

2003; Blackmore et al., 2007; Zhang et al., 2013). In each specimen, the development stages of 100 microspores were observed. Such parameters as the presence of tetrads, early/middle/late microspores and two-cell pollen were considered. The percentage of each development stage in a particular specimen was calculated as the ratio of the number of microspores related to a certain development stage to the total number of observed microspores multiplied by 100 %.

The statistical significance of the performed calculations was confirmed with ANOVA analysis and the Tukey test for $\alpha = 0.05$. The correlation between the measured parameters and microspore development stages was determined using the linearity regression (R) and correlation (CC) coefficients. The collected data were described and processed with the R software.

Results and discussion

During the cytological analysis of melon flower buds, 6 stages of microspore development were observed. These included tetrads, early/middle/late vacuolated microspores, early/late two-celled pollen (Fig. 1).

The diameter of the microspores increased as they developed and reached their maximum at the stage of late two-celled pollen (Fig. 2). It has been noted that each stage was characterized by a certain shape and size of the cells. The diameter of the early microspores formed after tetrad degradation

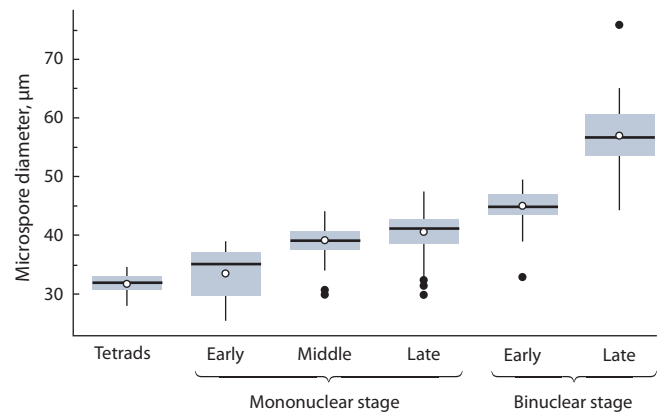


Fig. 2. Changes in male gametophyte diameters related to their development stages.

was $33.41 \pm 4.34 \mu\text{m}$; they were of uneven circular shape and had thin walls and large nuclei. The middle microspores were $39.06 \pm 2.33 \mu\text{m}$ in diameter, had a round shape and a centered nucleus. The late microspores were round and had a well-expressed three-lobed exine wall with the nucleus pressed to it by a big vacuole. Their diameter was $40.45 \pm 3.26 \mu\text{m}$. The cells of early two-celled pollen had $44.94 \pm 2.65 \mu\text{m}$ in diameter with well-expressed two nuclei: a larger vegetative

Correlations between flower-bud sizes, anther lengths and the stages of male gametophyte development in the melon

No.	Buds length, mm	Buds diameter, mm	Anther length, mm	Microspores developmental stages, %					
				Tetrads	Early	Mid	Late	Early two-celled pollen	Late two-celled pollen
1	<4	1.51 ± 0.02 ^{a*}	1.63 ± 0.19 ^a	48.00 ± 5.66	22.00 ± 8.49	6.00 ± 2.83	22.00 ± 2.83	2.00 ± 2.83	0.00 ± 0.00
2	4.0–4.9	2.30 ± 0.02 ^b	1.83 ± 0.16 ^a	0	30.00 ± 14.14	46.00 ± 25.46	22.00 ± 14.14	2.00 ± 2.83	0.00 ± 0.00
3	5.0–5.9	2.32 ± 0.00 ^b	2.50 ± 0.51 ^b	0	2.00 ± 2.83	50.00 ± 14.14	48.00 ± 11.31	0.00 ± 0.00	0.00 ± 0.00
4	6.0–8.9	2.96 ± 0.37 ^b	2.89 ± 0.23 ^c	0	0.40 ± 1.26	40.40 ± 24.91	56.80 ± 23.61	2.40 ± 6.31	0.00 ± 0.00
5	9.0–11.9	3.97 ± 0.34 ^c	2.96 ± 0.20 ^c	0	0	0.67 ± 1.63	14.67 ± 34.00	51.33 ± 50.62	33.33 ± 50.13
6	>12	5.16 ± 0.27 ^d	3.12 ± 0.22 ^c	0	0	0	0	0	100.00

* Data marked with the same letters do not differ at $p = 0.05$.

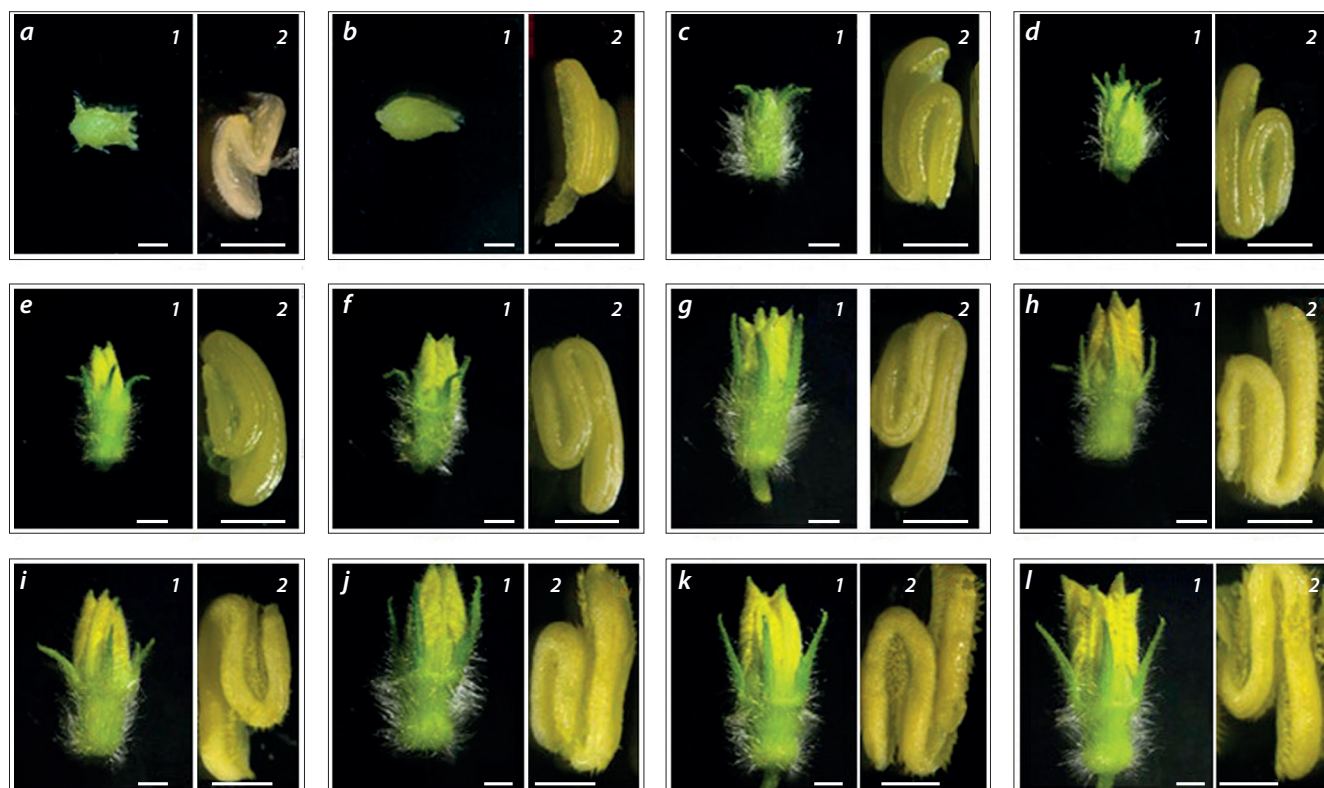


Fig. 3. Changing the morphological characteristics of melon buds (1, bar = 20 μ m) and anthers (2, bar = 10 μ m) in relation to flower-bud sizes: a – 3.6–4.0 mm; b – 4.0–4.9 mm; c – 5.0–5.9 mm; d – 6.0–6.9 mm; e – 7.0–7.9 mm; f – 8.0–8.9 mm; g – 9.0–9.9 mm; h – 10.0–10.9 mm; i – 11.0–11.9 mm; j – 12.0–12.9 mm; k – 13.0–13.9 mm; l – more than 14.0 mm.

and a more vividly-colored generative one. The diameter of the late two-celled pollen comprised $56.93 \pm 4.81 \mu$ m, its cell shapes varying from round to oval, so one anther could contain pollen grains of different shapes. The pollen's cytoplasm became dense and nontransparent making it more difficult to observe the nucleus.

The results of the correlation analysis to bring together the morphological features of melon flower buds and corresponding microspore development changes enabled us to subdivide the buds into 6 groups. Each group could include microspores

of different stages, so at least one of these stages prevailed (see the Table). It was noted that a single anther could have microspores that belonged to different development stages, which corresponds to the observations of other researchers who studied this issue in other cultures.

The tetrads were found in green oval-shaped pubescent flower buds that were fully covered in sepals and had a length of less than 4 mm and a diameter of 1.85 mm (Fig. 3, a). The buds' anthers were of light-beige color and had 1.6–1.63 mm in length.

The early microspores were found in flower buds of 3.8–7.0 mm in length, their biggest portion (30±14.14%) concentrated in buds of 4.0–4.9 mm. The buds' anthers changed their color to green-yellow, their length comprised 1.63–2.74 mm (see Fig. 3, b). The early microspores were found in smaller amounts compared to the other development stages.

The middle microspores concentrated in flower buds of 4.0 to 10.9 mm in length. The buds' anthers were 2.15±0.05 mm in length and had a yellowish glazing surface (see Fig. 3, c). The microspores prevailed (50±14.14%) in the buds of 5.0–5.9 mm in length. Such buds had a clear morphological difference from younger buds: their sepals were open, so one could see the corolla tip.

The late vacuolated microspores prevailed in buds of 6.0–8.9 mm in length. At this stage, the buds kept growing in size, so the corolla extended beyond the sepals. However, the anthers' morphology remained unchanged (see Fig. 3, d–f) as did their length.

The early two-celled pollen prevailed in buds of 9.0–12.0 mm in length (see Fig. 3, g–i). Their anthers' length, compared to the previous stage, remained unchanged, their surfaces containing mature pollen grains.

As for buds larger than 12 mm in length, they contained only two-celled pollen. The transition from the late to mature stage was characterized by a small increase in bud size, its petals starting to open (see Fig. 3, j–l). The anthers increased in size and opened too, so a large number of pollen grains could be seen on their surface.

Statistical analysis of anther lengths gave us linear regression coefficient $R^2 = 0.52$, which meant that this parameter could not be used as a predictor of microspore development stages in the melon, which corresponded to the results obtained for some other cultures such as the tomato and aubergine (Segui-Simarro, Nuez, 2005; Salas et al., 2012). In (Adhikari, Kang, 2017), the authors obtained a similar coefficient ($R^2 = 0.59$) when studying a relation between anther length and microspore development stages in the tomato.

Many researchers recommend using flower-bud length to select proper plant material to cultivate isolated microspores for it is a convenient and reliable morphological parameter for many plant species. They also recommend bud diameter as an indicator for flower bud selection. A study published in 2019 demonstrated that the best results in the embryogenesis of lucerne microspores were obtained when cultivating late microspores from flower buds of 6.02–6.20 mm in length and 1.50–1.72 mm in diameter (Yi et al., 2019). In 2017, a correlation between flower-bud size (length and diameter), anther length and microspore development stages in the tomato was published (Adhikari, Kang, 2017).

In our study, a linear regression analysis showed there was a clear linear dependence ($p < 0.05$) between the flower-bud characteristics and microspore development stages. The regression coefficients (R^2) varied from 0.767 to 0.783. The strongest correlation was for flower-bud diameter ($r = 0.885$, $R^2 = 0.783$) (Fig. 4), followed by flower-bud ($r = 0.880$, $R^2 = 0.775$) (Fig. 5) and anther ($r = 0.876$, $R^2 = 0.763$) lengths, the last being the least reliable feature.

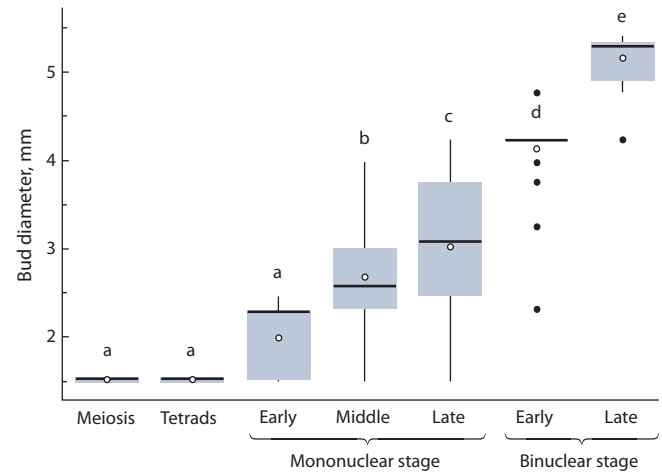


Fig. 4. Correlation between the melon's flower bud diameter and male gametophyte development stages.

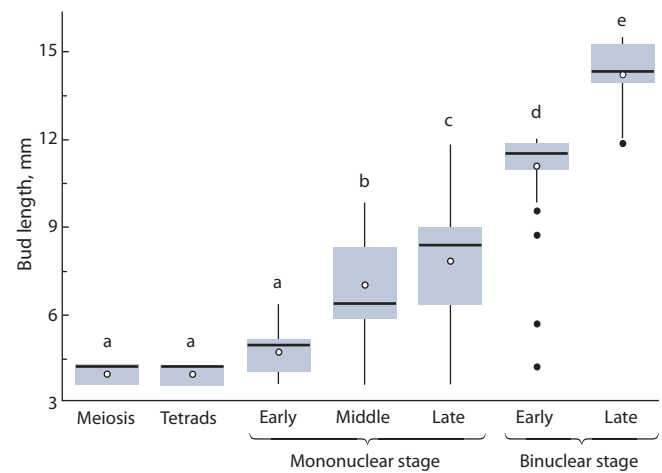


Fig. 5. Correlation between the melon's flower bud length and male gametophyte development stages (a–e correspond to different bud groups).

Conclusion

The correlation between the morphological characteristics of the flower buds and anthers of the melon (*Cucumis melo* L.) and the development stages of its microspores enables one to select a proper material for cultivation of isolated microspores *in vitro*. The characteristics in question are flower-bud diameter and length and the length of visible corolla. Since the correlation coefficient is higher for the diameter and length of flower buds, these parameters are easier to use.

The obtained results can be applied for further development of the technology to produce melon DHs in isolated microspore culture.

References

- Abdollahi M.R., Najafi S., Sarikhani H., Moosavi S.S. Induction and development of anther-derived gametic embryos in cucumber (*Cucumis sativus* L.) by optimizing the macronutrient and agar concentrations in culture medium. *Turk. J. Biol.* 2016;40:571-579. DOI 10.3906/biy-1502-55.

- Adhikari P.B., Kang W.H. Association of floral bud and anther size with microspore developmental stage in Campari tomato. *Korean J. Hortic. Sci. Technol.* 2017;35(5):608-617. DOI 10.12972/kjhst.20170065.
- Babbar S.B., Agarwal P.K., Sahay S., Bhojwani S.S. Isolated microspore culture of *Brassica*: an experimental tool for developmental. *Indian J. Biotechnol.* 2004;3:185-202.
- Binarova P., Hause G., Cenklova V., Cordewener J.H.G., Van Lookeren Campagne M.M. A short severe heat shock is required to induce embryogenesis in late bicellular pollen of *Brassica napus* L. *Sex. Plant Reprod.* 1997;10:200-208. DOI 10.1007/s004970050088.
- Blackmore S., Wortley A.H., Skvarla J.J., Rowley J.R. Pollen wall development in flowering plants. *New Phytol.* 2007;174(3):483-498. DOI 10.1111/j.1469-8137.2007.02060.x.
- Chen J., Vanek E., Pieper M. Method for Producing Haploid, Dihaploid and Doubled Haploid Plants by Isolated Microspore Culture. Patent Int. Publ. No. WO 2017/017108 A1. Publ. date Feb. 2, 2017.
- Custers J.B.M., Cordewener J.H.G., Fiers M.A., Maasen B.T.H., van Lookeren Campagne M.M., Liu C.M. Androgenesis in *Brassica*: a model system to study the initiation of plant embryogenesis. In: Bhojwani S.S., Soh W.T. (Eds.) *Current Trends in The Embryology of Angiosperms*. Dordrecht: Springer, 2001;451-469. DOI 10.1007/978-94-017-1203-3_18.
- De Moraes A.P., Bered F., De Carvalho F.I.F., Kaltchuk-Santos E. Morphological markers for microspore developmental stage in maize. *Braz. Arch. Biol. Technol.* 2008;51(5):911-916. DOI 10.1590/S1516-89132008000500006.
- Djatchouk T.I., Khomyakova O.V., Akinina V.N., Kibkalo I.A., Pominov A.V. Microspore embryogenesis *in vitro*: the role of stresses. *Vavilovskii Zhurnal Genetiki i Seleksii = Vavilov Journal of Genetics and Breeding.* 2019;23(1):86-94. DOI 10.18699/VJ19.466. (in Russian)
- Dunwell J.M. Haploids in flowering plants: origins and exploitation. *Plant Biotechnol. J.* 2010;8:377-424. DOI 10.1111/j.1467-7652.2009.00498.x.
- Ferrie A.M.R., Caswell K.L. Isolated microspore culture techniques and recent progress for haploid and doubled haploid plant production. *Plant Cell Tissue Organ Cult.* 2011;104:301-309. DOI 10.1007/s11240-010-9800-y.
- Germanà M.A. Anther culture for haploid and doubled haploid production. *Plant Cell Tissue Organ Cult.* 2011;104:283-300. DOI 10.1007/s11240-010-9852-z.
- Gorecka K., Kowalska U., Krzyżanowska D., Kiszczak W. Obtaining carrot (*Daucus carota* L.) plants in isolated microspore cultures. *J. Appl. Genet.* 2010;51(2):141-147. DOI 10.1007/BF03195722.
- Han N., Kim S.U., Park H.Y., Na H. Microspore-derived embryo formation and morphological changes during the isolated microspore culture of radish (*Raphanus sativus* L.). *Korean J. Hortic. Sci. Technol.* 2014;32(3):382-389. DOI 10.7235/hort.2014.13170.
- Hooghorst I., Torrico O., Hooghorst S., Nogués S. *In situ* parthenogenetic doubled haploid production in melon "Piel de Sapo" for breeding purposes. *Front. Plant Sci.* 2020;11:378. DOI 10.3389/fpls.2020.00378.
- Kozar E.V., Domblides E.A., Soldatenko A.V. Factors affecting DH plants *in vitro* production from microspores of European radish. *Vavilovskii Zhurnal Genetiki i Seleksii = Vavilov Journal of Genetics and Breeding.* 2020;24(1):31-39. DOI 10.18699/VJ20.592.
- Lotfi M., Alan A.R., Henning M.J., Jahn M.M., Earle E.D. Production of haploid and doubled haploid plants of melon (*Cucumis melo* L.) for use in breeding for multiple virus resistance. *Plant Cell Rep.* 2003;21(11):1121-1128. DOI 10.1007/s00299-003-0636-3.
- Maluszynski M., Kasha K., Forster B.P., Szarejko I. (Eds.) *Doubled Haploid Production in Crop Plants: A manual*. Netherlands: Kluwer Acad. Publ., 2003.
- Nguyen M.L., Ta T.H.T., Huyen T.N.B.T., Voronina A.V. Anther-derived callus formation in bitter melon (*Momordica charantia* L.) as influenced by microspore development stage and medium composition. *Selskokhozyaystvennaya Biologiya = Agricultural Biology.* 2019;54(1):140-148. DOI 10.15389/agrobiology.2019.1.140eng.
- Niazian M., Shariatpanahi M.E. *In vitro*-based doubled haploid production: recent improvements. *Euphytica.* 2020;216:69. DOI 10.1007/s10681-020-02609-7.
- Parra-Vega V., Renau-Morata B., Sifres A., Seguí-Simarro J.M. Stress treatments and *in vitro* culture conditions influence microspore embryogenesis and growth of callus from anther walls of sweet pepper (*Capsicum annuum* L.). *Plant Cell Tissue Organ Cult.* 2013;112(3):353-360. DOI 10.1007/s11240-012-0242-6.
- Salas P., Rivas-Sendra A., Prohens J., Seguí-Simarro J.M. Influence of the stage for anther excision and heterostyly in embryogenesis induction from eggplant anther cultures. *Euphytica.* 2012;184:235-250. DOI 10.1007/s10681-011-0569-9.
- Sauton A. Doubled haploid production in melon. In: *Proceedings of the EUCARPIA Meeting on Cucurbit Genetics and Breeding*. Avignon-Montfavet, France, 1988;06(01-02):119-128.
- Sebastian P., Schaefer H., Telford I.R.H., Renner S.S. Cucumber (*Cucumis sativus*) and melon (*C. melo*) have numerous wild relatives in Asia and Australia, and the sister species of melon is from Australia. *Proc. Natl. Acad. Sci. USA.* 2010;107(32):14269-14273. DOI 10.1073/pnas.1005338107.
- Seguí-Simarro J.M., Nuez F. Meiotic metaphase I to telophase II as the most responsive stage during microspore development for callus induction in tomato (*Solanum lycopersicum*) anther cultures. *Acta Physiol. Plant.* 2005;27:675-685. DOI 10.1007/s11738-005-0071-x.
- Shmykova N.A., Khimich G.A., Korotseva I.B., Domblides E.A. Prospective of development of doubled haploid plants of Cucurbitaceae family. *Ovoshchi Rossii = Vegetable Crops of Russia.* 2015a;3-4:28-31. DOI 10.18619/2072-9146-2015-3-4-28-31. (in Russian)
- Shmykova N.A., Shumilina D.V., Suprunova T.P. Doubled haploid production in *Brassica* L. *Vavilovskii Zhurnal Genetiki i Seleksii = Vavilov Journal of Genetics and Breeding.* 2015b;19(1):111-120. DOI 10.18699/VJ15.014. (in Russian)
- Sumarmi S., Daryono B.S., Rachmawati D., Indrianto A. Determination of soybean (*Glycine max* L. [Merrill]) microspores development stage based on the length of flower buds. *J. Biol. Res.* 2014;20:6-11. DOI 10.23869/bphjbr.20.1.20142.
- Takahata Y., Keller W.A. High frequency embryogenesis and plant regeneration in isolated microspore culture of *Brassica oleracea* L. *Plant Sci.* 1991;74:235-242. DOI 10.1016/0168-9452(91)90051-9.
- Telmer C.A., Simmonds D., Newcomb W. Determination of developmental stage to obtain high frequencies of embryogenic microspores in *Brassica napus*. *Physiol. Plant.* 1992;84:417-424. DOI 10.1111/j.1399-3054.1992.tb04685.x.
- Touraev A., Pfosser M., Vicente O., Heberle-Bors E. Stress as the major signal controlling the developmental fate of tobacco microspores: towards a unified model of induction of microspore/pollen embryogenesis. *Planta.* 1996;200:144-152.
- Vergne P., Delvallee I., Dumas C. Rapid assessment of microspore and pollen development stage in wheat and maize using DAPI and membrane permeabilization. *Stain Technol.* 1987;62:299-304. DOI 10.3109/10520298709108014.
- Weber S., Unker W., Friedt W. Improved doubled haploid production protocol for *Brassica napus* using microspore colchicine treatment *in vitro* and ploidy determination by flow cytometry. *Plant Breeding.* 2005;124:511-513. DOI 10.1111/j.1439-0523.2005.01114.x.
- Winarto B., Teixeira da Silva J.A. Microspore culture protocol for Indonesian *Brassica oleracea*. *Plant Cell Tissue Organ Cult.* 2011;107:305-315. DOI 10.1007/s112400110081z.

Yi D., Sun J., Su Y., Tong Z., Zhang T., Wang Z. Doubled haploid production in alfalfa (*Medicago sativa* L.) through isolated microspore culture. *Sci. Rep.* 2019;9:9458. DOI 10.1038/s41598-019-45946-x.

Zhan Y., Chen J.F., Malik A.A. Embryoid induction and plant regeneration of cucumber (*Cucumis sativus* L.) through microspore culture. *Acta Hort. Sin.* 2009;36(2):221-226.

Zhang C., Tsukuni T., Ikeda M., Sato M., Okada H., Ohashi Y., Matsuno H., Yamamoto T., Wada M., Yoshikawa N., Matsumoto S., Li J., Mimida N., Watanabe M., Suzuki A., Komori S. Effects of the microspore development stage and cold pre-treatment of flower buds on embryo induction in apple (*Malus × domestica* Borkh.) anther culture. *J. Jpn. Soc. Hortic. Sci.* 2013;82(2):114-124. DOI 10.2503/jjshs1.82.114.

ORCID ID

M.L. Nguyen orcid.org/0000-0002-0652-891X
T.N.B.T. Huyen orcid.org/0000-0003-0467-9391
D.M. Trinh orcid.org/0000-0002-3662-2392
A.V. Voronina orcid.org/0000-0003-0249-246X

Conflict of interest. The authors declare no conflict of interest.

Received July 23, 2021. Revised September 6, 2021. Accepted September 6, 2021.

Developmental and hormonal regulation of *Arabidopsis thaliana* ornithine-delta-aminotransferase

A.A. Egorova^{1, 2}✉, S.V. Gerasimova^{1, 2}, A.V. Kochetov^{1, 2}

¹ Institute of Cytology and Genetics of the Siberian Branch of the Russian Academy of Sciences, Novosibirsk, Russia

² Novosibirsk State University, Novosibirsk, Russia

✉ egorova@bionet.nsc.ru

Abstract. Ornithine aminotransferase (OAT) catalyzes transfer of the delta-amino group from L-ornithine to oxo-glutarate. In plants, this reaction biochemically connects urea cycle, proline cycle, and polyamine biosynthesis pathway. OAT activity is shown to be associated with biotic and abiotic stress responses and nitrogen metabolism, but its physiological role is still unclear. In our study, we decided to investigate transcriptional regulation of the *OAT* gene in *Arabidopsis thaliana* under normal conditions and in response to various growth regulators. In the present work, the reporter gene construct containing the *Escherichia coli* β -glucuronidase gene (*gus*) under control of the *A. thaliana* *OAT* gene promoter was introduced into the genome of *A. thaliana* ecotype Columbia plants using the floral dip method; GUS activity was assayed in different experimental conditions including hormone treatment, low and high nitrogen and salinity. The GUS activity was analyzed histochemically. Plants were incubated with staining solution containing X-Gluc. We show that under standard growth conditions, the promoter is active during germination and in developing floral organs. *OAT* promoter activity specifically activates in response to different forms of auxin (IAA, NAA, and 2,4D), cytokinin (6-BAP), ethylene precursor (ACC), high nitrogen and salinity. Analysis of the *OAT* expression by qRT-PCR confirmed the pattern observed using the GUS reporter system. The *OAT* gene showed a significantly elevated expression in four-day-old seedlings and in plant roots in response to auxins and cytokinins. The analysis of the *OAT* promoter structure reveals cis-acting regulatory DNA elements associated with auxin regulation and abiotic stresses. The results of the study indicate that the *OAT* gene is involved in developmental processes and is regulated by auxin and cytokinins. Key words: ornithine aminotransferase; *Arabidopsis thaliana*; auxin; nitrogen; development.

For citation: Egorova A.A., Gerasimova S.V., Kochetov A.V. Developmental and hormonal regulation of *Arabidopsis thaliana* ornithine-delta-aminotransferase. *Vavilovskii Zhurnal Genetiki i Seleksii* = *Vavilov Journal of Genetics and Breeding*. 2022;26(2):153-158. DOI 10.18699/VJGB-22-19

Регуляция дельта-орнитинаминотрансферазы *Arabidopsis thaliana* в развитии и в ответ на гормоны

A.A. Egorova^{1, 2}✉, С.В. Герасимова^{1, 2}, А.В. Кочетов^{1, 2}

¹ Федеральный исследовательский центр Институт цитологии и генетики Сибирского отделения Российской академии наук, Новосибирск, Россия

² Новосибирский национальный исследовательский государственный университет, Новосибирск, Россия

✉ egorova@bionet.nsc.ru

Аннотация. Фермент орнитинаминотрансфераза (OAT) катализирует перенос дельта-аминогруппы от L-орнитина на альфа-кетоглутарат. В растениях эта реакция связывает цикл мочевины, пролина и путь биосинтеза пролина. В литературе активность OAT связывают с ответом на биотические и абиотические стрессы, метаболизмом азота, но физиологическая роль этого фермента до сих пор остается неясной. В нашем исследовании мы изучали транскрипционную регуляцию гена OAT в *Arabidopsis thaliana* в нормальных условиях и в ответ на различные ростовые регуляторы. Репортерная конструкция, содержащая ген β -глюкуронидазы (*gus*) *Escherichia coli* под контролем промотора гена OAT из *A. thaliana* была интродуцирована в геном растений *A. thaliana*. Активность GUS оценивалась в различных экспериментальных условиях, включающих воздействие гормонов, низких и высоких концентраций азота, солевой стресс. Для выявления активности GUS мы использовали гистохимический метод, растения обрабатывали раствором, содержащим X-Gluc. В нормальных условиях промотор был активен при прорастании семени и в развивающихся пестиках и пыльниках. Промотор гена OAT специфично активируется в ответ на различные формы ауксина (IAA, NAA, 2,4D), цитокинина (6-BAP), предшественника этилена (ACC), высокие концентрации азота и NaCl. Результаты анализа экспрессии гена OAT соответствуют наблюдаемому паттерну активности промотора, полученному с использованием репортерной системы GUS. Экспрессия гена OAT значительно повышалась в четырехдневных проростках и в ответ на ауксины и цитокинины. При анализе структуры промотора гена OAT обнаружены цис-элементы, связанные с ответами на ауксин и абиотические стрессы. Наши результаты позволяют сделать вывод о связи гена OAT с процессами развития растений и о его регуляции ауксинами и цитокининами.

Ключевые слова: орнитинаминотрансфераза; *Arabidopsis thaliana*; ауксин; азот; развитие.

Introduction

The ornithine- δ -aminotransferase (OAT) is a mitochondrial pyridoxal-5-phosphate (PLP)-dependent enzyme that transfers an amino group from ornithine to oxo-glutarate with formation of glutamate-1-semialdehyde (GSA) and glutamate (Gerasimova et al., 2011b). Although the biochemical function of OAT is known, its biological role in plants is not fully understood. On the one hand, OAT is involved in metabolism of ornithine, which takes part in numerous biochemical processes in plants, such as arginine metabolism, synthesis of polyamines and alkaloids (Funck et al., 2008; Majumdar et al., 2015). On the other hand, one of the products of the reaction mediated by OAT, namely GSA, is involved in proline production. It readily interconverts into the cyclic 1-pyrroline-5-carboxylate (P5C), an intermediate in the proline biosynthesis, in a non-enzymatic fashion (Ginguay et al., 2017). Proline is involved in plant stress response (Kochetov et al., 2004; Hayat et al., 2012) and development (Kavi Kishor et al., 2015). It has already been shown in various experiments on several plant species that overexpression of the *OAT* gene is associated with increased proline content and resistance to abiotic stresses (Roosens et al., 1998, 2002; Wu et al., 2003). It is tempting to assume that OAT might link biological processes related to proline, ornithine and P5C metabolism, such as nitrogen recycling, stress response, secondary metabolism, growth and development.

We have previously shown that *OAT* overexpression in tobacco increases salt stress resistance. Interestingly, the level of proline accumulation in *OAT* overexpressing lines did not differ from that of WT plants under both normal and stress conditions, suggesting that OAT might contribute to stress resistance through processes not related to proline synthesis (Gerasimova et al., 2010). On a model of transgenic tobacco plants expressing GUS under the control of putative *Arabidopsis thaliana* *OAT* promoter we showed that the promoter activity is associated with meristems and zones of active growth (Gerasimova et al., 2011a). This observation suggests that the *OAT* gene might be involved in developmental processes. The present study aims to investigate transcriptional regulation of the *OAT* gene in *A. thaliana* under normal conditions and in response to various growth regulators.

Materials and methods

Development of transgenic *Arabidopsis* harboring AtOAT promoter construct. The 1844 bp region upstream of the *OAT* gene translation start (TAIR, AT5G46180) was cloned in the promoterless vector pBI101 with the formation of the P1844 construct (Gerasimova et al., 2011a). The resulting vector contains the expression cassette harboring the β -glucuronidase (*gus*) reporter gene under the control of putative *A. thaliana* *OAT* promoter. *A. thaliana* plants ecotype Columbia were grown at 22 °C in a long-day growth conditions (16 h of light and 8 h of dark). Construct P1844 was transformed into *Agrobacterium tumefaciens* strain AGL0, which was used to transform *A. thaliana* by floral dip method (Clough, Bent, 1998). T1 transformants were screened on 1/2 MS agar plates containing 50 mg/L kanamycin, transferred to pots and grown to maturity until the T2 generation seeds were harvested. T2 seeds were germinated on 1/2 MS agar plates containing 50 mg/L kanamycin and resistant plants were tested for the presence of GUS activity by histochemical assay. Six indepen-

dent transgenic T2 lines showing the presence of GUS activity in seedlings were selected for further experiments. Plants from the selected lines were grown to maturity and T3 generation seeds were harvested. Thus, six independent T3 transgenic lines have been obtained.

GUS staining. The histochemical staining method (Jefferson et al., 1987) was used to visualize GUS (*Escherichia coli* β -glucuronidase) activity in seedlings grown on agar plates and plant parts grown in soil (5-week-old plants). Whole seedlings and different plant parts were incubated in X-Gluc solution (2 mM X-Gluc, 50 mM NaPO₄, pH 7, 0.5 % (v/v) Triton-X) for 24 h at 37 °C. Chlorophyll was removed by repeated washing in 70 % (v/v) ethanol. GUS activity was observed using a ZEISS Stemi 2000-C microscope coupled with an AxioCam HRC camera.

Experimental treatments. Surface-sterilized seeds of six independent transgenic *A. thaliana* lines (T3) were germinated on MS plates supplemented with 1 % sucrose, 0.7 % agar. To detect promoter activity during germination, histochemical assay was performed for seedlings at 3rd, 5th, 6th and 14th day after sowing (DAS) on plates. For experimental treatments, one-week-old seedlings were transferred to the same medium supplemented with the following growth regulators (from Sigma-Aldrich): auxins (1 mg/L NAA, 2 mg/L IAA, 0.5 mg/L 2,4-D), cytokinins (1 mg/L 6-BAP, 100 μ M trans-zeatin, 10 μ M and 100 μ M kinetin), gibberellic acid (10 μ M GA3), 100 μ M abscisic acid, 1 mM methyl jasmonate, ethylene precursor (50 μ M ACC), high nitrogen (10 mM NH₄NO₃), high salinity (200 mM NaCl). For low nitrogen treatment, MS NH₄NO₃-free medium (Duchefa Biochemie) was used. GUS activity was assayed after 1, 4, 6 and 8 days of treatment. For cold and heat treatment, two-week-old transgenic plants were used. For cold treatment, plates with seedlings were incubated at +4 °C for 4 h, then for 2 h at 22 °C; for heat treatment, plates were incubated at +50 °C for 15 min, then 6 h at 22 °C.

Gene expression analysis (RNA isolation and qRT-PCR). Wild type Col-0 seed was surface sterilized with 12.5 % bleach (Aqualon) and 70 % ethanol and germinated on 1/2 MS medium (16-h daylight, 22 °C). To measure expression of the *OAT* gene during germination and early development, total RNA was isolated from whole seedlings at 4th, 7th and 14th DAS. For experimental treatments, one-week seedlings were transferred to 1/2 MS medium supplemented with different growth regulators (1 mg/L NAA, 2 mg/L IAA, 0.5 mg/L 2,4-D, 1 mg/L 6-BAP, 50 μ M ACC), and control, to 1/2 MS medium. For each treatment, experiment was performed in three biological replicates. There were 30 seedlings per each biological replicate. Total RNA was isolated from roots of seedlings after 6 days of treatment with the RNeasy Plant Mini Kit (Qiagen). RNA was treated with DNase (QIAGEN RNase-Free DNase Set). The concentration of RNA was measured by NanoDrop 2000 (Thermo Scientific). The quality of RNA was evaluated using Bioanalyzer 2100 (Agilent). First strand cDNA was synthesized from 1 μ g of total RNA using BIORAD iScript™ Reverse Transcription Supermix for RT-qPCR. For qRT-PCR analysis, cDNA was diluted ten times. PCR was performed in a final volume of 15 μ L: 3 μ L of 5x Low Rox buffer (SibEnzyme), 0.15 μ L of each primer (10 μ M) and the taqman probe solution, 3 μ L of diluted

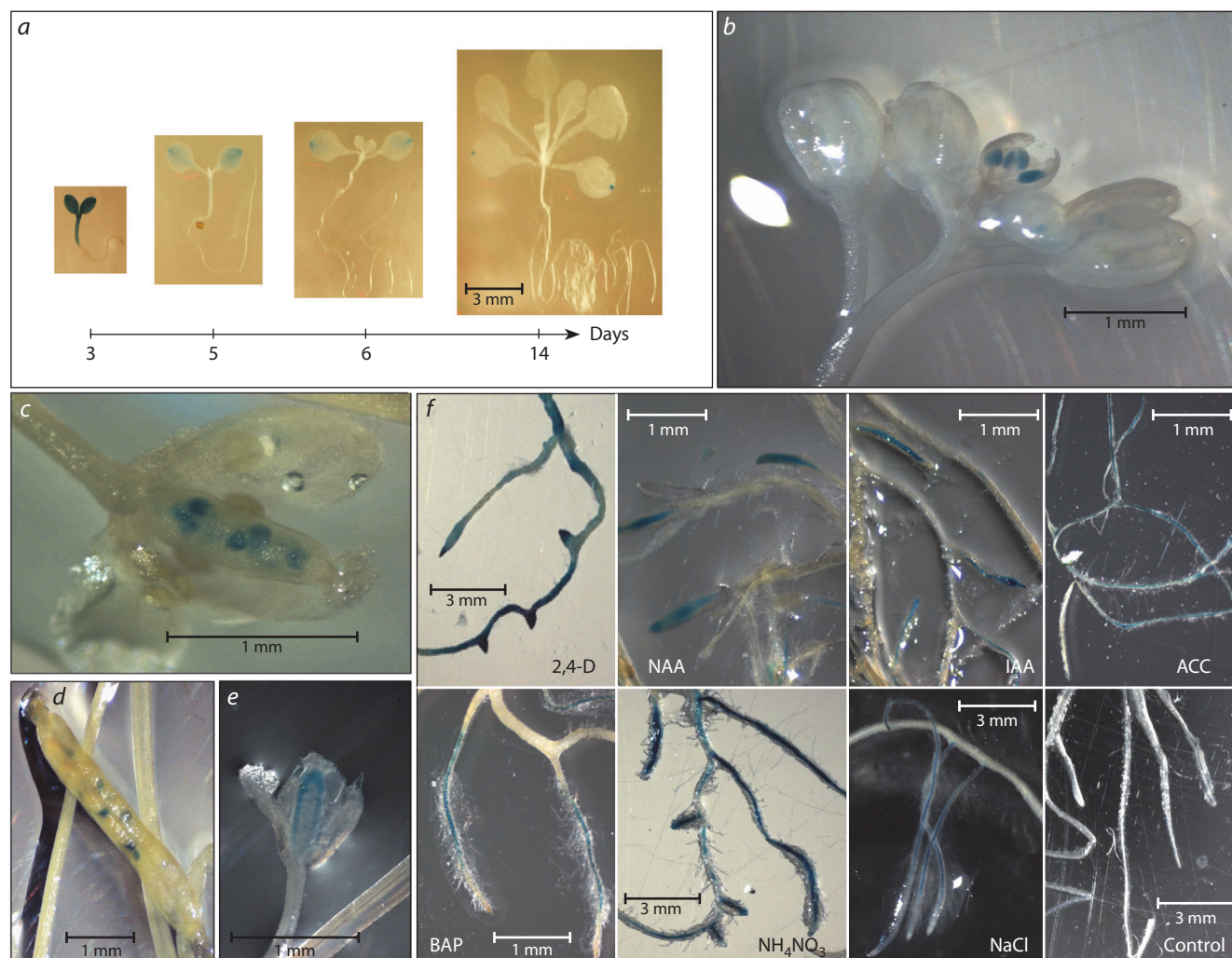


Fig. 1. Histochemical GUS analysis of transgenic *A. thaliana* lines:

a–e, tissue-specific GUS expression during plant development: *a*, different stages of seedling development; *b*, GUS expression in immature anthers; *c*, GUS expression in ovules; *d*, developing silique with GUS expression in seeds; *e*, developing carpel; *f*, roots of plants treated with different inducers. Age of plants on pictures *b–e* – 1.5 months, on picture *f* – 13 days.

cDNA. The primers and probes were designed using IDT's PrimerQuest Tool (<https://eu.idtdna.com/PrimerQuest/>). The comparative threshold cycle method was used to determine relative gene expression, with the expression of EF1- α and F-box (accession no. At1g13320 and At5g15710) serving as an internal control. The structures of primers and probes are given in Suppl. Table 1¹. The relative expression levels of *OAT* mRNA in all the treated samples were quantified using an Applied biosystems 7500 Real Time PCR System. Each reaction was performed in three technical replicates using the following program of the qRT-PCR; 95 °C for 10 min; 45 cycles of 95 °C for 15 s, 68 °C for 60 s. Statistical analysis was performed using Student's *t*-test. *p*-values < 0.05 were considered significant.

Web tools used for cis-acting regulatory DNA elements search and expression data analysis. Search of cis-acting regulatory elements was performed using the PLACE database (Higo et al., 1999). Gene expression data from different

microarray and RNA-seq experiments were extracted from Expression Atlas and Arabidopsis eFP Browser Web tools (Winter D. et al., 2007; Papatheodorou et al., 2018).

Results

Tissue-specific promoter activation at different developmental stages and under experimental treatments. Strong GUS staining was detected in hypocotyls and cotyledons of seedlings at 3–4th DAS. At later stages, the GUS activity was observed only in cotyledons. In 6- and 14- DAS seedlings, the GUS activity was found only in the distal parts of cotyledons (Fig. 1). During flower development, the GUS activity was observed in anthers, carpels and developing seeds of growing siliques (see Fig. 1, Suppl. Table 2).

To get a deeper insight into the transcriptional regulation of *OAT*, transgenic seedlings were subjected to experimental treatments including different concentrations of growth regulators and phytohormones auxins, cytokinins, gibberellin, ABA, methyl jasmonate, ethylene precursor (ACC), low and high nitrogen, high salinity, cold and heat stress (see Fig. 1, Suppl.

¹ Supplementary Tables 1–4 are available in the online version of the paper: <http://www.bionet.nsc.ru/vogis/download/pict-2022-26/appx4.pdf>

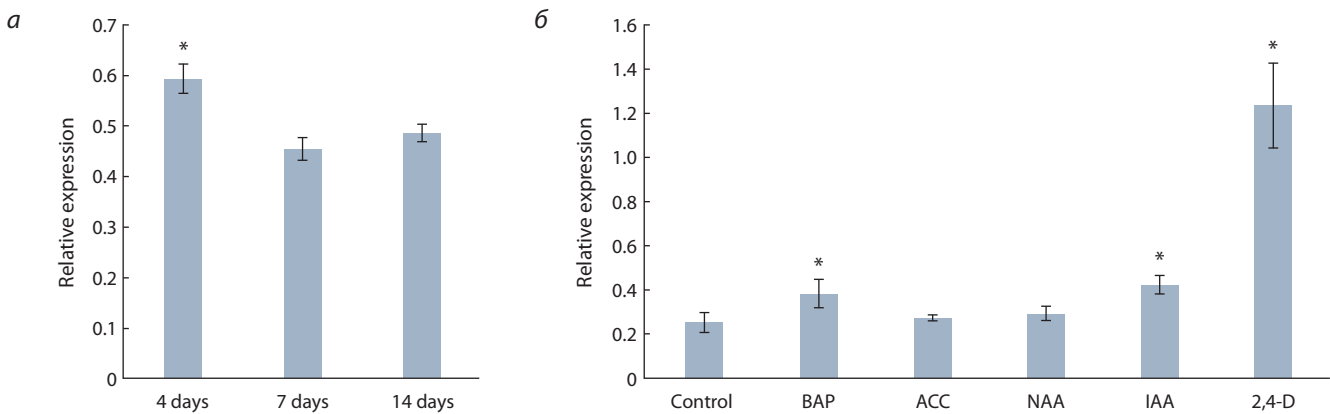


Fig. 2. The relative expression of *OAT*: *a*, in whole 4-, 7- and 14-days seedlings; *b*, in roots of seedlings, which were grown for 6 days on medium with inducers.

An asterisk indicates statistical significance in a one-way ANOVA ($p \leq 0.05$). Each bar represents the mean of three biological replicates \pm SE.

Table 2). We observed tissue-specific *OAT* promoter activity in response to different forms of auxin (IAA, NAA, and 2,4-D), cytokinin (6-BAP), and ACC. The strongest GUS activity was observed in response to 2,4-D in whole plant. Treatment with IAA and NAA caused GUS activation in root tips; treatment with 6-BAP – in the zone of root hairs. Treatment with ACC, salinity and nitrogen activated promoter along the whole root.

***OAT* gene expression analysis.** The qRT-PCR results showed that transcript levels of the *OAT* gene are significantly higher in four-day-old seedlings, than at later developmental stages (Fig. 2, *a*). In experimental treatments, the *OAT* gene showed significantly ($p \leq 0.05$) elevated expression in response to different forms of auxin (IAA and 2,4-D) and cytokinin (6-BAP) in comparison to control conditions. Treatment with synthetic auxin 2,4-D led to 3-fold increase in *OAT* expression level in roots (see Fig. 2, *b*).

Cis-acting regulatory DNA elements search and transcriptomic data analysis. Cis-acting regulatory DNA elements search revealed putative transcription factors binding sites, corresponding to different physiological processes, including hyperosmotic and hypoosmotic stress response, auxin response, axillary bud dormancy control, specific regulation in ontogenesis (Suppl. Table 3). Meta-analysis of microarray and RNA-seq data (Winter D. et al., 2007; Papatheodorou et al., 2018) shows that the *OAT* expression level changes in response to cold, drought, heat, wounding, osmotic and salt stress. Expression increases in response to pathogens *Botrytis cinerea*, *Pseudomonas syringae*, *Phytophthora infestans* and some other infections. Altered *OAT* gene expression was observed in response to different hormones: it increased in response to 3 h of treatment with ABA, methyl jasmonate, and decreased in response to 3 h of treatment with brassinosteroids. The *OAT* gene demonstrates high expression in seeds, siliques, embryos, senescent leaves, floral organs in *A. thaliana* (Suppl. Table 4).

Discussion

For more than a decade *OAT* has been considered an enzyme involved in metabolic response to different stress conditions, such as osmotic stress, pathogen attack and ROS production, nitrogen starvation, etc. (Funck et al., 2008; Verslues, Sharma, 2010; Qamar et al., 2015). This enzyme belongs to the net-

work of nitrogen-metabolizing pathways in plants, affected by various environmental stimuli. It has been shown that plants accumulate proline during stress conditions (Verbruggen, Hermans, 2008). The results of Funck et al. (2008) and our previous study did not support the hypothesis of *OAT* contribution to proline accumulation. Instead, a specific role of the *OAT* gene in plant developmental and growth processes under both normal and stress conditions is hypothesized (Gerasimova et al., 2010, 2011a). This study provides a deeper insight into the role of the *OAT* gene in plant development.

The important metabolic role of the *OAT* was clearly shown in an experiment where *OAT*-deficient plants failed to develop with arginine or ornithine as the sole nitrogen source (Funck et al., 2008). This result demonstrated that *OAT* is required for utilization of arginine and ornithine. The present study demonstrates high *OAT* promoter activity and elevated *OAT* transcript level during seed germination. These results are in agreement with available transcriptomic data (Winter D. et al., 2007). In arginine catabolism, *OAT* acts downstream of arginase (Funck et al., 2008). Arginine is regarded as a major nitrogen storage compound in seeds. Urease and arginase activities increase sharply during germination in *A. thaliana* (Zonia et al., 1995) and other plant species (Winter G. et al., 2015). Taken together, these data provide evidence for *OAT* involvement in nitrogen reorganization during seed germination together with other enzymes of arginine catabolism.

Our work also shows that the *OAT* gene promoter is active during inflorescence development. This observation is in accordance with recent findings showing that the *OAT* enzyme plays a role in flower development and seed setting in rice (Liu et al., 2018). It has been reported that rice plants with a mutated *OAT* gene (*OsOAT* mutants) have different abnormalities in inflorescence and seed development. The mutant phenotype of the *OsOAT* mutant could be rescued by application of urea (Liu et al., 2018). Authors assumed that *OAT* mediates arginase activity and plays a role in regulation of nitrogen reutilization, which is critical for developing tissues (Liu et al., 2018).

Taking into account the association between the *OAT* gene expression and proline accumulation (Roosens et al., 1998, 2002; Wu et al., 2003), it can be assumed that *OAT* enzyme

activity may also play a role in control of proline level during inflorescence development. It has been reported that some proline metabolic enzymes can regulate a number of developmental processes including flowering time (Mattioli et al., 2008), pollen development (Mattioli et al., 2012; Biancucci et al., 2015a) and root growth (Biancucci et al., 2015b). Proline is known to be accumulated in reproductive organs of many plant species (Kavi Kishor et al., 2015). Ornithine to proline conversion is mediated by the plant oncogene RolD (Trovato et al., 2001), the overexpression of which stimulates flowering and affects inflorescence architecture in transgenic tobacco plants (Mauro et al., 1996). This study shows that the *OAT* promoter is active in inflorescences on different developmental stages (see Fig. 1), suggesting that the *OAT* enzyme can convert ornithine to proline directly or indirectly via arginine catabolism and glutamate production and might serve as a regulator of proline level during inflorescence development.

Tissue-specific activation of the *OAT* transcription in roots in response to auxin and cytokinin treatments, as well as the presence of the auxin-responsive element in the *OAT* promoter (see Suppl. Table 3) allow us to assume specific regulation of the *OAT* gene during root growth and development. Recent findings show the importance of nutrient and especially nitrogen signaling for root development and its interplay with hormone regulation. Thus, cytokinins negatively regulate uptake of nitrogen, but enhance nitrate distribution and translocation (Gu et al., 2018). Auxin level was shown to be elevated in roots of plants growing on a low-nitrogen medium, while in roots of plants growing on a medium with high nitrate concentration the auxin level was decreased. The reduction of auxin content correlated with the degree of inhibition of root growth and lateral root development (Kiba et al., 2011). The root growth regulation is associated with local reorganization of nitrogen metabolism (Kiba, Krapp, 2016). Thereby, *OAT* may play an important role in hormone-dependent fine-tuning of nitrogen metabolism during the process of root development.

Conclusion

The data regarding the *OAT* transcription activation in a wide spectrum of experimental conditions, which was shown in our experiment and other studies, support the hypothesis that ornithine aminotransferase provides a link between different biochemical pathways of nitrogen conversion and contributes to the complicated signaling network regulating plant development.

References

Ballas N., Wong L.M., Theologis A. Identification of the auxin-responsive element, *AuxRE*, in the primary indoleacetic acid-inducible gene, *PS-IAA4/5*, of pea (*Pisum sativum*). *J. Mol. Biol.* 1993;233:580-596. DOI 10.1006/jmbi.1993.1537.

Biancucci M., Mattioli R., Forlani G., Funck D., Costantino P., Trovato M. Role of proline and GABA in sexual reproduction of angiosperms. *Front. Plant Sci.* 2015a;6:680. DOI 10.3389/fpls.2015.00680.

Biancucci M., Mattioli R., Moubayidin L., Sabatini S., Costantino P., Trovato M. Proline affects the size of the root meristematic zone in *Arabidopsis*. *BMC Plant Biol.* 2015b;15:263. DOI 10.1186/s12870-015-0637-8.

Clough S.J., Bent A.F. Floral dip: a simplified method for *Agrobacterium*-mediated transformation of *Arabidopsis thaliana*. *Plant J.* 1998;16:735-743. DOI 10.1046/j.1365-3113.1998.00343.x.

Funck D., Stadelhofer B., Koch W. Ornithine-delta-aminotransferase is essential for arginine catabolism but not for proline biosynthesis. *BMC Plant Biol.* 2008;8:40. DOI 10.1186/1471-2229-8-40.

Gerasimova S.V., Gorelova V.V., Dorogina O.V., Zhmud E.V., Koval V.S., Romanova A.V., Kochetov A.V., Shumny V.K. Analysis of transcriptional activity of the *Arabidopsis thaliana* ornithine-delta-aminotransferase gene promoter. *Russ. J. Genet.* 2011a;47:625-628. DOI 10.1134/S1022795411050073.

Gerasimova S.V., Kochetov A.V., Ibragimova S.S., Shumnyi V.K. Functions of delta-ornithine aminotransferase in plants. *Uspekhi Sovremennoi Biologii = Advances in Current Biology.* 2011b;131:531-542. (in Russian)

Gerasimova S.V., Kolodyazhnaya Y.S., Titov S.E., Romanova A.V., Koval V.S., Kochetov A.V., Shumnyi V.K. Tobacco transformants expressing the *Medicago truncatula* ornithine aminotransferase cDNA. *Russ. J. Genet.* 2010;46(7):890-893. DOI 10.1134/S102279541007015X.

Gilles L., Bluteau D., Boukour S., Chang Y., Zhang Y., Robert T., Dessen P., Debili N., Bernard O.A., Vainchenker W., Raslova H. MAL/SRF complex is involved in platelet formation and megakaryocyte migration by regulating MYL9 (MLC2) and MMP9. *Blood.* 2009;114(19):4221-4232. DOI 10.1182/blood-2009-03-209932.

Ginguy A., Cynober L., Curis E., Nicolis I. Ornithine aminotransferase, an important glutamate-metabolizing enzyme at the crossroads of multiple metabolic pathways. *Biology.* 2017;6(1):18. DOI 10.3390/biology6010018.

Gu J., Li Z., Mao Y., Struik P.C., Zhang H., Liu L., Wang Z., Yang J. Roles of nitrogen and cytokinin signals in root and shoot communications in maximizing of plant productivity and their agronomic applications. *Plant Sci.* 2018;274:320-331. DOI 10.1016/j.plantsci.2018.06.010.

Hayat S., Hayat Q., Alyemeni M.N., Wani A.S., Pichtel J., Ahmad A. Role of proline under changing environments. *Plant Signal. Behav.* 2012;7:1456-1466. DOI 10.4161/psb.21949.

Higo K., Ugawa Y., Iwamoto M., Korenaga T. Plant cis-acting regulatory DNA elements (PLACE) database: 1999. *Nucleic Acids Res.* 1999;27:297-300. DOI 10.1093/nar/27.1.297.

Jefferson R.A., Kavanagh T.A., Bevan M.W. GUS fusions: beta-glucuronidase as a sensitive and versatile gene fusion marker in higher plants. *EMBO J.* 1987;6:3901-3907. DOI 10.1073/pnas.1411926112.

Kavi Kishor P.B., Kumari P.H., Sunita M.S.L., Sreenivasulu N. Role of proline in cell wall synthesis and plant development and its implications in plant ontogeny. *Front. Plant Sci.* 2015;6:544. DOI 10.3389/fpls.2015.00544.

Kiba T., Krapp A. Plant nitrogen acquisition under low availability: regulation of uptake and root architecture. *Plant Cell Physiol.* 2016;57:707-714. DOI 10.1093/pcp/pcw052.

Kiba T., Kudo T., Kojima M., Sakakibara H. Hormonal control of nitrogen acquisition: roles of auxin, abscisic acid, and cytokinin. *J. Exp. Bot.* 2011;62:1399-1409. DOI 10.1093/jxb/erq410.

Kochetov A.V., Titov S.E., Kolodyazhnaya Y.S., Komarova M.L., Koval V.S., Makarova N.N., Ilyinskiy Y.Y., Trifonova E.A., Shumny V.K. Tobacco transformants bearing antisense suppressor of proline dehydrogenase gene are characterized by higher proline content and cytoplasm osmotic pressure. *Russ. J. Genet.* 2004;40:216-218. DOI 10.1023/B:RUGE.0000016999.53466.e1.

Liu C., Xue Z., Tang D., Shen Y., Shi W., Ren L., Li Y., Cheng Z. Ornithine δ -aminotransferase is critical for floret development and seed setting through mediating nitrogen reutilization in rice. *Plant J.* 2018;96:842-854. DOI 10.1111/tj.14072.

Majumdar R., Minocha R., Minocha S.C. Ornithine: at the crossroads of multiple paths to amino acids and polyamines. In: D'Mello J.P.F. (Ed.) *Amino Acids in Higher Plants*. Ch. 9. Oxfordshire, UK: CABI, 2015;156-176.

Mattioli R., Biancucci M., Lonoce C., Costantino P., Trovato M. Proline is required for male gametophyte development in *Arabidopsis*. *BMC Plant Biol.* 2012;12:236. DOI 10.1186/1471-2229-12-236.

- Mattioli R., Marchese D., D'Angeli S., Altamura M.M., Costantino P., Trovato M. Modulation of intracellular proline levels affects flowering time and inflorescence architecture in *Arabidopsis*. *Plant Mol. Biol.* 2008;66:277-288. DOI 10.1007/s11103-007-9269-1.
- Mauro M.L., Trovato M., De Paolis A., Gallelli A., Costantino P., Altamura M.M. The plant oncogene rolD stimulates flowering in transgenic tobacco plants. *Dev. Biol.* 1996;180:693-700. DOI 10.1006/dbio.1996.0338.
- Papatheodorou I., Fonseca N.A., Keays M., Tang Y.A., Barrera E., Bazant W., Burke M., Füllgrabe A., Fuentes A.M.-P., George N., Huerta L., Koskinen S., Mohammed S., Geniza M., Preece J., Jaiswal P., Jarnuczak A.F., Huber W., Stegle O., Vizcaino J.A., Brazma A., Petryszak R. Expression Atlas: gene and protein expression across multiple studies and organisms. *Nucleic Acids Res.* 2018;46:D246-D251. DOI 10.1093/nar/gkx1158.
- Qamar A., Mysore K.S., Senthil-Kumar M. Role of proline and pyrroline-5-carboxylate metabolism in plant defense against invading pathogens. *Front. Plant Sci.* 2015;6:503. DOI 10.3389/fpls.2015.00503.
- Roosens N.H., Al Bitar F., Loenders K., Angenon G., Jacobs M. Overexpression of ornithine- δ -aminotransferase increases proline biosynthesis and confers osmotolerance in transgenic plants. *Mol. Breed.* 2002;9:73-80. DOI 10.1023/A:1026791932238.
- Roosens N.H., Thu T.T., Iskandar H.M., Jacobs M. Isolation of the ornithine- δ -aminotransferase cDNA and effect of salt stress on its expression in *Arabidopsis thaliana*. *Plant Physiol.* 1998;117:263-271. DOI 10.1104/pp.117.1.263.
- Satoh R., Nakashima K., Seki M., Shinozaki K., Yamaguchi-Shinozaki K. ACTCAT, a novel cis-acting element for proline- and hypoosmolarity-responsive expression of the *ProDH* gene encoding proline dehydrogenase in *Arabidopsis*. *Plant Physiol.* 2002;130:709-719. DOI 10.1104/pp.009993.
- Suzuki M., Ketterling M.G., McCarty D.R. Quantitative statistical analysis of cis-regulatory sequences in ABA/VP1- and CBF/DREB1-regulated genes of *Arabidopsis*. *Plant Physiol.* 2005;139:437-447. DOI 10.1104/pp.104.058412.
- Tatematsu K., Ward S., Leyser O., Kamiya Y., Nambara E. Identification of cis-elements that regulate gene expression during initiation of axillary bud outgrowth in *Arabidopsis*. *Plant Physiol.* 2005;138(2):757-766. DOI 10.1104/pp.104.057984.
- Trovato M., Maras B., Linhares F., Costantino P. The plant oncogene *rolD* encodes a functional ornithine cyclodeaminase. *Proc. Natl. Acad. Sci. USA.* 2001;98:13449-13453. DOI 10.1073/pnas.231320398.
- Verbruggen N., Hermans C. Proline accumulation in plants: a review. *Amino Acids.* 2008;35(4):753-759. DOI 10.1007/s00726-008-0061-6.
- Verslues P.E., Sharma S. Proline metabolism and its implications for plant-environment interaction. *Arabidopsis Book.* 2010;8:e0140. DOI 10.1199/tab.0140.
- Winter D., Vinegar B., Nahal H., Ammar R., Wilson G.V., Provart N.J. An "Electronic Fluorescent Pictograph" browser for exploring and analyzing large-scale biological data sets. *PLoS One.* 2007;2(8):e718. DOI 10.1371/journal.pone.0000718.
- Winter G., Todd C.D., Trovato M., Forlani G., Funck D. Physiological implications of arginine metabolism in plants. *Front. Plant Sci.* 2015;6:534. DOI 10.3389/fpls.2015.00534.
- Wu L., Fan Z., Guo L., Li Y., Zhang W., Qu L.J., Chen Z. Over-expression of an *Arabidopsis* δ -*OAT* gene enhances salt and drought tolerance in transgenic rice. *Chinese Sci. Bull.* 2003;48:2594-2600. DOI 10.1360/03wc0218.
- Zonia L.E., Stebbins N.E., Polacco J.C. Essential role of urease in germination of nitrogen-limited *Arabidopsis thaliana* seeds. *Plant Physiol.* 1995;107:1097-1103. DOI 10.1104/pp.107.4.1097.

ORCID ID

A.A. Egorova orcid.org/0000-0002-6745-3077
S.V. Gerasimova orcid.org/0000-0001-8626-1831
A.V. Kochetov orcid.org/0000-0003-3151-5181

Author contributions. S.V. Gerasimova, A.A. Egorova designed and performed the experiment, analyzed the data, wrote the manuscript, A.V. Kochetov coordinated the project.

Acknowledgements. We thank Vera Gorelova for help in conducting the experiments and writing the manuscript. The work is supported by the Ministry of Science and Higher Education of Russian Federation (FWNR-2022-0017).

Conflict of interest. The authors declare no conflict of interest.

Received October 28, 2021. Revised January 20, 2022. Accepted January 21, 2022.

Original Russian text www.bionet.nsc.ru/vogis/

Estradiol-dependent and independent effects of FGF21 in obese female mice

T.V. Jakovleva¹✉, A.Yu. Kazantseva¹, A.D. Dubinina¹, N.Yu. Balybina¹, K.O. Baranov², E.N. Makarova¹, N.M. Bazhan^{1,3}

¹ Institute of Cytology and Genetics of the Siberian Branch of the Russian Academy of Sciences, Novosibirsk, Russia

² Institute of Molecular and Cellular Biology of the Siberian Branch of the Russian Academy of Sciences, Novosibirsk, Russia

³ Novosibirsk State University, Novosibirsk, Russia

✉ tatanajakovleva@yandex.ru

Abstract. The fibroblast growth factor 21 (FGF21) synthesized in the liver, acting as a hormone, increases insulin sensitivity and energy expenditure. FGF21 administration has potent beneficial effects on obesity and diabetes in humans, cynomolgus monkey, and rodents. The therapeutic effects of FGF21 have been studied mainly in males. They are not always manifested in females, and they are accompanied by sex-specific activation of gene expression in tissues. We have suggested that one of the causes of sexual dimorphism in response to FGF21 is the effect of estradiol (E2). Currently, it is not known how estradiol modifies the pharmacological effects of FGF21. The objective of this study was to study the influence of FGF21 on metabolic characteristics, food intake, and the expression of carbohydrate and fat metabolism genes in the liver, adipose tissue, and hypothalamus in female mice with alimentary obesity and low (ovariectomy) or high (ovariectomy + E2) blood estradiol level. In ovariectomized (OVX) females, the development of obesity was induced by the consumption of a high sweet-fat diet (standard chow, lard, and cookies) for 8 weeks. We investigated the effects of FGF21 on body weight, blood levels, food preferences and gene expression in tissues when FGF21 was administered separately or in combination with E2 for 13 days. In OVX obese females, FGF21, regardless of E2-treatment, did not affect body weight, and adipose tissue weight, or glucose tolerance but increased the consumption of standard chow, reduced blood glucose levels, and suppressed its own expression in the liver (*Fgf21*), as well as the expression of the *G6pc* and *Acaca* genes. This study is the first to show the modification of FGF21 effects by estradiol: inhibition of FGF21-influence on the expression of *Irs2* and *Pklr* in the liver and potentiation of the FGF21-stimulated expression of *LepR* and *Klb* in the hypothalamus. In addition, when administered together with estradiol, FGF21 exerted an inhibitory effect on the expression of *Cpt1a* in subcutaneous white adipose tissue (scWAT), whereas no stimulating FGF21 effects on the expression of *Insr* and *Acacβ* in scWAT or inhibitory FGF21 effect on the plasma insulin level were observed. The results suggest that the absence of FGF21 effects on body and adipose tissue weights in OVX obese females and its beneficial effect on food intake and blood glucose levels are not associated with the action of estradiol. However, estradiol affects the transcriptional effects of FGF21 in the liver, white adipose tissue, and hypothalamus, which may underlie sex differences in the FGF21 effect on the expression of metabolic genes and, possibly, in pharmacological FGF21 effects.

Key words: FGF21; estradiol; liver; adipose tissue; food preference; gene expression; sex differences.

For citation: Jakovleva T.V., Kazantseva A.Yu., Dubinina A.D., Balybina N.Yu., Baranov K.O., Makarova E.N., Bazhan N.M. Estradiol-dependent and independent effects of FGF21 in obese female mice. *Vavilovskii Zhurnal Genetiki i Selektzii* = *Vavilov Journal of Genetics and Breeding*. 2022;26(2):159-168. DOI 10.18699/VJGB-22-20

Зависимые и независимые от уровня эстрадиола эффекты FGF21 у самок мышей с ожирением

Т.В. Яковлева¹✉, А.Ю. Казанцева¹, А.Д. Дубинина¹, Н.Ю. Балыбина¹, К.О. Баранов², Е.Н. Макарова¹, Н.М. Бажан^{1,3}

¹ Федеральный исследовательский центр Институт цитологии и генетики Сибирского отделения Российской академии наук, Новосибирск, Россия

² Институт молекулярной и клеточной биологии Сибирского отделения Российской академии наук, Новосибирск, Россия

³ Новосибирский национальный исследовательский государственный университет, Новосибирск, Россия

✉ tatanajakovleva@yandex.ru

Аннотация. Синтезируемый в печени фактор роста фибробластов 21 (FGF21), действуя как гормон, повышает чувствительность к инсулину и расход энергии. Введение FGF21 оказывает мощное благотворное воздействие у людей, обезьян и грызунов с ожирением и диабетом второго типа. Терапевтические эффекты FGF21 исследованы главным образом на самцах, они не всегда проявляются у самок и сопровождаются половой специфической активацией экспрессии генов в тканях. Мы предположили, что одной из причин полового диморфизма в ответе на FGF21 является действие эстрадиола (E2). В настоящее время неизвестно, как эстрадиол

влияет на проявление фармакологических эффектов FGF21. Задачей данного исследования было изучение влияния FGF21 на метаболические характеристики, потребление пищи и экспрессию генов углеводного и жирового обмена в печени, жировой ткани и гипоталамусе у самок мышей с алиментарным ожирением на фоне низкого (овариэктомия) и высокого (овариэктомия + E2) уровня эстрадиола в крови. У овариэктомизированных самок развитие ожирения индуцировали потреблением сладко-жирной диеты (стандартный корм, сало, печень) в течение 8 недель. Мы оценили эффекты FGF21 на массу тела, показатели крови, выбор компонентов диеты, экспрессию генов в тканях при раздельном и совместном введении с E2 в течение 13 дней. У овариэктомизированных самок с ожирением FGF21, независимо от введения E2, не влиял на массу тела и жировой ткани, толерантность к глюкозе, повышал потребление стандартного корма, снижал уровень глюкозы в крови, подавлял в печени собственную экспрессию (*Fgf21*), а также экспрессию генов *Gbpc* и *Acaca*. Впервые показано влияние эстрадиола на эффекты FGF21: ингибирование FGF21-влияния на экспрессию *Irs2* и *Pklr* в печени и потенцирование FGF21-стимулированной экспрессии *LepR* и *Klb* в гипоталамусе. Кроме того, на фоне введения эстрадиола не проявлялось ингибирующее влияние FGF21 на уровень инсулина в крови, а в подкожной белой жировой ткани проявлялось ингибирующее влияние FGF21 на экспрессию *Cpt1a* и не проявлялось активирующее влияние FGF21 на экспрессию генов *Insr* и *Acacβ*. Полученные данные позволяют заключить, что у овариэктомизированных самок с ожирением отсутствие эффектов FGF21 на массу тела и жировой ткани и его благотворное влияние на потребление пищи и уровень глюкозы в крови не связаны с действием эстрадиола. Однако эстрадиол влияет на транскрипционные эффекты FGF21 в печени, белом жире и гипоталамусе, что может лежать в основе половых различий в его действии на экспрессию метаболических генов и, возможно, половых различий его фармакологических эффектов.

Ключевые слова: FGF21; эстрадиол; печень; жировая ткань; пищевое предпочтение; экспрессия генов; половые различия.

Introduction

Fibroblast growth factor 21 (FGF21) is synthesized in the liver, secreted into blood and acts as a hormone (Kharitonov et al., 2005). Its level increases significantly at metabolic stress; specifically, in the cold, fasting, and obesity (Fisher et al., 2011). FGF21 is involved in the regulation of carbohydrate-lipid metabolism. Its pharmacological doses improve metabolic parameters in animals and people with obesity: they increase energy expenditure and insulin sensitivity and reduce blood glucose levels (Kharitonov et al., 2005; Coskun et al., 2008). In addition, FGF21 affects taste preferences: it reduces the consumption of sweets and alcohol and increases protein consumption (Talukdar et al., 2016; Allard et al., 2019; Larson et al., 2019).

Currently, FGF21 and its synthetic analogues are used in designing drugs for the treatment of metabolic syndrome in obesity. However, the vast majority of preclinical studies of its pharmacological action were performed on males. Our studies of the effect of FGF21 in mice showed that its pharmacological effects in females and males might differ. In female C57Bl mice with obesity induced by the consumption of high sweet-fat diet, FGF21 reduced body weight, but, unlike males, did not affect glucose tolerance or the expression of metabolic genes in the liver or in brown adipose tissue (Bazhan et al., 2019). In obese C57Bl mice fed a mixture of high-fat and standard diets, administration of FGF21 improved some metabolic indices in mice of both sexes but induced female-specific activation of gene expression in abdominal adipose tissue (Makarova et al., 2021). In female *A^y* mice with genetically induced obesity, unlike males, FGF21 did not affect body weight, blood insulin levels, or POMC expression in the hypothalamus, but increased food intake and liver weight and modified the expression of metabolic genes in the liver and in white adipose tissue (Makarova et al., 2020).

The causes of the sex differences in the pharmacological effects of FGF21 are still unknown. We assumed that sex differences in responses to FGF21 were associated with the influence of estrogens. Estradiol and FGF21 exert similar effects on metabolic parameters. Estradiol, like FGF21, reduces food intake, body weight, blood glucose and insulin levels and increases glucose tolerance in ovariectomized and intact obese females (Gao et al., 2006; Thammacharoen et al., 2009). According to the available data, estradiol and FGF21 have different receptors and the same signaling pathways (Fisher et al., 2011; Vrtačnik et al., 2014). In addition, estradiol can affect the level of FGF21 in blood. The expression of *Fgf21* in the liver determines the blood hormone level and depends on the stage of the estrous cycle, positively correlating with the blood level of estradiol (Hua et al., 2018). Exogenous estradiol can also stimulate the expression of *Fgf21* in the liver and increase the blood FGF21 level (Allard et al., 2019).

We suggested that FGF21 and estradiol interact in the regulation of carbohydrate-lipid metabolism, and the pharmacological effects of FGF21 depend on the blood estradiol level. Therefore, the aim of this study was to compare the effects of FGF21 on metabolic parameters, food choice, and the expression of genes involved in carbohydrate and fat metabolism in the liver, adipose tissue, and hypothalamus in female mice with alimentary obesity and different levels of estrogenic activity.

Materials and methods

Animals. All experiments were performed according to the Guide for the Care and Use of Laboratory Animals (1996) and the Russian National Guidelines for the Care and Use of Laboratory Animals.

Female mice of C57BL/6J strain were kept at the vivarium for conventional animals of the Institute of Cytology and Ge-

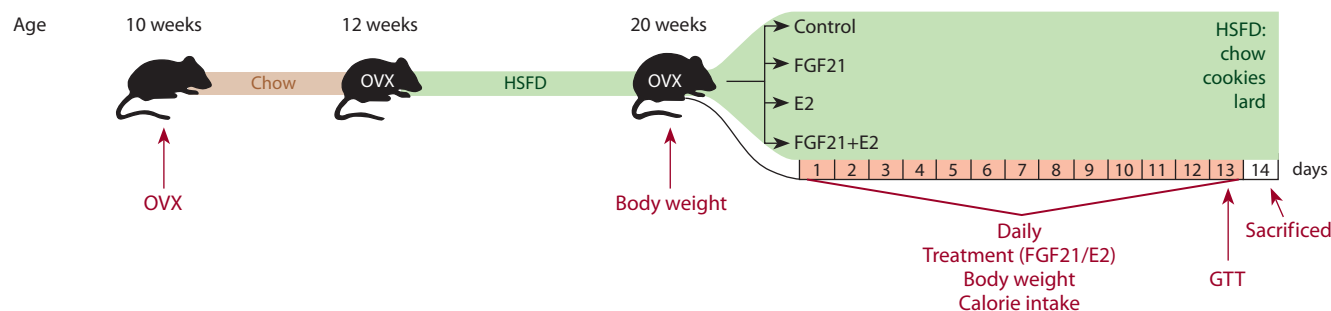


Fig. 1. Scheme of the experiment.

OVX – ovariectomy; GTT – glucose tolerance test; Chow – *ad libitum* access to commercial mouse chow; HSF – high sweet fat diet (standard laboratory chow, sweet cookies, lard); Treatment – ovariectomized females with diet-induced obesity received fibroblast growth factor 21 (FGF21) at a dose of 1 mg per 1 kg of body weight subcutaneously and estradiol (E2) at a dose of 20 mg/animal orally separately or together for 13 days. Control females received subcutaneously phosphate buffered saline (PBS) and oil orally.

netics, Novosibirsk. The mice were housed at the 12-h/12-h light/dark regime (light from 07:30 to 19:30) at the ambient temperature 22–24 °C and free access to water and food. At the age of 10 weeks, all females were ovariectomized. To induce obesity, mice were fed with mixed diet, which consisted of standard laboratory chow, sweet cookies and lard, for two weeks after surgery. The animals consumed this diet for 8 weeks before and during the entire period (2 weeks) of drug administration (Fig. 1).

Mouse recombinant FGF21 (1 mg per 1 kg) dissolved in Phosphate Buffered Saline (PBS) or PBS itself were injected subcutaneously ($V \approx 200 \mu\text{L}$) at the end of the light period (17:00–19:00) for 13 days. The expression and purification of mouse FGF21 were performed by Dr. Baranov, as described earlier (Makarova et al., 2021). Estradiol (E2 Sigma, USA, 20 $\mu\text{g}/\text{animal}$) dissolved in oil or oil itself were administered orally ($V = 100 \mu\text{L}$) at the same time as FGF21.

Obese ovariectomized female mice were randomly divided into four experimental groups (6–8 animals per group): (1) control females, which received vehicles (oil and PBS); (2) FGF21-females, which received FGF21 and oil; (3) E2-females, which received E2 and PBS; and (4) FGF21+E2-females, which received both FGF21 and E2.

The glucose tolerance test (GTT) was performed on day 13 of the experiment, after which each group received the last due treatment with drugs or solvents. One day after the last treatment, the females were weighed and decapitated (14:00–16:00). E2 increased the uterus weight ($43.5 \pm 6.5 \text{ mg}$ without estradiol ($n = 15$) vs $114.0 \pm 8.6 \text{ mg}$ ($n = 12$) after E2-treatment, $p < 0.001$ Student test), indicating the effectiveness of the selected dose of the hormone. After decapitation, liver, subcutaneous (scWAT) white adipose tissue, abdominal (abWAT) white adipose tissue, and brown adipose tissue (BAT) were excised and immediately weighed. Blood and tissue samples were taken. Tissue samples for gene expression assays were immediately frozen in liquid nitrogen and stored until RNA isolation.

Diet. Standard chow was purchased from BioPro (Novosibirsk, Russia). The energy value of chow diet was 250 kcal/100 g. Pork lard and cookies were bought in a food store. The

energy value of cookies was 458 kcal/100 g. The energy value of lard (subcutaneous fat) was 800 kcal/100 g. The number of calories consumed with each component of the diet was calculated as the weight of the component in grams multiplied by the energy value of the component. The percentage of calories consumed with each component of the diet (share of total) was calculated as the number of calories consumed by the female with the component divided by the total number of calories consumed and multiplied by 100.

Ovariectomy. The animals were anesthetized by an intraperitoneal injection of 2.5 % avertin (a mixture of 2,2,2-tribromethanol (Sigma-Aldrich Inc., USA) and 2-methyl-2-butanol (Sigma-Aldrich Inc.) in the volume 400 μL . Bilateral ovariectomy was performed through a skin incision in the lumbar region.

Glucose tolerance test (GTT). Before the test, food was removed from the animals at 08:00, and the test started at 15:00. Animals were injected with glucose (AO REACHEM, Moscow, Russia) intraperitoneally at the dose 1 g/kg body weight. Blood glucose concentrations were measured using a Lifescan One Touch Basic Plus glucometer (LifeScan Inc., Switzerland) before glucose administration (fasting glucose) and 15, 30, 60, and 120 minutes after glucose administration. The Area Under the Curve (AUC) was presented as $\text{mmol/L} \times \text{hour}$.

Plasma assays. Concentrations of insulin, leptin, adiponectin, and corticosterone were measured using Rat/Mouse Insulin ELISA, Mouse Leptin ELISA (EMD Millipore, USA), Mouse Adiponectin/Acrp30 Quantikine ELISA (R&D Systems, USA), and CORTICOSTERONE rat/mouse ELISA (Xema Co. Ltd. in Moscow, Russia) kits, respectively. Concentrations of glucose, triglycerides, cholesterol, and free fatty acids were measured colorimetrically using Fluitest GLU, Fluitest TG, Fluitest CHOL (Analyticon Biotechnologies GmbH, Germany), and NEFA FS DiaSys (DiaSys Diagnostic Systems GmbH, Germany) kits, respectively. Fasting significantly increases endogenous FGF21 production and its level in the blood. As, the aim of this study was to compare the effect of prolonged FGF21 administration on metabolic parameters rather than the acute effects of FGF21, biochemical (and other) parameters were measured in fed animals.

Hepatic triglyceride content. Liver samples were homogenized in PBS (50 mg in 400 μ L) and centrifuged at 1000 rpm. The supernatant was stored at -20°C . Triglyceride levels were assayed using the Fluitest TG commercial kit (Analyticon Biotechnologies GmbH, Germany) according to manufacturer's recommendations.

Relative quantitative real-time PCR. Total RNA was isolated from tissue samples using ExtractRNA kit (Evrogen, Moscow, Russia) according to the manufacturer's recommendations. First-strand cDNA was synthesized using Moloney murine leukemia virus (MMLV) reverse transcriptase (Evrogen) and oligo(dT) as a primer. TaqMan gene expression assays (Applied Biosystems, USA) were used for relative quantitation real-time PCR. The genes tested involved fibroblast growth factor 21 (*Fgf21*, Mm00840165_g1), peroxisome proliferator-activated receptor gamma coactivator (*Ppargc1a*, Mm01208835_m1), carnitine palmitoyltransferase 1A/1B (*Cpt1a/b*, Mm01231183_m1/Mm00487191_g1), acetyl-CoA carboxylase alpha/beta (*Acaca/b*, Mm01304257_m1/Mm01204671_m1), insulin receptor (*Insr*, Mm01211875_m1), insulin receptor substrate 1/2 (*Irs1/2*, Mm01278327_m1/Mm03038438_m1), protein-tyrosine phosphatase 1B (*Ptpn1*, Mm00448427_m1), pyruvate kinase (*Pklr*, Mm00443090_m1), glucokinase (*Gck*, Mm00439129_m1), glucose-6-phosphatase (*G6pc*, Mm00839363_m1), phosphoenolpyruvate carboxykinase (*Pck*, Mm01247058_m1), solute carrier family 2 member 2 (*Slc2a2*, Mm00446229_m1), solute carrier family 2 member 4 (*Slc2a4*, Mm00436615_m1), estrogen receptor 1 (*Esr1*, Mm00433149_m1), signal transducer and activator of transcription 3 (*Stat3*, Mm01219775_m1), peroxisome proliferator-activated receptor alpha/gamma (*Ppara/g*, Mm00440939_m1/Mm00440940_m1), hormone-sensitive lipase (*Lipe*, Mm00495359_m1), adipose triglyceride lipase (*Atgl*, Mm00503040_m1), fatty acid synthase (*Fasn*, Mm00662319_m1), uncoupling protein 1 (*Ucp1*, Mm01244861_m1), deiodonase-2 (*Dio2*, Mm00515664_m1), corticotropin releasing hormone (*Crh*, Mm01293920_s1), agouti related neuropeptide (*Agrp*, Mm00475829_g1), neuropeptide Y (*Npy*, Mm01410146_m1), proopiomelanocortin (*Pomc*, Mm00435874_m1), leptin receptor (*Lepr*, Mm00440181_m1), klotho beta (*Klb*, Mm00473122_m1), cyclophilin A (*Ppia*, Mm02342430_g1), and beta-actin (*Actb*, Mm00607939_s1). Cyclophilin A and beta-actin were used as endogenous controls. The PCR and fluorescence detection were performed on an Applied Biosystems VIIA 7 Real-Time PCR System. Relative quantification was performed by the comparative threshold cycle (CT) method.

Statistical analysis. Each result is presented as the arithmetic mean \pm SE. Two-way ANOVA with factors 'FGF21' (PBS or FGF21) and 'E2' (oil or E2) was used to analyze FGF21 and E2 effects on metabolic parameters with multiple comparisons by the post hoc Tukey test or Mann-Whitney U test in case of inequality of variances. Repeated measures ANOVA with factors 'FGF21', 'E2' and 'Time' (time after glucose load) was used to analyze the results of the GTT. Differences were considered significant at $p < 0.05$. Calculations were performed with the STATISTICA 10.0 software package (StatSoft Russia, Moscow, Russia).

Results

Food intake, body weight, weights of liver and adipose tissues

At the end of the experiment, E2-treated ovariectomized (OVX) obese females had lower weights of the body and of abdominal and subcutaneous adipose tissues (abWAT and scWAT, respectively) than oil-treated females ($p < 0.05$, $p < 0.05$, and $p < 0.01$, respectively) (Fig. 2, a). Fibroblast growth factor 21 (FGF21) did not affect the parameters whether administered alone or with estradiol. There were no significant effects of the administration of E2, or FGF21, or both on the weight of brown adipose tissue (BAT), hepatic weight, or hepatic triglyceride content (Fig. 3, a, see Fig. 2, a).

Estradiol reduced the number of calories consumed with the high-fat component of the diet (lard) and the total number of calories consumed ($p < 0.01$ and $p < 0.05$, respectively), but did not affect the contribution of various components of the diet to the calorie content of the food consumed (Fig 4, a). FGF21, regardless of E2, increased the number of calories consumed with standard chow and contribution of standard chow to the calorie content of the food consumed.

Thus, in obese OVX females, estradiol reduced body weight, apparently due to the decrease in WAT weight. Both drugs influenced the food preferences, and their effects were independent.

Insulin sensitivity, plasma hormone and metabolite levels

In obese OVX females, there were no significant effects of separate or joint administration of drugs on the plasma levels of corticosterone, free fatty acids (FFA), triglycerides (TG), or cholesterol (Fig. 5). FGF21 had no effect on plasma levels of leptin or adiponectin, but estradiol reduced both ($p < 0.001$). Estradiol reduced the plasma insulin and blood fasting glucose levels and increased glucose tolerance ($p < 0.001$ in all cases) (Fig. 6, a, b). When administered separately, FGF21 also reduced the plasma insulin level ($p < 0.05$, post hoc Tukey test). In females having received both drugs, insulin levels did not differ from those in FGF21- or E2-females, but they were significantly lower than in control females ($p < 0.05$, post hoc Tukey test). Regardless of E2-treatment, glucose tolerance in females treated with FGF21 did not differ from control females and the fed plasma glucose level was lower than in control females, although the differences were below the level of significance ($p = 0.07$).

Thus, estradiol increased insulin sensitivity in obese OVX females. FGF21, regardless of E2-treatment, did not affect glucose tolerance or the fasting glucose level, but lowered the fed glucose level. FGF21 also had a beneficial effect on the plasma insulin level, but this effect was recorded only in E2-untreated females.

Metabolic gene expression

In scWAT, in obese OVX females, FGF21 and estradiol, when administered separately, increased the expression of insulin receptor gene (*Insr*) and acetyl-coA carboxylase beta gene (*Acacb*, suppression of fatty acid oxidation) (see Fig. 2, b).

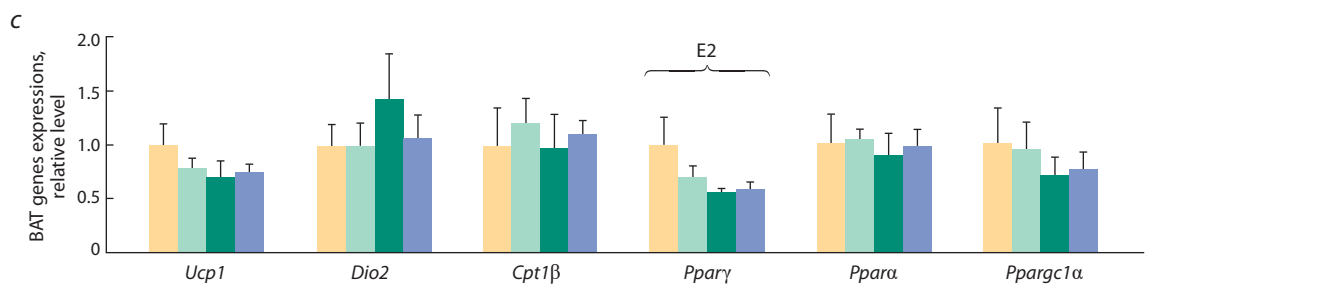
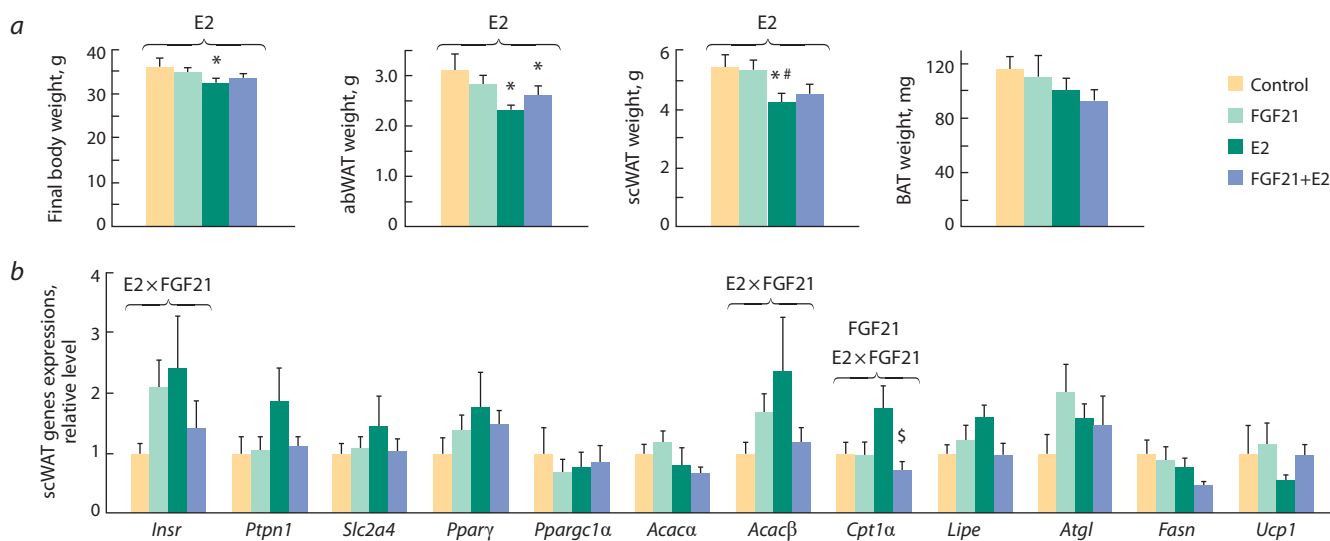


Fig. 2. *a*, Body weight, the weight of abdominal (abWAT) and subcutaneous (scWAT) white adipose tissues and the weight of brown adipose tissue (BAT); *b*, *c*, the mRNA levels of genes regulating metabolism in scWAT and BAT, respectively.

The ANOVA factors whose influence on the parameter is significant are shown above brackets (E2, FGF21, or E2×FGF21). *vs Control, #vs FGF21, \$vs E2, post hoc Tukey test.

Insr – insulin receptor; *Ptpn1* – protein-tyrosine phosphatase 1B; *Slc2a4* – solute carrier family 2 member 4; *Ppargγ* – peroxisome proliferator-activated nuclear receptor gamma; *Ppargc1α* – peroxisome proliferator-activated receptor gamma coactivator; *Acaca* – acetyl-coenzyme A carboxylase alpha; *Acacβ* – acetyl-CoA carboxylase beta; *Cpt1α* – carnitine palmitoyltransferase 1A; *Lipe* – hormone-sensitive lipase; *Atgl* – adipose triglyceride lipase; *Fasn* – fatty acid synthase; *Ucp1* – uncoupling protein 1; *Dio2* – deiodonase-2; *Cpt1β* – carnitine palmitoyltransferase 1B; *Ppara* – peroxisome proliferator-activated receptor alpha coactivator.

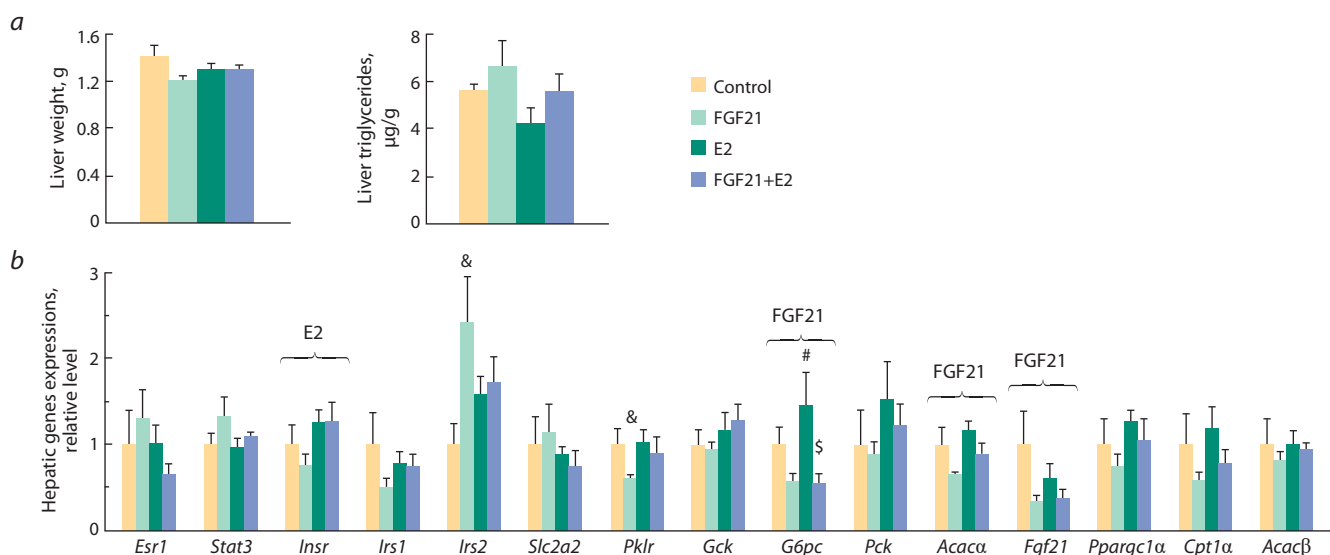


Fig. 3. Liver: *a*, weight, triglyceride content; *b*, mRNA levels of genes regulating glucose and lipid metabolism.

The ANOVA factors whose influence on the parameter is significant are shown above brackets (E2, FGF21, or E2×FGF21). # vs FGF21, \$ vs E2, post hoc Tukey test; & vs control, Mann-Whitney U test.

Esr1 – estrogen receptor 1; *Stat3* – signal transducer and activator of transcription 3; *Insr* – insulin receptor; *Irs1/2* – insulin receptor substrate 1/2; *Slc2a2* – solute carrier family 2 member 2; *Pklr* – pyruvate kinase; *Gck* – glucokinase; *G6pc* – glucose-6-phosphatase; *Pck* – phosphoenolpyruvate carboxykinase; *Acaca* – acetyl-coenzyme A carboxylase alpha; *Fgf21* – fibroblast growth factor 21; *Ppargc1α* – peroxisome proliferator-activated receptor gamma coactivator; *Cpt1α* – carnitine palmitoyltransferase 1A; *Acacβ* – acetyl-CoA carboxylase beta.

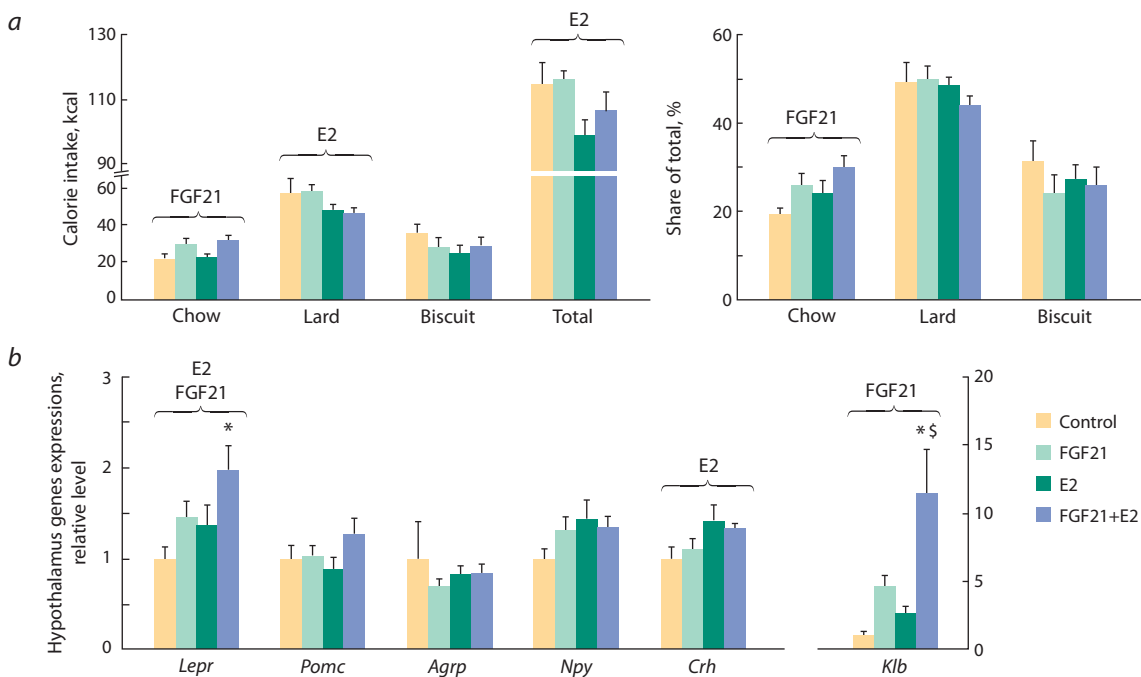


Fig. 4. *a*, The number of calories consumed during the experiment (with each component and the total amount) and the percentage of each component (share of total); *b*, hypothalamic levels of mRNAs of genes associated with the control of food intake.

ANOVA factors whose influence on the parameter is significant are shown above the brackets (E2, FGF21, or E2xFGF21). * vs Control; \$ vs E2, post hoc Tukey test.

Lepr – leptin receptor; *Pomc* – proopiomelanocortin; *AgRP* – agouti related peptide; *Npy* – neuropeptide Y; *Crh* – corticotropin releasing hormone; *Klb* – klotho beta.

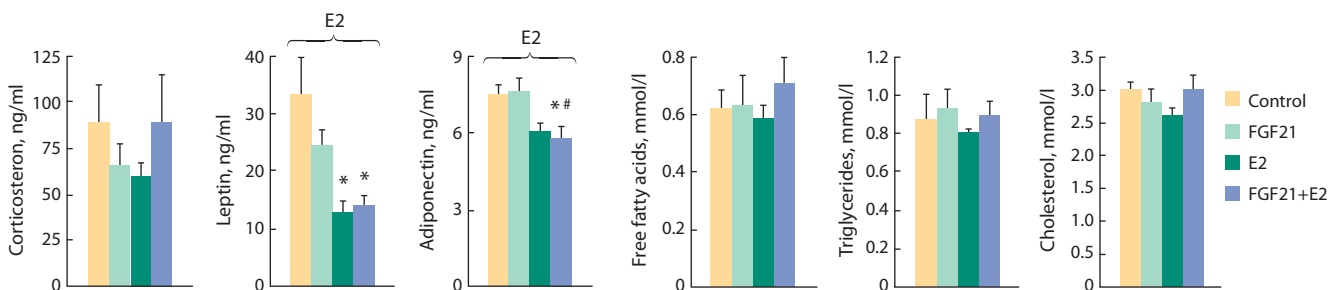


Fig. 5. The level of hormones and metabolites in the blood plasma.

ANOVA factors, whose influence on the parameter is significant, are shown above the brackets (E2, FGF21 or E2xFGF21). * vs Control; # vs FGF21, post hoc Tukey test.

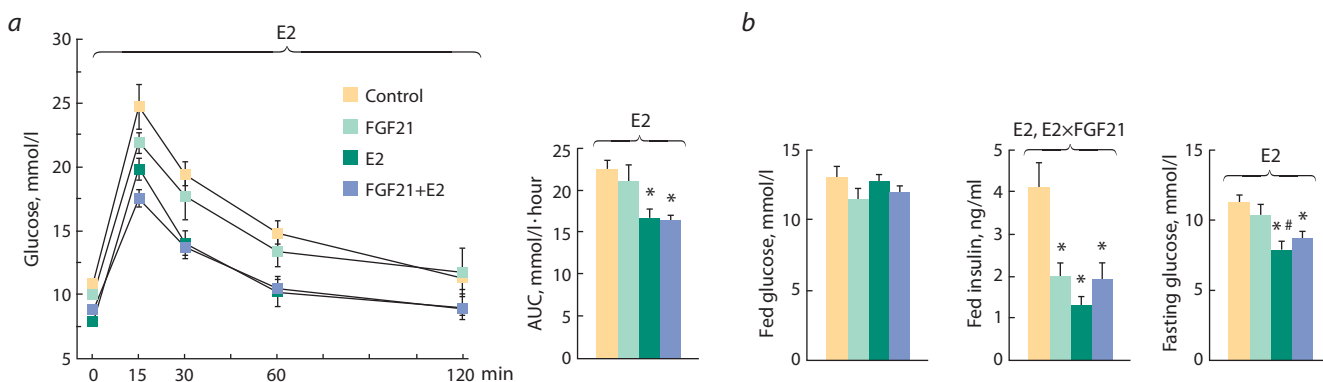


Fig. 6. *a*, Glucose tolerance test: blood glucose levels before (0 min) and 15, 30, 60, and 120 minutes after glucose administration, and the area under the curve (AUC) of blood glucose levels; *b*, fed plasma levels of glucose and insulin, fasting blood glucose levels.

ANOVA factors whose influence on the parameter is significant are shown above brackets (E2, FGF21 or E2xFGF21). * vs Control, # vs FGF21, post hoc Tukey test.

In females who received both drugs, the expression of these genes was lower than in females who received one of them, and it did not differ from that in control females (influence of factor interaction $p < 0.05$ in both cases). In addition, when administered separately, FGF21 did not affect the expression of the *Cpt1a* gene for carnitine palmitoyltransferase 1 α gene (activation of fatty acid oxidation) but suppressed its expression in E2-treated females (influence of factor interaction $p < 0.05$). In females receiving both drugs, the mRNA level of this gene was significantly lower than in E2-females ($p < 0.05$, post hoc Tukey test) and did not differ from control females.

There was no significant effect of separate or joint administration of drugs on gene expression in abWAT. In BAT, estradiol reduced the expression of the transcription factor peroxisome proliferator-activated nuclear receptor gamma (*Ppar γ*) ($p < 0.05$) (see Fig. 2, c). Regardless of the estradiol status, there were no effects of FGF21 on the expression of genes involved in thermogenesis and fatty acid beta-oxidation in BAT.

Thus, in obese OVX females, the catabolic effect of estradiol was associated with its stimulating influence on the expression of *Insr*, *Acac β* in scWAT and *Ppar γ* in BAT. Despite the absence of the catabolic effect of FGF21, it exerted transcriptional effects in scWAT (stimulated the expression of *Insr* and *Acac β*), but only in oil-treated females; in E2-treated females, the stimulating effect of FGF21 on gene expression was not manifested.

In the hypothalamus, changes in food consumption caused by the E2 action were associated with higher expression of the genes for leptin receptor (*Lepr*) and corticotropin-releasing hormone (*Crh*) ($p < 0.05$ and $p < 0.01$, respectively) (see Fig. 4, b). The effect of FGF21 on food consumption was associated with an increase in *Lepr* expression ($p < 0.05$), which was more pronounced in females receiving E2. In addition, FGF21 increased the expression of its own coreceptor, klotho beta (*Klb*) ($p < 0.01$), and this effect was also more pronounced in females receiving E2.

Thus, the effect of drugs on the choice of food components was associated with a change in the hypothalamic expression of genes associated with the regulation of food consumption, and estradiol enhanced the transcriptional effects of FGF21.

In the liver of obese OVX females, estradiol increased the expression of the insulin receptor gene (*Insr*) ($p < 0.05$) (see Fig. 3, b). FGF21, regardless of E2-treatment, suppressed its own expression (*Fgf21*) and the expression of genes associated with fatty acid synthesis and oxidation (acetyl-coenzyme A carboxylase alpha, *Acaca*, and carnitine palmitoyltransferase 1a, *Cpt1a* (tendency)), and with gluconeogenesis (glucose-6-phosphatase, *G6pc*) ($p < 0.05$, $p < 0.05$, $p = 0.08$ and $p < 0.01$, respectively). When administered separately, FGF21 increased the expression of insulin receptor substrate type 2 gene (*Irs2*) and suppressed the expression of pyruvate kinase (*Pklr*, a key enzyme in glycolysis) ($p < 0.05$, FGF21-females vs control females, Mann–Whitney U test in both

cases). In females treated with both FGF21 and estradiol, the mRNA levels of *Irs2* and *Pklr* did not differ from those in E2-females or control females.

Thus, independent transcriptional effects of FGF21 and estradiol in the liver were shown: FGF21-effects on *G6pc*, *Acaca*, and *Fgf21* expression and an E2-effect on *Insr* expression. However, the effects of FGF21 on *Irs2* and *Pklr* expression manifested themselves only when the drug was administered without estradiol, and they were absent from animals receiving both drugs, which suggests an inhibition of the effects of FGF21 by E2.

Discussion

In this work, we investigated whether the blood estradiol level modifies the pharmacological action of FGF21 in obese females. It is known that chronic FGF21 treatment improves many metabolic parameters in obese male mice; in particular, weight loss and lipoprotein profiles. It increases insulin sensitivity and energy expenditure, normalizes blood glucose and triglyceride levels, improves the liver state, and suppresses gluconeogenesis (Kharitonov et al., 2005; Coskun et al., 2008; Xu et al., 2009; Chau et al., 2010; Véniant et al., 2012; Fisher, Maratos-Flier, 2016; BonDurant, Potthoff, 2018). Also, FGF21 changes taste preferences, increasing protein consumption and reducing sugar consumption by male mice (Talukdar et al., 2016; Hill et al., 2019; Larson et al., 2019).

According to our data, estradiol given to OVX obese females reduced body and adipose tissues weights, the total number of calories consumed, fed insulin plasma level, and fasting glucose blood level and increased glucose tolerance. These observations agree with the generally accepted opinion as to the effect of estradiol on these parameters in female mice with obesity (Riant et al., 2009; Yan et al., 2019). We were first to demonstrate that the anorexigenic effect of estradiol in obese OVX females is due to the suppression of the consumption of a high-fat component of diet (lard), and this effect is associated with the activation of the expression of the corticotropin-releasing hormone gene (*Crh*) in the hypothalamus. However, some effects of FGF21 observed in obese males were not detected in obese OVX females. For example, FGF21, regardless of E2-treatment, did not affect body or adipose tissues weights; levels of lipids, leptin, or adiponectin in plasma; or the expression of genes associated with the regulation of thermogenesis in BAT, hypothalamic food consumption regulation, or with lipid metabolism in scWAT or in the liver. These results are consistent with data on the effect of FGF21 in non-ovariectomized obese females (Bazhan et al., 2019), and they suggest that there are sex-related factors other than estradiol that suppress the pharmacological effects of FGF21 in obese females.

We showed that the stimulating effect of FGF21 on the consumption of standard food in obese OVX females did not depend on E2-treatment, and it appeared to be similar to the FGF21 effect on food consumption in males. FGF21 is known to increase the consumption of protein (casein enriched with cystine) by males (Larson et al., 2019). In our experiment,

standard food had the maximum amount of protein, compared with lard and cookies. Both hormones, FGF21 and estradiol, affected the choice of food components, the influence of each was aimed to reduce the caloric content of consumed food; herewith, estradiol reduced the high-fat component of diet, and FGF21 increased intake of standard food. Both hormones increased the expression of leptin receptors (*Lepr*) in the hypothalamus. Genes for the hypothalamic neuropeptides pro-opiomelanocortin (*Pomc*), agouti related peptide (*AgRP*) and neuropeptide Y (*Npy*) are leptin targets (Cowley et al., 2001), and they are involved in the regulation of food consumption. We found no effect of FGF21 or estradiol on their expression, thus we assume that the activation of the hypothalamic expression of *Lepr* and, accordingly, enhance hypothalamic leptin sensitivity in response to the administration of FGF21 or estradiol do not mediate the effects of these hormones on food consumption. In this regard, the mechanism of FGF21 effect on food consumption remains unclear and requires further study, whereas the anorexigenic effect of estradiol is apparently due to the increase in hypothalamic *Crh* expression and activation of the CRF system. It should be noted that in the hypothalamus, FGF21 stimulated not only *Lepr* expression but also the expression of its own co-receptor klotho beta (*Klb*); the maximum expression of *Lepr* and *Klb* being recorded when drugs were administered jointly. The results indicate that the pharmacological use FGF21 can increase the sensitivity of the hypothalamus to regulatory factors, and estradiol can potentiate the central effects of FGF21.

We show that FGF21 administered to obese OVX females increases the expression of *Insr* and *Acacβ* in scWAT and *Irs2* in the liver but suppresses the hepatic expression of glucose-6-phosphatase (*G6pc*), *Pklr*, *Acaca*, *Cpt1a*, and itself (*Fgf21*). It is known that chronic administration of FGF21 to obese males increases the expression of *Insr*, *Acacβ* and suppresses the expression of *Cpt1a* in scWAT, and in the liver stimulates the expression of *Insr* and suppresses its own expression (*Fgf21*) and the expression of *Acaca* and *Cpt1a* (Coskun et al., 2008; Fisher et al., 2011). Consequently, the transcriptional effects of FGF21 in obese OVX females not treated with estradiol were similar to those in obese males and beneficial. They were aimed at increasing insulin sensitivity in the liver and adipose tissue, and they contributed to a decrease in glucose and fatty acid plasma levels. In obese OVX females having received both drugs, the beneficial transcriptional effects of FGF21 persisted only in the liver: FGF21 suppressed the expression of *G6pc*, *Acaca*, *Cpt1a*, and itself.

When co-administered with estradiol, FGF21 suppressed the expression of *Cpt1a* in scWAT, but the effect of FGF21 on the expression of *Insr* and *Acacβ* in scWAT, *Irs2* and *Pklr* in the liver was not pronounced. Consequently, the effect of FGF21 on hepatic *G6pc* expression, is independent of estradiol and is associated with a decrease in fed glucose plasma levels. We assume that these FGF21 effects (suppression of *G6pc* expression and lower plasma glucose level) were mediated by activation of hypothalamic *Lepr* expression, since the ability of leptin, affecting the activity of POMC neurons, to normal-

ize blood glucose levels and increase insulin sensitivity in the liver has been shown (Berglund et al., 2012).

Thus, the study of the transcriptional effects of FGF21 in the liver, adipose tissue, and hypothalamus shows that there are different types of interaction between FGF21 and estradiol in regulating the expression of metabolic genes in obese OVX females: (1) FGF21 can act independently of E2, (2) estradiol may inhibit or enhance the effects of FGF21, and (3) the interplay of hormones can lead to mutual suppression of their effects, observed when they are administered separately. The ability of exogenous FGF21 to suppress the effects of estradiol in females suggests a possible adverse effect of pharmacological FGF21; in particular, on the female reproductive function.

What mechanisms may mediate the estradiol influence on the pharmacological effects of FGF21? FGF21 has been shown to bind to a receptor complex consisting of fibroblast growth factor receptor type 1 (FGFR1) and klotho beta co-receptor (Kurosu et al., 2007). In the hypothalamus, adipose tissue, and the pancreas, the receptor and co-receptor of FGF21 are expressed, as well as all types of estradiol receptors (Kurosu et al., 2007; Nadal et al., 2009; Fisher et al., 2011; Bian et al., 2019; Pan et al., 2019). These tissues are the target of FGF21 and estradiol. Estrogen receptor alpha and G-protein-coupled estrogen receptor are expressed in the liver (Palmisano et al., 2017), so the liver is the target of estradiol. The level of FGFR1 in the liver is very low (Fisher et al., 2011); however, some direct effects of FGF21 can be observed in the liver with its pharmacological administration, as a result of a large dose of the drug (Owen et al., 2015). The interaction of FGF21 and estradiol in the regulation of metabolic parameters may depend on the molecular mechanism regulating the expression of target genes, as well as on the type and level of receptors in the tissue, thus being tissue-specific. The molecular mechanism of this interaction requires additional study.

Conclusion

To sum up, we state that ovariectomized obese females are resistant to the catabolic action of FGF21, and this resistance is not associated with the action of estradiol. The ability of FGF21 to increase the consumption of standard food and reduce blood glucose levels does not depend on estradiol either. However, FGF21 and estradiol appear to interact in the regulation of gene expression and blood insulin levels: (i) estradiol can suppress the transcriptional effects of FGF21 in the liver and potentiate its effect in the hypothalamus; (ii) in adipose tissue, the interaction of FGF21 and estradiol can suppress the activating effect of each of the drugs observed with separate administration or contribute to the manifestation of the inhibitory effect of FGF21; and (iii) in E2-treated animals, FGF21 exerts no inhibitory effect on the blood insulin level.

Estradiol-dependent effects of FGF21 can manifest themselves differently in male and female bodies, different in estrogen activity. Thereby, they determine the sexual dimorphism of the pharmacological effects of FGF21 in obese animals.

References

- Allard C., Bonnet F., Xu B., Coons L., Albarado D., Hill C., Fagherazzi G., Korach K.S., Levin E.R., Lefante J., Morrison C., Mauvais-Jarvis F. Activation of hepatic estrogen receptor- α increases energy expenditure by stimulating the production of fibroblast growth factor 21 in female mice. *Mol. Metab.* 2019;22:62-70. DOI 10.1016/j.molmet.2019.02.002.
- Bazhan N., Yakovleva T., Denisova E., Dubinina A., Makarova E. Antidiabetic FGF21 action depended on sex and exerted only in male mice with diet induced obesity. *Obes. Facts.* 2019; 12(Suppl.1):189. DOI 10.1159/000489691.
- Berglund E.D., Vianna C.R., Donato J., Jr., Kim M.H., Chuang J.C., Lee C.E., Lauzon D.A., Lin P., Brule L.J., Scott M.M., Copparrini R., Elmquist J.K. Direct leptin action on POMC neurons regulates glucose homeostasis and hepatic insulin sensitivity in mice. *J. Clin. Invest.* 2012;122(3):1000-1009. DOI 10.1172/JCI59816.
- Bian C., Bai B., Gao Q., Li S., Zhao Y. 17 β -estradiol regulates glucose metabolism and insulin secretion in rat islet β cells through GPER and Akt/mTOR/GLUT2 pathway. *Front. Endocrinol. (Lausanne)*. 2019;10:531. DOI 10.3389/fendo.2019.00531.
- BonDurant L.D., Potthoff M.J. Fibroblast growth factor 21: a versatile regulator of metabolic homeostasis. *Annu. Rev. Nutr.* 2018;38: 173-196. DOI 10.1146/annurev-nutr-071816-064800.
- Chau M.D., Gao J., Yang Q., Wu Z., Gromada J. Fibroblast growth factor 21 regulates energy metabolism by activating the AMPK-SIRT1-PGC-1 α pathway. *Proc. Natl. Acad. Sci. USA.* 2010; 107(28):12553-12558. DOI 10.1073/pnas.1006962107.
- Coskun T., Bina H.A., Schneider M.A., Dunbar J.D., Hu C.C., Chen Y., Moller D.E., Kharitonov A. Fibroblast growth factor 21 corrects obesity in mice. *Endocrinology.* 2008;149(12):6018-6027. DOI 10.1210/en.2008-0816.
- Cowley M.A., Smart J.L., Rubinstein M., Cerdán M.G., Diano S., Horvath T.L., Cone R.D., Low M.J. Leptin activates anorexigenic POMC neurons through a neural network in the arcuate nucleus. *Nature.* 2001;411(6836):480-484. DOI 10.1038/35078085.
- Fisher F.M., Estall J.L., Adams A.C., Antonellis P.J., Bina H.A., Flier J.S., Kharitonov A., Spiegelman B.M., Maratos-Flier E. Integrated regulation of hepatic metabolism by fibroblast growth factor 21 (FGF21) *in vivo*. *Endocrinology.* 2011;152(8):2996-3004. DOI 10.1210/en.2011-0281.
- Fisher F.M., Maratos-Flier E. Understanding the physiology of FGF21. *Annu. Rev. Physiol.* 2016;78:223-241. DOI 10.1146/annurev-physiol-021115-105339.
- Gao H., Bryzgalova G., Hedman E., Khan A., Efendic S., Gustafsson J.A., Dahlman-Wright K. Long-term administration of estradiol decreases expression of hepatic lipogenic genes and improves insulin sensitivity in ob/ob mice: a possible mechanism is through direct regulation of signal transducer and activator of transcription 3. *Mol. Endocrinol.* 2006;20(6):1287-1299. DOI 10.1210/me.2006-0012.
- Hill C.M., Laeger T., Dehner M., Albarado D.C., Clarke B., Wanders D., Burke S.J., Collier J.J., Qualls-Creekmore E., Solon-Biet S.M., Simpson S.J., Berthoud H.R., Münzberg H., Morrison C.D. FGF21 signals protein status to the brain and adaptively regulates food choice and metabolism. *Cell Rep.* 2019;27(10): 2934-2947.e3. DOI 10.1016/j.celrep.2019.05.022.
- Hua L., Zhuo Y., Jiang D., Li J., Huang X., Zhu Y., Li Z., Yan L., Jin C., Jiang X., Che L., Fang Z., Lin Y., Xu S., Li J., Feng B., Wu D. Identification of hepatic fibroblast growth factor 21 as a mediator in 17 β -estradiol-induced white adipose tissue browning. *FASEB J.* 2018;32(10):5602-5611. DOI 10.1096/fj.201800240R.
- Kharitonov A., Shiyanova T.L., Koester A., Ford A.M., Micanovic R., Galbreath E.J., Sandusky G.E., Hammond L.J., Moyers J.S., Owens R.A., Gromada J., Brozinick J.T., Hawkins E.D., Wroblewski V.J., Li D.S., Mehrbod F., Jaskunas S.R., Shanafelt A.B. FGF-21 as a novel metabolic regulator. *J. Clin. Invest.* 2005;115(6):1627-1635. DOI 10.1172/JCI23606.
- Kurosu H., Choi M., Ogawa Y., Dickson A.S., Goetz R., Eliseenkova A.V., Mohammadi M., Rosenblatt K.P., Klierer S.A., Kuro-O M. Tissue-specific expression of β Klotho and fibroblast growth factor (FGF) receptor isoforms determines metabolic activity of FGF19 and FGF21. *J. Biol. Chem.* 2007;282(37):26687-26695. DOI 10.1074/jbc.M704165200.
- Larson K.R., Chaffin A.T., Goodson M.L., Fang Y., Ryan K.K. Fibroblast growth factor-21 controls dietary protein intake in male mice. *Endocrinology.* 2019;160(5):1069-1080. DOI 10.1210/en.2018-01056.
- Makarova E., Kazantseva A., Dubinina A., Yakovleva T., Balybina N., Baranov K., Bazhan N. The same metabolic response to FGF21 administration in male and female obese mice is accompanied by sex-specific changes in adipose tissue gene expression. *Int. J. Mol. Sci.* 2021;22(19):10561. DOI 10.3390/ijms221910561.
- Makarova E.N., Yakovleva T.V., Balybina N.Y., Baranov K.O., Denisova E.I., Dubinina A.D., Feofanova N.A., Bazhan N.M. Pharmacological effects of fibroblast growth factor 21 are sex-specific in mice with the *lethal yellow (A^y)* mutation. *Vavilovskii Zhurnal Genetiki i Selektzii = Vavilov Journal of Genetics and Breeding.* 2020;24(2):200-208. DOI 10.18699/VJ20.40-o.
- Nadal A., Alonso-Magdalena P., Soriano S., Ropero A.B., Quesada I. The role of oestrogens in the adaptation of islets to insulin resistance. *J. Physiol.* 2009;587(Pt.21):5031-5037. DOI 10.1113/jphysiol.2009.177188.
- Owen B.M., Mangelsdorf D.J., Klierer S.A. Tissue-specific actions of the metabolic hormones FGF15/19 and FGF21. *Trends Endocrinol. Metab.* 2015;26(1):22-29. DOI 10.1016/j.tem.2014.10.002.
- Palmisano B.T., Zhu L., Stafford J.M. Role of estrogens in the regulation of liver lipid metabolism. *Adv. Exp. Med. Biol.* 2017;1043: 227-256. DOI 10.1007/978-3-319-70178-3_12.
- Pan Y., Wang B., Zheng J., Xiong R., Fan Z., Ye Y., Zhang S., Li Q., Gong F., Wu C., Lin Z., Li X., Pan X. Pancreatic fibroblast growth factor 21 protects against type 2 diabetes in mice by promoting insulin expression and secretion in a PI3K/Akt signaling-dependent manner. *J. Cell. Mol. Med.* 2019;23(2):1059-1071. DOI 10.1111/jcmm.14007.
- Riant E., Waget A., Cogo H., Arnal J.F., Burcelin R., Gourdy P. Estrogens protect against high-fat diet-induced insulin resistance and glucose intolerance in mice. *Endocrinology.* 2009;150(5): 2109-2117. DOI 10.1210/en.2008-0971.
- Talukdar S., Zhou Y., Li D., Rossulek M., Dong J., Somayaji V., Weng Y., Clark R., Lanba A., Owen B.M., Brenner M.B., Trimmer J.K., Gropp K.E., Chabot J.R., Erion D.M., Rolph T.P., Goodwin B., Calle R.A. A long-acting FGF21 molecule, PF-05231023, decreases body weight and improves lipid profile in non-human primates and type 2 diabetic subjects. *Cell Metab.* 2016;23(3): 427-440. DOI 10.1016/j.cmet.2016.02.001.
- Thammacharoen S., Geary N., Lutz T.A., Ogawa S., Asarian L. Divergent effects of estradiol and the estrogen receptor- α agonist PPT on eating and activation of PVN CRH neurons in ovariectomized rats and mice. *Brain Res.* 2009;1268:88-96. DOI 10.1016/j.brainres.2009.02.067.
- Véniant M.M., Komorowski R., Chen P., Stanislaus S., Winters K., Hager T., Zhou L., Wada R., Hecht R., Xu J. Long-acting FGF21 has enhanced efficacy in diet-induced obese mice and in obese rhesus monkeys. *Endocrinology.* 2012;153(9):4192-4203. DOI 10.1210/en.2012-1211.

Vrtačnik P., Ostanek B., Mencej-Bedrač S., Marc J. The many faces of estrogen signaling. *Biochem. Med. (Zagreb)*. 2014;24(3):329-342. DOI 10.11613/BM.2014.035.

Xu J., Stanislaus S., Chinooswong N., Lau Y.Y., Hager T., Patel J., Ge H., Weiszmann J., Lu S.C., Graham M., Busby J., Hecht R., Li Y.S., Li Y., Lindberg R., Véniant M.M. Acute glucose-lowering and insulin-sensitizing action of FGF21 in insulin-resistant mouse models – association with liver and adipose tissue effects. *Am. J.*

Physiol. Endocrinol. Metab. 2009;297(5):E1105-E1114. DOI 10.1152/ajpendo.00348.2009.

Yan H., Yang W., Zhou F., Li X., Pan Q., Shen Z., Han G., Newell-Fugate A., Tian Y., Majeti R., Liu W., Xu Y., Wu C., Allred K., Allred C., Sun Y., Guo S. Estrogen improves insulin sensitivity and suppresses gluconeogenesis via the transcription factor Foxo1. *Diabetes*. 2019;68(2):291-304. DOI 10.2337/db18-0638.

ORCID ID

T.V. Jakovleva orcid.org/0000-0001-7628-5856
A.Yu. Kazantseva orcid.org/0000-0003-4192-2020
A.D. Dubinina orcid.org/0000-0003-3907-3488
N.Yu. Balybina orcid.org/0000-0001-7168-1438
K.O. Baranov orcid.org/0000-0002-4029-6518
E.N. Makarova orcid.org/0000-0002-6417-9893
N.M. Bazhan orcid.org/0000-0002-7246-4758

Acknowledgements. This work was supported by the Russian Science Foundation, project 17-15-01036-П. The use of the equipment of the Department of Experimental Animal Genetic Resources, ICG, was supported by the Russian Ministry of Education and Science, project RFMEFI62117X0015.

Conflict of interest. The authors declare no conflict of interest.

Received October 29, 2021. Revised November 23, 2021. Accepted November 24, 2021.

The impact of the *Hsp67Bc* gene product on *Drosophila melanogaster* longevity, fecundity, and acute heat stress tolerance

D. Malkeyeva , S.A. Fedorova, E. Kiseleva

Institute of Cytology and Genetics of the Siberian Branch of the Russian Academy of Sciences, Novosibirsk, Russia

 malkeyeva@bionet.nsc.ru

Abstract. *Drosophila melanogaster* Hsp67Bc is a heat- and cold-inducible small heat shock protein that participates in the prevention of aggregation of misfolded proteins and in macroautophagy regulation. Overexpression of the *Hsp67Bc* gene has been shown to enhance macroautophagy in *Drosophila* S2 cells, and the deletion of this gene leads to the formation of a slightly increased number of autophagic vacuoles in the fruit fly brain neurons. Recently, we found that *Hsp67Bc*-null *D. melanogaster* flies have poor tolerance to cold stress (0 °C) of various durations. In the present work, we investigated how the *Hsp67Bc* gene deletion affects the fitness of fruit flies under normal conditions and their tolerance to elevated temperatures at different developmental stages. Larvae and pupae were not adversely affected by the *Hsp67Bc* gene deletion, and adult *Hsp67Bc*-null flies showed an extended lifespan in comparison with the control at normal (24–25 °C) and elevated temperature (29 °C), and after acute heat stress (37 °C, 2 h). At the same time, the fecundity of the mutant females was lower by 6–13 % in all tested environments, except for permanent maintenance at 29 °C, where the mean numbers of eggs laid by the mutant and control flies were equal. We explain this phenomenon by a reduced number of ovarioles in *Hsp67Bc*-null females and enhanced macroautophagy in their germaria, which promotes the death of forming egg chambers. In addition, short heat stress (37 °C, 2 h), which increased the control line's longevity (an effect common for a wide range of organisms), had a negative impact on the lifespan of *Hsp67Bc*-null flies. Therefore, *Hsp67Bc*-null *D. melanogaster* have an extended lifespan under normal and elevated temperature conditions, and reduced fecundity and thermal stress tolerance. Key words: *Drosophila* longevity; thermal stress tolerance; elevated temperature; heat stress; small heat shock proteins; autophagy.

For citation: Malkeyeva D., Fedorova S.A., Kiseleva E. The impact of the *Hsp67Bc* gene product on *Drosophila melanogaster* longevity, fecundity, and acute heat stress tolerance. *Vavilovskii Zhurnal Genetiki i Selekcii* = *Vavilov Journal of Genetics and Breeding*. 2022;26(2):169-178. DOI 10.18699/VJGB-22-21

Влияние продукта гена *Hsp67Bc* на продолжительность жизни, плодовитость и устойчивость *Drosophila melanogaster* к кратковременному тепловому стрессу

Д.А. Малькеева , С.А. Фёдорова, Е.В. Киселева

Федеральный исследовательский центр Институт цитологии и генетики Сибирского отделения Российской академии наук, Новосибирск, Россия

 malkeyeva@bionet.nsc.ru

Аннотация. Hsp67Bc *Drosophila melanogaster* – индуцируемый в ответ на тепловой и холодовой стресс малый белок теплового шока, участвующий в предотвращении агрегации поврежденных белков и в регуляции макроаутофагии. Было показано, что повышенная экспрессия гена *Hsp67Bc* стимулирует макроаутофагию в клетках S2 дрозофилы, а его делеция приводит к небольшому увеличению количества аутофагических вакуолей в нейронах мозга мух. Недавно нами обнаружено, что нуль-аллельные по гену *Hsp67Bc* особи *D. melanogaster* имеют сниженную устойчивость к холодовому стрессу (0 °C) различной длительности. В настоящей работе мы исследовали, как наличие делеции в гене *Hsp67Bc* повлияет на жизнеспособность *D. melanogaster* в нормальных условиях и на их устойчивость к повышенной температуре на разных стадиях развития. Делеция *Hsp67Bc* не оказала на личинок и куколок дрозофил неблагоприятного воздействия; нуль-аллельные по гену *Hsp67Bc* имаго имели увеличенную по сравнению с контролем продолжительность жизни при нормальной (24–25 °C) и повышенной (29 °C) температуре, а также после кратковременного теплового стресса (37 °C, 2 ч). В то же время плодовитость мутантных самок была снижена на 6–13 % по сравнению с контролем при всех исследованных температурных режимах, за исключением постоянного содержания при 29 °C, при котором среднее число откладываемых яиц не различалось между контрольной и мутантной линиями. Мы связываем этот феномен со сниженным количеством овариол у нуль-аллельных по гену *Hsp67Bc* самок, а также с усиленной макроаутофагией в их гермариях, приводящей к росту числа гибнущих формирующихся яйцевых камер.

Кроме того, кратковременный тепловой стресс (37 °C, 2 ч), приводивший к увеличению продолжительности жизни *D. melanogaster* контрольной линии (что является распространенной реакцией у живых организмов), отрицательно влиял на продолжительность жизни мух с делецией *Hsp67Bc*. Таким образом, *D. melanogaster* с делецией в гене *Hsp67Bc* имеют увеличенную продолжительность жизни в нормальных условиях и при повышенной температуре и сниженные плодовитость и устойчивость к температурному стрессу.

Ключевые слова: продолжительность жизни *Drosophila*; устойчивость к температурному стрессу; повышенная температура; тепловой стресс; малые белки теплового шока; аутофагия.

Introduction

During ontogenesis, all living organisms experience stress. The effects of stress-inducing agents on cells include oxidative modification of proteins, which leads to their misfolding (Jolly, Morimoto, 2000). Misfolded proteins are detrimental to the cell because they may gain deleterious biological functions and are prone to forming insoluble aggregates (Jolly, Morimoto, 2000). To maintain homeostasis, cells synthesize heat shock proteins (HSPs): a group of conservative proteins that ensure correct folding of peptides, prevent aggregation of denatured proteins, and resolubilize protein aggregates (Jolly, Morimoto, 2000). This response is universal among all the known pro- and eukaryotes (Lindquist, 1986). Expression of the majority of *HSP* genes is up-regulated in stressful conditions such as heat and cold stress, hypoxia, bacterial and viral infections, and oxidative stress (Lindquist, 1986; Sørensen et al., 2003). Some HSPs are constitutively expressed and are necessary for growth and development of organisms under normal conditions (Kampinga et al., 2009; Sarkar et al., 2011). In a study by Raut et al. (2017) on *Drosophila*, knockdown of 42 out of 95 tested *HSP* genes led to F1 lethality indicating their crucial role in the fly development.

Drosophila melanogaster Hsp67Bc belongs to the small heat shock protein family of HSPs (Vos et al., 2016). It shares a function of preventing damaged protein aggregation with other members of the family (Vos et al., 2016). In addition, *Hsp67Bc* was shown to be involved in the regulation of macroautophagy – a conservative catabolic process allowing the recycling of cytoplasm components – alongside Starvin protein (Carra et al., 2010; Parzych, Klionsky, 2014). Overexpression of the *Hsp67Bc* gene separately or together with *stv* resulted in protein synthesis inhibition and macroautophagy stimulation (Carra et al., 2010).

Our studies on the *Hsp67Bc* gene deletion in *D. melanogaster* revealed that in brain neurons of *Hsp67Bc*-null flies infected by a pathogenic *Wolbachia* bacteria strain *wMelPop*, the number of autophagosomes and autolysosomes (organelles formed in the process of macroautophagy that sequester cytoplasm components and digest them) was increased, and the cross-sectional area of autolysosomes was more than 1.5-fold larger than in the control line with the wild-type *Hsp67Bc* gene (Malkeyeva et al., 2021). These observations may indicate that in the absence of the *Hsp67Bc* gene product, macroautophagy is slightly enhanced and autophagosome maturation process is affected. Furthermore, we showed that the *Hsp67Bc* gene product plays an important role in tolerance to cold stress in the fruit fly (Malkeyeva et al., 2020). *Hsp67Bc*-null adult flies needed more time to recover from chill coma than the control flies, and adult females with the *Hsp67Bc* gene deletion had a 1.6–3-fold lower survival after cold stress of various dura-

tions (2, 4, and 12 h at 0 °C) as compared to the control line (Malkeyeva et al., 2020).

In this study, we investigated fitness of *Hsp67Bc*-null *D. melanogaster* under normal conditions (24–25 °C) and their tolerance to elevated temperatures (29 °C or 2 h at 37 °C) at different stages of ontogenesis (larva, pupa, and imago). We found that the adult mutant flies had an increased lifespan at all the tested temperatures, in comparison with the control line with an intact *Hsp67Bc* gene. *Hsp67Bc*-null adult flies, however, had slightly reduced fecundity under normal conditions and after heat stress (37 °C, 2 h) and were negatively affected by acute heat stress (37 °C, 2 h) that prolonged longevity of the control line. Thus, despite having extended lifespan in comparison with the control line under all tested conditions, *Hsp67Bc*-null flies had lower fecundity and were less tolerant to acute heat stress.

Materials and methods

***Drosophila melanogaster* lines.** In this study, we used *Hsp67Bc*-null *D. melanogaster* line *Hsp67Bc*-0 we created by an imprecise excision of a *P*-element located in proximity to the *Hsp67Bc* gene transcription start. Fly line *Hsp67Bc*-2 containing a wild-type variant of *Hsp67Bc* obtained by a precise cutting out of the mentioned *P*-element was used as a control. The procedure for obtaining the fly lines is described in our recent article (Malkeyeva et al., 2020).

Heat stress applied to larvae and pupae. For these experiments, wandering late 3rd instar (L3) larvae were transferred from their rearing vials to the walls of vials with fresh cornmeal-agar medium, at 20 per vial. The larvae were then either directly transferred to a 37 °C environment (water bath in an incubator) for 2 h incubation or allowed to first reach the developmental stage that was to be treated. In particular, these were pupal stages P1–P2 (white prepupae, 1–2 h after pupation), P5 (18–20 h after pupation), or P7–P8 (46–48 h after pupation) (Bainbridge, Bownes, 1981). The cottons sealing the vials were slightly moisturized with water before the start of heat treatment to prevent drying of the larvae and pupae. After the heat stress treatment, the flies were kept at 24–25 °C until eclosion. Survivors to the pupa stage (in case of late L3 treatment) and to the adult stage (for all treatment groups) were then counted. In each experiment, 39–107 flies of each genotype were used.

Analysis of the lifespan and fecundity of adult *D. melanogaster* kept at either normal or elevated temperature. The flies were collected from rearing vials on the 1st day after eclosion and placed into vials with a fresh cornmeal-agar medium, at eight males and eight females per vial. The flies then underwent one of four treatments. The 1st group was kept at 24–25 °C (normal conditions); the 2nd group was subjected

to heat treatment at 37 °C for 2 h at 1 day of age and then was returned to the 24–25 °C environment; the 3rd group was heat treated (37 °C, 2 h) at 7 days of age, then returned to the 24–25 °C environment; the 4th group was transferred to a 29 °C environment at 1 day of age and kept at the elevated temperature. Each experimental group contained 45–62 males and 51–62 females of relevant genotypes.

All the flies were kept under the specified conditions until the death of all individuals, with survivors transferred to fresh food daily or every other day. In parallel, fecundity was measured in these *Drosophila* starting from day 2 in the 1st, 2nd, and 4th groups and starting from day 8 in the 3rd group (one day after the heat treatment). *D. melanogaster* females were allowed to lay eggs for 24 h in vials with fresh medium, then the parents were transferred to new food, and the eggs were counted. The number of eggs in a vial was then divided by the number of females that oviposited in that very vial. The egg per female ratio was evaluated on days 2–11, 15–17, and 22–24 in the 1st, 2nd, and 4th experimental groups; in the 3rd group, the ratio was measured on days 8–10, 13–15, and 20–22.

Protein starvation assay. For this assay, newly eclosed adult *D. melanogaster* individuals were collected every 2 h from their rearing vials and transferred to vials with protein-free medium containing 100 g/L sucrose, 5 g/L agar and 0.78 g/L methyl 4-hydroxybenzoate. The flies were transferred to a fresh medium every other day.

LysoTracker Red (LTR) staining. On the 5th and 15th days of the protein starvation experiment, ovaries of the starved adult *D. melanogaster* females and females kept on standard food were dissected in 0.01 M PBS (Medigen) (pH 7.4) and stained with 100 nM LysoTracker Red DND-99 (Life Technologies) and DAPI. The LTR staining was performed as follows: the dissected ovaries were first placed into a droplet of a 100 nM LTR solution in 0.01 M PBS for 10 min incubation, washed thrice in PBS, and then fixed in 4 % paraformaldehyde for 20 min; next, the ovaries were washed three times with a 0.1 % Triton X-100 solution in PBS and mounted on a slide with a drop of DAPI-containing *SlowFade* Gold Antifade Mountant (Thermo Fisher Scientific). To make sure the antifade mountant penetrates inner ovarioles, we let the ovaries stay without a cover slip for ~15 min before sealing them under it with nail polish. The samples were stored in the dark at 4 °C until analysis under the LSM 780 confocal microscope (Zeiss) with the Plan-Apochromat 20x/0.8 M27 objective.

Statistical analyses. Survival and recovery curves were compared by the log-rank test. The fecundity, lifespan, number of ovarioles, and number of dying egg chambers per ovariole datasets were tested for normality by the Shapiro–Wilk test; normally distributed data were compared by the heteroscedastic *t* test; data with non-normal distribution were compared by the Mann–Whitney *U* test. Differences in fecundity between the control and mutant fly lines throughout the experiment were evaluated at each point by the heteroscedastic *t* test, followed by the Benjamini–Krieger–Yekutieli method to control the false discovery rate. Analyses of the proportion (%) of LTR-positive germaria obtained in the LTR-staining experiments were performed by the chi-squared test. Differences were considered statistically significant at $p \leq 0.05$.

The Shapiro–Wilk test and the Mann–Whitney *U* test were conducted using Statistics Kingdom statistics calculators (<https://www.statskingdom.com>).

Results

Hsp67Bc-null *D. melanogaster* under normal conditions

To expand our knowledge on the functions of *Hsp67Bc* in the fruit fly we created a *D. melanogaster* line carrying a deletion of almost the entire *Hsp67Bc* gene (described in detail in our recent article (Malkeyeva et al., 2020)). The flies carrying the deletion in the *Hsp67Bc* gene in the homozygous state (*Hsp67Bc*-0) were viable and fertile, and had no visible morphological deviations from the control. The *Hsp67Bc*-0 line had extended longevity under normal conditions (24–25 °C) as compared to the control *Hsp67Bc*-2 line (Fig. 1, *a–c*). The mean lifespan of *Hsp67Bc*-null *D. melanogaster* significantly exceeded that of the control by 35 % in males and by 34 % in females at 24–25 °C (see Fig. 1, *c*). Thus, it was 70.9 ± 1.3 days in the mutant males as compared to 52.4 ± 1.9 days in the control males ($p < 0.001$) and 63.9 ± 2.2 days in *Hsp67Bc*-0 females, compared to 47.8 ± 2.4 days in the control line ($p < 0.001$). On the contrary, the mean fecundity measured during the first month of life was 5.9 % lower ($p = 0.809$) in *Hsp67Bc*-0 females than in the control (see Fig. 1, *d*).

Because under normal conditions the absence of the *Hsp67Bc* gene increased the mean lifespan of the flies while causing only a minor decrease in fecundity, and because no cases of the loss of this gene in wild fruit fly populations have been reported to date, a question arose about the role of the *Hsp67Bc* gene in *D. melanogaster*. It is known that heat shock proteins (which include *Hsp67Bc*) are essential for stress tolerance in all the living organisms (Lindquist, 1986; Sørensen et al., 2003). In our previous study, we discovered involvement of the *Hsp67Bc* gene product in cold stress tolerance in *D. melanogaster* (Malkeyeva et al., 2020). In addition, the *Hsp67Bc* gene expression was shown to increase in response to heat stress (Vos et al., 2016). Therefore, we decided to investigate the impact of the deletion in the *Hsp67Bc* gene on elevated temperature tolerance in the flies.

The effect of heat stress on survival of *Hsp67Bc*-null larvae and pupae

According to FlyBase (<https://flybase.org>), the *Hsp67Bc* gene expression levels are the highest in wandering 3rd instar (late L3) larvae and pupae of *D. melanogaster*, in particular, white prepupae, 12 h pupae, and 48 h pupae. We decided to check how heat stress would affect *Hsp67Bc*-0 flies at those stages of development, in addition to the adult stage.

The larvae and pupae were placed in a 37 °C environment for 2 h, after which they were returned to 24–25 °C to recover and continue development. The survival rates of the larvae and pupae were computed as a proportion (%) of eclosed individuals (Fig. 2, *a*). The mean survival rates to adult stage were similar between the control and *Hsp67Bc*-null pupae, varying between 95.0 ± 2.9 % (12 h *Hsp67Bc*-0 pupae) and 100 % (48 h *Hsp67Bc*-0 pupae). Statistically significant differences were observed between the survival rates of the control and mutant flies at wandering L3 larva stage: the mutant larvae

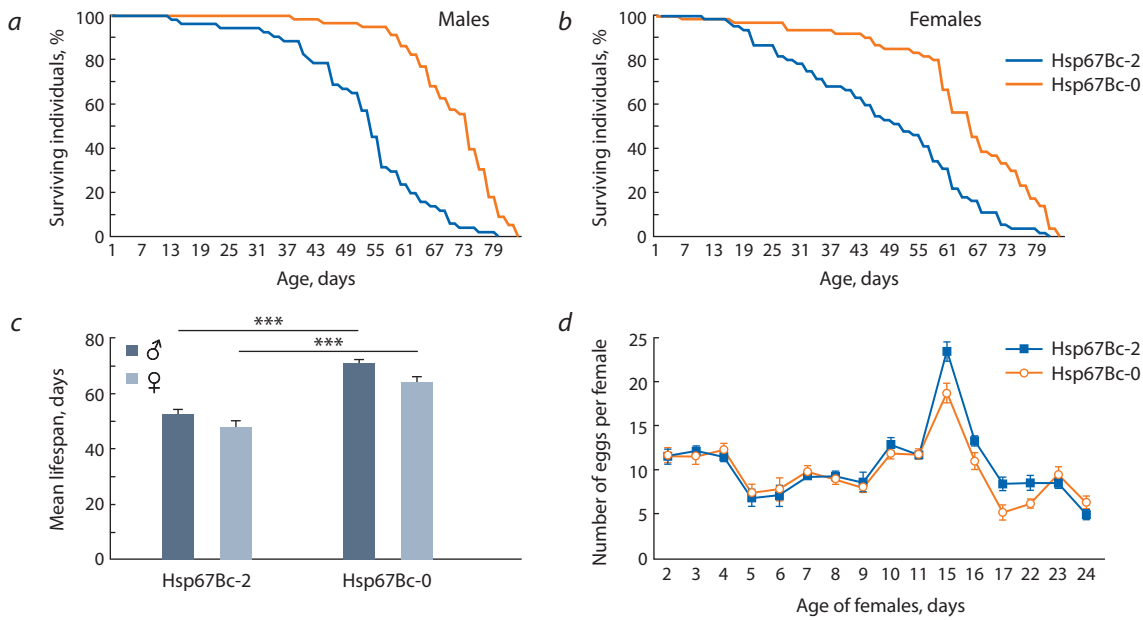


Fig. 1. The survival, lifespan, and fecundity of *Hsp67Bc*-null (*Hsp67Bc-0*) and control (*Hsp67Bc-2*) *D. melanogaster* under normal conditions (24–25 °C).

Survival curves of males (a) and females (b); the mean lifespan (c); fecundity (eggs per female) dynamics of mutant and control females throughout the first month of life (d). The error bars denote standard error of the mean (SEM). *** $p < 0.001$.

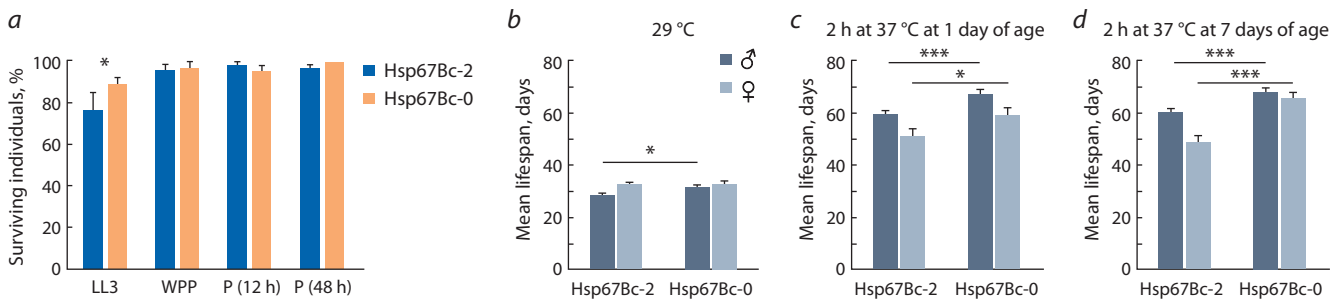


Fig. 2. Survival rates of larvae, white prepupae, and pupae of *Hsp67Bc*-null (*Hsp67Bc-0*) and control (*Hsp67Bc-2*) flies after acute heat stress (37 °C, 2 h), and the mean lifespan of adult mutant and control flies under different regimens involving heat treatment.

a, the proportion (%) of wandering L3 larvae (LL3), white prepupae (WPP), 11–13 h pupae (P (12 h)), and of 47–49 h pupae (P (48 h)) surviving to the adult stage after 2 h of heat treatment (37 °C); b, the mean lifespan of the adult males and females constantly kept at 29 °C; c, the mean lifespan of the adult flies kept at 24–25 °C after 2 h heat treatment (37 °C) at 1 day of age; d, the mean lifespan of the adult flies kept at 24–25 °C after 2 h heat treatment (37 °C) at 7 days of age. The error bars represent SEM. * $0.010 < p < 0.050$; *** $p < 0.001$.

showed higher survival rate as compared to the control line (88.9 ± 3.1 % in the *Hsp67Bc-0* line against 76.6 ± 8.3 % in the control, $p = 0.044$).

The impact of elevated temperature on *Hsp67Bc*-null adult flies

In continuation of the temperature stress experiments on larvae and pupae, *Hsp67Bc-0* and control adult flies were subjected to one of the two variants of elevated temperature treatment. The first variant was life-long maintenance at 29 °C starting from one day of age; the second variant included heat stress (2 h at 37 °C) at either one or seven days of age with subsequent maintenance at 24–25 °C until death of all individuals. The fly ages for heat stress treatment (2 h at 37 °C) were chosen based on FlyBase (<https://flybase.org>) data indicating that the *Hsp67Bc* protein levels are much higher in 1-day-old flies than in 7-day-old flies.

Constant maintenance at 29 °C significantly shortened the lifespan of both control and *Hsp67Bc*-null flies, as compared to maintenance under normal conditions (24–25 °C) without heat treatment (see Fig. 2, b, Fig. 1, c). The mean lifespan of males was 28.1 ± 0.9 days in the control line and 31.3 ± 0.8 days in the mutant line. Still, the mean lifespan of *Hsp67Bc*-null males was 11.5 % higher than that of the control line at 29 °C ($p = 0.010$), and the mutant males passed 50 % survival between days 33 and 34 of the experiment, whereas the control ones had passed it already between days 29 and 30 (Fig. 3). Females of the control line had a mean lifespan of 32.4 ± 0.7 days and *Hsp67Bc-0* females had a mean lifespan of 32.5 ± 1.1 days. Unlike males, females of the control and mutant lines had similar survival dynamics and lifespan at 29 °C (see Fig. 2, b, Fig. 3). Of note, although the mean lifespan of *Hsp67Bc*-null *Drosophila* was exceeding or equal to that of the control flies at the 29 °C environment, the re-

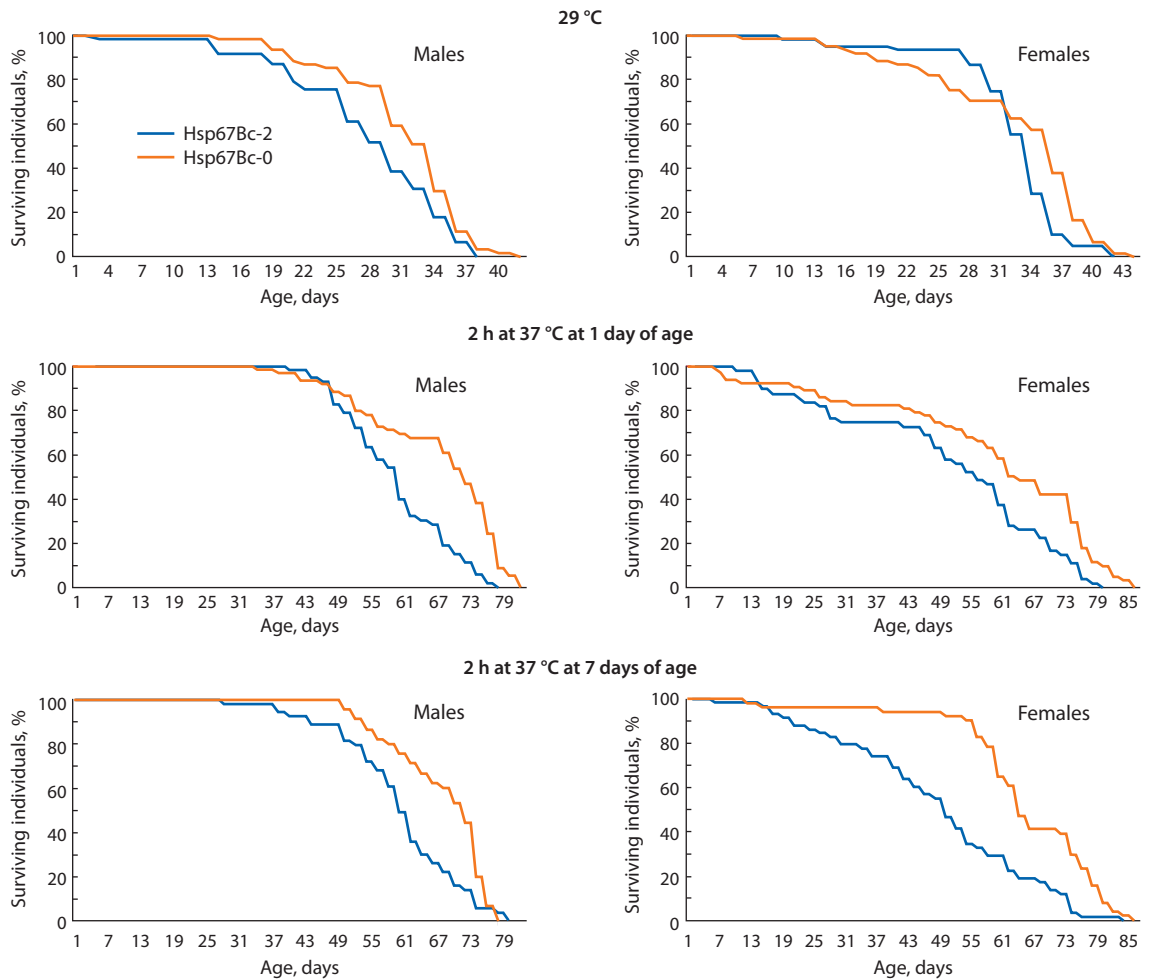


Fig. 3. Survival curves of adult *Hsp67Bc*-null (*Hsp67Bc*-0) and control (*Hsp67Bc*-2) flies kept at 29 °C or at 24–25 °C after 2 h heat treatment (37 °C) at either 1 or 7 days of age.

duction of longevity caused by maintenance at the elevated temperature (29 °C) was more prominent in the mutant flies than in the control ones. Thus, maintenance at 29 °C reduced the lifespan of *Hsp67Bc*-2 males and females 1.9-fold and 1.5-fold, respectively, as compared to normal conditions (24–25 °C) without heat stress, whereas the decline was 2.3-fold in *Hsp67Bc*-null males and 2.0-fold in *Hsp67Bc*-0 females (see Fig. 1, c, Fig. 2, b).

Heat shock (37 °C, 2 h) did not cause death in neither the control nor *Hsp67Bc*-null fly line. The mean lifespan of *Hsp67Bc*-0 flies was higher as compared to the control among both males and females at both variants of heat treatment (at one or seven days of age) (see Fig. 2, c, d). Survival dynamics also significantly differed between the lines with $p \leq 0.010$ (see Fig. 3). The mean lifespan of *Hsp67Bc*-0 males heat-treated at one or seven days of age was higher than that of the control males by ~13 % ($p < 0.001$) and was 67.0 ± 1.7 days in *Hsp67Bc*-0 males heat-shocked at one day of age and 67.9 ± 1.3 days in the mutant males heat-shocked at seven days of age (see Fig. 2, c, d). The mean lifespan of *Hsp67Bc*-null females that underwent heat stress at one day of age exceeded that of the control females by ~16 % (58.9 ± 2.8 days, $p = 0.014$); between the control and mutant females heat-treated at seven days of age, the difference in

the mean lifespan was ~35 % (65.4 ± 2.0 days, whereas that of *Hsp67Bc*-2 females was 48.5 ± 2.4 days, $p < 0.001$) (see Fig. 2, c, d). Of note, the applied heat stress (37 °C, 2 h) had a different impact on the control and *Hsp67Bc*-null flies. In comparison with the maintenance under normal conditions (24–25 °C, without treatment), it increased longevity of the control males and females by 1.5–14.5 % (see Fig. 1, c, Fig. 2, c, d). On the contrary, in the *Hsp67Bc*-0 line, heat stress at 37 °C reduced the mean lifespan of females treated at one day of age by 7.8 %, and the mean lifespan of males heat-shocked at one and seven days of age by 5.5 and 4.2 %, respectively (see Fig. 1, c, Fig. 2, c, d).

These findings may suggest that even though the *Hsp67Bc* gene deletion causes an increase in the lifespan of flies at both normal and elevated temperature, it has a detrimental effect on tolerance to acute heat stress, which normally improves the longevity of flies (Hercus et al., 2003; Le Bourg, 2011; Sarup et al., 2014).

The effect of elevated temperature on *D. melanogaster* fecundity

In parallel with lifespan and survival, we measured fecundity of the control and *Hsp67Bc*-null females as the number of eggs laid in each vial within 24 h divided by the number of

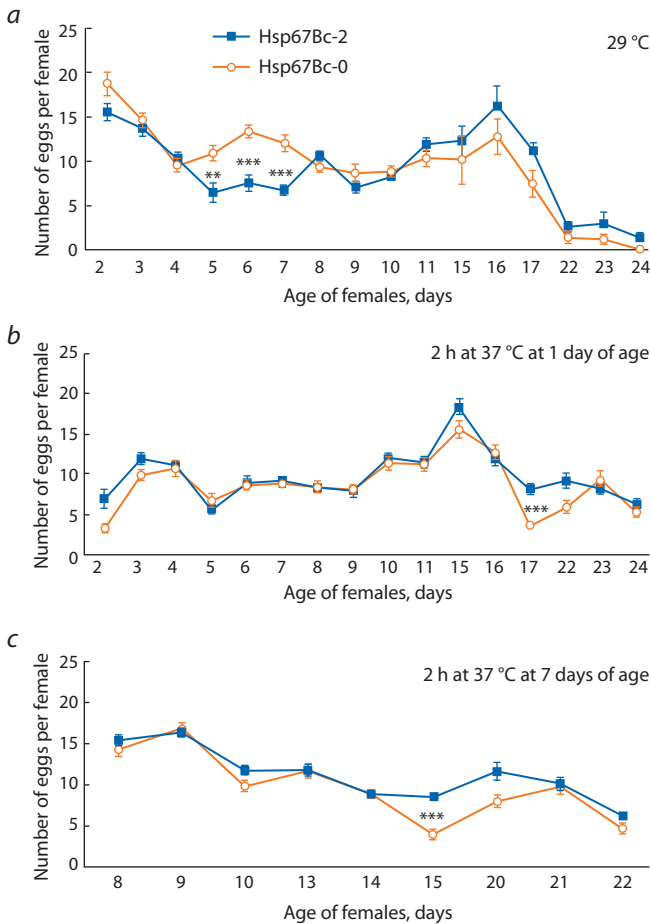


Fig. 4. Fecundity (eggs per female) measured throughout the first month of life of the *Hsp67Bc*-null (*Hsp67Bc*-0) and control (*Hsp67Bc*-2) females kept at 29 °C (a) or at 24–25 °C after 2 h heat treatment (37 °C) at either 1 day (b) or 7 days (c) of age.

The error bars denote SEM. ** 0.001 < p ≤ 0.010; *** p ≤ 0.001.

females kept in those very vials. The mean egg per female ratio calculated throughout the experiment did not statistically differ between the control and mutant lines in any of the heat treatment groups (29 °C, 2 h at 37 °C at one day of age, and 2 h at 37 °C at seven days of age). Nevertheless, *Hsp67Bc*-null females had slightly reduced fecundity as compared to the control flies after being subjected to heat shock (37 °C, 2 h). The differences between the lines were more prominent than at 24–25 °C without treatment. Thus, the mean number of eggs per female was 10.5 % lower in the mutant flies that underwent the heat treatment at one day of age as compared to the control (8.71 eggs/female in *Hsp67Bc*-0 line and 9.73 eggs/female in *Hsp67Bc*-2 line, $p = 0.564$); in the mutant flies subjected to heat stress at seven days of age, this value was 12.8 % (9.77 eggs/female in *Hsp67Bc*-0 line and 11.2 eggs/female in the control, $p = 0.427$).

The egg/female ratio measured each day significantly differed between the mutant and control lines only on some of the days of the experiment (Fig. 4). It is worth mentioning that heat shock (37 °C, 2 h) at one day of age was detrimental for the fecundity of females. The next day after the heat treatment, the number of laid eggs per female was much less than under normal conditions without treatment in both the control and

mutant lines (see Fig. 4, b, Fig. 1, d). The decrease was more prominent in *Hsp67Bc*-null flies (72 % decrease in *Hsp67Bc*-0 line as compared to 40 % reduction in the control line).

In search for the cause of the reduced mean fecundity in *Hsp67Bc*-null females kept at 24–25 °C, we analyzed the morphology of ovaries in the control and mutant lines. In the ovaries of both the control and mutant flies, egg chambers at all stages of oogenesis were present. However, the mutant females had lower number of ovarioles than the control ones. Five- and 15-day-old *Hsp67Bc*-2 females had 16.9–18.4 ovarioles per ovary, whereas *Hsp67Bc*-0 females had 14.6–16.2 ovarioles per ovary ($p = 0.680$ in case of the 5-day-old flies and $p < 0.001$ in case of the 15-day-old flies). This finding may partially explain the difference in the fecundity of the two lines.

The number of ovarioles may be influenced by nutrient deprivation in *D. melanogaster* (Sarıkaya et al., 2012). Dietary restriction stimulates macroautophagy, a process of intracellular component degradation, in regulation of which *Hsp67Bc* was shown to participate (Amano et al., 2006; Carra et al., 2010; Kroemer et al., 2010). Our recent studies on macroautophagy revealed a slight increase in autophagic vacuole number in the brain of adult *Hsp67Bc*-null flies (Malkeyeva et al., 2021). Therefore, we next decided to study the morphology of the control and *Hsp67Bc*-null *D. melanogaster* ovaries under the stress of protein starvation.

The impact of *Hsp67Bc* gene deletion on starvation-induced macroautophagy in *D. melanogaster* ovaries

It is known that starvation, including protein deprivation, induces macroautophagy in *Drosophila* ovaries at two nutrient status checkpoints: germarium and mid-oogenesis (Hou et al., 2008), which then leads to oogenesis slowdown and to an increase in the number of egg chambers eliminated from oogenesis (Barth et al., 2011). The discarded egg chambers degrade through apoptosis with the participation of autophagy (Bolobolova et al., 2020). To evaluate macroautophagy intensity, we used the LysoTracker Red DND-99 (LTR) dye, which had been shown to label acidic organelles, such as lysosomes and autolysosomes, in *D. melanogaster* (Scott et al., 2004; Klionsky et al., 2007). Massive acidification of the cytoplasm signifies death of forming egg chamber cells. We estimated the percentages of LTR-positive germaria in the control and *Hsp67Bc*-null flies kept on standard food and after five (Fig. 5) and 15 days of protein starvation.

As compared to the control line, in the ovaries of *Hsp67Bc*-null females kept on either the standard or protein-free medium, a higher number of LTR-positive germaria was observed (Fig. 6, see Fig. 5). During early oogenesis, the *Hsp67Bc* gene deletion resulted in a 1.2- to 1.5-fold increase in the LTR-positive-germaria proportion (see Fig. 6). Thus, in 5-day-old *Hsp67Bc*-0 females kept on the standard medium, 32.1 % of germaria were LTR-positive, relative to 21.1 % in the control *Hsp67Bc*-2 line ($p = 0.066$); in 5-day-old starved *Hsp67Bc*-null female ovaries, the percentage of LTR-positive germaria was as high as 77.9 % but was only 59.3 % in *Hsp67Bc*-2 females ($p = 0.045$). In 15-day-old *Hsp67Bc*-null females kept on the standard food, LTR-positive germaria constituted 31.1 %, whereas in the control line, this proportion was 24.3 % ($p = 0.348$); in 15-day-old starved flies, the percentages of LTR-positive germaria in ovaries were 73.3 % in the

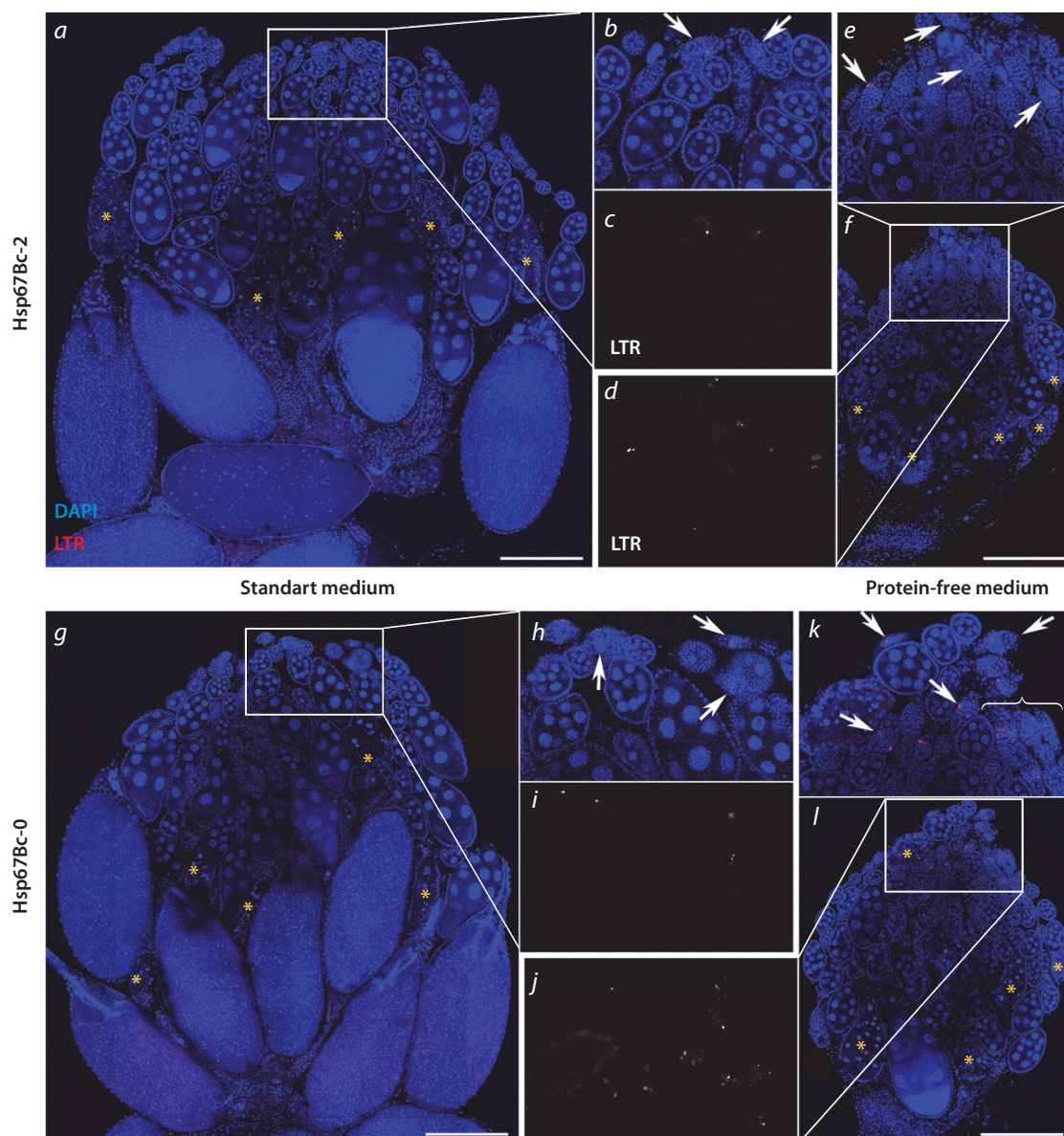


Fig. 5. LTR-labelled ovaries of *Hsp67Bc*-null (*Hsp67Bc*-0) and control (*Hsp67Bc*-2) adult *D. melanogaster* females kept on either the standard or protein-free medium for 5 days.

a, an ovary of a control female kept on the standard medium; *b*, *c*, the magnified white rectangle from panel *a* showing DAPI (blue) and LTR (red) channels (*b*) and a separate LTR channel (*c*); *d*–*f*, an ovary (*f*) of an *Hsp67Bc*-2 female kept on the protein-free medium, and its magnified fragment (white rectangle from panel *f*) showing DAPI and LTR channels (*e*) and a separate LTR channel (*d*); *g*–*i*, same as *a*–*f*, for the *Hsp67Bc*-0 line. Yellow asterisks denote egg chambers with highly condensed and/or fragmented nuclei; white arrows indicate LTR-positive germaria; because too many LTR-positive germaria are present in panel *k*, not all of them are indicated by arrows, and three of them are indicated by a brace. Scale bars are 200 µm.

Hsp67Bc-0 line and 60.4 % in the *Hsp67Bc*-2 line ($p = 0.226$). These data reflect an increase in macroautophagy intensity in the germaria of *Hsp67Bc*-null females.

During mid-oogenesis, we noted a decrease in the number of egg chambers with highly condensed chromatin (see Fig. 5), which is a marker of apoptotic cell death, in *Hsp67Bc*-null flies in comparison with the control, except for the 5-day-old females kept on the standard medium. In 5- and 15-day-old starved and in 15-day-old normally fed *Hsp67Bc*-null flies, the mean number of apoptotic egg chambers per ovariole was slightly lower than that in the control flies, the difference being significant only in 5-day-old starved flies (Fig. 6). Thus, the

observed egg chamber apoptosis was 37 % lower in 5-day-old starved mutant females than in the control females ($p = 0.008$). In 15-day-old starved flies, the mean number of apoptotic egg chambers per ovariole was 11 % lower in the *Hsp67Bc*-0 flies than that in the control individuals ($p = 0.528$); in 15-day-old females kept on the standard food, this number was 35 % lower in the mutant flies than in the *Hsp67Bc*-2 line ($p = 0.131$). Although we observed a lower mean number of apoptotically dying mid-oogenesis egg chambers in *Hsp67Bc*-null flies, we can hypothesize that this phenomenon is related to the observed increased apoptosis of forming egg chambers in germaria during early oogenesis in the mutant flies.

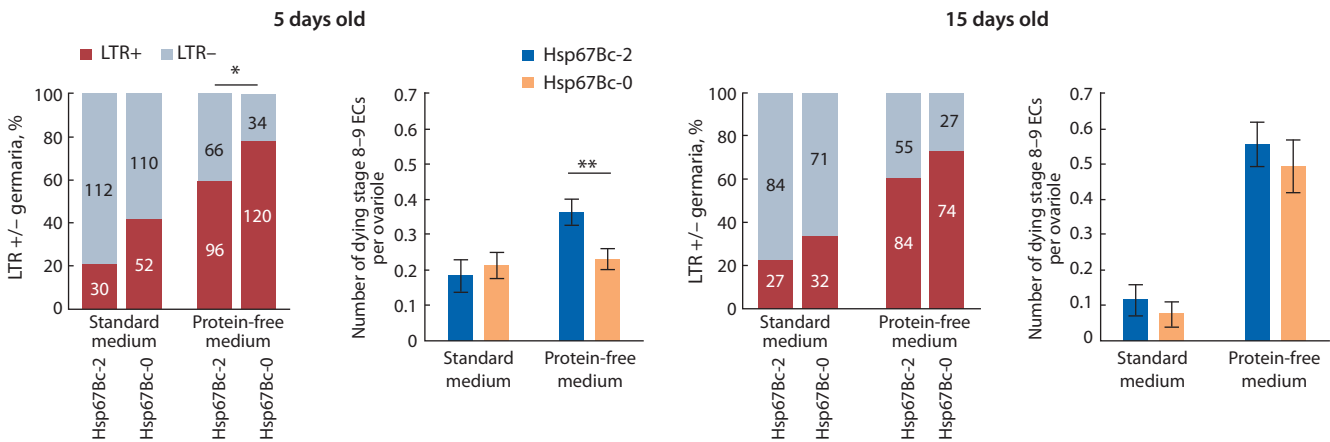


Fig. 6. Diagrams depicting ratios of LTR-positive (LTR+) and LTR-negative (LTR-) germaria and mean numbers of mid-oogenesis egg chambers (ECs) with highly condensed and/or fragmented nuclei per ovariole in the ovaries of 5- and 15-day-old mutant (*Hsp67Bc-0*) and control (*Hsp67Bc-2*) females kept on either the standard or protein-free medium.

The numerals written inside columns in the LTR+/- diagrams represent actual numbers of analyzed germaria. The error bars denote SEM. * 0.010 < *p* ≤ 0.050; ** 0.001 < *p* ≤ 0.010.

Discussion

In this study, we investigated the impact of the *Hsp67Bc* gene deletion on *D. melanogaster* fitness under normal conditions and on their heat-stress tolerance. *Hsp67Bc*-null flies showed extended lifespan as compared to the control line under normal conditions (24–25 °C), elevated temperature conditions (29 °C), and after acute heat stress (37 °C, 2 h) (see Fig. 1, Fig. 2). At the same time, the mean fecundity of the mutant females was slightly reduced at 24–25 °C without heat treatment and after the short heat stress (Fig. 1, *d*, Fig. 4, *b*, *c*).

The observed statistically insignificant decrease in *Hsp67Bc*-null female fecundity can be explained by a combination of the following factors. First, the mutants had reduced number of ovarioles, a trait that was reported by other researchers to result in lower egg yield (Yamamoto et al., 2021). Second, the quantity of LTR-positive germaria was higher in *Hsp67Bc*-null females as compared to the control line (Fig. 6), which indicates increased macroautophagy and enhanced death of forming egg chambers resulting in less eggs (Drummond-Barbosa, Spradling, 2001; Nezis et al., 2009). Contrary, in the mutant females, a lower number of mid-oogenesis egg chambers dying via apoptosis was present as compared to the control flies (Fig. 6). This last feature of the mutant ovaries may partially compensate the first two in terms of eventual egg yield making the difference between the lines statistically insignificant. In *D. melanogaster*, ovariole number is determined at the stage of 3rd instar larva and can be influenced by either genetic or environmental factors, such as rearing temperature and diet (Sarıkaya et al., 2012).

Nutrition plays an important role in defining the quantity of ovarioles: larvae kept on medium with reduced nutrient level develop into adult flies with less ovarioles (Sarıkaya et al., 2012). The decreased ovariole number in *Hsp67Bc*-null flies reared on the standard food may be caused by impaired larva nutrition due to reduced food intake or uptake, which was not registered in our studies. Alternatively, the number of ovarioles in mutant flies could be affected by slightly increased macroautophagy, which we detected in *Hsp67Bc*-null fly germaria and, previously, in brain neurons of adult flies

with the *Hsp67Bc* gene deletion (Malkeyeva et al., 2021). It is known that macroautophagy is strongly stimulated in response to starvation (Kroemer et al., 2010); therefore, enhanced macroautophagy on larval stage caused by the absence of the *Hsp67Bc* gene product may mimic nutrient deprivation conditions leading to formation of less ovarioles. The decrease in apoptotic stage 8 egg chambers in *Hsp67Bc*-null females may be a result of increased death of forming egg chambers and, hence, enhanced quality control in the germarium resulting in less defective mid-oogenesis egg chambers in *Hsp67Bc*-null fly ovaries in comparison with the control line.

Extended longevity caused by gene mutations has been reported in *D. melanogaster*. Lifespan is increased in fruit flies carrying hypomorphic mutations in the *InR* (*insulin-like receptor*), *chico*, and *methuselah* genes (Lin et al., 1998; Clansy et al., 2001; Tatar et al., 2001). Notably, products of all these genes are involved in macroautophagy modulation via target of rapamycin (TOR) pathway (Clansy et al., 2001; Wang et al., 2015; Graze et al., 2018; Yamamoto et al., 2021), and their down-regulation leads to macroautophagy stimulation. Similarly, macroautophagy stimulation by dietary restriction or TOR kinase inhibition expands lifespan of animals belonging to various taxa (Masoro, 2000; Kapahi et al., 2004). Moreover, it was shown that longevity extension of *chico*-null *D. melanogaster* is only possible with intact macroautophagy (Bjedov et al., 2020). In this work, we discovered that the number of LTR-positive germaria was slightly higher in *Hsp67Bc*-null *D. melanogaster* ovaries (Fig. 6), which signifies increased macroautophagy. Similarly, our recent study on ultrastructure of neurons in *Wolbachia*-infected *Drosophila* brains revealed an increment in the number of autophagic vacuoles in *Hsp67Bc-0* fly neurons, which, again, points towards enhanced macroautophagy (Malkeyeva et al., 2021). Bjedov et al. (2020) demonstrated that moderate enhancement of macroautophagy in a complex of tissues increases lifespan in *D. melanogaster*, while strong and ubiquitous stimulation of macroautophagy shortens it. Hence, the extension of lifespan we observed in *Hsp67Bc*-null flies may be caused by slight increase in macroautophagy in their tissues.

Although the *Hsp67Bc*-0 flies had an increased lifespan as compared to the control line under all the tested conditions (normal temperature, elevated temperature, and short heat stress), a decline in longevity was present in the mutant flies that were heat treated in relation to untreated *Hsp67Bc*-null flies. Heat shock had the opposite effect on the control line, with acute heat stress improving the longevity of the flies. Generally, mild heat (or other stress) treatment of young adults extends *Drosophila* longevity (Hercus et al., 2003; Le Bourg, 2011; Sarup et al., 2014), as we observed in the control flies. Our experiments with 2–12 h cold treatment of *Hsp67Bc*-null fly line revealed a decreased cold stress tolerance in the mutants (Malkeyeva et al., 2020). Taken together, our results point towards an adverse impact of the *Hsp67Bc* gene deletion on short temperature stress tolerance in adult *D. melanogaster*. While in the laboratory environment flies are rarely exposed to thermal and other stresses, conditions are different in the *D. melanogaster* natural habitat, where fruit flies may experience a wide variety of extreme stresses including heat shock and chill coma. Therefore, an extended lifespan under normal conditions does not guarantee survival in the wild, as was revealed in a study by Wit et al. (2013). It is important for the survival of poikilothermic animals like *Drosophila* to be able to cope with thermal stresses. Hence, the loss of the *Hsp67Bc* gene, the product of which promotes tolerance to acute thermal stresses, though extending lifespan under normal conditions, may be deleterious in a changing environment. Taking into account that *D. melanogaster* overwinter at the adult stage in temperate regions (Izquierdo, 1991), we assume that the *Hsp67Bc* gene was not eliminated from the fruit fly genome because of its prominent role in promoting acute heat and cold tolerance in adult flies.

Conclusion

Here, we studied the effect of the *Hsp67Bc* gene deletion on *D. melanogaster* lifespan and fecundity under normal conditions, and their tolerance to elevated temperature and acute heat stress. We did not detect any difference in survival of heat-shocked (37 °C, 2 h) pupae between the mutant and control lines, and the *Hsp67Bc*-null larvae showed improved survival. Adult *Hsp67Bc*-null flies had a greater lifespan than the control line at all the tested temperature regimes but lower fecundity and decreased acute heat tolerance. We hypothesize that the lifespan extension is caused by slightly increased macroautophagy in the mutant flies, which we observed in ovaries of *Hsp67Bc*-deficient *Drosophila* and – in our earlier work – in the brains of *Hsp67Bc*-null females. At the same time, the enhanced macroautophagy in germlaria, combined with a reduced number of ovarioles, may be the cause of the fecundity reduction in the mutant flies. In conclusion, although the *Hsp67Bc* gene deletion causes the increase in *D. melanogaster* lifespan in a stress-free environment, it has a negative effect on fruit fly acute heat stress tolerance, which may negate the longevity benefits in nature habitat, where stresses like extremely high and low temperature are common.

References

Amano A., Nakagawa I., Yoshimori T. Autophagy in innate immunity against intracellular bacteria. *J. Biochem.* 2006;140(2):161-166. DOI 10.1093/jb/mvj162.

Bainbridge S.P., Bownes M. Staging the metamorphosis of *Drosophila melanogaster*. *J. Embryol. Exp. Morphol.* 1981;66:57-80.

Barth J.M.I., Szabad J., Hafen E., Köhler K. Autophagy in *Drosophila* ovaries is induced by starvation and is required for oogenesis. *Cell Death Differ.* 2011;18:915-924. DOI 10.1038/cdd.2010.157.

Bjedov I., Cochemé H.M., Foley A., Wieser D., Woodling N.S., Castillo-Quan J.I., Norvaisas P., Lujan C., Regan J.C., Toivonen J.M., Murphy M.P., Thornton J., Kinghorn K.J., Neufeld T.P., Cabreiro F., Partridge L. Fine-tuning autophagy maximises lifespan and is associated with changes in mitochondrial gene expression in *Drosophila*. *PLoS Genet.* 2020;16:e1009083. DOI 10.1371/journal.pgen.1009083.

Bolobolova E.U., Dorogova N.V., Fedorova S.A. Major scenarios of genetically regulated cell death during oogenesis in *Drosophila melanogaster*. *Russ. J. Genet.* 2020;56:655-665. DOI 10.1134/S1022795420060034.

Carra S., Boncoraglio A., Kanon B., Brunsting J.F., Minoia M., Rana A., Vos M.J., Seidel K., Sibon O.C., Kampinga H.H. Identification of the *Drosophila* ortholog of HSPB8. *J. Biol. Chem.* 2010;285:37811-37822. DOI 10.1074/jbc.M110.127498.

Clancy D.J., Gems D., Harshman L.G., Oldham S., Stocker H., Hafen E., Leivers S.J., Partridge L. Extension of life-span by loss of CHICO, a *Drosophila* insulin receptor substrate protein. *Science.* 2001;292(5514):104-106. DOI 10.1126/science.1057991.

Drummond-Barbosa D., Spradling A.C. Stem cells and their progeny respond to nutritional changes during *Drosophila* oogenesis. *Dev. Biol.* 2001;231(1):265-278. DOI 10.1006/dbio.2000.0135.

Graze R.M., Tzeng R.-Y., Howard T.S., Arbeitman M.N. Perturbation of IIS/TOR signaling alters the landscape of sex-differential gene expression in *Drosophila*. *BMC Genom.* 2018;19:893. DOI 10.1186/s12864-018-5308-3.

Hercus M.J., Loeschcke V., Rattan S.I.S. Lifespan extension of *Drosophila melanogaster* through hormesis by repeated mild heat stress. *Biogerontology.* 2003;4:149-156. DOI 10.1023/A:1024197806855.

Hou Y.-C.C., Chittaranjan S., Barbosa S.G., McCall K., Gorski S.M. Effector caspase Dcp-1 and IAP protein Bruce regulate starvation-induced autophagy during *Drosophila melanogaster* oogenesis. *J. Cell Biol.* 2008;182:1127-1139. DOI 10.1083/jcb.200712091.

Izquierdo J.I. How does *Drosophila melanogaster* overwinter? *Entomol. Exp. Appl.* 1991;59:51-58. DOI 10.1111/j.1570-7458.1991.tb01485.x.

Jolly C., Morimoto R.I. Role of the heat shock response and molecular chaperones in oncogenesis and cell death. *J. Natl. Cancer. Inst.* 2000;92(19):1564-1572. DOI 10.1093/jnci/92.19.1564.

Kampinga H.H., Hageman J., Vos M.J., Kubota H., Tanguay R.M., Bruford E.A., Cheetham M.E., Chen B., Hightower L.E. Guidelines for the nomenclature of the human heat shock proteins. *Cell Stress Chaperones.* 2009;14:105-111. DOI 10.1007/s12192-008-0068-7.

Kapahi P., Zid B.M., Harper T., Koslover D., Sapin V., Benzer S. Regulation of lifespan in *Drosophila* by modulation of genes in the TOR signaling pathway. *Curr. Biol.* 2004;14(10):885-890. DOI 10.1016/j.cub.2004.03.059.

Klionsky D.J., Cuervo A.M., Seglen P.O. Methods for monitoring autophagy from yeast to human. *Autophagy.* 2007;3(3):181-206. DOI 10.4161/auto.3678.

Kroemer G., Mariño G., Levine B. Autophagy and the integrated stress response. *Mol. Cell.* 2010;40(2):280-293. DOI 10.1016/j.molcel.2010.09.023.

Le Bourg É. Using *Drosophila melanogaster* to study the positive effects of mild stress on aging. *Exp. Gerontol.* 2011;46:345-348. DOI 10.1016/j.exger.2010.08.003.

Lin Y.-J., Seroude L., Benzer S. Extended life-span and stress resistance in the *Drosophila* mutant *methuselah*. *Science.* 1998;282(5390):943-946. DOI 10.1126/science.282.5390.943.

Lindquist S. The heat-shock response. *Annu. Rev. Biochem.* 1986;55:1151-1191. DOI 10.1146/annurev.bi.55.070186.005443.

Malkeyeva D., Kiseleva E., Fedorova S. Small heat shock protein *Hsp67Bc* plays a significant role in *Drosophila melanogaster* cold-

- stress tolerance. *J. Exp. Biol.* 2020;223(Pt.21):jeb219592. DOI 10.1242/jeb.219592.
- Malkeyeva D.A., Kiseleva E.V., Fedorova S.A. Loss of *Hsp67Bc* leads to autolysosome enlargement in the *Drosophila* brain. *Cell Biol. Int.* 2021. DOI 10.1002/cbin.11721.
- Masoro E.J. Caloric restriction and aging: an update. *Exp. Gerontol.* 2000;35:299-305. DOI 10.1016/S0531-5565(00)00084-X.
- Nezis I.P., Lamark T., Velentzas A.D., Rusten T.E., Bjørkøy G., Johansen T., Papassideri I.S., Stravopodis D.J., Margaritis L.H., Stenmark H., Brech A. Cell death during *Drosophila melanogaster* early oogenesis is mediated through autophagy. *Autophagy.* 2009;5: 298-302. DOI 10.4161/auto.5.3.7454.
- Parzych K.R., Klionsky D.J. An overview of autophagy: morphology, mechanism, and regulation. *Antioxid. Redox Signal.* 2014;20(3): 460-473. DOI 10.1089/ars.2013.5371.
- Raut S., Mallik B., Parichha A., Amrutha V., Sahi C., Kumar V. RNAi-mediated reverse genetic screen identified *Drosophila* chaperones regulating eye and neuromuscular junction morphology. *G3: Genes Genomes Genetics. (Bethesda).* 2017;7(7):2023-2038. DOI 10.1534/g3.117.041632.
- Sarikaya D.P., Belay A.A., Ahuja A., Dorta A., Green D.A., Extavour C.G. The roles of cell size and cell number in determining ovariole number in *Drosophila*. *Dev. Biol.* 2012;363:279-289. DOI 10.1016/j.ydbio.2011.12.017.
- Sarkar S., Singh M.D., Yadav R., Arunkumar K.P., Pittman G.W. Heat shock proteins: molecules with assorted functions. *Front. Biol. (Beijing).* 2011;6(4):312. DOI 10.1007/s11515-011-1080-3.
- Sarup P., Sørensen P., Loeschcke V. The long-term effects of a life-prolonging heat treatment on the *Drosophila melanogaster* transcriptome suggest that heat shock proteins extend lifespan. *Exp. Gerontol.* 2014;50:34-39. DOI 10.1016/j.exger.2013.11.017.
- Scott R.C., Schuldiner O., Neufeld T.P. Role and regulation of starvation-induced autophagy in the *Drosophila* fat body. *Dev. Cell.* 2004;7(2):167-178. DOI 10.1016/j.devcel.2004.07.009.
- Sørensen J.G., Kristensen T.N., Loeschcke V. The evolutionary and ecological role of heat shock proteins. *Ecol. Lett.* 2003;6:1025-1037. DOI 10.1046/j.1461-0248.2003.00528.x.
- Tatar M., Kopelman A., Epstein D., Tu M.-P., Yin C.-M., Garofalo R.S. A mutant *Drosophila* insulin receptor homolog that extends life-span and impairs neuroendocrine function. *Science.* 2001;292(5514): 107-110. DOI 10.1126/science.1057987.
- Vos M.J., Carra S., Kanon B., Bosveld F., Klauke K., Sibon O.C.M., Kampinga H.H. Specific protein homeostatic functions of small heat-shock proteins increase lifespan. *Aging Cell.* 2016;15:217-226. DOI 10.1111/acel.12422.
- Wang J., Wang Z., Zhang Z., Hua Q., Wang M., Shi C., Xue L., Zhang R., Xie X. *Methuselah* regulates longevity via dTOR: a pathway revealed by small-molecule ligands. *J. Mol. Cell Biol.* 2015; 7:280-282. DOI 10.1093/jmcb/mjv018.
- Wit J., Kristensen T.N., Sarup P., Frydenberg J., Loeschcke V. Laboratory selection for increased longevity in *Drosophila melanogaster* reduces field performance. *Exp. Gerontol.* 2013;48:1189-1195. DOI 10.1016/j.exger.2013.07.012.
- Yamamoto R., Palmer M., Koski H., Curtis-Joseph N., Tatar M. Aging modulated by the *Drosophila* insulin receptor through distinct structure-defined mechanisms. *Genetics.* 2021;217(2):iyaa037. DOI 10.1093/genetics/iyaa037.

ORCID ID

D. Malkeyeva orcid.org/0000-0002-7308-8846
S.A. Fedorova orcid.org/0000-0001-8257-4654
E. Kiseleva orcid.org/0000-0001-6949-182X

Acknowledgements. LTR analyses were performed at the Multiple-access Center for Microscopy of Biological Objects (Institute of Cytology and Genetics SB RAS). This work was supported by budget project No. 0259-2021-0011.

Conflict of interest. The authors declare no conflict of interest.

Received November 19, 2021. Revised December 30, 2021. Accepted January 10, 2022.

Original Russian text www.bionet.nsc.ru/vogis/

The role of inflammatory system genes in individual differences in nonverbal intelligence

R.F. Enikeeva^{1, 2} , A.V. Kazantseva^{1, 2} , Yu.D. Davydova^{1, 2}, R.N. Mustafin^{2, 3}, Z.R. Takhirova², S.B. Malykh^{4, 5}, Y.V. Kovas^{2, 6}, E.K. Khusnutdinova^{1, 2, 5}

¹ Institute of Biochemistry and Genetics – Subdivision of the Ufa Federal Research Centre of the Russian Academy of Sciences, Ufa, Russia

² Bashkir State University, Department of genetics and fundamental medicine, Laboratory of neurocognitive genomics, Ufa, Russia

³ Bashkir State Medical University, Department of medical genetics and fundamental medicine, Ufa, Russia

⁴ Psychological Institute of the Russian Academy of Education, Moscow, Russia

⁵ Lomonosov Moscow State University, Department of psychology, Moscow, Russia

⁶ Goldsmiths, University of London, Department of psychology, London, United Kingdom

 Kazantsa@mail.ru; Enikeevarf@gmail.com

Abstract. Nonverbal intelligence represents one of the components of brain cognitive functions, which uses visual images and nonverbal approaches for solving required tasks. Interaction between the nervous and immune systems plays a specific role in individual differences in brain cognitive functions. Therefore, the genes encoding pro- and anti-inflammatory cytokines are prospective candidate genes in the study of nonverbal intelligence. Within the framework of the present study, we conducted the association analysis of six SNPs in the genes that encode proteins involved in inflammatory response regulation in the central nervous system (*CRP* rs3093077, *IL1A* rs1800587, *IL1B* rs16944, *TNF/LTA* rs1041981, rs1800629, and *P2RX7* rs2230912), with nonverbal intelligence in mentally healthy young adults aged 18–25 years without cognitive decline with inclusion of sex, ethnicity and the presence of the “risky” *APOE* ϵ 4 allele as covariates. Considering an important role of environmental factors in the development of brain cognitive functions in general and nonverbal intelligence in particular, we conducted an analysis of gene-by-environment ($G \times E$) interactions. As a result of a statistical analysis, rs1041981 and rs1800629 in the tumor necrosis factor gene (*TNF*) were shown to be associated with a phenotypic variance in nonverbal intelligence at the haplotype level (for AA-haplotype: $\beta_{ST} = 1.19$; $p = 0.033$; $p_{perm} = 0.047$) in carriers of the “risky” *APOE* ϵ 4 allele. Gene-by-environment interaction models, which determined interindividual differences in nonverbal intelligence, have been constructed: sibship size (number of children in a family) and smoking demonstrated a modulating effect on association of the *TNF/LTA* (rs1041981) ($\beta = 2.08$; $\beta_{ST} = 0.16$; $p = 0.001$) and *P2RX7* (rs2230912) ($\beta = -1.70$; $\beta_{ST} = -0.10$; $p = 0.022$) gene polymorphisms with nonverbal intelligence. The data obtained indicate that the effect of *TNF/LTA* on the development of cognitive functions is evident only in the presence of the “unfavorable” *APOE* ϵ 4 variant and/or certain environmental conditions.

Key words: nonverbal intelligence; cognitive functions; single nucleotide polymorphism (SNP); association analysis; microglia; inflammatory response.

For citation: Enikeeva R.F., Kazantseva A.V., Davydova Yu.D., Mustafin R.N., Takhirova Z.R., Malykh S.B., Kovas Y.V., Khusnutdinova E.K. The role of inflammatory system genes in individual differences in nonverbal intelligence. *Vavilovskii Zhurnal Genetiki i Seleksii* = *Vavilov Journal of Genetics and Breeding*. 2022;26(2):179-187. DOI 10.18699/VJGB-22-22

Роль генов воспалительного ответа организма в формировании индивидуальных различий в уровне невербального интеллекта

Р.Ф. Еникеева^{1, 2} , А.В. Казанцева^{1, 2} , Ю.Д. Давыдова^{1, 2}, Р.Н. Мустафин^{2, 3}, З.Р. Тахирова², С.Б. Малых^{4, 5}, Ю.В. Ковас^{2, 6}, Э.К. Хуснутдинова^{1, 2, 5}

¹ Институт биохимии и генетики – обособленное структурное подразделение Уфимского федерального исследовательского центра Российской академии наук, Уфа, Россия

² Башкирский государственный университет, кафедра генетики и фундаментальной медицины, лаборатория нейрокогнитивной геномики, Уфа, Россия

³ Башкирский государственный медицинский университет, кафедра медицинской генетики и фундаментальной медицины, Уфа, Россия

⁴ Психологический институт Российской академии образования, Москва, Россия

⁵ Московский государственный университет им. М.В. Ломоносова, факультет психологии, Москва, Россия

⁶ Голдсмит, Лондонский университет, международная лаборатория междисциплинарных исследований индивидуальных различий в обучении, департамент психологии, Лондон, Великобритания

 Kazantsa@mail.ru; Enikeevarf@gmail.com

Аннотация. Невербальный интеллект – один из компонентов когнитивных функций мозга, использующий визуальные образы и невербальные методы для решения поставленных задач. Особую роль в развитии индивидуальных различий в уровне когнитивных функций мозга отводят взаимодействию нервной и иммунной

систем. Гены, кодирующие про- и противовоспалительные цитокины, могут являться кандидатами при изучении невербального интеллекта. Проведен анализ ассоциаций шести локусов генов, белковые продукты которых принимают участие в регуляции воспалительного ответа в центральной нервной системе: *CRP* (rs3093077), *IL1A* (rs1800587), *IL1B* (rs16944), *TNF/LTA* (rs1041981, rs1800629), *P2RX7* (rs2230912), с уровнем невербального интеллекта у здоровых индивидов без когнитивных нарушений в возрасте 18–25 лет с включением половой, этнической принадлежности и наличия «рискового» аллеля $\epsilon 4$ гена *APOE* в качестве ковариат. С учетом важной роли средовых факторов, влияющих на формирование когнитивных функций мозга в целом и невербального интеллекта в частности, осуществлен анализ ген-средовых (G×E) взаимодействий. В результате статистического анализа показано, что полиморфные варианты rs1041981 и rs1800629 гена фактора некроза опухоли альфа (*TNF*) ассоциированы с фенотипическими вариациями в показателе невербального интеллекта на уровне гаплотипов (для гаплотипа AA: $\beta_{ST} = 1.19$; $p = 0.033$; $p_{perm} = 0.047$) в группе носителей «рискового» варианта $\epsilon 4$ гена *APOE*. Построены модели ген-средовых взаимодействий, детерминирующие межиндивидуальные различия в уровне невербального интеллекта: число детей в семье и табакокурение модулируют ассоциацию вариантов генов *TNF/LTA* (rs1041981) ($\beta = 2.08$; $\beta_{ST} = 0.16$; $p = 0.001$) и *P2RX7* (rs2230912) ($\beta = -1.70$; $\beta_{ST} = -0.10$; $p = 0.022$) с уровнем невербального интеллекта. Полученные данные свидетельствуют о том, что эффект гена *TNF/LTA* на формирование особенностей когнитивной сферы наблюдается только в случае наличия «неблагоприятного» варианта гена *APOE* и при сочетании определенных социальных факторов.

Ключевые слова: невербальный интеллект; когнитивные функции; однонуклеотидный полиморфный локус; анализ ассоциаций; микроглия; воспалительный ответ.

Introduction

Understanding the nature of human cognitive development represents one of the relevant issues in the modern-day psychiatric genetics. The possibility to enhance the efficacy of learning at any age directly depends on the knowledge of the mechanisms underlying the development of cognitive functions in the brain and the factors determining this process. Nonverbal intelligence as one of cognitive abilities implies an individual's ability to use problem-solving strategies and manipulate visual information without using verbal skills (Kuschner, 2013). In turn, verbal intelligence stands for language skills, receptive and expressive speech, vocabulary, and verbal abstract reasoning (Dawson, 2013). The differences in the brain functional architecture are related to the use of verbal and nonverbal skills (Feklicheva et al., 2021).

Nowadays, the study of nonverbal intelligence from a biological point of view is considered the most justified (Vyshedskiy et al., 2017), therefore, individual differences in intellectual development are explained by the effect of a number of physiological factors (anatomical and physiological parameters of the brain, signaling systems, etc.) (Li et al., 2009), which, in turn, are significantly affected by an individual's genome (Mustafin et al., 2020). Various socio-demographic parameters play an equally important role in the manifestation of individual variance in nonverbal intelligence (Franić et al., 2014).

Inflammatory mediators belong to one of the promising and poorly studied biological systems in relation to nonverbal intelligence. The only immune system cells in the central nervous system (CNS) parenchyma are microglial cells functioning as residential macrophages (Kierdorf, Prinz, 2017). In addition to the barrier function, microglial cells in the mature brain can produce various neurotrophic factors, such as BDNF (brain-derived neurotrophic factor) and GDNF (glial-derived neurotrophic factor) (Parkhurst et al., 2013). Moreover, contemporary studies reported that microglial cells had receptors for neurotransmitters, neuropeptides and

neuromodulators (Alekseeva et al., 2019), which indicates a link between microglia and neuronal activity, indicating the prospects for studying the inflammatory system relevant to cognitive functioning of the brain in general and nonverbal intelligence in particular. Accordingly, the genes responsible for regulating the activation and deactivation of microglial cells can mediate the development of nonverbal intelligence.

An important function of microglia is to maintain a balance of pro- and anti-inflammatory processes in the intact brain. Such balance is achieved by the production of anti-inflammatory cytokines by microglia: C-reactive protein (CRP), interleukin 1 α (IL1 α), interleukin 1 β (IL1 β), tumor necrosis factor alpha (TNF α). The imbalance in the functioning of microglial cells may cause cytokines accumulation in CNS (Ferro et al., 2021), which, in turn, is one of the reasons for the increased permeability of the blood-brain barrier (BBB). An impaired BBB integration promotes CNS infiltration by leukocytes and neuroinflammation, which may develop into a chronic form and result in abnormal synaptic plasticity of neurons, reduced number of synaptic connections and neurodegenerative processes (Haruwaka et al., 2019). Purinergic receptors are other important participants regulating the inflammatory response. Thus, activation of microglia in the CNS is carried out by purinergic signaling (Franke et al., 2007). According to published data, activation of the purinergic receptor P2X7 initiates innate immunity, thus contributing to an increased level of proinflammatory cytokines (mainly IL-1 β and IL-18) in the CNS, which results in increased inflammation and/or neurons death in various animal species, as well as in humans (Lister et al., 2007).

Another additional genetic risk factor for developing cognitive impairments is the presence of the $\epsilon 4$ variant in the apolipoprotein E (*APOE*) gene, which, according to literature, is associated with an increased risk of neurodegenerative diseases (Emrani et al., 2020), aging and longevity (Erdman et al., 2016). The *APOE* protein has three isoforms E2, E3

and E4 encoded by the $\epsilon 2$, $\epsilon 3$, and $\epsilon 4$ alleles, respectively. Multiple data evidence that the APOE reduces inflammation in the CNS in isoform-specific manner: $\epsilon 2$ and $\epsilon 3$ isoforms have anti-inflammatory and protective properties, while $\epsilon 4$ isoform exhibits low anti-inflammatory activity (Lanfranco et al., 2021). In addition, mice lacking the *APOE* gene demonstrate an enhanced level of proinflammatory cytokines in the CNS (Vitek et al., 2009), which indicates the *APOE* effect on regulating immune function. Therefore, there is a direct link between the *APOE* and microglial cells functioning and cytokine production.

Published data indicate the functional significance of rs1800629 (c.-488G>A) and rs1041981 (c.179C>A or Thr60Asn) in the *TNF/LTA* gene (Hameed et al., 2018), rs2230912 (c.1379A>G or Gln460Arg) in the *P2RX7* gene (Winham et al., 2019), rs1800587 (-889C>T) in the promoter region of the *IL1A* gene (Dominici et al., 2002), rs16944 (-511T>C) in the *IL1B* gene (Tayel et al., 2018), based on the evidence of modified expression of corresponding genes related to various allelic variants. In addition, a genome-wide association analysis of C-reactive protein levels detected the rs3093077 in the *CRP* gene in a large cohort of healthy individuals (Naitza et al., 2012).

Considering a functional role of the mentioned SNPs located in the genes involved in the regulation of inflammatory response in the CNS, within the framework of the present study we have performed the association analysis of the *CRP* (rs3093077), *IL1A* (rs1800587), *IL1B* (rs16944), *TNF/LTA* (rs1041981, rs1800629), *P2RX7* (rs2230912) gene loci with interindividual differences in the level of nonverbal intelligence for the first time. Moreover, a possible modulating effect of the *APOE* $\epsilon 4$ variant (which is determined based on genotyping of rs7412 and rs429358) and several socio-demographic parameters on the association of inflammatory response genes with nonverbal intelligence has been analysed.

Materials and methods

The present study involved 1011 individuals (80 % women, mean age 19.79 ± 1.69 years) of different ethnicity (535 Russians, 231 Tatars, 160 Udmurts, and 85 of mixed ethnicity). At the time of participation in the study, all the subjects were students at the universities of Russia and were not registered in the psychiatric database. Informed consent to participate in the study was obtained from all the participants. The design of this study was approved by the Ethics Committee of the Institute of Biochemistry and Genetics UFRC RAS.

The level of nonverbal intelligence was measured using a black-and-white version of the Raven Progressive Matrices (Raven, 2000), which represents the essential and widely used diagnostic instrument for the assessment of examined cognitive construct and is characterized by high validity and reproducibility (Feklicheva et al., 2021). The abovementioned approach includes a representation of figures, which are related to each other by certain dependence. One figure is missing, and a respondent has to choose one missing figure among 6–8 figures presented. The respondent has to establish a pattern

connecting the figures and to choose a missing figure among the presented ones. The test consists of 60 tables (5 series). The complexity of tasks enhances with an increase in the series and the task number in each series of tables.

To estimate a modulating effect of several socio-demographic parameters, which had been previously reported to influence cognitive abilities, the respondents were asked to present information regarding their ethnicity up to three generations, birth order and the sibship size, smoking status, rearing style, the presence of mental illness in close relatives, knowledge of their native language (Bashkir, Tatar, Udmurt, etc.). Information about the rearing style included such questions on child-parent relationships as the episodes of childhood maltreatment, rearing in a complete/incomplete family, family income, and maternal age at delivery of the respondent.

DNA samples isolated from the venous blood by phenol-chloroform extraction were used in the present study. A genotyping of the *IL1A* (rs1800587), *CRP* (rs3093077), *TNF α* (rs1041981, rs1800629), *P2RX7* (rs2230912), and *APOE* (rs7412, rs429358) gene SNPs was performed by real-time PCR with a fluorescent detection using the KASP method. Detection was carried out on the CFX96 DNA Analyzer (Bio-Rad, USA) with the endpoint fluorescence analysis. The genotypes in the *APOE* gene were grouped based on the presence of $\epsilon 2$, $\epsilon 3$, $\epsilon 4$ alleles.

The estimate of allele and genotype frequencies distribution was conducted using the Hardy–Weinberg equilibrium test. To verify the correspondence of scores distribution obtained via the Raven’s progressive matrices to the Gaussian distribution, we performed the Shapiro–Wilk *W*-test. To assess the main effect of gene polymorphisms together with gene-environment interactions (G×E) in individual variance in nonverbal intelligence, a series of linear regression analyses was carried out. Genotypes and social parameters were used as independent factors in the G×E analysis, while the level of nonverbal intelligence was used as a dependent variable. Statistical analysis included the verification of several linear regression models (additive, dominant, recessive); sex, ethnicity and the “risky” *APOE* $\epsilon 4$ allele were included as covariates. A correction for multiple comparisons was carried out using the FDR (false discovery rate) procedure or permutation (10,000) in the case of haplotype analysis. Statistical analysis was performed using the programs PLINK v.1.09, R, SPSS Statistics 23.0. Visualization was conducted in R v.4.1.2.

Results

Within the present study we analyzed the effect of eight SNPs in six genes: *CRP* (rs3093077), *IL1A* (rs1800587), *IL1B* (rs16944), *TNF/LTA* (rs1041981, rs1800629), *P2RX7* (rs2230912), *APOE* (rs7412, rs429358), which are involved in the regulation of inflammatory system, on individual differences in nonverbal intelligence in mentally healthy individuals. According to the Shapiro–Wilk *W*-test, nonverbal intelligence scores were congruent to the normal distribution ($p > 0.05$). A distribution of allele and genotype frequencies of all examined loci corresponded to the Hardy–Weinberg

Examined SNPs, the Hardy–Weinberg equilibrium test and the results of linear regression analysis of association of the genes with a nonverbal intelligence in the total sample and in subgroups

Gene	SNP	Alleles ^a	MAF	p_{HWE}	Total sample		Women		Men		APOE ε4+		APOE ε4–	
					β_{ST}	p	β_{ST}	p	β_{ST}	p	β_{ST}	p	β_{ST}	p
<i>IL1b</i>	rs16944	A/G	0.374	0.945	0.02	0.545	0.04	0.275	–0.07	0.366	0.07	0.306	< 0.01	0.913
					0.03	0.427	0.04	0.280	–0.02	0.762	0.02	0.718	0.02	0.652
<i>IL1A</i>	rs1800587	A/G	0.285	0.395	–0.01	0.827	–0.01	0.810	< –0.01	0.991	0.10	0.134	–0.04	0.323
					< 0.01	0.977	< –0.01	0.889	0.03	0.641	0.09	0.154	–0.03	0.437
<i>CRP</i>	rs3093077	G/T	0.105	0.052	–0.01	0.801	–0.01	0.834	–0.01	0.867	< –0.01	0.955	–0.01	0.746
					–0.02	0.566	–0.03	0.389	0.03	0.708	–0.02	0.712	–0.01	0.738
<i>TNF</i>	rs1041981	A/C	0.234	0.157	0.01	0.555	< –0.01	0.941	0.11	0.150	0.10	0.130	–0.01	0.771
					0.03	0.405	< 0.01	0.996	0.014	0.051	0.16	0.019^d	< –0.01	0.953
	rs1800629	A/G	0.118	0.448	0.02	0.486	–0.02	0.625	0.20	0.008^b	0.15	0.022^e	–0.021	0.588
					0.03	0.356	< –0.01	0.869	0.19	0.009^c	0.16	0.019^d	< –0.01	0.797
<i>P2RX7</i>	rs2230912	G/A	0.191	0.299	–0.03	0.403	–0.03	0.429	–0.03	0.702	0.02	0.736	–0.05	0.239
					< –0.01	0.946	–0.01	0.755	0.04	0.611	0.04	0.548	–0.01	0.685

Note. p_{HWE} – p -value for the Hardy–Weinberg equilibrium test; MAF – minor allele frequency; β_{ST} – standardized regression coefficient; p – p -value. The upper row indicates the results obtained from an additive model, the lower row – from a dominant model. Statistically significant values are shown in bold. ^a Minor/major alleles; ^b $p_{FDR} = 0.051$; ^c $p_{FDR} = 0.058$; ^d $p_{FDR} = 0.059$; ^e $p_{FDR} = 0.137$.

equilibrium ($p > 0.05$). The analysis of allele and genotype frequencies distribution demonstrated the absence of statistically significant differences between various ethnic groups ($p > 0.05$); therefore, a subsequent statistical analysis was conducted in the total group with previously reported requirement to include sex and ethnicity as covariates, as well as in men and women separately.

Statistical analysis of associations of eight SNPs in six genes involved in the regulation of inflammatory response with nonverbal intelligence, which was conducted via linear regression, revealed the effect of *TNF* (rs1800629) (for additive model: $\beta_{ST} = 0.15$; $p = 0.022$; $p_{FDR} = 0.137$; for dominant model: $\beta_{ST} = 0.16$; $p = 0.019$; $p_{FDR} = 0.059$) and rs1041981 (for dominant model: $\beta_{ST} = 0.16$; $p = 0.019$; $p_{FDR} = 0.059$) on individual differences in nonverbal intelligence among carriers of the “risky” *APOE* ε4 variant (see the Table, Fig. 1, *c, f*). However, this association became only a trend after correction for multiple comparisons. In particular, the carriers of rs1800629 and rs1041981 minor A-alleles demonstrated an increased nonverbal intelligence compared to individuals bearing G/G and C/C-genotypes (respectively) at the trend level, which was evident only under genetically determined diminished anti-inflammatory activity (*APOE* ε4 variant). In men, the association of *TNF* gene loci appeared to become insignificant after FDR-correction (see the Table, Fig. 1, *b, e*).

The linkage disequilibrium analysis conducted between the *TNF* (rs1800629 and rs1041981) succeeded to report a linkage

($D' = 0.741$, $r^2 = 0.235$), therefore, a haplotypic analysis was performed. Haplotype frequencies in the *TNF* gene (based on rs1041981, rs1800629) were the following: AA – 0.094, CA – 0.023, AG – 0.143, CG – 0.740. As a result of haplotypic analysis we detected the association of the *TNF**AA haplotype (rs1041981, rs1800629) ($\beta_{ST} = 1.19$; $p = 0.033$; $p_{perm} = 0.047$) with an enhanced level of nonverbal intelligence in individuals without cognitive decline, which remained statistically significant after correction for multiple comparisons.

In the present study we also conducted the analysis of gene-by-environment (G×E) interactions estimating the effect of 14 socio-demographic parameters. As a result of G×E interactions we observed that sibship size significantly affected the association of the rs1041981 in the *TNF* gene ($\beta = 2.08$; $\beta_{ST} = 0.16$; $p = 0.001$). Thus, it was revealed that carriers of the rs1041981 A-allele who were reared in the families with three and more children demonstrated a significantly higher level of nonverbal intelligence compared to those with the rs1041981 C/C-genotype (Fig. 2, *a*). Moreover, we observed that smoking had a modulating effect on the association of the *P2RX7* rs2230912 ($\beta = -1.70$; $\beta_{ST} = -0.10$; $p = 0.022$) with individual differences in nonverbal intelligence. In particular, we observed a dose-dependent effect of *P2RX7* rs2230912 minor G-allele on a decreased level of nonverbal intelligence among smoking individuals (see Fig. 2, *b*). In the present study, we failed to observe associations of the *IL1B* (rs16944), *IL1A* (rs1800587), *CRP* (rs3093077) gene polymorphisms with individual differences in nonverbal intelligence.

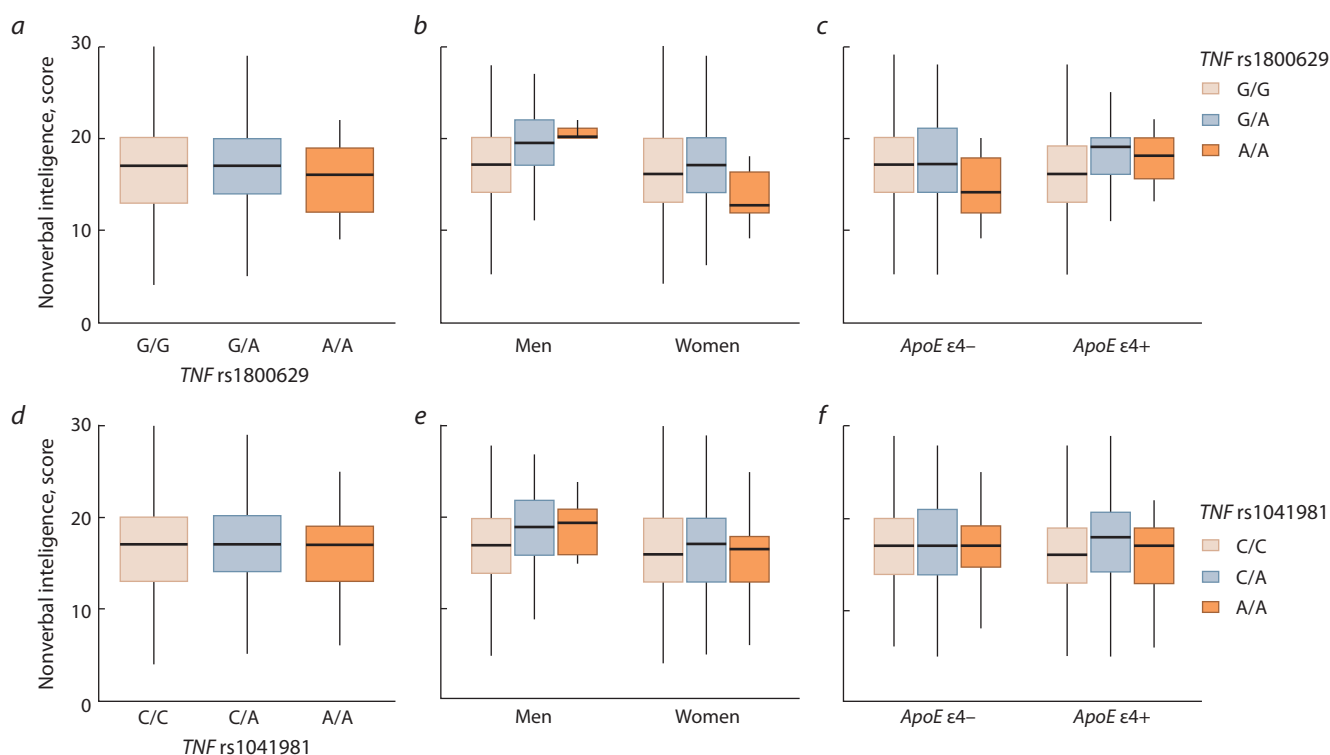


Fig. 1. Mean values of nonverbal intelligence depending on the genotypes in the *TNF* rs1800629 and rs1041981 gene polymorphisms in the total sample (a, d), in the groups differing by sex (b, e) and the presence/absence of the *APOE* ε4 variant (c, f).

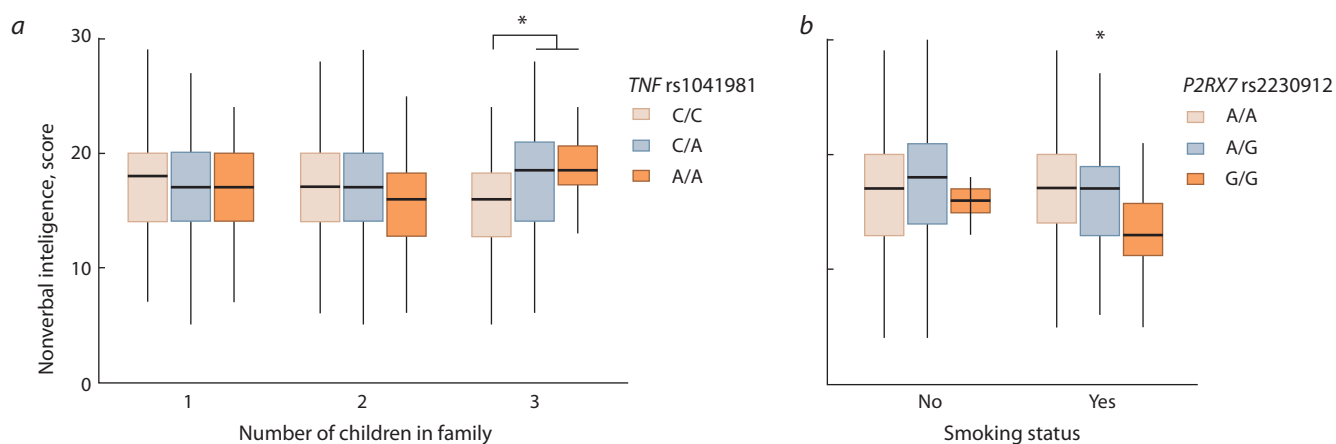


Fig. 2. The results of gene-by-environment interaction analysis demonstrating a modulating effect (a) of the sibship size on the association of the *TNF* (rs1041981) and (b) smoking on the association of the *P2RX7* (rs2230912) with nonverbal intelligence.

Statistically significant differences in nonverbal intelligence between the groups are marked with brackets. * $p_{FDR} < 0.05$.

Discussion

The inflammatory response system plays an important role in the development and normal functioning of cognitive abilities (Sartori et al., 2012; Fard, Stough, 2019). Within the framework of the present study, an attempt was made to identify evidence of the involvement of genes encoding inflammatory system proteins in the manifestation of individual differences in nonverbal intelligence. The results of our study identified the effect of tumor necrosis factor alpha (*TNF*) and purinergic receptor P2X7 (*P2RX7*) genes and social parameters such as

smoking and sibship size in childhood on the development of cognitive abilities. Previously, we had also identified a modulating effect of sibship size on manifestation of cognitive abilities (Kazantseva et al., 2016). The results obtained can provide valuable information for determining genetic mechanisms underlying the development of cognitive functions in general and nonverbal intelligence in particular.

To date, scarce research has been devoted to the study of the inflammatory response system related to normal cognitive functioning in the brain. There may be several explanations

for this. Cognitive functions represent a complex personality construct, the development of which is based on a large number of both biologically determined and environmental factors (Xu et al., 2015; Wang et al., 2019). In this regard, genetic data related to this cognitive phenotype are accumulating gradually, while the majority of studies are devoted to the examination of more obvious biological systems that can directly affect the transmission of information between the neurons, neurogenesis, differentiation of neurons, and others (Kazantseva et al., 2020, 2021). The second reason may be attributed to the assumption that the brain as an organ is completely isolated from immune processes. However, to date, more findings on the cellular components of innate and acquired immunity represented in the brain have been published (Filiano et al., 2015; Morimoto, Nakajima, 2019).

The inflammatory response refers to nonspecific innate immunity that occurs as a response to pathogen penetration. Scientific publications indicate that the inflammatory process in the brain is primarily associated with microglia functioning (Li, Barres, 2018), which represent a large population of immune cells in the central nervous system (Ginhoux et al., 2010). One of the main functions of microglia is to maintain the balance of inflammatory and anti-inflammatory processes in the intact brain (Li, Barres, 2018). The imbalance in these processes can transform into a pathological process, which initiates endogenous neuroinflammation (Wake et al., 2011) and damages neuronal integrity. In turn, the latter may be caused by the factors responsible for the activation of microglia and affect cognitive processes in the brain. This observation may partly explain the associations of SNPs in the gene encoding tumor necrosis factor alpha (*TNF*) with variations in nonverbal intelligence determined in the present study. Within the present study we demonstrated the association of minor alleles of *TNF* rs1800629 and rs1041981 polymorphisms (at the haplotype level) with a higher level of nonverbal intelligence in mentally healthy individuals. The $TNF\alpha$ protein is one of the pro-inflammatory cytokines, which plays an important role in the initiation and regulation of the cytokine cascade during the inflammatory reaction (Makhatadze, 1998). According to literature, $TNF\alpha$ deficiency results in uncontrolled inflammatory response, which, in turn, can cause chronic course of the inflammatory process and negatively affect the integrity of neurons (Raffaele et al., 2020).

The examined rs1800629 (c.-488G>A) in the *TNF* gene and rs1041981 (c.179C>A or Thr60Asn) in the *LTA* gene are functionally significant, and minor alleles are associated with an increased expression of the *TNF/LTA* genes (Hameed et al., 2018), which indicates that our data are consistent with previous research. Based on the data obtained, it can be assumed that an enhanced expression of the *TNF* gene is protective and contributes to more controlled inflammatory process in the brain, which positively affects human cognitive functioning.

It should be noted that a positive effect of minor alleles in the *TNF* gene on improving cognitive performance was observed only in the presence of the “unfavorable” $\epsilon 4$ allele in the *APOE* gene. Together with the involvement of the *APOE*

protein in cholesterol metabolism, it also demonstrates an immunomodulatory effect and the evidence indicating the role of the *APOE* in developing neurodegenerative diseases increasingly appear in the literature. To date, it is known that *APOE* can alter the CNS response to acute and chronic damage, thus actively regulating microglia activation and deactivation (Fitz et al., 2021).

The association of polymorphic variants in the *TNF* gene with nonverbal intelligence observed in the present study in carriers of the *APOE* “risky” $\epsilon 4$ variant can be explained by a close link of these proteins in the human body. In the study conducted by D.T. Laskowitz et al. (1997) it was shown that *APOE* was able to suppress the secretion of $TNF\alpha$ by glial cells, while $TNF\alpha$ deficiency in the CNS resulted in imbalanced inflammatory and anti-inflammatory processes in the intact brain. Thus, a favorable effect of the presence of minor alleles in the *TNF* gene (at the haplotype level) on cognitive abilities may be attributed to *APOE*-related changes in $TNF\alpha$ secretion and, hence, to a certain level of neuroinflammation.

The results of gene-environment studies are interesting. Thus, it was shown that the number of children in a family (sibship size) had a modulating effect on the association of the *TNF* rs1800629 with variations in nonverbal intelligence. In the literature, there are multiple contradictory findings concerning the role of the “intellectual climate” in the family in intelligence level. The results of the majority of studies indicate that younger children are less successful in learning and have lower scores on cognitive tests compared with their older siblings (Kanazawa, 2012). Such observations are explained by the fact that one child in the family receives more parental attention and time resources, while the appearance of each subsequent child is accompanied by insufficient parental time and resources. Nevertheless, such patterns are more relevant to verbal intelligence and may be extended to nonverbal one (Blake, 2020).

In the present study, no differences in cognitive abilities depending on the sibship size were observed. Nevertheless, the association of a higher level of nonverbal intelligence with *TNF* rs1041981 minor A-allele was observed only among individuals who were reared in a large family, while in groups of individuals with a different sibship size no *TNF*-dependent association with cognitive indicators was obtained. From another point of view, nonverbal intelligence positively correlates with family size, since children in large families demonstrate a better ability to understand nonverbal signals due to a decrease in verbal contacts (Morand, 1999). Therefore, genetically determined pro-inflammatory response of the organism associated with the expression of the *TNF* gene plays a significant role in the development of nonverbal intelligence in the case of rearing in a large family, which promotes the development of nonverbal processes (Morand, 1999). The data obtained by our group indicate a favorable effect of the *TNF* rs1041981 minor A-allele, which is associated with more controlled inflammatory process in the brain, on nonverbal intelligence, which manifests only under the conditions of limited verbal parental resources (i. e., a large family).

The second statistically significant result of gene-by-environment analysis carried out in the present study evidences a modulating effect of smoking on the association of the *P2RX7* rs2230912 with nonverbal intelligence. Namely, carriers of the rs2230912 G-allele in the *P2RX7* gene demonstrated a decreased level of nonverbal intelligence in smokers compared with carriers of other genotypes. The *P2RX7* receptor belongs to the purinergic signaling system, which regulates interaction of neurons and the functioning of glial cells, primarily, microglia (Lister et al., 2007).

According to literature, A to G transition in the *P2RX7* rs2230912 is accompanied by glutamate replacement with arginine at position 460, which is expressed in modified signal transmission by the translated P2RX7 protein (Winham et al., 2019). This receptor is involved in the secretion and degradation of extracellular ATP belonging to inflammation-inducing molecules. An impaired ATP metabolism results in enhanced concentration of this molecule in the intercellular space, which can promote a chronic inflammatory process in the CNS and negatively affect the integrity of neurons (Shevela et al., 2020). Another reason of abnormal ATP metabolism in the organism is cigarette smoke. One of the mechanisms of the effect of cigarette smoke on ATP metabolism may be attributed to its ability to modify the expression of the *TSPO* gene encoding the translocator protein, which is increased in the outer mitochondrial membrane responsible for ATP synthesis (Zeineh et al., 2019). In addition, recent studies linked cognitive impairment with nicotine addiction and the number of cigarettes smoked per day. According to large-scale longitudinal studies involving individuals with nicotine smoking, a decreased working memory volume and the ability to solve problems was revealed (Vermeulen et al., 2018).

The examined SNP (G-allele) and an increased expression of the P2RX7 protein were previously associated with a risk for developing affective and depressive disorders (Winham et al., 2019), which is partially consistent with our results on a lower level of cognitive functioning in carriers of the rs2230912 G-allele, which manifests only under the conditions of enhanced neuroinflammatory reaction (such as smoking). Based on the abovementioned data, it can be assumed that a reduced level of nonverbal intelligence may be related to the changes in ATP metabolism and associated neuroinflammatory process.

Conclusion

The present study has several limitations, since the results were obtained using an average sample size. Another limitation is the small number of examined gene polymorphisms, which makes our conclusions on the involvement of the inflammatory system genes incomplete. It should also be noted that within the framework of this study, no genetic correlation was assessed between the level of nonverbal and verbal intelligence, as well as other cognitive abilities, which does not allow us to make an unambiguous conclusion on the specificity of demonstrated genetic associations specifically for nonverbal intelligence. Nevertheless, the results obtained in the present study make a significant foundation and set a direction for the

study of genetically determined factors underlying the studied cognitive ability.

This research also has several strengths: for the first time, the association analysis of the genes involved in the regulation of the inflammatory response with nonverbal intelligence was carried out. In addition, this study also includes the analysis of gene-by-environment interactions, which helps to understand the biological nature of nonverbal intelligence and the role of the immune system in the manifestation of interindividual differences in this cognitive construct in mentally healthy individuals.

References

- Alekseeva O.S., Kirik O.V., Gilerovich E.G., Korzhevskii D.E. Microglia of the brain: origin, structure and functions. *Zhurnal Evolutsionnoy Biokhimii i Fiziologii = Journal of Evolutionary Biochemistry and Physiology*. 2019;55(4):231-241. DOI 10.1134/S0044452919040028. (in Russian)
- Blake J. Family Size and Achievement. Berkeley: University of California Press, 2020. DOI 10.1525/9780520330597.
- Dawson M. Verbal intelligence. In: Volkmar F.R. (Ed.). *Encyclopedia of Autism Spectrum Disorders*. New York: Springer, 2013;3243-3250. DOI 10.1007/978-1-4419-1698-3_375.
- Dominici R., Cattaneo M., Malferrari G., Archi D., Mariani C., Grimaldi L.M., Biunno I. Cloning and functional analysis of the allelic polymorphism in the transcription regulatory region of interleukin-1 alpha. *Immunogenetics*. 2002;54(2):82-86. DOI 10.1007/s00251-002-0445-9.
- Emrani S., Arain H.A., DeMarshall C., Nuriel T. *APOE4* is associated with cognitive and pathological heterogeneity in patients with Alzheimer's disease: a systematic review. *Alz. Res. Therapy*. 2020;12(1):141. DOI 10.1186/s13195-020-00712-4.
- Erdman V.V., Nasibullin T.R., Tuktarova I.A., Somova R.S., Mustafina O.E. Analysis of *FOXO1A* and *FOXO3A* gene allele association with human longevity. *Russ. J. Genet*. 2016;52(4):416-422. DOI 10.1134/S1022795416020034.
- Fard M.T., Stough C. A review and hypothesized model of the mechanisms that underpin the relationship between inflammation and cognition in the elderly. *Front. Aging Neurosci*. 2019;11:56. DOI 10.3389/fnagi.2019.00056.
- Feklicheva I., Zakharov I., Chipeeva N., Maslennikova E., Korobova S., Adamovich T., Ismatullina V., Malykh S. Assessing the relationship between verbal and nonverbal cognitive abilities using resting-state EEG functional connectivity. *Brain Sci*. 2021;11(1):94. DOI 10.3390/brainsci11010094.
- Ferro A., Auguste Y.S.S., Cheadle L. Microglia, cytokines, and neural activity: unexpected interactions in brain development and function. *Front. Immunol*. 2021;12:703527. DOI 10.3389/fimmu.2021.703527.
- Filiano A.J., Gadani S.P., Kipnis J. Interactions of innate and adaptive immunity in brain development and function. *Brain Res*. 2015;1617:18-27. DOI 10.1016/j.brainres.2014.07.050.
- Fitz N.F., Nam K.N., Wolfe C.M., Letronne F., Playso B.E., Iordanova B.E., Kozai T.D.Y., Biedrzycki R.J., Kagan V.E., Tyurina Y.Y., Han X., Lefterov I., Koldamova R. Phospholipids of APOE lipoproteins activate microglia in an isoform-specific manner in preclinical models of Alzheimer's disease. *Nat. Commun*. 2021;12(1):3416. DOI 10.1038/s41467-021-23762-0.
- Franić S., Dolan C.V., van Beijsterveldt C.E., Pol H.H.E., Bartels M., Boomsma D.I. Genetic and environmental stability of intelligence

- in childhood and adolescence. *Twin Res. Hum. Genet.* 2014;17(3): 151-163. DOI 10.1017/thg.2014.26.
- Franke H., Schepper C., Illes P., Krügel U. Involvement of P2X and P2Y receptors in microglial activation *in vivo*. *Purinergic Signal.* 2007;3(4):435-445. DOI 10.1007/s11302-007-9082-y.
- Ginhoux F., Greter M., Leboeuf M., Nandi S., See P., Gokhan S., Mehler M.F., Conway S.J., Ng L.G., Stanley E.R., Samokhvalov I.M., Merad M. Fate mapping analysis reveals that adult microglia derive from primitive macrophages. *Science.* 2010; 330(6005):841-845. DOI 10.1126/science.1194637.
- Hameed I., Masoodi S.R., Malik P.A., Mir S.A., Ghazanfar K., Ganai B.A. Genetic variations in key inflammatory cytokines exacerbates the risk of diabetic nephropathy by influencing the gene expression. *Gene.* 2018;661:51-59. DOI 10.1016/j.gene.2018.03.095.
- Haruwaka K., Ikegami A., Tachibana Y., Ohno N., Konishi H., Hashimoto A., Matsumoto M., Kato D., Ono R., Kiyama H., Moorhouse A.J., Nabekura J., Wake H. Dual microglia effects on blood brain barrier permeability induced by systemic inflammation. *Nat. Commun.* 2019;10(1):5816. DOI 10.1038/s41467-019-13812-z.
- Kanazawa S. Intelligence, birth order, and family size. *Pers. Soc. Psychol. Bull.* 2012;38(9):1157-1164. DOI 10.1177/0146167212445911.
- Kazantseva A.V., Enikeeva R.F., Davydova Yu.D., Mustafin R.N., Takhirova Z.R., Malykh S.B., Lobaskova M.M., Tikhomirova T.N., Khusnutdinova E.K. The role of the *KIBRA* and *APOE* genes in developing spatial abilities in humans. *Vavilovskii Zhurnal Genetiki i Selekcii = Vavilov Journal of Genetics and Breeding.* 2021;25(8):839-846. DOI 10.18699/VJ21.097. (in Russian)
- Kazantseva A.V., Enikeeva R.F., Romanova A.R., Bashkatov S.A., Galyautdinova S.I., Tikhomirova T.N., Malykh S.B., Khusnutdinova E.K. Neurexin family genes (*CNTNAP2* and *NRXN1*): their involvement in mathematics anxiety. *Meditsinskaya Genetika = Medical Genetics.* 2016;15(11):17-23. (in Russian)
- Kazantseva A.V., Enikeeva R.F., Romanova A.R., Galyautdinova S.I., Malykh S.B., Khusnutdinova E.K. Stress-associated cognitive functioning is controlled by variations in synaptic plasticity genes. *Russ. J. Genet.* 2020;56(1):88-95. DOI 10.1134/S1022795420010068.
- Kierdorf K., Prinz M. Microglia in steady state. *J. Clin. Invest.* 2017; 127(9):3201-3209. DOI 10.1172/JCI90602.
- Kuschnier E.S. Nonverbal intelligence. In: Volkmar F.R. (Eds.). *Encyclopedia of Autism Spectrum Disorders.* New York: Springer, 2013;82-139. DOI 10.1007/978-1-4419-1698-3_354.
- Lanfranco M.F., Sepulveda J., Kopetsky G., Rebeck G.W. Expression and secretion of apoE isoforms in astrocytes and microglia during inflammation. *Glia.* 2021;69(6):1478-1493. DOI 10.1002/glia.23974.
- Laskowitz D.T., Goel S., Bennett E.R., Matthew W.D. Apolipoprotein E suppresses glial cell secretion of TNF α . *J. Neuroimmunol.* 1997;76(1-2):70-74. DOI 10.1016/s0165-5728(97)00021-0.
- Li Q., Barres B.A. Microglia and macrophages in brain homeostasis and disease. *Nat. Rev. Immunol.* 2018;18(4):225-242. DOI 10.1038/nri.2017.125.
- Li Y., Liu Y., Li J., Qin W., Li K., Yu C., Jiang T. Brain anatomical network and intelligence. *PLoS Comput. Biol.* 2009;5(5):e1000395. DOI 10.1371/journal.pcbi.1000395.
- Lister M.F., Sharkey J., Sawatzky D.A., Hodgkiss J.P., Davidson D.J., Rossi A.G., Finlayson K. The role of the purinergic P2X7 receptor in inflammation. *J. Inflamm. (Lond.).* 2007;4:5. DOI 10.1186/1476-9255-4-5.
- Makhatadze N.J. Tumor necrosis factor locus: genetic organisation and biological implications. *Hum. Immunol.* 1998;59(9):571-579. DOI 10.1016/s0198-8859(98)00056-1.
- Morand D.A. Family size and intelligence revisited: the role of emotional intelligence. *Psychol. Rep.* 1999;84(2):643-649. DOI 10.2466/pr0.1999.84.2.643.
- Morimoto K., Nakajima K. Role of the immune system in the development of the central nervous system. *Front. Neurosci.* 2019;13: 916. DOI 10.3389/fnins.2019.00916.
- Mustafin R.N., Kazantseva A.V., Khusnutdinova E.K., Malykh S.B. Genetic mechanisms of cognitive development. *Russ. J. Genet.* 2020;56(8):891-902. DOI 10.1134/S102279542007011X.
- Naitza S., Porcu E., Steri M., Taub D.D., Mulas A., Xiao X., Strait J., Dei M., Lai S., Busonero F., Maschio A., Usala G., Zoledziwska M., Sidore C., Zara I., Pitzalis M., Loi A., Virdis F., Piras R., Deidda F., Whalen M.B., Crisponi L., Concas A., Podda C., Uzzau S., Scheet P., Longo D.L., Lakatta E., Abecasis G.R., Cao A., Schlessinger D., Uda M., Sanna S., Cucca F. A genome-wide association scan on the levels of markers of inflammation in Sardinians reveals associations that underpin its complex regulation. *PLoS Genet.* 2012;8(1):e1002480. DOI 10.1371/journal.pgen.1002480.
- Parkhurst C.N., Yang G., Ninan I., Savas J.N., Yates J.R. 3rd, Lafaille J.J., Hempstead B.L., Littman D.R., Gan W.B. Microglia promote learning-dependent synapse formation through brain-derived neurotrophic factor. *Cell.* 2013;155(7):1596-1609. DOI 10.1016/j.cell.2013.11.030.
- Raffaële S., Lombardi M., Verderio C., Fumagalli M. TNF production and release from microglia via extracellular vesicles: impact on brain functions. *Cells.* 2020;9(10):2145. DOI 10.3390/cells9102145.
- Raven J. The Raven's progressive matrices: change and stability over culture and time. *Cogn. Psychol.* 2000;41(1):1-48. DOI 10.1006/cogp.1999.0735.
- Sartori A.C., Vance D.E., Slater L.Z., Crowe M. The impact of inflammation on cognitive function in older adults. *J. Neurosci. Nurs.* 2012;44(4):206-217. DOI 10.1097/JNN.0b013e3182527690.
- Shevela E.Y., Markova E.V., Knyazheva M.A., Proskurina A.S., Efremov Y.R., Molodtsov V.V., Seledtsov I.A., Ostanin A.A., Bogachev S.S., Kolchanov N.A., Chernykh E.R. Changes in the hippocampal genes transcriptome in depression model mice upon intranasal exposure to M2 macrophage secretome factors. *Matematicheskaya Biologiya i Bioinformatika = Mathematical Biology and Bioinformatics.* 2020;15(2):357-393. DOI 10.17537/2020.15.357. (in Russian)
- Tayel S.I., Fouda E.A.M., Elshayeb E.I., Eldakamawy A.R.A., El-Kousy S.M. Biochemical and molecular study on interleukin-1 β gene expression and relation of single nucleotide polymorphism in promoter region with Type 2 diabetes mellitus. *J. Cell Biochem.* 2018;119(7):5343-5349. DOI 10.1002/jcb.26667.
- Vermeulen J.M., Schirmbeck F., Blankers M., van Tricht M., Brugge-man R., van den Brink W., de Haan L. Genetic Risk and Outcome of Psychosis (GROUP) investigators. Association between smoking behavior and cognitive functioning in patients with psychosis, siblings, and healthy control subjects: results from a prospective 6-year follow-up study. *Am. J. Psychiatry.* 2018;175(11):1121-1128. DOI 10.1176/appi.ajp.2018.18010069.
- Vitek M.P., Brown C.M., Colton C.A. APOE genotype-specific differences in the innate immune response. *Neurobiol. Aging.* 2009;30(9):1350-1360. DOI 10.1016/j.neurobiolaging.2007.11.014.
- Vyshedskiy A., Dunn R., Piryatinsky I. Neurobiological mechanisms for nonverbal IQ tests: implications for instruction of nonverbal

- children with autism. *Res. Ideas Outcomes*. 2017;3:e13239. DOI 10.3897/RIO.3.E13239.
- Wake H., Moorhouse A.J., Nabekura J. Functions of microglia in the central nervous system – beyond the immune response. *Neuron Glia Biol.* 2011;7(1):47-53. DOI 10.1017/S1740925X12000063.
- Wang Y., Du Y., Li J., Qiu C. Lifespan intellectual factors, genetic susceptibility, and cognitive phenotypes in aging: implications for interventions. *Front. Aging Neurosci.* 2019;11:129. DOI 10.3389/fnagi.2019.00129.
- Winham S.J., Bobo W.V., Liu J., Coombes B., Backlund L., Frye M.A., Biernacka J.M., Schalling M., Lavebratt C. Sex-specific effects of gain-of-function P2RX7 variation on bipolar disorder. *J. Affect. Disord.* 2019;245:597-601. DOI 10.1016/j.jad.2018.11.007.
- Xu C., Sun J., Duan H., Ji F., Tian X., Zhai Y., Wang S., Pang Z., Zhang D., Zhao Z., Li S., Gue M.M., Hjelmberg J.V., Christensen K., Tan Q. Gene, environment and cognitive function: a Chinese twin ageing study. *Age Ageing*. 2015;44(3):452-457. DOI 10.1093/ageing/afv015.
- Zeineh N., Nagler R., Gabay M., Weizman A., Gavish M. Effects of cigarette smoke on TSPO-related mitochondrial processes. *Cells*. 2019;8(7):694. DOI 10.3390/cells8070694.

ORCID ID

R.F. Enikeeva orcid.org/0000-0002-4301-5283
A.V. Kazantseva orcid.org/0000-0002-3744-8058
Yu.D. Davydova orcid.org/0000-0003-3508-4710
R.N. Mustafin orcid.org/0000-0002-4091-382X
S.B. Malykh orcid.org/0000-0002-3786-7447
Y.V. Kovas orcid.org/0000-0001-9633-6374
E.K. Khusnutdinova orcid.org/0000-0003-2987-3334

Acknowledgements. The study was partially supported by the Russian Science Foundation (project No.17-78-30028) in the part of psychological assessment and collection of biological materials, by the Ministry of Science and Higher Education of Russian Federation (project No. 075-15-2021-595) in the part of statistical and bioinformatics analysis and by the mega-grant of the Ministry of Science and Higher Education of the Republic of Bashkortostan in the part of genetic analysis.

Conflict of interest. The authors declare no conflict of interest.

Received October 4, 2021. Revised January 12, 2022. Accepted January 27, 2022.

Original Russian text www.bionet.nsc.ru/vogis/

TCF7L2 gene polymorphism in populations of five Siberian ethnic groups

L.E. Tabikhanova^{1,3}✉, L.P. Osipova^{1,3}, T.V. Churkina^{1,3}, E.N. Voronina^{2,3}, M.L. Filipenko^{2,3}

¹ Institute of Cytology and Genetics of the Siberian Branch of the Russian Academy of Sciences, Novosibirsk, Russia

² Institute of Chemical Biology and Fundamental Medicine of the Siberian Branch of the Russian Academy of Sciences, Novosibirsk, Russia

³ Novosibirsk State University, Novosibirsk, Russia

✉ tabikhan@bionet.nsc.ru

Abstract. Investigation of the frequencies of functionally significant gene variants in the context of medical biology and gene geography is a relevant issue for studying the genetic structure of human populations. The transition from a traditional to an urbanized lifestyle leads to a higher incidence of civilizational diseases associated with metabolic disorders, including type 2 diabetes mellitus. The goal of the present paper is to analyze the frequencies of functionally significant gene alleles in the metabolic profiles of indigenous Siberian peoples to identify the gene pool resilience, evaluate the susceptibility of various ethnic groups to metabolic disorders under changing environmental conditions, and predict the epidemiological situation that may occur in the near future. The study was performed in the monoethnic samples of eastern and western Buryats, Teleuts, Dolgans, and two territorial groups of Yakuts. A real-time PCR was used to determine the frequencies of single nucleotide polymorphisms (SNPs) *G103894T*, rs12255372, and *C53341T*, rs7903146 in the *TCF7L2* gene. The results obtained were compared to the frequencies identified for Russians from Eastern Siberia and the values available in the literature. The frequencies of the polymorphic variants studied in the samples from the indigenous Siberian peoples place them in between Caucasian and East Asian populations, following the geographic gradient of polymorphism distribution. A significantly lower occurrence of type 2 diabetes risk alleles *TCF7L2* (*G103894T*) and *TCF7L2* (*C53341T*) in the samples of indigenous Siberian peoples compared to Russians was observed, which agrees with their lower susceptibility to metabolic disorders compared to the newcomer Caucasian population. Taking into account urbanization, a reduced growth in type 2 diabetes incidence may be predicted in indigenous Siberian peoples, i. e. Buryats, Yakuts, Dolgans, and Teleuts, compared to the newcomer Caucasian population. A further study of population structure with respect to different metabolic profile genes is required to better understand the molecular genetic foundations of the adaptive potential of indigenous Siberian peoples.

Key words: Buryats; Teleuts; Yakuts; Dolgans; Russians from East Siberia; type 2 diabetes mellitus; genetic polymorphism; real-time PCR; *TCF7L2* (*G103894T*, rs12255372); *TCF7L2* (*C53341T*, rs7903146).

For citation: Tabikhanova L.E., Osipova L.P., Churkina T.V., Voronina E.N., Filipenko M.L. *TCF7L2* gene polymorphism in populations of five Siberian ethnic groups. *Vavilovskii Zhurnal Genetiki i Seleksii = Vavilov Journal of Genetics and Breeding*. 2022;26(2):188-195. DOI 10.18699/VJGB-22-23

Полиморфизм гена *TCF7L2* в популяциях пяти этносов Сибири

Л.Э. Табиханова^{1,3}✉, Л.П. Осипова^{1,3}, Т.В. Чуркина^{1,3}, Е.Н. Воронина^{2,3}, М.Л. Филипенко^{2,3}

¹ Федеральный исследовательский центр Институт цитологии и генетики Сибирского отделения Российской академии наук, Новосибирск, Россия

² Институт химической биологии и фундаментальной медицины Сибирского отделения Российской академии наук, Новосибирск, Россия

³ Новосибирский национальный исследовательский государственный университет, Новосибирск, Россия

✉ tabikhan@bionet.nsc.ru

Аннотация. Исследование частот функционально значимых вариантов генов в медико-биологическом и географическом контексте является актуальным направлением в изучении генетической структуры популяций человека. С переходом человечества от традиционного к урбанизированному образу жизни все большее распространение получают болезни цивилизации, связанные с нарушением метаболизма, в том числе сахарный диабет 2-го типа. Цель настоящей работы – проанализировать частоты функционально значимых аллелей генов метаболического профиля у коренных народов Сибири, чтобы определить «запас прочности» генофонда, оценить степень подверженности разных этнических групп заболеваниям метаболического спектра в меняющихся условиях внешней среды и спрогнозировать эпидемиологическую ситуацию в ближайшем будущем. Материалом исследования послужили этнические выборки восточных и западных бурят, телеутов, долган и двух территориальных групп якутов. Методом полимеразной цепной реакции в режиме реального времени определены частоты полиморфных вариантов, обусловленных однонуклеотидными заменами *G103894T*, rs12255372, и *C53341T*, rs7903146 гена *TCF7L2*. Полученные показатели сравнены с частотами в выборке русских Восточной Сибири и с литературными данными. В соответствии с общим географическим градиентом распределения полиморфных ва-

риантов, частоты их в выборках коренных сибирских народов находятся в промежуточном положении между европеоидами и популяциями Восточной Азии. Показана статистически значимо меньшая встречаемость аллелей риска сахарного диабета 2-го типа *TCF7L2* (*G103894T*) и *TCF7L2* (*G53341T*) в выборках коренных сибирских народов по сравнению с русскими, что согласуется с их меньшей подверженностью метаболическим нарушениям, чем у пришлое европеоидного населения. В условиях урбанизации можно также прогнозировать сниженный рост заболеваемости сахарным диабетом 2-го типа у коренных народов Сибири – бурят, якутов, долган и телеутов, по сравнению с пришедшим европеоидным населением. Для более полного понимания молекулярно-генетических основ адаптивного потенциала коренных народностей Сибири необходимо дальнейшее изучение структуры популяций по другим генам метаболического профиля.

Ключевые слова: буряты; телеуты; якуты; долганы; русские Восточной Сибири; сахарный диабет 2 типа; генетический полиморфизм; ПЦР в режиме реального времени; *TCF7L2* (*G103894T*, rs12255372); *TCF7L2* (*G53341T*, rs7903146).

Introduction

Investigation into the peculiarities of the population genetic structure of ethnic groups in the context of medical biology and gene geography is a relevant issue in human genetics. To better understand molecular genetic foundations of adaptive potential that ethnic groups develop as they evolve under specific climatic and geographic conditions and adapt to specific dietary patterns, it is important to analyze the frequencies of the candidate gene alleles proven to be functionally significant based on studies in individual populations.

Type 2 diabetes mellitus (DM2) is among the leading mortality and disability factors in a working-age population (Asfandiyarova, 2015). DM2 is a metabolic syndrome component and above that is linked to increased risk of multiple associated pathological states, primarily including cardiovascular diseases (infarctions, strokes, and cardiovascular failure) and chronic renal failure.

Incretin hormone secretion defect, a key element of DM2 pathogenesis, is associated with *TCF7L2* gene polymorphism since it is this gene's product that regulates the production of pancreatic β -cells from pluripotent stem cells and is involved in glucose-stimulated insulin secretion (Bennett et al., 2002). In addition, the gene also targets the brain, where *TCF7L2* determines the intensity of the anorexigenic effect and affects the central glucose homeostasis mechanism (Ametov et al., 2016). In the liver, the gene is involved in the regulation of triglycerides and low- and very low-density lipoprotein exchange. It is also involved in gluconeogenesis and acts as an insulin resistance mediator (Nobrega, 2013).

It was found that SNPs *G103894T*, rs12255372, and *C53341T*, rs7903146 in introns 3 and 4 of gene *TCF7L2* were associated with DM2 (Sladek et al., 2007; Timpson et al., 2009; Xi et al., 2014; Katsoulis et al., 2018). The link of *TCF7L2* (*G103894T*) and *TCF7L2* (*G53341T*) alleles with increased risk of DM2 was demonstrated in a number of populations around the world, including Russia (Saxena et al., 2006; Cauchi et al., 2007; Potapov et al., 2010; Bondar' et al., 2013; Avzaletdinova et al., 2016; Kaya et al., 2017; Melnikova et al., 2020). It was shown that the *TCF7L2* (*G53341T*) variant was linked to increased risk of DM2 compared to *TCF7L2* (*G103894T*), with homozygous alleles showing higher susceptibility to the disease than heterozygous ones (Anjum et al., 2018).

The *TCF7L2* polymorphisms are also linked to BMI, total body fat volume, as well as subcutaneous and visceral fat (Haupt et al., 2010; Smetanina, 2015). *TCF7L2* (*G53341T*) allele is associated with the risk of myocardial ischemia and myocardial infarction as syntropic diseases with common

pathogenetic elements (Melzer et al., 2006; Han et al., 2010; Orlov et al., 2011). Gene *TCF7L2* is also linked to renal embryogenesis, i. e. its polymorphisms are associated with various degrees of chronic renal failure, a vascular complication of DM2 (Franceschini et al., 2012; Ametov et al., 2016; Vikulova et al., 2017). It was proved that *TCF7L2* polymorphism in loci rs7903146 and rs12255372 was associated with risks of gastric, breast, and colorectal cancer (Rosales-Reynoso et al., 2016; Zhang et al., 2018). The effect of natural selection on locus rs7903146 in gene *TCF7L2* was discovered and a statistically significant link between *G53341T* allele frequency and several climatic geographic factors was shown (Trifonova et al., 2020).

Studies on the frequencies of gene alleles associated with the risk of DM2 and other metabolic disorders in indigenous Siberian populations have remained relevant throughout the recent decade (Bairova et al., 2013; Baturin et al., 2017; Hallmark et al., 2018; Kurtanov et al., 2018; Ievleva et al., 2019; Tabikhanova et al., 2019; Melnikova et al., 2020). However, the distribution of the polymorphic variants of functionally significant gene *TCF7L2* in Siberian populations remains understudied. Polymorphism frequencies in locus rs7903146 for some Siberian peoples, including Buryats and Yakuts, were presented in (Trifonova et al., 2020). Unfortunately, the authors did not indicate the area where genetic material was collected, which seems necessary for these large heterogeneous ethnic groups populating vast territories.

The present paper reports the results of a study into the frequencies of polymorphisms *G103894T*, rs12255372, and *C53341T*, rs7903146 in gene *TCF7L2* associated with several diseases in the populations of indigenous Siberian ethnic groups, namely Buryats, Teleuts, Yakuts and Dolgans, in comparison to Russians living in Siberia.

Materials and methods

The genetic material for the present research was collected in the field in 2000–2006. Blood samples were taken from apparently healthy volunteers under their informed consent and with the approval of the local healthcare authorities and the Ethics Committee of the Institute of Cytology and Genetics, SB RAS. Before blood sampling, all volunteers filled in a special demographic questionnaire to specify their ancestors' nationalities down to 3 to 4 generations.

The data obtained were used to form 7 population samples covering Southern and Eastern Siberia. Persons of Buryat nationality with no outsider ancestors living in Alkhanay and Orlovsky settlements in the Aginsky Buryat Okrug (ABO) of Zabaykalsky Krai were included in the Eastern Buryat group

($N = 132$). Ethnic Buryats from settlements of Ekhirit-Bulagatsky District of Ust-Ordynsky Buryat Okrug (UOB) of the Irkutsk Region ($N = 278$) were included in the Western sample. Also included in the study were Teleuts from the Belovo District of the Kemerovo Region ($N = 116$). Two ethnically homogeneous samples of Yakuts were formed as follows: the Nyurbinsky group included the residents of settlements Nyurbachan and Syultsy of the Nyurbinsky District ($N = 109$), and the Ust-Aldansky group – the residents of the Dyupsya settlement of the Ust-Aldansky District ($N = 100$). The residents of the town of Dudinka and settlements Volochanka and Ust-Avam of the Taymyr Dolgan-Nenets Okrug of Krasnoyarsk Krai identifying as ethnic Dolgans were included in the Dolgan sample ($N = 180$). The seventh sample combined Russians from Zabaykalsky Krai and the Irkutsk Region ($N = 133$).

DNA samples were isolated from the leukocyte fraction of venous blood using the BioSilica kits (Russia). Real-time SNP genotyping in genes *TCF7L2* (*G103894T*, rs12255372) and *TCF7L2* (*C53341T*, rs7903146) was performed applying competing TaqMan-probes complementary to polymorphic DNA segments. Primer and probe designs were selected using the sequences available in the NCBI database (<http://www.ncbi.nlm.nih.gov/>) with UGENE (version 1.14, <http://ugene.unipro.ru/>) and Oligo Analyzer (version 1.0.3, <https://eu.idtdna.com/pages/tools/oligoanalyzer>) software (Table 1).

Amplification was performed in 25- μ l final volume, the master mix included 300 nM primers, 100 nM TaqMan probes, 65 mM TrisHCl (pH 8.9), 16 mM $(\text{NH}_4)_2\text{SO}_4$, 2.5 mM MgCl_2 , 0.05 % Tween-20, 0.2 mM dNTP, 0.5–10 ng DNA, and 0.5 U Taq DNA polymerase (hot-start, Biosan, IHBFM). Reaction conditions were as follows: initial denaturation for 3 min at 96 °C was followed by 46 cycles including denaturation at 96 °C for 5 s, primer annealing, and extension at 61 °C for 30 s (each step is accompanied by recording fluorescent signals at FAM and HEX fluorophore emission wavelengths).

Allele variant frequencies in the populations were determined based on observed genotype frequencies. The match between empirically observed genotype frequency distribution and theoretically expected distribution at the Hardy–Weinberg equilibrium was tested using Pearson’s chi-squared (the equilibrium holds at $p > 0.05$). The statistical confidence of allele frequency differences between the studied samples was evaluated using the chi-squared test with Yates continuity correction; the results were considered statistically significant at $p < 0.025$ (corrected for multiple comparisons, $0.025 = 0.05/2$).

Results

Genotyping results for *TCF7L2* (*G103894T*, rs12255372) and (*C53341T*, rs7903146) in samples of Buryats, Teleuts, Yakuts, Dolgans, and Russians from Eastern Siberia are presented in Table 2.

Table 1. Primer and probe designs used for SNP genotyping in gene *TCF7L2*

Locus	Primers	Probes
<i>G103894T</i> , rs12255372	5'-aaggatgtgcaaatccagcag-3'	5'- FAM -tccaggcaagaattacat-BHQ-3'
	5'-tgaatctggcactcagaagag-3'	5'-HEX-ccaggcaagaatgacat-BHQ-3'
<i>C53341T</i> , rs7903146	5'-ggcttctctgctctcaaacct-3'	5'- FAM-agcacttttagatataatata-BHQ-3'
	5'-ctgccttcctgtaactgt-3'	5'- HEX-agcacttttagataatata-BHQ-3'

Table 2. Genotype distribution for gene *TCF7L2* in samples of Buryats, Teleuts, Yakuts, Dolgans, and Russians from Eastern Siberia

Population		Buryats		Teleuts	Yakuts		Dolgans	Russians from Eastern Siberia	
		Eastern	Western		Nyurbinsky District	Ust-Aldansky District			
<i>G103894T</i> , rs12255372	Genotype distribution, n (%)	<i>G/G</i>	116 (88.5)	251 (90.3)	96 (82.8)	96 (88.1)	87 (87)	159 (88.3)	78 (59.1)
		<i>G/T</i>	15 (11.5)	24 (8.6)	18 (15.5)	13 (11.9)	13 (13)	20 (11.1)	47 (35.6)
		<i>T/T</i>	0	3 (1.1)	2 (1.7)	0	0	1 (0.6)	7 (5.3)
	N , ppl	131	278	116	109	100	180	132	
	p (H–W)	0.905	0.668	0.817	0.907	0.899	0.940	0.993	
<i>C53341T</i> , rs7903146	Genotype distribution, n (%)	<i>C/C</i>	119 (90.1)	225 (81.6)	91 (79.1)	90 (90.1)	84 (87.5)	143 (85.1)	73 (54.9)
		<i>C/T</i>	13 (9.9)	49 (17.7)	22 (19.1)	9 (9.9)	12 (12.5)	24 (14.3)	51 (38.3)
		<i>T/T</i>	0	2 (0.7)	2 (1.8)	0	0	1 (0.6)	9 (6.8)
	N , ppl	132	276	115	99	96	168	133	
	p (H–W)	0.925	0.932	0.904	0.942	0.907	0.999	0.982	

Note. N is the sample size; n is the quantity; p (H–W) is the probability of Hardy–Weinberg equilibrium deviation.

Table 3. *TCF7L2* (103894T) allele frequency in some populations (ethnic groups) and comparison of populations (*p*-value)

Population/ ethnic group	N, ppl	<i>TCF7L2</i> (103894T) frequency, %	Population comparison (<i>p</i> -value)						
			Buryats		Teleuts	Yakuts		Dolgans	Russians from Eastern Siberia
			Eastern	Western		Nyurbinsky District	Ust-Aldansky District		
Eastern Buryats*	131	5.7		0.991	0.153	0.955	0.873	0.971	<i>p</i> < 0.001
Western Buryats*	278	5.4	0.991		0.051	0.878	0.691	0.763	<i>p</i> < 0.001
Teleuts*	116	9.5	0.153	0.051		0.227	0.336	0.168	<i>p</i> < 0.001
Yakuts, Nyurbinsky District*	109	6.0	0.955	0.878	0.227		0.993	0.896	<i>p</i> < 0.001
Yakuts, Ust-Aldansky District*	100	6.5	0.873	0.691	0.336	0.993		0.996	<i>p</i> < 0.001
Dolgans*	180	6.1	0.971	0.763	0.168	0.896	0.996		<i>p</i> < 0.001
Russians from Eastern Siberia*	132	23.1	<i>p</i> < 0.001	<i>p</i> < 0.001	<i>p</i> < 0.001	<i>p</i> < 0.001	<i>p</i> < 0.001	<i>p</i> < 0.001	<i>p</i> < 0.001
Chinese Dai in Xishuangbanna, China**	93	1.1	0.024	0.022	<i>p</i> < 0.001	0.020	0.013	0.013	<i>p</i> < 0.001
Han Chinese, Beijing, China**	103	0	0.001	0.001	<i>p</i> < 0.001	0.001	<i>p</i> < 0.001	<i>p</i> < 0.001	<i>p</i> < 0.001
Southern Han Chinese, China**	105	1.0	0.013	0.012	<i>p</i> < 0.001	0.011	0.007	0.007	<i>p</i> < 0.001
Japanese, Tokyo, Japan**	104	2.4	0.125	0.116	0.004	0.109	0.076	0.073	<i>p</i> < 0.001
Kinh (Viet), Ho Chi Minh City, Vietnam**	99	0.5	0.006	0.005	<i>p</i> < 0.001	0.005	0.003	0.003	<i>p</i> < 0.001
Population of the state of Utah, descendants of Northern and Western European settlers**	99	27.8	<i>p</i> < 0.001	<i>p</i> < 0.001	<i>p</i> < 0.001	<i>p</i> < 0.001	<i>p</i> < 0.001	<i>p</i> < 0.001	0.296
Finns, Finland**	99	21.7	<i>p</i> < 0.001	<i>p</i> < 0.001	<i>p</i> < 0.001	<i>p</i> < 0.001	<i>p</i> < 0.001	<i>p</i> < 0.001	0.807
English people and Scots**	91	26.4	<i>p</i> < 0.001	<i>p</i> < 0.001	<i>p</i> < 0.001	<i>p</i> < 0.001	<i>p</i> < 0.001	<i>p</i> < 0.001	0.493
Iberians, Spain**	107	37.4	<i>p</i> < 0.001	<i>p</i> < 0.001	<i>p</i> < 0.001	<i>p</i> < 0.001	<i>p</i> < 0.001	<i>p</i> < 0.001	<i>p</i> < 0.001
Toscani, Italy**	107	31.8	<i>p</i> < 0.001	<i>p</i> < 0.001	<i>p</i> < 0.001	<i>p</i> < 0.001	<i>p</i> < 0.001	<i>p</i> < 0.001	0.043

Note. Here and in Table 4: * marks the data obtained by the authors, ** marks the data from the literature (The 1000 Genomes..., 2012); *p* < 0.025, at which differences were considered statistically significant are marked in bold.

The genotype distribution matched the Hardy–Weinberg equilibrium for all polymorphic loci and samples. The frequencies of alleles *TCF7L2* (103894T) and *TCF7L2* (53341T) in the studied samples and some ethnic groups described in the literature (The 1000 Genomes..., 2012), as well as comparison of populations (*p*-value), are presented in Tables 3–4.

It was shown that *TCF7L2* (103894T) allele frequency in the Russians sample (23.1 %) matched that in other Caucasian groups (22–37 %) (The 1000 Genomes..., 2012). The frequency in the studied samples of indigenous Siberian peoples varies from 5.4 % for Western Buryats to 9.5 % for Teleuts, with no statistically significant differences observed. However, the allele frequency in all samples of indigenous populations was significantly lower than in Russians from Eastern Siberia and other Caucasian groups described in the literature (The 1000 Genomes..., 2012). At the same time, it was significantly higher than in several East Asian populations, i. e. Chinese and Vietnamese. We could also see a significant difference between Teleuts and Japanese not observed for other studied groups.

This in-between position of indigenous Siberian populations, as exemplified by Buryats and Teleuts, had been demonstrated earlier in the polymorphism frequencies of some other metabolic profile genes (Tabikhanova et al., 2019).

TCF7L2 (53341T) allele frequency in the Russians sample (25.9 %) matched that in other Caucasian groups (23–40 %) (The 1000 Genomes..., 2012). The studied samples of indigenous populations showed a significantly lower value compared to Russians varying from 4.5 % in Yakuts from the Nyurbinsky District to 11.3 % in Teleuts. Statistically significant differences were discovered between Teleuts and the samples with the lowest frequency values, namely Eastern Buryats (4.9 %) and Yakuts from the Nyurbinsky District. The data on *TCF7L2* (53341T) allele frequency in the samples of Buryats (6.3 %) and Yakuts (4.3 %) resembling the results obtained in our study were presented by Trifonova et al. (2020). Unfortunately, the authors did not indicate sample sizes and the participants' places of residence, so confidence evaluation was impossible to perform. The frequency values do not show

Table 4. *TCF7L2* (53341T) allele frequency in some populations (ethnic groups) and comparison of populations (*p*-value)

Population/ ethnic group	N, ppl	<i>TCF7L2</i> (53341T) frequency, %	Population comparison (<i>p</i> -value)						
			Buryats		Teleuts	Yakuts		Dolgans	Russians from Eastern Siberia
			Eastern	Western		Nyurbinsky District	Ust-Aldansky District		
Eastern Buryats*	132	4.9		0.030	0.014	0.983	0.660	0.224	<i>p</i> < 0.001
Western Buryats*	276	9.6	0.030		0.556	0.037	0.213	0.399	<i>p</i> < 0.001
Teleuts*	115	11.3	0.014	0.556		0.017	0.106	0.190	<i>p</i> < 0.001
Yakuts, Nyurbinsky District*	99	4.5	0.983	0.037	0.017		0.573	0.205	<i>p</i> < 0.001
Yakuts, Ust-Aldansky District*	96	6.3	0.660	0.213	0.106	0.573		0.672	<i>p</i> < 0.001
Dolgans*	168	7.7	0.224	0.399	0.190	0.205	0.672		<i>p</i> < 0.001
Russians from Eastern Siberia*	133	25.9	<i>p</i> < 0.001	<i>p</i> < 0.001	<i>p</i> < 0.001	<i>p</i> < 0.001	<i>p</i> < 0.001	<i>p</i> < 0.001	
Chinese Dai in Xishuangbanna, China**	93	2.2	0.220	0.002	<i>p</i> < 0.001	0.335	0.086	0.017	<i>p</i> < 0.001
Han Chinese, Beijing, China**	103	2.4	0.245	0.001	<i>p</i> < 0.001	0.375	0.094	0.017	<i>p</i> < 0.001
Southern Han Chinese, China**	105	2.9	0.386	0.003	0.001	0.552	0.162	0.033	<i>p</i> < 0.001
Japanese, Tokyo, Japan**	104	2.9	0.388	0.003	0.001	0.554	0.164	0.033	<i>p</i> < 0.001
Kinh (Viet), Ho Chi Minh City, Vietnam**	99	1.0	0.037	<i>p</i> < 0.001	<i>p</i> < 0.001	0.068	0.011	0.001	<i>p</i> < 0.001
Population of the state of Utah, descendants of Northern and Western European settlers**	99	31.3	<i>p</i> < 0.001	<i>p</i> < 0.001	<i>p</i> < 0.001	<i>p</i> < 0.001	<i>p</i> < 0.001	<i>p</i> < 0.001	0.240
Finns, Finland**	99	22.7	<i>p</i> < 0.001	<i>p</i> < 0.001	0.002	<i>p</i> < 0.001	<i>p</i> < 0.001	<i>p</i> < 0.001	0.494
English people and Scots**	91	25.8	<i>p</i> < 0.001	<i>p</i> < 0.001	<i>p</i> < 0.001	<i>p</i> < 0.001	<i>p</i> < 0.001	<i>p</i> < 0.001	0.931
Iberians, Spain**	107	39.7	<i>p</i> < 0.001	<i>p</i> < 0.001	<i>p</i> < 0.001	<i>p</i> < 0.001	<i>p</i> < 0.001	<i>p</i> < 0.001	0.002
Toscani, Italy**	107	37.4	<i>p</i> < 0.001	<i>p</i> < 0.001	<i>p</i> < 0.001	<i>p</i> < 0.001	<i>p</i> < 0.001	<i>p</i> < 0.001	0.009

significant differences between the samples of Eastern Buryats and Yakuts from the Nyurbinsky District and the samples of indigenous East Asian populations, namely Chinese, Japanese and Vietnamese, available in the literature. Yakuts from the Ust-Aldansky District demonstrated a significantly higher *TCF7L2* (53341T) allele frequency than Vietnamese, while Dolgans showed differences compared to some Chinese populations as well. Western Buryats and Teleuts showed significantly higher allele frequencies than all the East Asian samples described in the literature. It was also shown that this polymorphism frequency in populations of indigenous Siberian peoples was significantly lower than in the Caucasian groups described in the literature (The 1000 Genomes..., 2012). Thus, *TCF7L2* (53341T) allele frequencies also confirm the trend that places samples of indigenous Siberian peoples in-between East Asian and Caucasian populations.

Discussion

Investigation of the frequencies of functionally significant gene variants in the context of medical biology and gene geography is a relevant issue for studying the population ge-

netic structure of indigenous Siberian peoples. In the present paper, we have determined the frequencies of the 103894T and 53341T alleles in gene *TCF7L2* associated with DM2 and other metabolic disorders in the populations of Buryats, Yakuts, Dolgans, and Teleuts, as well as a sample of Russians from Eastern Siberia. It was shown that these frequencies in Russians fall within the same range as in other Caucasian populations. Meanwhile, the populations of indigenous Siberian ethnic groups show significantly lower *TCF7L2* (103894T) and *TCF7L2* (53341T) polymorphism frequencies, which places them in-between Caucasian and East Asian populations.

It was shown in several papers that indigenous Siberian and Far Eastern ethnic groups, as well as the ethnic groups from the European part of Russia with a mongoloid component in their gene pool, had lower incidence rates of metabolic syndrome and its DM2 component compared to Caucasians (Tsyretorova et al., 2015; Kichigin et al., 2017; Cygankova et al., 2018). It is primarily explained by the traditional lifestyle implying a sufficient amount of physical activity and diet consisting mostly of animal source foods rich in proteins and fats with limited carbohydrate component (Bairova et al., 2013).

Ethnic peculiarities in DM2 prevalence and manifestations are also caused by distinctions from the European gene pool, i. e. a unique combination of frequencies of functionally significant genes developed as a result of adaptation to local environmental conditions (Baturin et al., 2017; Hallmark et al., 2018). Differences in living conditions between indigenous and newcomer populations are alleviated due to urbanization, centuries-long traditions, and acquired dietary patterns change, and, as a result, civilizational diseases associated with metabolic disorders, including DM2, become increasingly common in indigenous populations (Ovsyannikova et al., 2007; Tsyretorova et al., 2015; Cygankova et al., 2018). Investigation of the polymorphism distribution of the functionally significant genes associated with risks of diseases in indigenous Siberian populations makes it possible to identify the gene pool resilience, evaluate the susceptibility of various ethnic groups to metabolic disorders under changing environmental conditions, and predict the epidemiological situation in the near future.

Lower prevalence of DM2 among indigenous Siberian populations agrees with reduced populational frequencies of studied alleles *TCF7L2 (103894T)* and *TCF7L2 (53341T)* associated with DM2 and several syntropic diseases, discovered in the present paper. The reduced frequencies of these polymorphisms may affect the incidence rates of the diseases in the studied populations. With urbanization taken into account, one might predict reduced growth in incidence rates of DM2 and other pathological states associated with studied polymorphisms in indigenous Siberian ethnic groups compared to newcomer Caucasians.

The high frequency of *TCF7L2 (53341T)* polymorphism in Teleuts from the Kemerovo Region compared to Buryats and Yakuts may be attributed to a Caucasian component that this ethnic group adopted in their gene pool in the process of formation (Ostaptseva et al., 2006). With more comfortable living conditions close to cities of Prokopyevsk, Kemerovo, and Novokuznetsk and a richer European-type diet, Teleuts may face an increased risk of DM2 and associated diseases. Increased incidence of cardiovascular diseases has been observed in this ethnic group in recent decades (Ovsyannikova et al., 2007). However, polymorphism frequencies of other functionally significant genes are to be investigated to draw better-grounded conclusions.

Conclusions

Ethnic peculiarities in the frequency distribution of polymorphisms in gene *TCF7L2 (G103894T, rs12255372)* and (*C53341T, rs7903146*) in the populations of Buryats, Yakuts, Dolgans, and Teleuts, as well as a sample of Russians from Eastern Siberia, have been studied in the present paper. Locus rs12255372 has been studied in various territorial groups of Buryats and Yakuts for the first time, and the same goes for loci rs12255372 and rs7903146 in the Dolgan and Teleut populations. It has been shown that the samples of indigenous Siberian populations fall in-between Caucasian and East Asian populations with respect to studied polymorphism frequencies, following the geographic polymorphism distribution gradient.

Significantly lower occurrence of *TCF7L2 (103894T)* and *TCF7L2 (53341T)* alleles associated with DM2 and other metabolic disorders in the samples of indigenous Siberian

peoples compared to Russians was demonstrated, which agrees with their lower susceptibility to metabolic disorders, including DM2, compared to the newcomer Caucasian population described in the literature. With the transition to urbanized lifestyle taken into account, one might predict reduced growth in incidence rates of DM2 and other pathological states associated with the studied polymorphisms in indigenous Siberian ethnic groups, namely Buryats, Yakuts, Dolgans, and Teleuts, compared to newcomer Caucasians.

To better understand the nature of ethnic differences, further investigation into population structure with respect to other metabolic profile genes is required.

References

- Ametov A.S., Kamynina L.L., Akhmedova Z.G. The clinical aspects of effectiveness of incretin therapy (Wnt-pathogenic path and polymorphism of gene *TCF7L2*). *Rossiyskiy Meditsinskiy Zhurnal = Medical Journal of the Russian Federation*. 2016;22(1):47-51. DOI 10.18821/0869-2106-2016-22-1-47-51. (in Russian)
- Anjum N., Jehangir A., Liu Y. Two *TCF7L2* variants associated with type 2 diabetes in the Han nationality residents of China. *J. Coll. Physicians Surg. Pak*. 2018;28(10):794-797.
- Asfandiyarova N.S. A review of mortality in type 2 diabetes mellitus. *Sakharnyi Diabet = Diabetes Mellitus*. 2015;18(4):12-21. DOI 10.14341/DM6846. (in Russian)
- Avzaletdinova D.S., Sharipova L.F., Kochetova O.V., Morugova T.V., Erdman V.V., Somova R.S., Mustafina O.E. The association of *TCF7L2* rs7903146 polymorphism with type 2 diabetes mellitus among Tatars of Bashkortostan. *Sakharnyi Diabet = Diabetes Mellitus*. 2016;19(2):119-124. DOI 10.14341/DM2004138-45. (in Russian)
- Bairova T.A., Dolgikh V.V., Kolesnikova L.I., Pervushina O.A. Nutri-genetics and risk factors of cardiovascular disease: associated research in Eastern Siberia populations. *Byulleten' VSNIS SO RAMN = Bulletin of the East Siberian Scientific Center SB RAMS*. 2013; 4(92):87-92. (in Russian)
- Baturin A.K., Sorokina E.Yu., Pogozheva A.V., Keshabyants E.E., Kobelkova I.V., Kambarov A.O., Elizarova E.V., Tutelyan V.A. The association of rs993609 polymorphisms of gene *FTO* and rs659366 polymorphisms of gene *UCP2* with obesity among Arctic Russian population. *Voprosy Pitaniya = Problems of Nutrition*. 2017;86(3): 32-39. (in Russian)
- Bennett C.N., Ross S.E., Longo K.A., Bajnok L., Hemati N., Johnson K.W., Harrison S.D., MacDougald O.A. Regulation of Wnt signaling during adipogenesis. *J. Biol. Chem*. 2002;277(34):30998-31004. DOI 10.1074/jbc.M204527200.
- Bondar' I.A., Filipenko M.L., Shabel'nikova O.Yu., Sokolova E.A. Rs7903146 variant of *TCF7L2* gene and rs18012824 variant of *PPARG2* gene (*Pro12Ala*) are associated with type 2 diabetes mellitus in Novosibirsk population. *Sakharnyi Diabet = Diabetes Mellitus*. 2013;4:17-22. DOI 10.14341/DM2013417-22. (in Russian)
- Cauchi S., El Achhab Y., Choquet H., Dina C., Krempler F., Weitgasser R., Nejjari C., Patsch W., Chikri M., Meyre D., Froguel P. *TCF7L2* is reproducibly associated with type 2 diabetes in various ethnic groups: a global meta-analysis. *J. Mol. Med*. 2007;85(7):777-782. DOI 10.1007/s00109-007 0203-4.
- Cygankova D.P., Mulerova T.A., Ogarkov M.Yu., Saarela Ye.Yu., Barbarash O.L. Traditional lifestyle change as a reason for metabolic disorders risk increase in residents of Gornaya Shoriya. *Consilium Medicum*. 2018;20(5):66-70. DOI 10.26442/2075-1753_2018.5. 66-71. (in Russian)
- Franceschini N., Shara N.M., Wang H., Voruganti V.S., Laston S., Haack K., Lee E.T., Best L.G., MacCluer J.W., Cohran B., Dyer T.D.,

- Howard B.V., Cole S.A., North K.E., Umans J.G. The association of genetic variants of type 2 diabetes with kidney function. *Kidney Int.* 2012;82(2):220-225. DOI 10.1038/ki.2012.107.
- Hallmark B., Karafet T.M., Hsieh P.H., Osipova L.P., Watkins J.C., Hammer M.F. Genomic evidence of local adaptation to climate and diet in indigenous Siberians. *Mol. Biol. Evol.* 2018;36(2):315-327. DOI 10.1093/molbev/msy211.
- Han X., Luo Y., Ren Q., Zhang X., Wang F., Sun X., Zhou X., Ji L. Implication of genetic variants near *SLC30A8*, *HHEX*, *CDKAL1*, *CDKN2A/B*, *IGF2BP2*, *FTO*, *TCF2*, *KCNQ1*, and *WFS1* in type 2 diabetes in a Chinese population. *BMC Med. Genet.* 2010;11:81. DOI 10.1186/1471-2350-11-81.
- Haupt A., Thamer C., Heni M., Ketterer C., Machann J., Schick F., Machicao F., Stefan N., Claussen C.D., Häring H.U., Fritsche A., Staiger H. Gene variants of *TCF7L2* influence weight loss and body composition during lifestyle intervention in a population at risk for type 2 diabetes. *Diabetes.* 2010;59(3):747-750. DOI 10.2337/db09-1050.
- Ievleva K.D., Bairova T.A., Sheneman E.A., Ayurova Zh.G., Bal'zheva V.V., Novikova E.A., Bugun O.V., Rychkova L.V., Kolesnikova L.I. The protective effect of the G-allele of *PPARG2* rs1801282 polymorphism against overweight and obesity in Mongoloid adolescents. *Zhurnal Mediko-Biologicheskikh Issledovaniy = Journal of Medical and Biological Research.* 2019;7(4):452-463. DOI 10.17238/issn2542-1298.2019.7.4.452. (in Russian)
- Katsoulis K., Paschou S.A., Hatzis E., Tigas S., Georgiou I., Tsatsoulis A. *TCF7L2* gene variants predispose to the development of type 2 diabetes mellitus among individuals with metabolic syndrome. *Hormones (Athens).* 2018;17(3):359-365. DOI 10.1007/s42000-018-0047-z.
- Kaya E.D., Arikoğlu H., Kayış S.A., Öztürk O., Gönen M.S. Transcription factor 7-like 2 (*TCF7L2*) gene polymorphisms are strong predictors of type 2 diabetes among nonobese diabetics in the Turkish population. *Turk. J. Med. Sci.* 2017;47(1):22-28. DOI 10.3906/sag-1507-160.
- Kichigin V.A., Kochemirova T.N., Akimova V.P. Ethnic peculiarities in prevalence of cardiovascular risk factors in urban population. *Acta Medica Eurasica.* 2017;4:16-23. (in Russian)
- Kurtanov Kh.A., Sydykova L.A., Pavlova N.I., Filippova N.P., Doldokhov V.V., Apsolikhova G.A., Solov'eva N.A., D'yakonova A.T., Neustroeva L.M., Varlamova M.A., Borisova N.V. Polymorphism of the adiponutrin gene (*PNPLA3*) in the indigenous inhabitants of the Republic of Sakha (Yakutia) with type 2 diabetes mellitus. *Al'manakh Klinicheskoy Meditsiny = Almanac of Clinical Medicine.* 2018;46(3):258-263. DOI 10.18786/2072-0505-2018-46-3-258-263. (in Russian)
- Mel'nikova E.S., Rymar O.D., Ivanova A.A., Mustafina S.V., Shapkina M.Ju., Bobak M., Maljutina S.K., Voevoda M.I., Maximov V.N. Association of polymorphisms of genes *TCF7L2*, *FABP2*, *KCNQ1*, *ADIPOQ* with the prognosis of the development of type 2 diabetes mellitus. *Terapevticheskiy arkhiv = Therapeutic Archive.* 2020;92(10):40-47. DOI 10.26442/00403660.2020.10.000393. (in Russian)
- Melzer D., Murray A., Hurst A.J., Weedon M.N., Bandinelli S., Corsi A.M., Ferrucci L., Paolisso G., Guralnik J.M., Frayling T.M. Effects of the diabetes linked *TCF7L2* polymorphism in a representative older population. *BMC Med.* 2006;4:34. DOI 10.1186/1741-7015-4-34.
- Nobrega M.A. *TCF7L2* and glucose metabolism: time to look beyond the pancreas. *Diabetes.* 2013;62(3):706-708. DOI 10.2337/db12-1418.
- Orlov P.S., Kulikov I.V., Ustinov S.N., Gafarov V.V., Malyutina S.K., Romashchenko A.G., Voyevoda M.I., Maksimov V.N. Association analysis of some single nucleotide polymorphism markers of the second type of diabetes with myocardial infarction. *Byulleten' SO RAMN = Bulletin of Siberian Branch of Russian Academy of Medical Sciences.* 2011;31(5):19-24. (in Russian)
- Ostaptseva A.V., Shabaldin A.V., Akhmatianova V.R., Minina V.I., Glushkov A.N., Druzhinin V.G., Zorkoltseva I.V., Shabaldin E.V., Glushkova O.A., Makarchenko O.S., Ageyeva T.N. Molecular genetic analysis of interleukin 4 gene polymorphism among Teleutians, Shorians, and Caucasians of Kemerovo region. *Meditsinskaya Immunologiya = Medical Immunology.* 2006;8(5-6):737-740. (in Russian)
- Ovsyannikova O.V., Podkhomutnikov V.M., Kolbasko A.V., Luzina F.A., Gus'kova E.V. Cardiovascular disease in rural Kuzbass aborigines – Teleut. *Rossiyskiy Kardiologicheskii Zhurnal = Russian Journal of Cardiology.* 2007;6:59-62. (in Russian)
- Potapov V.A., Nosikov V.V., Shamkhalova M.N., Shestakova M.V., Smetanina S.A., Bel'chikova L.N., Suplotova L.A. *TCF7L2* rs12255372 and *SLC30A8* rs13266634 confer susceptibility to type 2 diabetes in a Russian population. *Russ. J. Genet.* 2010;46(8):1001-1008. DOI 10.1134/S1022795410080132.
- Rosales-Reynoso M.A., Arredondo-Valdez A.R., Juárez-Vázquez C.I., Wence-Chavez L.I., Barros-Núñez P., Gallegos-Arreola M.P., Flores-Martínez S.E., Morán-Moguel M.C., Sánchez-Corona J. *TCF7L2* and *CCND1* polymorphisms and its association with colorectal cancer in Mexican patients. *Cell Mol. Biol.* 2016;62(11):13-20. DOI 10.14715/cmb/2016.62.11.3.
- Saxena R., Gianniny L., Burt N.P., Lyssenko V., Giuducci C., Sjögren M., Florez J.C., Almgren P., Isomaa B., Orho-Melander M., Lindblad U., Daly M.J., Tuomi T., Hirschhorn J.N., Ardlie K.G., Groop L.C., Altshuler D. Common single nucleotide polymorphisms in *TCF7L2* are reproducibly associated with type 2 diabetes and reduce the insulin response to glucose in nondiabetic individuals. *Diabetes.* 2006;55(10):2890-2895. DOI 10.2337/db06-0381.
- Sladek R., Rocheleau G., Rung J., Dina C., Shen L., Serre D., Boutin P., Vincent D., Belisle A., Hadjadj S., Balkau B., Heude B., Charpentier G., Hudson T.J., Montpetit A., Pshezhetsky A.V., Prentki M., Posner B.I., Balding D.J., Meyre D., Polychronakos C., Froguel P. A genome-wide association study identifies novel risk loci for type 2 diabetes. *Nature.* 2007;445(7130):881-885. DOI 10.1038/nature05616.
- Smetanina S.A. Molecular-genetic and hormonal-metabolic associations among women of the Russian population of reproductive age with obesity and early menarche. *Meditsinskaya Nauka i Obrazovaniye Urala = Medical Science and Education in Ural.* 2015; 2(1):126-129. (in Russian)
- Tabikhanova L.E., Osipova L.P., Voronina E.N., Bragin A.O., Filipenko M.L. Polymorphism of lipid exchange genes in some populations of South and East Siberia. *Vavilovskii Zhurnal Genetiki i Selekcii = Vavilov Journal of Genetics and Breeding.* 2019;23(8):1011-1019. DOI 10.18699/VJ19.578.
- The 1000 Genomes Project Consortium. An integrated map of genetic variation from 1,092 human genomes. *Nature.* 2012;491(7422): 56-65. DOI 10.1038/nature11632.
- Timpson N.J., Lindgren C.M., Weedon M.N., Randall J., Ouwehand W.H., Strachan D.P., Rayner N.W., Walker M., Hitman G.A., Doney A.S., Palmer C.N., Morris A.D., Hattersley A.T., Zeggini E., Frayling T.M., McCarthy M.I. Adiposity-related heterogeneity in patterns of type 2 diabetes susceptibility observed in genome-wide association data. *Diabetes.* 2009;58(2):505-510. DOI 10.2337/db08-0906.
- Trifonova E.A., Popovich A.A., Bocharova A.V., Vagaitseva K.V., Stepanov V.A. The role of natural selection in the formation of the genetic structure of populations by SNP markers in association with body mass index and obesity. *Mol. Biol.* 2020;54(3):349-360. DOI 10.1134/S0026893320030176.

- Tsyretorova S.S., Bardymova T.P., Protasov K.V., Donirova O.S., Mistyakov M.V. Ethnic features of diabetes mellitus and coronary heart disease. *Sibirskiy Meditsinskiy Zhurnal (Irkutsk) = Siberian Medical Journal (Irkutsk)*. 2015;136(5):15-21. (in Russian)
- Vikulova O.K., Zheleznyakova A.V., Lebedeva N.O., Nikitin A.G., Nosikov V.V., Shestakova M.V. Genetic factors in the development of kidney chronic disease in patients with diabetes mellitus. *Russ. J. Genet.* 2017;53(4):420-432. DOI 10.1134/S1022795417030140.
- Xi B., Takeuchi F., Meirhaeghe A., Kato N., Chambers J.C., Morris A.P., Cho Y.S., Zhang W., Mohlke K.L., Kooner J.S., Shu X.O., Pan H., Tai E.S., Pan H., Wu J.Y., Zhou D., Chandak G.R., DIAGRAM Consortium, AGEN-T2D Consortium, SAT2D Consortium. Associations of genetic variants in/near body mass index-associated genes with type 2 diabetes: a systematic meta-analysis. *Clin. Endocrinol. (Oxf.)*. 2014;81(5):702-710. DOI 10.1111/cen.12428.
- Zhang M., Tang M., Fang Y., Cui H., Chen S., Li J., Xiong H., Lu J., Gu D., Zhang B. Cumulative evidence for relationships between multiple variants in the *VTG1A* and *TCF7L2* genes and cancer incidence. *Int. J. Cancer*. 2018;142(3):498-513. DOI 10.1002/ijc.31074.

ORCID ID

L.E. Tabikhanova orcid.org/0000-0002-5547-8189
L.P. Osipova orcid.org/0000-0001-7602-1156
T.V. Churkina orcid.org/0000-0003-1398-6537
E.N. Voronina orcid.org/0000-0002-3405-6980
M.L. Filipenko orcid.org/0000-0002-8950-5368

Acknowledgements. The study of Buryat, Teleut, Yakut, and Dolgan populations was supported by the Russian Scientific Foundation, project No. 19-15-00219. The Russian sample was studied under the state assignment of the Institute of Cytology and Genetics, SB RAS (project No. 0259-2021-0014).

Conflict of interest. The authors declare no conflict of interest.

Received August 5, 2021. Revised October 29, 2021. Accepted November 10, 2021.

Original Russian text www.bionet.nsc.ru/vogis/

Canopy temperature depression for drought- and heat stress tolerance in wheat breeding

S.B. Lepekhov 

Federal Altai Scientific Centre of Agro-BioTechnologies, Barnaul, Russia
 sergei.lepehov@yandex.ru

Abstract. An infrared thermometer was first used to assess drought and heat tolerance in plant breeding more than 40 years ago. Soon afterward, this method became widely used throughout the world. However, Russia has not yet applied the described method for evaluating stress tolerance. This paper presents an overview of using infrared thermometry in plant breeding. Taking wheat as an example, it shows major advantages and disadvantages of canopy temperature depression (CTD) values measured by the infrared thermometer. The paper also demonstrates that genotypes with higher CTD values, and therefore with a lower canopy temperature, use more available soil moisture under drought stress to cool the canopy by transpiration. It refers to CTD as an integrative trait that reflects an overall plant water status. Its coefficient of variation lies in the interval of 10 to 43 %. A large number of publications illustrate a close relation between CTD values and yield and indicate a high heritability of the former. Meanwhile, the same works show that yield has a higher heritability. Moreover, some researchers doubt that CTD should be used in applied wheat breeding as there are many factors that influence it. CTD has a high correlation with other traits that reflect plant water status or their adaptation to drought or heat stress. Quantitative trait loci (QTLs) associated with CTD are localized in all chromosomes, except for 3D. These QTLs often explain a small part of phenotypic variance (10–20 %, more likely less than 10 %), which complicates the pyramiding of canopy temperature genes through marker-assisted selection. The paper concludes that the evaluation of CTD appears to be a reliable, relatively simple, labor-saving, objective, and non-invasive method that sets it apart from other methods as well as shows the best results under terminal drought and heat stress conditions.

Key words: CTD; wheat; drought tolerance; heat tolerance; selection criteria.

For citation: Lepekhov S.B. Canopy temperature depression for drought- and heat stress tolerance in wheat breeding. *Vavilovskii Zhurnal Genetiki i Seleksii = Vavilov Journal of Genetics and Breeding*. 2022;26(2):196-201. DOI 10.18699/VJGB-22-24

Показатель снижения температуры растительного полога в селекции пшеницы на засухоустойчивость и жаростойкость

С.Б. Лепехов 

Федеральный Алтайский научный центр агробиотехнологий, Барнаул, Россия
 sergei.lepehov@yandex.ru

Аннотация. Прошло более 40 лет с начала использования инфракрасного термометра для оценки засухо- и жаростойкости в селекции растений. За это время метод широко распространился во всем мире. Однако в России описываемый способ оценки стрессоустойчивости сортов до сих пор не применяется. Нами сделан обзор результатов использования инфракрасного термометра в селекции растений. На примере пшеницы описаны основные достоинства и недостатки показателя CTD (canopy temperature depression), оцениваемого посредством инфракрасного термометра. Генотипы с более высоким значением CTD, а значит, более прохладным пологом в условиях засухи, используют большее количество доступной почвенной влаги для охлаждения за счет транспирации. CTD – интегрирующий признак, который диагностирует текущий водный статус растений. Коэффициент вариации показателя CTD находится в пределах 10–43 %. В значительном количестве работ показана его тесная взаимосвязь с урожайностью и высокая наследуемость, однако в целом больший коэффициент наследуемости имела урожайность. Применение показателя CTD в практической селекции пшеницы оспаривается рядом исследователей из-за значительного количества влияющих на него факторов. CTD тесно связан с другими признаками, отражающими водный статус растений или результат адаптации к засухе или жаре. Локусы количественных признаков, ассоциированные с CTD, обнаружены на всех хромосомах, за исключением хромосомы 3D. Выявленные локусы часто описывают небольшую часть фенотипической изменчивости (10–20 %, чаще менее 10 %), что затруднит пирамидирование генов, связан-

ных с температурой полога, посредством маркерной селекции. Оценка показателя CTD надежна, технически проста и производительна и при надлежащем ее использовании позволяет объективно определить одну из сторон жаро- и засухоустойчивости сортов, сохранив растения в живом виде, что выгодно отличает ее от других методов. Наилучший результат описываемый метод демонстрирует в условиях терминальной засухи.

Ключевые слова: показатель CTD; пшеница; засухоустойчивость; жаростойкость; критерий отбора.

Introduction

Every year 200 million hectares of wheat (*Triticum aestivum* L.) cultivated worldwide suffer economic losses from drought and heat (Ortiz et al., 2008) for wheat is very sensitive to heat stress. Optimal temperature for photosynthesis in wheat is approximately 25 °C (Nagai, Makino, 2009). It has been estimated that 1 °C increase above the optimal temperature at the grain filling stage decreases wheat yield by 3–4 % (Wardlaw et al., 1989).

Breeding drought-tolerant cultivars is one of the possible ways to reduce damage from drought. However, it requires much time and effort as it includes the evaluation of a large number of plants and is complicated by a low and inconsistent correlation between the phenotype and the yield under drought conditions, with multiple mechanisms of adaptation being involved. The selection that is based solely on yield indicators complicates breeding for drought tolerance because the yield shows low heritability under drought stress (Sofi et al., 2019). With that in mind, to evaluate many genotypes in a short period of time, it is important to single out other traits associated with drought tolerance (Sohail et al., 2020).

The paper suggests several physiological traits to identify tolerant genotypes. It refers to physiological traits as traits that contribute to mechanisms playing a role in plant adaptation to stress (Reynolds et al., 2009), such as coleoptile length, ability to stay green, stem water soluble carbohydrate, leaf water potential, canopy temperature, and so on.

This paper presents an overview of using infrared thermometry in plant breeding.

CTD and method of its measuring

Canopy temperature is an integrative trait that reflects the plant water status or the resultant equilibrium between the root water uptake and shoot transpiration (Berger et al., 2010). Under the high solar radiation and drought conditions, stomatal conductance decreases, soil moisture deficit reduces normal transpiration rate, which in turn increases canopy temperature (Rebetzke et al., 2013). Thus, canopy temperature can be used to study drought and heat tolerance in plants. Instead of canopy temperature, researchers often calculate canopy temperature depression (CTD) that refers to a metric, indicating the difference between air temperature and canopy temperature (Jackson et al., 1981). If the canopy temperature is lower than the air temperature under the influence of transpiration, then CTD is expressed as a positive value, but becomes negative if the reverse is true. Genotypes with higher CTD values and a cooler canopy temperature under drought stress use more available soil moisture to cool the canopy by transpiration. Given that Russian research lacks an established definition for ‘canopy temperature depression’, the paper refers to it as CTD defined in English research.

Canopy temperature is measured by a handheld infrared thermometer or thermal camera (Yousfi et al., 2019). It is done in the afternoon in clear weather conditions on windless days. The most considerable genotypic differences in CTD are reported from 2 to 3 p. m. (Thapa et al., 2018) at high temperatures and low relative humidity (Zhang X. et al., 2018). The researcher should stay close to the plot not to cast shadow on the place of measurement (Pinto et al., 2010). If a plot is sown in rows, it is best to stand to one side of it so that the infrared thermometer is pointed at an angle to the rows. If ground cover is low, it is best to point the thermometer at a low angle to the horizontal to minimize the likelihood of viewing soil (Reynolds et al., 2001). The infrared thermometer is held at approximately 50 cm above the canopy, and the measurements are taken at 1 m from the edge of the plot (Mason et al., 2011; Sohail et al., 2020). The best phase to perform measurements is the grain filling period (Thapa et al., 2018).

The infrared thermometer was first used for scheduling crop irrigation in the 1970s (Jackson et al., 1977) and for studying drought tolerance in the 1980s (Blum et al., 1982). In late 1980s, CIMMYT began to use CTD measurements as selection criteria in breeding for drought and heat tolerance in various experiments. Bulks showing high CTD values are selected in F₃ generation (Blum, 2005). Canopy temperature measurements can significantly improve the selection of drought tolerant genotypes because of their high speed (≈10 seconds per plot), simplicity, and relative economic efficiency. CTD is also integrative of the whole canopy due to scoring many plants at once, thus reducing error associated with plant-to-plant variation (Cossani, Reynolds, 2012).

Factors influenced on the measuring accuracy of CTD

However, this method has some limitations. First, the measuring accuracy depends on microclimate of the plant stand. Second, rapid changes in environmental conditions, for example on cloudy days, demonstrate high variability of the results (Chaves, 2013). Third, CTD is influenced by many biological and environmental factors, such as air temperature and relative humidity, soil moisture, wind, solar radiation, evapotranspiration, leaf adjustment to water deficit (Bahar et al., 2008), plant density (White et al., 2012), spike size, color and size of leaves (Balota et al., 2008), angle of leaves (Zhang Y. et al., 2011), peduncle length and awns (Bonari et al., 2020). Finally, plant organs differ in their self-cooling abilities, and thus, canopy temperature with spikes is 2 °C higher than the one without them (Olivares-Villegas et al., 2007).

The fact that these limitations have already been identified allows us to conclude that CTD and its features are well researched. Some environmental flux during the measurement period is inevitable, but correcting data against reference plots,

use of replication, and repetition of data collection during the crop cycle can compensate for this (Reynolds et al., 2001).

Association of CTD with other traits of wheat

CTD values demonstrate a significant correlation with yield under drought and heat stress in a large number of experiments (Gao et al., 2016; Liang et al., 2018; Sohail et al., 2020). They have regression relationships: if CTD decreases by 1 °C, the yield declines by 1.5 and 1.7 q/ha (Kaur et al., 2018). In this regard, the trait should be considered as a significant selection criterion in breeding programs not only in Mexico, but also in other countries of the world (Al-Ghzawi et al., 2018; Thapa et al., 2018). Newer cultivars of wheat have cooler canopy (Thapa et al., 2018), although the cultivars that are released in different decades under favorable growing conditions or irrigation do not show this correlation (Balota et al., 2017).

Various studies identify high correlation between CTD and other traits that reflect plant water status or their adaptation to drought or heat, including stomatal conductance (Bonari et al., 2020), delay in the senescence of leaves (Fang et al., 2017), leaf and stem wax (Mondal et al., 2015), depth and distribution of root system in soil (Pinto, Reynolds, 2015), spike sterility (Sohail et al., 2020), and 1000 grain weight (Gulnaz et al., 2019).

Variation and heritability of CTD

The coefficient of variation of CTD in different studies ranges from middle (10–14 % (Sharma P. et al., 2017; Jokar et al., 2018)) to high (26–43 % (Kumar et al., 2017; Sharma D. et al., 2018)). Dryland conditions make CTD values negative (Thapa et al., 2018) and increase genotypic differences (Pinto et al., 2010). In this respect, CTD value appears to be a better parameter for drought tolerance than yield under drought stress. Some research suggests that canopy temperature has a larger genetic value – if compared to direct selection based on yield and other traits – as it is an indirect index to the selection of certain types of cultivars and shows higher heritability and genetic correlation with yield (Rebetzke et al., 2013). Although some studies put CTD heritability at 0.65–0.80 (Kumar et al., 2017; Khan et al., 2020), there is a vast amount of research that calculates heritability for both CTD and yield and concludes that the latter has the larger heritability (see the Table).

One of the possible reasons for the low heritability of CTD value is environmental influence (Gao et al., 2016). Thus, literature review demonstrates that CTD cannot be referred to as the better selection criteria if compared to yield criteria under drought stress. This indicator is better used as an additional parameter in measuring drought tolerance in cultivars.

Genetic basis for canopy temperature depression

CTD genetic control has been extensively studied during the last two decades. For example, in their study, Acuña-Galindo et al. (2015) analyzed 30 pieces of research from 2002 to 2011 and identified four meta-QTLs (MQTLs) containing two or more QTLs for the trait that were associated with drought and heat tolerance, including CTD value that was identified in independent studies, populations, or environments. These MQTLs were localized on chromosomes 1B (34±2 cM),

Heritability coefficient for CTD and yield of common wheat in different studies

Heritability coefficient		References
CTD	Yield	
0.25, 0.32, 0.67	0.74, 0.82, 0.85	Olivares-Villegas et al., 2007
0.82, 0.11 and 0.34, 0.81	0.56 and 0.60	Reynolds et al., 2007
0.49	0.65–0.90	Pinto et al., 2010
0.51	0.61	Rathey et al., 2011
0.81	0.66	Paliwal et al., 2012
0.66	0.95	Bellundagi et al., 2013
0.24, 0.29	0.59	Lopes et al., 2013
0.22	0.62	Sukumaran et al., 2015
0.83	0.91	Rahman et al., 2016
0.52–0.61	0.66	Sharma D. et al., 2018

2B (68±2 cM), 3B (139±4 cM), and 7A (100±6 cM). The research also described single QTLs for CTD: these MQTLs were localized on chromosomes 3B, 4A, 7A, while chromosome 5A contained three MQTLs. QTLs associated with CTD were co-localized with QTLs that controlled other adaptive traits (yield, biomass, days to heading, grains per spike, 1000 grain weight, and water-soluble carbohydrates). While summarizing the results of their and prior research, Pinto et al. (2010) suggested that QTLs for canopy temperature were localized on chromosomes 1A, 1B, 1D, 2A, 2B, 3A, 3B, 4A, 4B, 5A, 5B, 6A, 6B, 6D, 7A, and 7B. The research undertaken after 2011 discovered QTLs for CTD on almost all chromosomes, except for 1D, 3A, 3D, and 6D (Paliwal et al., 2012; Lopes et al., 2013; Mason et al., 2013; Rebetzke et al., 2013; Mondal et al., 2015; Sukumaran et al., 2015; Awlachev et al., 2016; Gao et al., 2016; Mohammed et al., 2021).

Some research showed that QTLs associated with CTD were co-localized or closely localized with genes *Rht-B1* (Gao et al., 2016), *Rht-D1* (semi-dwarf wheat with warmer canopy), *Ppd-D1* (Rebetzke et al., 2013), *Vrn-A1* (Mondal et al., 2015), and transcription factor *Dreb1* (Khalid et al., 2019).

These loci for canopy temperature are responsible for 10–20 % of the phenotypic variation (Paliwal et al., 2012; Mondal et al., 2015; Awlachev et al., 2016) or even less than 10 % (Rebetzke et al., 2013; Sukumaran et al., 2015), and this is understandable as CTD is an integrative trait that is correlated to many mechanisms of drought tolerance (Lopes et al., 2013). Moreover, canopy cooling at different stages is controlled by loci with different localization (Lopes et al., 2013; Gao et al., 2016); therefore, the result of CTD measurements depends on the plant growth stage (Gulnaz et al., 2019). It is likely that the small genetic effects of multiple QTLs combined with the smaller population sizes commonly used in breeding will limit the pyramiding of multiple alleles for CTD through marker-assisted selection (Rebetzke et al., 2013).

Problems of using CTD in applied breeding

CTD indicates any kind of stress: high temperature, water or nutrient shortage (Kaur et al., 2018). Nitrogen fertilizers increase CTD values (Yang et al., 2018). Thus, this parameter shows not only water, but also a nitrogen nutrient status of plants (Guo et al., 2016). CTD is also related to NDVI (Yousfi et al., 2019), and canopy temperature may increase due to *Zymoseptoria tritici* infection (Wang et al., 2019). At the same time, high canopy temperatures provide unfavorable conditions for the development of stripe rust (Cheng et al., 2015). As the environmental factors have the aggregate effect on plants, CTD measurements that are performed for screening of drought tolerance without drought stress may produce incorrect results.

In addition to the well-studied negative correlation between yield and CTD values under drought or heat stress, the researchers highlight the controversy of their relationships in various environments (Balota et al., 2017). For example, in a high-yielding environment, cultivars with relatively high CTD values tend to produce higher yields than those with low CTD values, while in a low-yielding environment, the relationship between these traits disappears (Lu et al., 2020). However, it is explained by the fact that differences in plant tolerance become noticeable only if limiting factors are intense (Udovenko, 1973). Some studies show insignificant or positive correlation between CTD and yield (Rahman et al., 2016; Bala, Sikder, 2017), while others identify that under drought stress, high-yielding genotypes have both positive and negative CTD values (Sofi et al., 2019).

The research shows that a relatively large proportion of yield phenotypic variation under drought stress can be explained by a small number of traits, including CTD values. In most cases, they would be amenable to reliable quantification in parents and verification of expression in segregating progeny (Reynolds et al., 2007). However, it was impossible to accurately measure CTD values in some research because the plant canopy failed to cover the ground (Liang et al., 2018) or the yield was highly dependent on limited amounts of soil-stored water (Royo et al., 2002). Thus, Balota et al. (2017) identified the difficulty of using CTD values in applied plant breeding, for in that work a potential effect of neighbor plots plant height on canopy temperature was present.

More than that, a certain amount of caution is advisable in selecting genotypes with high CTD values in water-limited environments as more vigorous, later-flowering wheats may produce more biomass by the time canopy temperature is measured. Biomass and transpiration are physiologically linked, so that higher-biomass lines seem to deplete soil water faster, causing stomata to close and canopies to warm. Selection of cooler canopy temperature under conditions of soil-water depletion could favor the development of lines with low yield potential and smaller biomass (Rebetzke et al., 2013) or identification of specific genotypes (Jokar et al., 2018).

Conclusion

All things considered, the paper suggests that in general the evaluation of CTD appears to be a reliable, relatively simple, labor saving, and objective method that may be used to assess plant tolerance to heat or drought stress. Moreover, it is

a non-invasive method, and this sets it apart from others. To better evaluate cultivars tolerance to drought or heat stress, a substantial number of traits should be considered, therefore making CTD a meaningful contribution to knowledge on drought tolerance. Still, it is important to realize that this method shows the best results under terminal drought and heat stress conditions.

References

- Acuña-Galindo M.A., Mason R.E., Subramanian N.K., Hays D.B. Meta-analysis of wheat QTL regions associated with adaptation to drought and heat stress. *Crop Sci.* 2015;55(2):477-492. DOI 10.2135/cropsci2013.11.0793.
- Al-Ghazawi A.L.A., Khalaf Y.B., Al-Ajlouni Z.I., AL-Quraan N.A., Musallam I., Hani N.B. The effect of supplemental irrigation on canopy temperature depression, chlorophyll content, and water use efficiency in three wheat (*Triticum aestivum* L. and *T. durum* Desf.) varieties grown in dry regions of Jordan. *Agriculture.* 2018;8(5):67. DOI 10.3390/agriculture8050067.
- Awlachew Z.T., Singh R., Kaur S., Bains N.S., Chhuneja P. Transfer and mapping of the heat tolerance component traits of *Aegilops speltoides* in tetraploid wheat *Triticum durum*. *Mol. Breed.* 2016;36:78. DOI 10.1007/s11032-016-0499-2.
- Bahar B., Yildirim M., Barutcular C., Genç I. Effect of CTD on grain yield and yield component in bread and durum wheat. *Not. Bot. Horti Agrobot. Cluj-Napoca.* 2008;36(1):34-37. DOI 10.15835/nbha36187.
- Bala P., Sikder S. Heat stress indices, correlation and regression analysis of wheat genotypes for yield potential. *Int. J. Curr. Agric. Sci.* 2017;7(4):190-194.
- Balota M., Green A.J., Griffey C.A., Pitman R., Thomason W. Genetic gains for physiological traits associated with yield in soft red winter wheat in the Eastern United States from 1919 to 2009. *Eur. J. Agron.* 2017;84:76-83. DOI 10.1016/j.eja.2016.11.008.
- Balota M., Peters T.R., Payne W.A., Evelt S.R. Morphological and physiological traits related with canopy temperature depression in three-closely related wheat lines. *Crop Sci.* 2008;48(5):1897-1910. DOI 10.2135/cropsci2007.06.0317.
- Bellundagi A., Singh G.P., Prabhu K.V., Arora A., Neelu J., Ramya P., Singh A.M., Singh P.K., Ahlawat A. Early ground cover and other physiological traits as efficient selection criteria for grain yield under moisture deficit stress conditions in wheat (*Triticum aestivum* L.). *Indian J. Plant Physiol.* 2013;18:277-281. DOI 10.1007/s40502-013-0047-6.
- Berger B., Parent B., Tester M. High-throughput shoot imaging to study drought responses. *J. Exp. Bot.* 2010;61(13):3519-3528. DOI 10.1093/jxb/erq201.
- Blum A. Drought resistance, water-use efficiency, and yield potential – are they compatible, dissonant, or mutually exclusive? *Aust. J. Agric. Res.* 2005;56(11):1159-1168. DOI 10.1071/AR05069.
- Blum A., Mayer J., Gozlan G. Infrared thermal sensing of plant canopies as a screening technique for dehydration avoidance in wheat. *Field Crops Res.* 1982;5:137-146. DOI 10.1016/0378-4290(82)90014-4.
- Bonari A., Edalat M., Ghadiri H., Kazemeini S.A., Modarresi M. The study of temperature depression and its association with grain yield in six wheat cultivars under heat stress conditions and salicylic acid application. *Iran Agric. Res.* 2020;39(1):99-108. DOI 10.22099/iar.2020.31975.1318.
- Chaves M.M. Thermography to explore plant-environment interactions. *J. Exp. Bot.* 2013;64(13):3937-3949. DOI 10.1093/jxb/ert029.
- Cheng J.-J., Li H., Ren B., Zhou C.-J., Kang Z.-S., Huang L.-L. Effect of canopy temperature on the stripe rust resistance of wheat. *N.Z.J. Crop Hortic. Sci.* 2015;43(4):306-315. DOI 10.1080/01140671.2015.1098708.
- Cossani C.M., Reynolds M.P. Physiological traits for improving heat tolerance in wheat. *Plant Physiol.* 2012;160(4):1710-1718. DOI 10.1104/pp.112.207753.

- Fang Q., Zhang X., Chen S., Shao L., Sun H. Selecting traits to increase winter wheat yield under climate change in the North China Plain. *Field Crops Res.* 2017;207:30-41. DOI 10.1016/j.fcr.2017.03.005.
- Gao F., Liu J., Yang L., Wu X., Xiao Y., Xia X., He Z. Genome-wide linkage mapping of QTL for physiological traits in a Chinese wheat population using the 90K SNP array. *Euphytica.* 2016;209(3):789-804. DOI 10.1007/s10681-016-1682-6.
- Gulnaz S., Zulkiffal M., Sajjad M., Ahmed J., Musa M., Abdullah M., Ahsan A., Refman A. Identifying Pakistani wheat landraces as genetic resources for yield potential, heat tolerance and rust resistance. *Int. J. Agric. Biol.* 2019;21(3):520-526. DOI 10.17957/IJAB/15.0924.
- Guo J., Tian G., Zhou Y., Wang M., Ling N., Shen Q., Guo S. Evaluation of the grain yield and nitrogen nutrient status of wheat (*Triticum aestivum* L.) using thermal imaging. *Field Crops Res.* 2016;196:463-472. DOI 10.1016/j.fcr.2016.08.008.
- Jackson R.D., Idso S.B., Reginato R.J., Pinter P.J. Canopy temperature as a crop water-stress indicator. *Water Resour. Res.* 1981;17(4):1133-1138. DOI 10.1029/WR017i004p01133.
- Jackson R.D., Reginato R.J., Idso S.B. Wheat canopy temperature – practical tool for evaluating water requirements. *Water Resour. Res.* 1977;13(3):651-656. DOI 10.1029/WR013i003p00651.
- Jokar F., Karimizadeh R., Masoumiasl A., Fahliani R.A. Canopy temperature and chlorophyll content are effective measures of drought stress tolerance in durum wheat. *Not. Sci. Biol.* 2018;10(4):575-583. DOI 10.25835/nsb10410288.
- Kaur S., Singh S.P., Kingra P.K. Canopy temperature as indicator of thermal and nutrient stresses in wheat crop. *Mausam.* 2018;69(2): 309-314.
- Khalid M., Afzal F., Gul A., Amir R., Subhani A., Ahmed Z., Mahmood Z., Xia X., Rasheed A., He Z. Molecular characterization of 87 functional genes in wheat diversity panel and their association with phenotypes under well-watered and water-limited conditions. *Front. Plant Sci.* 2019;10:717. DOI 10.3389/fpls.2019.00717.
- Khan A., Ahmad M., Shah M.K.N., Ahmed M. Genetic manifestation of physio-morphic and yield related traits conferring thermotolerance in wheat. *Pak. J. Bot.* 2020;52(5):1545-1552. DOI 10.30848/PJB2020-5(27).
- Kumar J., Kumar M., Singh S.K., Singh L. Estimation of genetic variability and heritability in bread wheat under abiotic stress. *Int. J. Pure Appl. Biosci.* 2017;5(1):156-163. DOI 10.18782/2320-7051.2475.
- Liang X., Liu Y., Chen J., Adams C. Late-season photosynthetic rate and senescence were associated with grain yield in winter wheat of diverse origins. *J. Agron. Crop Sci.* 2018;204(1):1-12. DOI 10.1111/jac.12231.
- Lopes M.S., Reynolds M.P., McIntyre C.L., Mathews K.L., Kamali M.R.J., Mossad M., Feltaous Y., Tahir I.S.A., Chatrath R., Ogbonaya F., Baum M. QTL for yield and associated traits in the Seri/Babax population grown across several environments in Mexico, in the West Asia, North Africa, and South Asia regions. *Theor. Appl. Genet.* 2013;126(4):971-984. DOI 10.1007/s00122-012-2030-4.
- Lu Y., Yan Z., Li L., Gao C., Shao L. Selecting traits to improve the yield and water use efficiency of winter wheat under limited water supply. *Agric. Water Manag.* 2020;242:106410. DOI 10.1016/j.agwat.2020.106410.
- Mason R.E., Hays D.B., Mondal S., Ibrahim A.M.H., Basnet B.R. QTL for yield, yield components and canopy temperature depression in wheat under late sown field conditions. *Euphytica.* 2013;194:243-259. DOI 10.1007/s10681-013-0951-x.
- Mason R.E., Mondal S., Beecher F., Hays D. Genetic loci linking improved heat tolerance in wheat (*Triticum aestivum* L.) to lower leaf and spike temperatures under controlled conditions. *Euphytica.* 2011;180:181-194. DOI 10.1007/s10681-011-0349-6.
- Mohammed S., Huggins T., Mason E., Beecher F., Chick C., Sengodan P., Paudel A., Ibrahim A., Tilley M., Hays D. Mapping the genetic loci regulating leaf epicuticular wax, canopy temperature and drought susceptibility index in *Triticum aestivum* L. *Crop Sci.* 2021;61:2294-2305. DOI 10.1002/csc2.20458.
- Mondal S., Mason R.E., Huggins T., Hays D.B. QTL on wheat (*Triticum aestivum* L.) chromosomes 1B, 3D and 5A are associated with constitutive production of leaf cuticular wax and may contribute to lower leaf temperatures under heat stress. *Euphytica.* 2015;201: 123-130. DOI 10.1007/s10681-014-1193-2.
- Nagai T., Makino A. Differences between rice and wheat in temperature responses of photosynthesis and plant growth. *Plant Cell Physiol.* 2009;50(4):744-755. DOI 10.1093/pcp/pcp029.
- Olivares-Villegas J.J., Reynolds M.P., McDonald G.K. Drought-adaptive attributes in the Seri/Babax hexaploid wheat population. *Funct. Plant Biol.* 2007;34(3):189-203. DOI 10.1071/FP06148.
- Ortiz R., Sayre K.D., Govaerts B., Gupta R., Subbarao G.V., Ban T., Hodson D., Dixon J.M., Ortiz-Monasterio J.I., Reynolds M. Climate change: can wheat beat the heat? *Agric. Ecosyst. Environ.* 2008;126(1-2):46-58. DOI 10.1016/j.agee.2008.01.019.
- Paliwal R., Roder M.S., Kumar U., Srivastava J.P., Joshi A.K. QTL mapping of terminal heat tolerance in hexaploid wheat (*T. aestivum* L.). *Theor. Appl. Genet.* 2012;125(3):561-575. DOI 10.1007/s00122-012-1853-3.
- Pinto R.S., Reynolds M.P., Mathews K.L., McIntyre C.L., Olivares-Villegas J.J., Chapman S.C. Heat and drought adaptive QTL in a wheat population designed to minimize confounding agronomic effects. *Theor. Appl. Genet.* 2010;121(6):1001-1021. DOI 10.1007/s00122-010-1351-4.
- Pinto R.S., Reynolds M.P. Common genetic basis for canopy temperature depression under heat and drought stress associated with optimized root distribution in bread wheat. *Theor. Appl. Genet.* 2015;128:575-585. DOI 10.1007/s00122-015-2453-9.
- Rahman M., Barma N., Biswas B., Khan A., Rahman J. Study on morpho-physiological traits in spring wheat (*Triticum aestivum* L.) under rainfed condition. *Bangladesh J. Agric. Res.* 2016;41(2):235-250. DOI 10.3329/bjar.v41i2.28227.
- Rathey A., Shorter R., Chapman S. Evaluation of CIMMYT conventional and synthetic spring wheat germplasm in rainfed sub-tropical environments. II. Correlated response for grain yield components and physiological traits due to selection for grain yield. *Field Crops Res.* 2011;124(2):195-204. DOI 10.1016/j.fcr.2011.02.006.
- Rebetzke G.J., Rathey A.R., Farquhar G.D., Richards R.A., Condon A.G. Genomic regions for canopy temperature and their genetic association with stomatal conductance and grain yield in wheat. *Funct. Plant Biol.* 2013;40(1):14-33. DOI 10.1071/FP12184.
- Reynolds M., Manes Y., Izanloo A., Langridge P. Phenotyping approaches for physiological breeding and gene discovery in wheat. *Ann. Appl. Biol.* 2009;155(3):309-320. DOI 10.1111/j.1744-7348.2009.00351.x.
- Reynolds M.P., Ortiz-Monasterio J.I., McNab A. Application of physiology in wheat breeding. Mexico: CIMMYT, 2001.
- Reynolds M.P., Pierre C.S., Saad A.S.I., Vargas M., Condon A.G. Evaluating potential genetic gains in wheat associated with stress-adaptive trait expression in elite genetic resources under drought and heat stress. *Crop Sci.* 2007;47(S3):S-172-S-189. DOI 10.2135/cropsci2007.10.0022IPBS.
- Royo C., Villegas D., Del Moral L.F.G., Elhani S., Aparicio N., Rharabti Y., Araus J.L. Comparative performance of carbon isotope discrimination and canopy temperature depression as predictors of genotypes differences in durum wheat yield in Spain. *Aust. J. Agric. Res.* 2002;53(3):561-569. DOI 10.1071/AR01016.
- Sharma D., Jaiswal J.P., Singh N.K., Chauhan A., Gahtyari N.C. Developing a selection criterion for terminal heat tolerance in bread wheat based on various morpho-physiological traits. *Int. J. Curr. Microbiol. Appl. Sci.* 2018;7(7):2716-2726. DOI 10.20546/ijcmas.2018.707.318.
- Sharma P., Sareen S., Saini M.S. Assessing genetic variation for heat stress tolerance in Indian bread wheat genotypes using morpho-

- physiological traits and molecular markers. *Plant Genet. Resour.* 2017;15(6):539-547. DOI 10.1017/S1479262116000241.
- Sofi P.A., Ara A., Gull M., Rehman K. Canopy temperature depression as an effective physiological trait for drought screening. In: Ondrasek G. (Ed.) *Drought-Detection and Solutions*. London: IntechOpen, 2019;77-92. DOI 10.5772/intechopen.85966.
- Sohail M., Hussain I., Qamar M., Tanveer S.K., Abbas S.H., Ali Z., Imtiaz M. Evaluation of spring wheat genotypes for climatic adaptability using canopy temperature as physiological indicator. *Pak. J. Agric. Sci.* 2020;33(1):89-96. DOI 10.17582/journal.pjar/2020/33.1.89.96.
- Sukumaran S., Dreisigacker S., Lopes M., Chavez P., Reynolds M.P. Genome-wide association study for grain yield and related traits in an elite spring wheat population grown in temperate irrigated environments. *Theor. Appl. Genet.* 2015;128(2):353-363. DOI 10.1007/s00122-014-2435-3.
- Thapa S., Jessup K.E., Pradhan G.P., Rudd J.C., Liu S., Mahan J.R., Devkota R.N., Baker J.A., Xue Q. Canopy temperature depression at grain filling correlates to winter wheat yield in the U.S. Southern High Plains. *Field Crops Res.* 2018;217:11-19. DOI 10.1016/j.fcr.2017.12.005.
- Udovenko G.V. Character of adaptation reaction and causes of different resistance of plants to extremal conditions. *Trudy po Prikladnoy Botanike, Genetike i Seleksii = Proceedings on Applied Botany, Genetics, and Breeding*. 1973;49(3):258-268. (in Russian)
- Wang Y., Zia-Khan S., Owusu-Adu S., Miedaner T., Müller J. Early detection of *Zymoseptoria tritici* in winter wheat by infrared thermography. *Agriculture*. 2019;9(7):139. DOI 10.3390/agriculture9070139.
- Wardlaw I.F., Dawson I.A., Munibi P., Fewster R. The tolerance of wheat to high temperatures during reproductive growth. I. Survey procedures and general response patterns. *Aust. J. Agric. Res.* 1989;40(1):1-13. DOI 10.1071/AR9890001.
- White J.W., Andrade-Sanchez P., Gore M.A., Bronson K.F., Cof-felt T.A., Conley M.M. Field-based phenomics for plant genetics research. *Field Crop Res.* 2012;133:101-112. DOI 10.1016/j.fcr.2012.04.003.
- Yang D.Q., Dong W.H., Luo Y.L., Song W.T., Cai T., Li Y., Yin Y.P., Wang Z.L. Effects of nitrogen application and supplemental irrigation on canopy temperature and photosynthetic characteristics in winter wheat. *J. Agric. Sci. Technol.* 2018;156(1):13-23. DOI 10.1017/S0021859617000946.
- Yousfi S., Gracia-Romero A., Kellas N., Kaddour M., Chadouli A., Karrou M., Araus J.L., Serret M.D. Combined use of low-cost remote sensing techniques and $\delta^{13}C$ to assess bread wheat grain yield under different water and nitrogen conditions. *Agronomy*. 2019;9(6):285. DOI 10.3390/agronomy9060285.
- Zhang X., Zhang X., Chen S., Sun H., Shao L., Liu X. Optimized timing of using canopy temperature to select high-yielding cultivars of winter wheat under different water regimes. *Exp. Agric.* 2018;54(2):257-272. DOI 10.1017/S0014479716000235.
- Zhang Y., Zhang Y., Wang Z., Wang Z. Characteristics of canopy structure and contributions of non-leaf organs to yield in winter wheat under different irrigated conditions. *Field Crops Res.* 2011;123(3):187-195. DOI 10.1016/j.fcr.2011.04.014.

ORCID ID

S.B. Lepekhov orcid.org/0000-0003-1561-6345

Acknowledgements. The research is carried out under the Federal Altai Scientific Centre of Agro-BioTechnologies government contract No. 0534-2021-0003 (theme: "The use of molecular genetics and biotechnological research methods in plant breeding").

Conflict of interest. The author declares no conflict of interest.

Received October 8, 2021. Revised November 9, 2021. Accepted November 10, 2021.

Original Russian text www.bionet.nsc.ru/vogis/

A review of hyperspectral image analysis techniques for plant disease detection and identification

A.F. Cheshkova 

Siberian Federal Scientific Center of AgroBioTechnology of the Russian Academy of Sciences, Krasnoobsk, Novosibirsk region, Russia
 cheshanna@yandex.ru

Abstract. Plant diseases cause significant economic losses in agriculture around the world. Early detection, quantification and identification of plant diseases are crucial for targeted application of plant protection measures in crop production. Recently, intensive research has been conducted to develop innovative methods for diagnosing plant diseases based on hyperspectral technologies. The analysis of the reflection spectrum of plant tissue makes it possible to classify healthy and diseased plants, assess the severity of the disease, differentiate the types of pathogens, and identify the symptoms of biotic stresses at early stages, including during the incubation period, when the symptoms are not visible to the human eye. This review describes the basic principles of hyperspectral measurements and different types of available hyperspectral sensors. Possible applications of hyperspectral sensors and platforms on different scales for diseases diagnosis are discussed and evaluated. Hyperspectral analysis is a new subject that combines optical spectroscopy and image analysis methods, which make it possible to simultaneously evaluate both physiological and morphological parameters. The review describes the main steps of the hyperspectral data analysis process: image acquisition and preprocessing; data extraction and processing; modeling and analysis of data. The algorithms and methods applied at each step are mainly summarized. Further, the main areas of application of hyperspectral sensors in the diagnosis of plant diseases are considered, such as detection, differentiation and identification of diseases, estimation of disease severity, phenotyping of disease resistance of genotypes. A comprehensive review of scientific publications on the diagnosis of plant diseases highlights the benefits of hyperspectral technologies in investigating interactions between plants and pathogens at various measurement scales. Despite the encouraging progress made over the past few decades in monitoring plant diseases based on hyperspectral technologies, some technical problems that make these methods difficult to apply in practice remain unresolved. The review is concluded with an overview of problems and prospects of using new technologies in agricultural production.

Key words: hyperspectral technologies; plant diseases; image analysis; spectral analysis.

For citation: Cheshkova A.F. A review of hyperspectral image analysis techniques for plant disease detection and identification. *Vavilovskii Zhurnal Genetiki i Seleksii = Vavilov Journal of Genetics and Breeding*. 2022;26(2):202-213. DOI 10.18699/VJGB-22-25

Обзор современных методов обнаружения и идентификации болезней растений на основе анализа гиперспектральных изображений

А.Ф. Чешкова 

Сибирский федеральный научный центр агробиотехнологий Российской академии наук, р.п. Краснообск, Новосибирская область, Россия
 cheshanna@yandex.ru

Аннотация. Болезни растений приводят к значительным экономическим потерям в секторе сельскохозяйственного производства во всем мире. Раннее выявление, количественная оценка и идентификация болезней имеют решающее значение для целенаправленного применения мер защиты в растениеводстве. В настоящее время ведутся интенсивные научные исследования по разработке инновационных методов диагностики болезней растений, основанных на гиперспектральных технологиях. Анализ спектра отражения растительной ткани позволяет проводить классификацию здоровых и больных растений, оценивать тяжесть заболевания, дифференцировать виды патогенов и выявлять симптомы биотических стрессов на ранних стадиях, в том числе в инкубационный период, когда симптомы не видны человеческому глазу. В обзоре описаны основные принципы измерения спектра отражения растительной ткани. Обсуждаются и оцениваются возможности применения различных типов гиперспектральных сенсоров и платформ для диагностики болезней растений. Гиперспектральный анализ является новой областью, соединяющей в себе методы оптической спектроскопии и методы анализа изображений, которые позволяют одновременно оценивать как физиологические, так и морфологические параметры. Описаны главные этапы анализа гиперспектральных данных: получение и предварительная обработка изображения;

извлечение и обработка данных; моделирование и анализ данных. Приведен перечень алгоритмов и методов, применяемых на каждом из этапов. Рассмотрены основные области применения гиперспектральных сенсоров в диагностике болезней растений, такие как обнаружение болезни, дифференциация и идентификация типа заболевания, оценка степени поражения, оценка устойчивости генотипов. Приведен всесторонний обзор научных публикаций, подчеркивающий преимущества гиперспектральных технологий при исследовании взаимодействий между растениями и патогенами в различных масштабах измерений. Несмотря на обнадеживающий прогресс, достигнутый за последние несколько десятилетий в мониторинге болезней растений на основе гиперспектральных технологий, остаются нерешенными некоторые технические проблемы, препятствующие применению этих методов на практике. В заключение обсуждаются проблемы и перспективы практического использования новых технологий в сельскохозяйственном производстве.

Ключевые слова: гиперспектральные технологии; болезни растений; анализ изображений; спектральный анализ.

Introduction

Plant diseases cause crop losses, reduce the quality of agricultural products and can even threaten human health. Farmers need modern and effective tools for early detection and identification of plant diseases (Mahlein et al., 2019b). Traditional diagnostic methods such as visual assessment and microbiological laboratory analysis are time-consuming and labor-intensive, which limits their application in large-scale farms.

Currently, new non-invasive methods for diagnosing plant diseases using sensor technologies, robotics, computer vision and machine learning are rapidly developing (Singh A. et al., 2015; Demidchik et al., 2020; Zheng et al., 2021). These methods are high throughput and provide a real-time support for assessing a range of physiological parameters (Walter et al., 2015). A large amount of information obtained from modern sensors is transformed into new knowledge using computer data processing and modeling, reducing the distance from fundamental science to practical implementation (Afonnikov et al., 2016; Tardieu et al., 2017). New approaches allow, due to automation, to significantly speed up the diagnosis of diseases and increase its accuracy by eliminating the human subjectivity (Fahlgren et al., 2015; Lobos et al., 2017).

At present, a variety of imaging methods are being used for plant diseases detection, such as fluorescence imaging, thermal infrared imaging, visible RGB imaging, imaging spectroscopy and other techniques (Bock et al., 2010; Li L. et al., 2014).

Among them, hyperspectral imaging technique comes with numerous advantages (Mahlein, 2016; Mahlein et al., 2018; Dubrovskaya et al., 2018). According to the Scopus statistics, there are 412 relevant papers from 2005 to 2020 where 'plant disease' and 'hyperspectral' are used as key words for the search (Fig. 1). Hyperspectral analysis combines optical spectroscopy and image analysis methods, allowing both physiological and morphological parameters to be evaluated simultaneously.

The aim of the paper is to provide the reader with an overview of modern technologies for the diagnosis of plant diseases based on the analysis of hyperspectral images. The first part of the article discusses the main principles and tools of hyperspectral technologies. Next, algorithms and methods for analyzing hyperspectral images are described. Further,

the main areas of application of hyperspectral sensors in the diagnosis of plant diseases are considered. The paper is concluded with some problems and prospects of using new technologies.

Basic principles and tools of hyperspectral technologies

Interaction of light (electromagnetic radiation) and plants

Light can interact with plant tissue in the following ways: reflection, scattering, absorption and transmission. The reflectance characteristic of a plant results from the biochemical compounds present in the leaves, and the physical characteristics of leaves (Mishra et al., 2017). The interaction between light and plants also depends on the wavelength. In the visible wavelength range (400–700 nm), the surface of the plant has a low reflectivity due to the absorption of light by photosynthetic pigments (chlorophylls, anthocyanins and carotenoids). In the near infrared (700–1100 nm), the reflectance increases due to light scattering in the intercellular space. In the short wave infrared range (1100–2500 nm), healthy plants have a low reflectance due to the absorption of light by water, proteins and other carbon components (Lowe et al., 2017). The green color of the leaf is consistent with the characteristic reflection peak at 550 nm.

Spectral profiles of healthy and diseased plants can differ. As a result of the impact of biotic and abiotic stressors, the biochemical composition of plant tissues changes, which is reflected in the change in the color and shape of leaves, transpiration rate, canopy morphology, and, consequently, in the spectral characteristics of plants (Zhang J. et al., 2019). Moreover, each individual interaction of a plant and a pathogen has certain spatial and temporal dynamics, and these processes affect different ranges of the electromagnetic spectrum. For example, a change in photosynthetic activity caused by pathogens leads to a change in reflectivity in the visible range of the spectrum. Changes at the cellular level have a large impact on the near infrared spectrum. Tissue necrosis leads to increased reflection in the shortwave infrared range (Zhang N. et al., 2020).

Such relationships between cause and consequence can be used to study the biochemistry of plants and to perform controlled experiments.

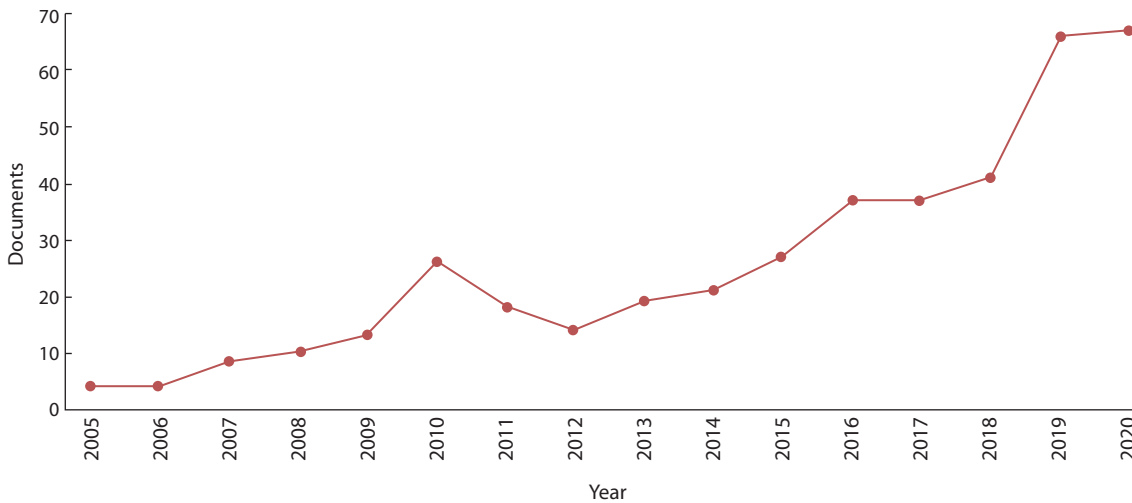


Fig. 1. Number of published articles by year on plant diseases with hyperspectral data (Scopus).

Hyperspectral sensors and platforms

The basic principle of hyperspectral sensors is comparable to the principle behind RGB and multispectral cameras (Thomas et al., 2018b). All these systems measure the amount of light reaching the sensor and store the information. Unlike RGB cameras (3 spectral bands) or multispectral cameras (<20 spectral bands), a hyperspectral sensor measures up to several hundred bands of the electromagnetic spectrum in the wavelength range of the sensor. Each of these spectral bands measures only a few nanometers of the electromagnetic spectrum, leading to a high spectral resolution of the hyperspectral sensor.

There are two main types of sensors: image sensors and non-imaging sensors. Non-imaging sensors measure the average reflectance spectrum in a certain area of a surface without storing spatial information. The size of the averaging area depends on the focal length, angle of view and distance to the object. Most non-imaging sensors are portable and do not require complicated measurement platforms. They have a wide spectral range (300–2500 nm), a high spectral resolution (1–3 nm), and low weight (1–5 kg). The most popular among them are spectrometers ASD FieldSpec (Analytical Spectral Devices Inc., USA), SVC (Spectral Vista Corporation, USA), ImSpector (Spectral Imaging Ltd., Finland).

These devices are widely used in laboratory, greenhouse and field conditions (Naidu et al., 2009; Zhang J. et al., 2017; Couture et al., 2018; Bohnenkamp et al., 2019; Mahlein et al., 2019a). There are also micro-spectrometers such as the STS-VIS spectrometer (Ocean Optics Inc., USA) suitable for use with UAVs (Burkart et al., 2015). Since early symptoms of plant disease often appear below 1 mm, their detection with spectrometers is limited. This is due to the averaging of the spectrum of healthy and diseased tissue in the measurement area (Mahlein et al., 2012).

Hyperspectral image sensors form a spectral profile for each individual pixel, thereby combining spectral and spatial resolution. The resulting image is a three-dimensional data array (hypercube) containing two dimensions of spatial information and additionally one dimension of spectral information. Depending on the type of sensors used, there are four ways to obtain a hypercube of data (Fig. 2): whisk-broom, push-broom, spectral scanning, and snapshot (Wu, Sun, 2013).

Hyperspectral image sensors usually cover a limited spectral range: VNIR (300–1000 nm) or SWIR (1000–2500 nm) with a spectral resolution of 1–7 nm. Spatial resolution ranges from micrometers to centimeters depending on the distance to the object and sensor characteristics.

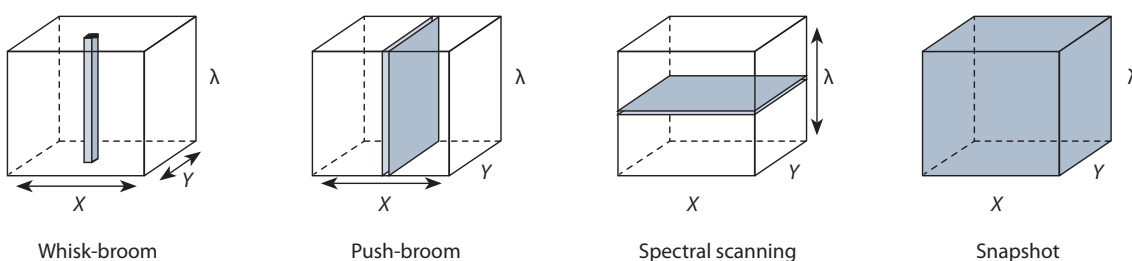


Fig. 2. Acquisition approaches of hyperspectral images.

Scanning directions are shown by arrows, and gray areas show data acquired each time.

In the case of using point or line scanning sensors (whisk-broom, push-broom), it is necessary to move the object or the camera to register the spectrum of each individual point or line. In scientific research, the most commonly used scanning cameras are Specim (Spectral Imaging Ltd., Finland), Headwall (Headwall Hyperspec Ltd., Canada), Photonfocus (Photonfocus AG, Switzerland), Pika L (Resonon Inc., USA). Most hyperspectral scanning cameras in the laboratory are installed on specialized mobile platforms that provide linear movement and stabilization of the camera (Leucker et al., 2016; Yeh et al., 2016). Stationary rail systems are used in greenhouses (Thomas et al., 2018a). Vehicles (Vigneau et al., 2011; Williams et al., 2017) or UAVs (Huang W. et al., 2007; Abdulridha et al., 2019) are used in the field. The disadvantage of scanning sensors is the relatively long image acquisition time, depending on the size of the measured area, which complicates the shooting of moving objects. This disadvantage is eliminated in portable Specim IQ camera with a built-in scanner (Behmann et al., 2018; Alt et al., 2020; Barreto et al., 2020).

Spectral scanning sensors use LCTF filters that pass only certain wavelengths changing rapidly during shooting (Choudhary et al., 2009; Wang et al., 2012). These sensors create 2D spatial images for each wavelength in the spectral range. Their use does not require moving the object or camera to obtain a hypercube. The acquisition time is mainly dependent on the exposure time, which is generally faster than point or line scans. If the object is moving, then this measuring principle can lead to inconsistent spectra, since the individual bands are observed at different times.

Recently, snapshot sensors that do not require scanning an object to obtain a hypercube have been developed. They use the mosaic principle of conventional RGB cameras. These sensors provide a significantly higher image recording rate, but lower spatial resolution compared to traditional ones. Well-known cameras of this type are Rikola, Senop (Senop Ltd., Finland), Ultris, FireFleye (Cubert Ltd., Canada). The compact size, short image acquisition time and the ability to create a sequence of hyperspectral images of a moving object make them optimal for use in UAVs (Aasen et al., 2015; Sankaran et al., 2015; Franceschini et al., 2019).

Hyperspectral image processing methods and algorithms

From the data analysis perspective the use of multi-scale datasets of hyperspectral images, characterized by a huge amount of data with a high level of collinearity, is a very challenging, emerging topic that requires non-trivial solutions. To face this challenge, the methods of discriminant and cluster analysis, machine learning, and neural networks have been successfully adopted (ElMasry et al., 2016; Lowe et al., 2017).

Available software tools for hyperspectral image analysis process are ENVI (Research Systems Inc.), MATLAB (The Math-Works Inc.), Python (Python Software Foundation), R (R Software Foundation).

The hyperspectral image analysis process usually includes the following steps (Fig. 3): (1) image acquisition and preprocessing, (2) data extraction and processing, (3) data modeling and analysis.

Image acquisition and preprocessing

The first important step in the analysis of plant diseases is to obtain high-quality hyperspectral images that meet the objectives of research. The right choice of sensors and platforms, the correct setting of the spatial and spectral resolution, lighting scheme, scan rate, frame rate and exposure time are prerequisites for obtaining accurate results (Wu, Sun, 2013).

The next step is image preprocessing, which includes calibration and spectrum correction. The goals of the calibration process are to standardize the spectral and spatial axes of the hyperspectral image, evaluate accuracy and reproducibility of the acquired data under different operating conditions, eliminate curvature effect and instrumental errors (Rinnan et al., 2009; Vidal, Amigo, 2012).

The standard practice is reflection calibration, which uses two reference images, black and white. The black image is acquired when the camera lens is completely covered with its opaque cap. The white reference image is obtained using a white surface board (e. g. Teflon) with a reflectivity of about 99.9 % to obtain the highest possible intensity for each pixel at each wavelength. These two reference images are then used to correct the raw hyperspectral images by using the following equation:

$$R = \frac{I_S - I_D}{I_W - I_D},$$

where R is the corrected hyperspectral image, I_S is the raw hyperspectral image, I_D is the dark image, and I_W is the white reference image.

To eliminate the effect of surface curvature, spectral image normalization (Polder et al., 2004), adaptive spherical transform (Tao, Wen, 1999) or Lambert transform (Gomez-Sanchis et al., 2008) are used during calibration.

The goal of spectrum correction is to improve image quality (Savitzky, Golay, 1964; Barnes et al., 1989; Burger, 2006; Esquerre et al., 2012). For example, smoothing algorithms (moving average, Savitzky–Golay, median filter, and Gaussian filter), as well as Fourier and wavelet transforms, are used to reduce noise from the spectral data. The first and second derivatives are used to correct the shift of the spectrum baseline. Multiplicative scattering correction (MSC) and standard normal variate (SNV) are used to reduce the spectral variability due to scattering.

Data extraction and processing

At this step of hyperspectral image analysis process, image segmentation is performed and features are selected for further analysis.

Image segmentation is used as a pre-processing step and is typically performed before the formal spectral analysis in order to extract the target objects from the background or form a mask for the formation of the region of inte-

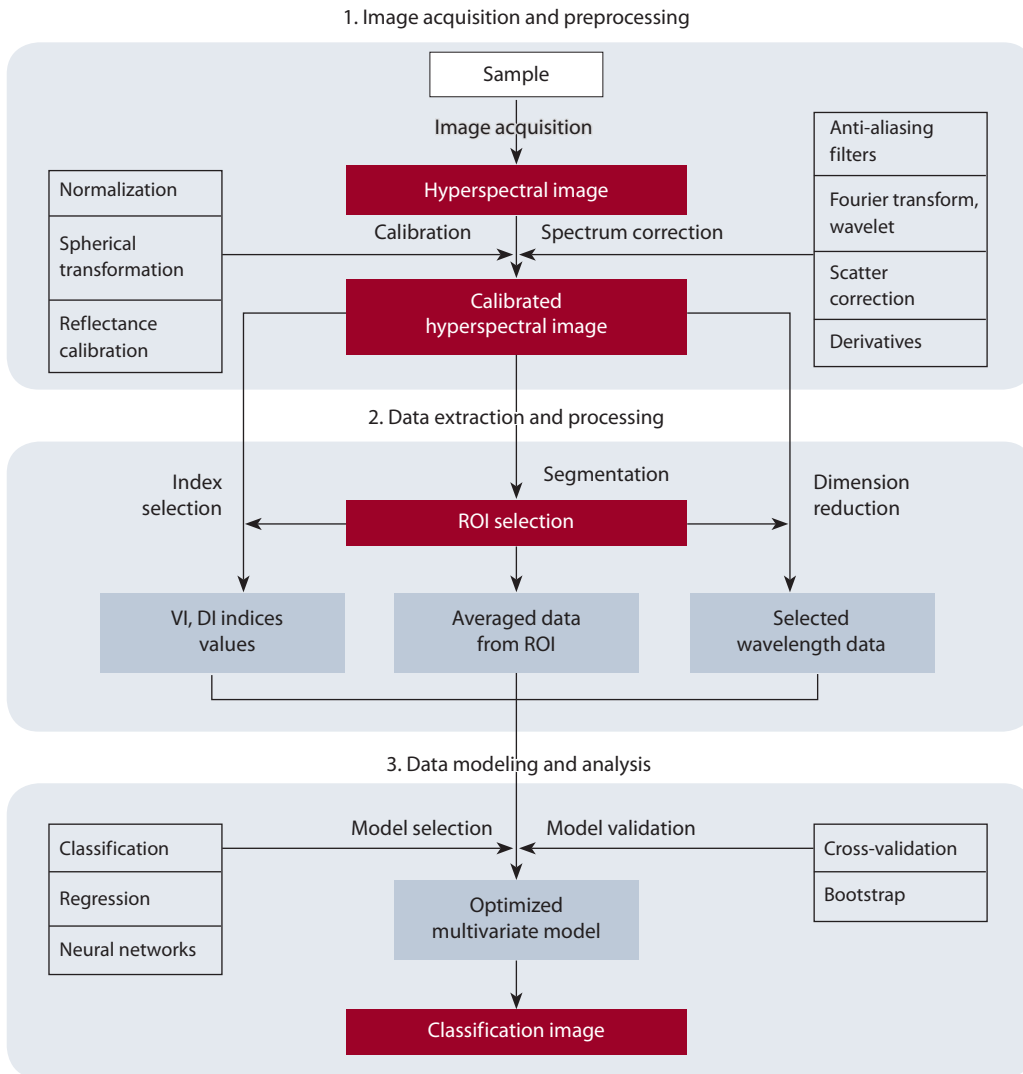


Fig. 3. Flowchart of a series of typical steps for analyzing hyperspectral image data.

rests (ROIs) for further information extraction. The following segmentation methods are used: threshold-based (Pandey et al., 2017); K-means (Behmann et al., 2014); watershed algorithm (Li J. et al., 2019); edge detection (Sun et al., 2017; Williams et al., 2017).

Feature extraction can be considered to be the most important step in hyperspectral-based classification. Its goal is to extract and form new feature vectors for plant disease detection by combining and optimizing the spectral, spatial and texture features, then feed them to a set of classifiers or machine learning algorithms.

Vegetation indices (VI) or disease indices (DI) can be used as features (Huete et al., 2002; Gitelson et al., 2006; Mahlein et al., 2013; Candiago et al., 2015). In this case, only a small number of wavelengths are required for analysis. When analyzing the entire spectrum, the following methods are used to reduce the dimension and eliminate autocorrelations: principal component analysis; minimum noise fraction algorithm;

linear discriminant analysis; stepwise discriminant analysis; partial least square discriminant analysis (Steddom et al., 2003; Delalieux et al., 2007; Naidu et al., 2009; Moshou et al., 2011; Yuan et al., 2014b; Zhou et al., 2019).

Data modeling and analysis

The last step in image analysis is to select a model and apply it to the data. Depending on the objectives of the study, these can be classification models (for diagnosing and differentiating diseases), or regression models (for predicting and assessing the relationship between the target variables and the spectral response).

The most commonly used models are:

- classification models of machine learning and neural networks: spectral angle mapper, support vector machine, k -nearest neighbor, maximum likelihood (Moshou et al., 2004; Liu et al., 2010; Rumpf et al., 2010; Yeh et al., 2013; Li Y. et al., 2017);

- regression models: multiple linear regression, binary logistic regression, partial least squares regression, Dirichlet aggregation regression (Huang W. et al., 2007; Singh D. et al., 2007; Yang et al., 2007; Huang J. et al., 2012).

Areas of application of hyperspectral technologies in diagnostics of plant diseases

The main tasks in the diagnosis of plant diseases are detection, differentiation, identification, assessment of the disease severity, assessment of the genotypes disease resistance. These tasks are solved at various levels of organization of living systems in the corresponding measurement scales.

Measurements at the cellular or tissue scales are carried out in laboratories using hyperspectral microscopes to observe fungal spores and detect metabolic changes in tissues caused by plant-pathogen interactions. Experiments at the cellular level are usually carried out in the context of fundamental research and to some extent for the identification of pathogens and the assessment of genotype resistance.

Measurements at the level of individual organs (leaf, ear, stem, root, fruit) and at the level of the whole plant are carried out in laboratory, greenhouse or field conditions with the aim of early detection and differentiation of the disease.

Canopy-level measurements are more often applied in plant disease mapping and severity assessment.

Below is a brief overview of scientific publications on hyperspectral technologies in plant diseases diagnostics in the context of different areas of application (see the Table).

Disease detection

The aim of disease detection is to differentiate healthy and infected plants. In this case, the subject of research is only one specific disease, its symptoms and dynamics.

A study of Mahlein et al., 2019a compares the feasibility of different sensors to characterize *Fusarium* head blight. Under controlled conditions, time-series measurements were performed with infrared thermography, chlorophyll fluorescence imaging, and hyperspectral imaging. Infrared thermography allowed the visualization of temperature differences within the infected spikelets beginning 5 days after inoculation. Also, on the 5th day, a disorder of the photosynthetic activity was confirmed by chlorophyll fluorescence imaging of spikelets. Pigment-specific simple ratio derived from hyperspectral imaging allowed discrimination between *Fusarium*-infected and non-inoculated spikelets on the 3rd day. Support vector machine method was used for classification. The classification accuracy was 78, 56 and 78 %, respectively.

A study of Abduridha et al., 2019 compares two methods for detecting citrus canker with hyperspectral imaging. In the laboratory, a hyperspectral (400–1000 nm) imaging system was utilized for the detection of citrus canker at several disease development stages (i. e., asymptomatic, early, and late symptoms) by using two classification methods: (i) radial basis function (RBF) and (ii) *k*-nearest neighbor (KNN). The same imaging system mounted on a UAV was used to

detect citrus canker on tree canopies in the orchard. The overall classification accuracy of the RBF was higher (94, 96, and 100 %) than the KNN method (94, 95, and 96 %) for detecting canker in leaves. Among the 31 studied vegetation indices, the water index (WI) and the Modified Chlorophyll Absorption in Reflectance Index (ARI and TCARI 1) more accurately detected canker in laboratory and in orchard conditions, respectively. The UAV-based technique achieved 100 % classification accuracy for identifying healthy and canker-infected trees.

Diseases identification and differentiation

In disease identification, the goal is to determine the type of pathogen affecting the plant. The subject of research is several types of diseases, their distinctive features.

Mahlein et al., 2013 developed specific spectral disease indices (SDIs) for the differentiation of diseases in crops. Sugar beet plants and three leaf diseases *Cercospora* leaf spot, sugar beet rust and powdery mildew were used as model system. Hyperspectral signatures of healthy and diseased sugar beet leaves were assessed with a non-imaging spectroradiometer at different development stages and disease severities of pathogens. Significant and most relevant wavelengths and two band normalized differences from 450 to 950 nm, describing the impact of a disease on sugar beet leaves, were extracted from the data-set using the RELIEF-F algorithm. To develop hyperspectral indices, the best weighted combination of a single wavelength and a normalized wavelength difference was searched. Healthy sugar beet leaves and leaves, infected with *Cercospora* leaf spot, sugar beet rust and powdery mildew were classified with a high accuracy and sensitivity (balanced classification accuracy: 89, 92, 87, and 85 %, respectively).

A study of Bohnenkamp et al., 2019 establishes a method for detecting and distinguishing between brown rust (*Puccinia triticina*) and yellow rust (*P. striiformis*) on wheat leaves based on hyperspectral imaging. The experiment was conducted at the leaf scale under controlled laboratory conditions. A reference spectrum from sporescale observations was used. Least-squares factorization was applied on hyperspectral images to unveil the presence of the spectral signal of rust spores in mixed spectra on wheat leaves. For the first time, this study shows an interpretable decomposition of the spectral reflectance mixture during pathogenesis.

Disease severity assessment

Quantitative diagnosis of plant disease severity is one of the main directions of hyperspectral disease analysis. The evaluation criteria for plant disease severity are often the disease index and incidence. In addition, according to the pathogens and symptoms they caused, the pigment content, water content, and even structural parameters are often regarded as indirect evaluation criteria.

Zhao Y.-R. et al., 2016 used hyperspectral imaging to determine the spatial distribution of chlorophyll and carotenoid

List of major contributions to different areas of application of hyperspectral images to plant diseases diagnostics

Target	Crop	Disease	Scale/sensor/platform	Methods and algorithms	Reference
Detection	Wheat	Fusarium Head Blight	Spikelet/ ImSpector V10E, N25E/ moving platform	Support vector machine (SVM)	Mahlein et al., 2019a
	Citrus	Citrus canker	Canopy/ Pika L/ UAV	Vegetation indices, <i>k</i> -nearest neighbor (KNN), radial basis function (RBF)	Abdulridha et al., 2019
	Onion	Sour skin (<i>Burkholderia cepacia</i>)	Onion/ SU320KTS-1.7RT SWIR camera, LCTF filter/ tripod	Principal component analysis (PCA), Fisher's discriminant analysis (FDA)	Wang et al., 2012
	Sugar beet	Root rot disease (<i>Rhizoctonia solani</i>)	Plant/ Specim IQ/ tripod	<i>k</i> -nearest neighbor (KNN), partial least squares (PLS), random forest (RF), support vector machine (SVM)	Barreto et al., 2020
Identification	Sugar beet	<i>Cercospora</i> leaf spot, sugar beet rust, powdery mildew	Leaf/ ASD FieldSpec Pro/ tripod	Disease indexes, algorithm RELIEF-F	Mahlein et al., 2013
Differentiation	Wheat	Brown and yellow rust (<i>Puccinia triticina</i> and <i>P. striiformis</i>)	Leaf/ ImSpector V10E/ moving platform	Least-squares factorization (LSF)	Bohnenkamp et al., 2019
		Yellow rust, powdery mildew, wheat aphid	Leaf/ ASD FieldSpec/ tripod	Partial least square regression (PLSR), Fisher's linear discriminant analysis (FLDA)	Yuan et al., 2014a
		Fusarium head blight (<i>F. graminearum</i> , <i>F. culmorum</i>)	Spike/ ImSpector V10E, ImSpector N25E/ moving platform	Vegetation indices, support vector machine (SVM)	Alisaac et al., 2018
Severity assessment	Barley	Powdery mildew	Canopy (plot)/ Specim V10E/ rail system	Support vector machine (SVM), Simplex Volume Maximization (SiVM)	Thomas et al., 2018a
	Potato	Late blight in potato	Canopy (plot)/ Rikola/ UAV	Simplex Volume Maximization (SiVM)	Franceschini et al., 2019
	Cucumber	Angular leaf spot	Leaf/ ImSpector V10/ moving platform	Partial least square regression (PLSR)	Zhao et al., 2016
	Wheat	Powdery mildew	Leaf/ ASD FieldSpec/ tripod	Partial least square regression (PLSR), multivariate linear regression (MLR)	Zhang J. et al., 2012
	Tomato	Bacteriosis (<i>Pseudomonas cichorii</i>)	Leaf/ Hyperspec Headwall/ moving platform	Principal component analysis (PCA)	Rajendran et al., 2016
Assessment of genotype resistance	Sugar beet	Leaf spot <i>Cercospora</i>	Leaf/ ImSpector V10E/ moving platform	Vegetation indices	Leucker et al., 2016
	Grape	Grape downy mildew (<i>Plasmopara viticola</i>)	Leaf/ ASD AgriSpec spectrometer, ImSpector V10E/ moving platform	Vegetation indices	Oerke et al., 2016
	Barley	Powdery mildew	Cell, tissue/ Specim V10E camera, Z6 APO microscope/ moving platform	Simplex Volume Maximization (SiVM)	Kuska et al., 2015

contents in cucumber leaves infected with angular spot. The pigment content was measured by biochemical analyzes. Partial least square regression (PLSR) models were used to develop quantitative analysis of the relationship between the disease severity, the spectra and the pigment contents. In addition, regression coefficients in PLSR models were employed to select important wavelengths for modeling. Finally, chlorophyll and carotenoid distributions in cucumber leaves with the angular spot infection were mapped by applying the optimal models pixel-wise to the hyperspectral images.

Zhang J. et al., 2012 detected wheat powdery mildew disease severity via spectral measurement and analysis. In this study, hyperspectral reflectances of normal and powdery mildew infected leaves were measured with a spectroradiometer in a laboratory. The severity of the disease was determined on a nine-point scale of the disease index. A total of 32 spectral features were extracted from the lab spectra and examined through a correlation analysis and an independent t-test associated with the disease severity. Two regression models: multivariate linear regression (MLR) and partial least square regression (PLSR) were developed for estimating the disease severity of powdery mildew. Based on the cross-validation result, seven spectral indices minimizing the relative root mean square error were selected. The PLSR model outperformed the MLR model, with a relative root mean square error of 0.23 and a coefficient of determination of 0.80 when using seven indices.

Assessment of genotypes resistance

Analysis of the pathogen-host interaction makes it possible to determine the resistance of genotypes to a specific disease and is an important part of breeding. In breeding practice, phenotyping of plant genotypes is carried out by means of labor-intensive and expensive visual assessment. In this context, hyperspectral analysis is a promising non-invasive method for speeding up and automating traditional phenotyping methods.

Leucker et al., 2016 evaluated the resistance of 5 different sugar beet genotypes to *Cercospora* leaf spot in their study. The experiment was carried out under controlled laboratory conditions. Lesions of *Cercospora* leaf spot were rated by classical quantitative and qualitative methods in combination with non-invasive hyperspectral imaging. It was found that the spectral characteristics of the affected leaf areas depend on the density of pathogen spores on the surface and on their spatial distribution. Accordingly, the number of conidia per diseased leaf area on resistant plant was lower. The assessment of lesion phenotypes by hyperspectral imaging with regard to sporulation may be an appropriate method for identifying subtle differences of genotypes in disease resistance.

Kuska et al., 2015 used a hyperspectral microscope to determine the resistance of barley cultivars to powdery mildew (*Blumeria graminis*). The reflection of inoculated and non-inoculated leaves was recorded daily with a hyper-

spectral linescanner in the visual (400–700 nm) and near infrared (700–1000 nm) range 3 to 14 days after inoculation. The susceptible genotypes showed an increase in reflectance in the visible range according to symptom development. However, the spectral signature of the resistant genotype did not show significant changes over the experimental period.

Problems and prospects of using hyperspectral technologies for the diagnosis of plant diseases

Despite the encouraging progress in monitoring plant diseases based on hyperspectral technologies made over the past few decades, some technical problems remain unresolved that make these methods difficult to apply in practice. Studies seeking solutions to these challenges will shape future trends.

Currently, low-altitude, airborne and satellite multispectral systems are widely used in agricultural production to monitor the canopy based on vegetation indices (Hatfield, Pinter, 1993; Huang Y.B. et al., 2013). But reliable remote sensing monitoring of plant diseases and pests is usually achieved when symptoms are fully exhibited, which may be too late for guiding the prevention. Despite significant results in scientific research on the use of hyperspectral sensors for early detection of plant diseases, their practical application in field and greenhouse conditions in precision farming systems is still an unresolved problem.

Most of these studies have been conducted in controlled conditions, often utilizing artificial illumination and precisely regulating the directions of incoming light and reflected light being registered by positioning the camera or sensor at a defined angle toward the leaf tissue. The illumination conditions in the field are very different from laboratory ones, which creates enormous difficulties for reliably quantifying diseases in a natural canopy. Canopy regions located in sunlight appear much brighter than canopy layers situated in the shade. Tissue color depends on the angle of the tissue toward both the incoming sunlight and the reflected outgoing light. Heterogeneities in image brightness change from minute to minute. Therefore, setting a threshold for distinguishing between healthy and diseased tissue would mean taking the overall brightness of the specific image within the location into account, as well as the angle of incidence of light, which is currently a matter of intense research (Guo et al., 2013; Yu et al., 2017).

Another unsolved problem is to accurately detect a specific disease under realistic field conditions where several crop stressors may occur simultaneously. Currently, most monitoring studies or applications are conducted in experimental fields or areas with prior information about the type of pathogen. For an area that lacks corresponding information, it is challenging to achieve a reliable and accurate monitoring result. Many pathogens, as well as abiotic stressors, have similar symptoms and, therefore, a similar spectral signature. Some state-of-the-art algorithms, such as deep learning algorithms, may play an important role in differentiating biotic

and abiotic stressors in field and greenhouse conditions (Liu et al., 2010; Mahlein et al., 2019b). Besides, it is necessary to promote the establishment of a knowledge base with the background information about diseases (i. e., geographical distribution, favorable habitats, soil types, climate conditions). The prior information may lower uncertainty in the monitoring of plant diseases.

Conclusion

Plant diseases are causing significant economic losses in the agricultural production around the world, especially given the climate change that has taken place in recent years. A promising technology for a non-invasive, fast, efficient and reliable way to detect and identify plant diseases is the use of hyperspectral sensors and platforms.

New technologies are expanding human perception by providing information beyond the visible spectrum. The analysis of the reflection spectrum of plant tissue makes it possible to classify healthy and diseased plants, assess the severity of the disease, differentiate the types of pathogens, and identify the symptoms of biotic stresses at early stages, including during the incubation period, when the symptoms are not visible to the human eye.

Due to the huge amount of information, the most promising methods for processing hyperspectral data are machine learning and neural networks. Currently, hyperspectral methods for diagnosing plant diseases are still at an early stage of development. In addition to its being an expensive technology, many technical difficulties limit its application in production. However, with advances in sensor technology and data analysis techniques, hyperspectral imaging can be expected to become one of the important tools for studying plant diseases.

References

- Aasen H., Burkhart A., Bolten A., Bareth G. Generating 3D hyperspectral information with lightweight UAV snapshot cameras for vegetation monitoring: from camera calibration to quality assurance. *ISPRS J. Photogramm. Remote Sens.* 2015;108:245-259. DOI 10.1016/j.isprsjprs.2015.08.002.
- Abdulridha J., Batuman O., Ampatzidis Y. UAV-based remote sensing technique to detect citrus canker disease utilizing hyperspectral imaging and machine learning. *Remote Sens.* 2019;11:1373. DOI 10.3390/rs11111373.
- Afonnikov D.A., Genaev M.A., Doroshkov A.V., Komyshev E.G., Pshenichnikova T.A. Methods of high-throughput plant phenotyping for large-scale breeding and genetic experiments. *Russ. J. Genet.* 2016;52(7):688-701. DOI 10.1134/S1022795416070024.
- Alisaac E., Behmann J., Kuska M.T., Dehne H.-W., Mahlein A.-K. Hyperspectral quantification of wheat resistance to *Fusarium* head blight: comparison of two *Fusarium* species. *Eur. J. Plant Pathol.* 2018;152:869-884. DOI 10.1007/s10658-018-1505-9.
- Alt V.V., Gurova T.A., Elkin O.V., Klimenko D.N., Maximov L.V., Pestunov I.A., Dubrovskaya O.A., Genaev M.A., Erst T.V., Genaev K.A., Komyshev E.G., Khlestkin V.K., Afonnikov D.A. The use of Specim IQ, a hyperspectral camera, for plant analysis. *Vavilovskii Zhurnal Genetiki i Selekcii = Vavilov Journal of Genetics and Breeding.* 2020;24(3):259-266. DOI 10.18699/VJ19.587. (in Russian)
- Barnes R., Dhanoa M., Lister S.J. Standard normal variate transformation and de-trending of near-infrared diffuse reflectance spectra. *Appl. Spectrosc.* 1989;43:772-777. DOI 10.1366/0003702894202201.
- Barreto A., Paulus S., Varrelmann M., Mahlein A.-K. Hyperspectral imaging of symptoms induced by *Rhizoctonia solani* in sugar beet: comparison of input data and different machine learning algorithms. *J. Plant Dis. Prot.* 2020;127:441-451. DOI 10.1007/s41348-020-00344-8.
- Behmann J., Acebron K., Emin D., Bennertz S., Matsubara S., Thomas S., Bohnenkamp D., Kuska M.T., Jussila J., Salo H., Mahlein A.-K., Rascher U. Specim IQ: evaluation of a new, miniaturized handheld hyperspectral camera and its application for plant phenotyping and disease detection. *Sensors.* 2018;18:441. DOI 10.3390/s18020441.
- Behmann J., Steinucken J., Plumer L. Detection of early plant stress responses in hyperspectral images. *ISPRS J. Photogramm. Remote Sens.* 2014;93:98-111. DOI 10.1016/j.isprsjprs.2014.03.016.
- Bock C.H., Poole G.H., Parker P.E., Gottwald T.R. Plant disease severity estimated visually, by digital photography and image analysis, and by hyperspectral imaging. *Crit. Rev. Plant Sci.* 2010;29:59-107. DOI 10.1080/07352681003617285.
- Bohnenkamp D., Kuska M.T., Mahlein A.-K., Behmann J. Hyperspectral signal decomposition and symptom detection of wheat rust disease at the leaf scale using pure fungal spore spectra as reference. *Plant Pathol.* 2019;68:1188-1195. DOI 10.1111/ppa.13020.
- Burger J. Hyperspectral NIR image analysis. Data Exploration, Correction, and Regression. Doctoral Dissertation. Arkitektkopia, Umea, Sweden, 2006.
- Burkart A., Aasen H., Alonso L., Menz G., Bareth G., Rascher U. Angular dependency of hyperspectral measurements over wheat characterized by a novel UAV based goniometer. *Remote Sens.* 2015;7(1):725-746. DOI 10.3390/rs70100725.
- Candiago S., Remondino F., De Giglio M., Dubbini M., Gattelli M. Evaluating multispectral images and vegetation indices for precision farming applications from UAV images. *Remote Sens.* 2015;7(4):4026-4047. DOI 10.3390/rs70404026.
- Choudhary R., Mahesh S., Paliwal J., Jayas D.S. Identification of wheat classes using wavelet features from near infrared hyperspectral images of bulk samples. *Biosyst. Eng.* 2009;102(2):115-127. DOI 10.1016/j.biosystemseng.2008.09.028.
- Couture J.J., Singh A., Charkowski A.O., Groves R.L., Gray S.M., Bethke P.C., Townsend P.A. Integrating spectroscopy with potato disease management. *Plant Dis.* 2018;102:2233-2240. DOI 10.1094/PDIS-01-18-0054-RE.
- Delalieux S., van Aardt J., Keulemans W., Schrevens E., Coppin P. Detection of biotic stress (*Venturia inaequalis*) in apple trees using hyperspectral data: non-parametric statistical approaches and physiological implications. *Eur. J. Agron.* 2007;27:130-143. DOI 10.1016/j.eja.2007.02.005.
- Demidchik V.V., Shashko A.Yu., Bondarenko V.Yu., Smolikova G.N., Przhevalskaya D.A., Chernysh M.A., Pozhvanov G.A., Barkovskij A.V., Smolich I.I., Sokolik A.I., Medvedev S.S. Plant phenomics: fundamental bases, software and hardware platforms, and machine learning. *Russ. J. Plant Physiol.* 2020;67(3):397-412. DOI 10.1134/S1021443720030061.

- Dubrovskaya O.A., Gurova T.A., Pestunov I.A., Kotov K.Yu. Methods of detection of diseases on wheat crops according to remote sensing (overview). *Sibirskii Vestnik Sel'skokhozyaistvennoi Nauki = Siberian Herald of Agricultural Science*. 2018;48(6): 76-89. DOI 10.26898/0370-8799-2018-6-11. (in Russian)
- ElMasry G.M., Nakauchi S. Image analysis operations applied to hyperspectral images for non-invasive sensing of food quality – a comprehensive review. *Biosyst. Eng.* 2016;142:53-82. DOI 10.1016/j.biosystemseng.2015.11.009.
- Esquerre C., Gowen A.A., Burger J., Downey G., O'Donnell C.P. Suppressing sample morphology effects in near infrared spectral imaging using chemometric data pre-treatments. *Chemom. Intell. Lab. Syst.* 2012;117:129-137. DOI 10.1016/j.chemolab.2012.02.006.
- Fahlgren N., Gehan M.A., Baxte I. Lights, camera, action: high-throughput plant phenotyping is ready for a close-up. *Curr. Opin. Plant Biol.* 2015;24:93-99. DOI 10.1016/j.pbi.2015.02.006.
- Franceschini M.H.D., Bartholomeus H., van Apeldoorn D.F., Suomalainen J., Kooistra L. Feasibility of unmanned aerial vehicle optical imagery for early detection and severity assessment of late blight in potato. *Remote Sens.* 2019;11:224. DOI 10.3390/rs11030224.
- Gitelson A.A., Keydan G.P., Merzlyak M.N. Three-band model for noninvasive estimation of chlorophyll, carotenoids, and anthocyanin contents in higher plant leaves. *Geophys. Res. Lett.* 2006; 33(11):L11402. DOI 10.1029/2006GL026457.
- Gomez-Sanchis J., Molto E., Camps-Valls G., Gomez-Chova L., Aleixos N., Blasco J. Automatic correction of the effects of the light source on spherical objects. An application to the analysis of hyperspectral images of citrus fruits. *J. Food Eng.* 2008;85(2): 191-200. DOI 10.1016/j.jfoodeng.2007.06.036.
- Guo W., Rage U.K., Ninomiya S. Illumination invariant segmentation of vegetation for time series wheat images based on decision tree model. *Comput. Electron. Agric.* 2013;96:58-66. DOI 10.1016/j.compag.2013.04.010.
- Hatfield J.L., Pinter P.J. Remote-sensing for crop protection. *Crop. Prot.* 1993;12:403-413. DOI 10.1016/0261-2194(93)90001-Y.
- Huang J., Liao H., Zhu Y., Sun J., Sun Q., Liu X. Hyperspectral detection of rice damaged by rice leaf folder (*Cnaphalocrocis medinalis*). *Comput. Electron. Agric.* 2012;82:100-107. DOI 10.1016/j.compag.2012.01.002.
- Huang W., Lamb D.W., Niu Z., Zhang Y., Liu L., Wang J. Identification of yellow rust in wheat using in-situ spectral reflectance measurements and airborne hyperspectral imaging. *Precis. Agric.* 2007;8:187-197. DOI 10.1007/s11119-007-9038-9.
- Huang Y.B., Thomson S.J., Hoffmann W.C., Lan Y.B., Fritz B.K. Development and prospect of unmanned aerial vehicle technologies for agricultural production management. *Int. J. Agric. Biol. Eng.* 2013;6(3):1-10. DOI 10.3965/j.ijabe.20130603.001.
- Huete A., Didan K., Miura T., Rodriguez E.P., Gao X., Ferreira L.G. Overview of the radiometric and biophysical performance of the MODIS vegetation indices. *Remote Sens. Environ.* 2002;83(1):195-213. DOI 10.1016/S0034-4257(02)00096-2.
- Kuska M.T., Wahabzada M., Leucker M., Dehne H.-W., Kersting K., Oerke E.-C., Steiner U., Mahlein A.-K. Hyperspectral phenotyping on the microscopic scale: towards automated characterization of plant-pathogen interactions. *Plant Methods.* 2015;11:28-41. DOI 10.1186/s13007-015-0073-7.
- Leucker M., Mahlein A.-K., Steiner U., Oerke E.-C. Improvement of lesion phenotyping in *Cercospora beticola* – sugar beet interaction by hyperspectral imaging. *Phytopathology.* 2016;106:177-184. DOI 10.1094/PHYTO-04-15-0100-R.
- Li J., Zhang R., Li J., Wang Z., Zhang H., Zhan B., Jiang Y. Detection of early decayed oranges based on multispectral principal component image combining both bi-dimensional empirical mode decomposition and watershed segmentation method. *Post-harvest Biol. Technol.* 2019;158:110986-110996. DOI 10.1016/j.postharvbio.2019.110986.
- Li L., Zhang Q., Huang D. A review of imaging techniques for plant phenotyping. *Sensors.* 2014;14:20078-20111. DOI 10.3390/s14120078.
- Li Y., Zhang H., Shen Q. Spectral-spatial classification of hyperspectral imagery with 3D convolutional neural network. *Remote Sens.* 2017;9:67. DOI 10.3390/rs9010067.
- Liu Z.-Y., Wu H.-F., Huang J.-F. Application of neural networks to discriminate fungal infection levels in rice panicles using hyperspectral reflectance and principal components analysis. *Comput. Electron. Agric.* 2010;72:99-106. DOI 10.1016/j.compag.2010.03.003.
- Lobos G.A., Camargo A.V., del Pozo A., Araus J.L., Ortiz R., Doonan J.H. Editorial: plant phenotyping and phenomics for plant breeding. *Front. Plant Sci.* 2017;8:2181. DOI 10.3389/fpls.2017.02181.
- Lowe A., Harrison N., French A.P. Hyperspectral image analysis techniques for the detection and classification of the early onset of plant disease and stress. *Plant Methods.* 2017;13:80-91. DOI 10.1186/s13007-017-0233-z.
- Mahlein A.-K. Plant disease detection by imaging sensors-parallels and specific demands for precision agriculture and plant phenotyping. *Plant Dis.* 2016;100:241-251. DOI 10.1094/PDIS-03-15-0340-FE.
- Mahlein A.-K., Alisaac E., Masri A.A., Behmann J., Dehne H.-W., Oerke E.-C. Comparison and combination of thermal, fluorescence, and hyperspectral imaging for monitoring *Fusarium* head blight of wheat on spikelet scale. *Sensors.* 2019a;19:2281. DOI 10.3390/s19102281.
- Mahlein A.-K., Kuska M.T., Thomas S., Wahabzada M., Behmann J., Rascher U., Kersting K. Quantitative and qualitative phenotyping of disease resistance of crops by hyperspectral sensors: seamless interlocking of phytopathology, sensors, and machine learning is needed! *Curr. Opin. Plant Biol.* 2019b;50:156-162. DOI 10.1016/j.pbi.2019.06.007.
- Mahlein A.-K., Kuska M.T., Behmann J., Polder G., Walter A. Hyperspectral sensors and imaging technologies in phytopathology: state of the art. *Annu. Rev. Phytopathol.* 2018;56:535-558. DOI 10.1146/annurev-phyto-080417-050100.
- Mahlein A.-K., Rumpf T., Welke P., Dehne H.-W., Plümer L., Steiner U., Oerke E.-C. Development of spectral indices for detecting and identifying plant diseases. *Remote Sens. Environ.* 2013;128: 21-30. DOI 10.1016/j.rse.2012.09.019.
- Mahlein A.-K., Steiner U., Hillnhütter C., Dehne H.-W., Oerke E.-C. Hyperspectral imaging for small-scale analysis of symptoms caused by different sugar beet diseases. *Plant Methods.* 2012;8:3. DOI 10.1186/1746-4811-8-3.
- Mishra P., Asaari M., Herrero-Langreo A., Lohumi S., Diezma B., Scheunders P. Close range hyperspectral imaging of plants: a review. *Biosyst. Eng.* 2017;164:49-67. DOI 10.1016/j.biosystemseng.2017.09.009.
- Moshou D., Bravo C., Oberti R., West J.S., Ramon H., Vougioukas S., Bochtis D. Intelligent multi-sensor system for the detec-

- tion and treatment of fungal diseases in arable crops. *Biosyst. Eng.* 2011;108:311-321. DOI 10.1016/j.biosystemseng.2011.01.003.
- Moshou D., Bravo C., West J., Wahlen S., McCartney A., Ramon H. Automatic detection of 'yellow rust' in wheat using reflectance measurements and neural networks. *Comput. Electron. Agric.* 2004;44:173-188. DOI 10.1016/j.compag.2004.04.003.
- Naidu R.A., Perry E.M., Pierce F.J., Mekuria T. The potential of spectral reflectance technique for the detection of *Grapevine leaf-roll-associated virus-3* in two red-berried wine grape cultivars. *Comput. Electron. Agr.* 2009;66:38-45. DOI 10.1016/j.compag.2008.11.007.
- Oerke E.-C., Herzog K., Toepfer R. Hyperspectral phenotyping of the reaction of grapevine genotypes to *Plasmopara viticola*. *J. Exp. Bot.* 2016;67(18):5529-5543. DOI 10.1093/jxb/erw318.
- Pandey P., Ge Y., Stoerger V., Schnable J.C. High throughput *in vivo* analysis of plant leaf chemical properties using hyperspectral imaging. *Front. Plant Sci.* 2017;8:1348-1359. DOI 10.3389/fpls.2017.01348.
- Polder G., van der Heijden G.W.A.M., van der Voet H., Young I.T. Measuring surface distribution of carotenes and chlorophyll in ripening tomatoes using imaging spectrometry. *Postharvest Biol. Technol.* 2004;34(2):117-129.
- Rajendran D.K., Park E., Nagendran R., Hung N.B., Cho B.-K., Kim K.-H. Visual analysis for detection and quantification of *Pseudomonas cichorii* disease severity in tomato plants. *Plant Pathol. J.* 2016;32:300-310. DOI 10.5423/PPJ.OA.01.2016.0032.
- Rinnan A., Berg F., Engelsen S. Review of the most common pre-processing techniques for near-infrared spectra. *Trends Anal. Chem.* 2009;28(10):1201-1222. DOI 10.1016/j.trac.2009.07.007.
- Rumpf T., Mahlein A.-K., Steiner U., Oerke E.-C., Dehne H.-W., Plumer L. Early detection and classification of plant diseases with Support Vector Machines based on hyperspectral reflectance. *Comput. Electron. Agric.* 2010;74:91-99. DOI 10.1016/j.compag.2010.06.009.
- Sankaran S., Khot L.R., Espinoza C.Z., Jarolmasjed S., Sathuvali V.R., Vandemark G.J., Miklas P.N., Carter A.H., Pumphrey M.O., Knowles N.R., Pavak K.J. Low-altitude, high-resolution aerial imaging systems for row and field crop phenotyping: a review. *Eur. J. Agron.* 2015;70:112-123. DOI 10.1016/j.eja.2015.07.004.
- Savitzky A., Golay M.J. Smoothing and differentiation of data by simplified least squares procedures. *Anal. Chem.* 1964;36:1627-1639. DOI 10.1021/ac60214a047.
- Singh A., Ganapathysubramanian B., Singh A.K., Sarkar S. Machine learning for high-throughput stress phenotyping in plants. *Trends Plant Sci.* 2016;21(2):110-124. DOI 10.1016/j.tplants.2015.10.015.
- Singh D., Sao R., Singh K.P. A remote sensing assessment of pest infestation on sorghum. *Adv. Space Res.* 2007;39:155-163. DOI 10.1016/j.asr.2006.02.025.
- Steddom K., Heidel G., Jones D., Rush C.M. Remote detection of rhizomania in sugar beets. *Phytopathology.* 2003;93:720-726. DOI 10.1094/PHYTO.2003.93.6.720.
- Sun G., Zhang A., Ren J., Ma J., Wang P., Zhang Y., Jia X. Gravitation-based edge detection in hyperspectral images. *Remote Sens.* 2017;9:592. DOI 10.3390/rs9060592.
- Tao Y., Wen Z. An adaptive spherical image transform for high-speed fruit defect detection. *Trans. ASABE.* 1999;42(1):241-246.
- Tardieu F., Cabrera-Bosquet L., Pridmore T., Bennett M. Plant phenomics, from sensors to knowledge. *Curr. Biol.* 2017;27:R770-R783. DOI 10.1016/j.cub.2017.05.055.
- Thomas S., Behmann J., Steier A., Kraska T., Muller O., Rascher U., Mahlein A.-K. Quantitative assessment of disease severity and rating of barley cultivars based on hyperspectral imaging in a non-invasive, automated phenotyping platform. *Plant Methods.* 2018a;14:45. DOI 10.1186/s13007-018-0313-8.
- Thomas S., Kuska M.T., Bohnenkamp D. Benefits of hyperspectral imaging for plant disease detection and plant protection: a technical perspective. *J. Plant Dis. Prot.* 2018b;125:5-20. DOI 10.1007/s41348-017-0124-6.
- Vidal M., Amigo J.M. Pre-processing of hyperspectral images. Essential steps before image analysis. *Chemom. Intell. Lab.* 2012;117:138-148. DOI 10.1016/j.chemolab.2012.05.009.
- Vigneau N., Ecartot M., Rabatel G., Roumet P. Potential of field hyperspectral imaging as a non destructive method to assess leaf nitrogen content in wheat. *Field Crops Res.* 2011;122:25-31. DOI 10.1016/j.fcr.2011.02.003.
- Walter A., Liebisch F., Hund A. Plant phenotyping: from bean weighing to image analysis (review). *Plant Methods.* 2015;11:14. DOI 10.1186/s13007-015-0056-8.
- Wang W., Li C., Tollner E.W., Gitaitis R.D., Rains G.C. Shortwave infrared hyperspectral imaging for detecting sour skin (*Burkholderia cepacia*)-infected onions. *J. Food Eng.* 2012;109(1):38-48. DOI 10.1016/j.jfoodeng.2011.10.001.
- Williams D., Britten A., McCallum S., Jones H., Aitkenhead M., Karley A., Loades K., Prashar A., Graham J. A method for automatic segmentation and splitting of hyperspectral images of raspberry plants collected in field conditions. *Plant Methods.* 2017;13:74-85. DOI 10.1186/s13007-017-0226-y.
- Wu D., Sun D.-W. Advanced applications of hyperspectral imaging technology for food quality and safety analysis and assessment: A review – Part I: Fundamentals. *Innov. Food Sci. Emerg. Technol.* 2013;19:1-14. DOI 10.1016/j.ifset.2013.04.014.
- Yang C., Cheng C., Chen R. Changes in spectral characteristics of rice canopy infested with brown planthopper and leafhopper. *Crop Sci.* 2007;47:329-335. DOI 10.2135/cropsci2006.05.0335.
- Yeh Y.F., Chung W., Liao J., Chung C., Kuo Y., Lin T. A comparison of machine learning methods on hyperspectral plant disease assessments. *IFAC Proc.* 2013;46:361-365. DOI 10.3182/20130327-3-JP-3017.00081.
- Yeh Y., Chung W., Liao J., Chung C., Kuo Y., Lin T. Strawberry foliar anthracnose assessment by hyperspectral imaging. *Comput. Electron. Agric.* 2016;122:1-9. DOI 10.1016/j.compag.2016.01.012.
- Yu K., Kirchgessner N., Grieder C., Walter A., Hund A. An image analysis pipeline for automated classification of imaging light conditions and for quantification of wheat canopy cover time series in field phenotyping. *Plant Methods.* 2017;13:15. DOI 10.1186/s13007-017-0168-4.
- Yuan L., Huang Y., Loraamm R.W., Nie C., Wang J., Zhang J. Spectral analysis of winter wheat leaves for detection and differentiation of diseases and insects. *Field Crops Res.* 2014a;156:199-207. DOI 10.1016/j.fcr.2013.11.012.
- Yuan L., Zhang J., Shi Y., Nie C., Wei L., Wang J. Damage mapping of powdery mildew in winter wheat with high-resolution satellite image. *Remote Sens.* 2014b;6:3611-3623. DOI 10.3390/rs6053611.
- Zhang J., Huang Y., Pu R., Gonzalez-Moreno P., Yuan L., Wu K., Huang W. Monitoring plant diseases and pests through remote sensing technology: a review. *Comput. Electron. Agric.* 2019;165:104943-104956. DOI 10.1016/j.compag.2019.104943.

- Zhang J., Pu R., Wang J., Huang W., Yuan L., Luo J. Detecting powdery mildew of winter wheat using leaf level hyperspectral measurements. *Comput. Electron. Agric.* 2012;85:13-23. DOI 10.1016/j.compag.2012.03.006.
- Zhang J., Wang N., Yuan L., Chen F., Wu K. Discrimination of winter wheat disease and insect stresses using continuous wavelet features extracted from foliar spectral measurements. *Biosyst. Eng.* 2017;162:20-29. DOI 10.1016/j.biosystemseng.2017.07.003.
- Zhang N., Yang G., Pan Y., Yang X., Chen L., Zhao C. A review of advanced technologies and development for hyperspectral-based plant disease detection in the past three decades. *Remote Sens.* 2020;12:3188. DOI 10.3390/rs12193188.
- Zhao Y.-R., Li X., Yu K.-Q., Cheng F., He Y. Hyperspectral imaging for determining pigment contents in cucumber leaves in response to angular leaf spot disease. *Sci. Rep.* 2016;6:27790. DOI 10.1038/srep27790.
- Zheng C., Abd-Elrahman A., Whitaker V. Remote sensing and machine learning in crop phenotyping and management, with an emphasis on applications in strawberry farming. *Remote Sens.* 2021; 13:531. DOI 10.3390/rs13030531.
- Zhou R.-Q., Jin J.-J., Li Q.-M., Su Z.-Z., Yu X.-J., Tang Y., Luo S.-M., He Y., Li X.-L. Early detection of *Magnaporthe oryzae*-infected barley leaves and lesion visualization based on hyperspectral imaging. *Front. Plant Sci.* 2019;9:1962. DOI 10.3389/fpls.2018.01962.

ORCID ID

A.F. Cheshkova orcid.org/0000-0003-2265-7129

Acknowledgements. This work was supported by the Russian Science Foundation, project No. 0533-2021-0007.**Conflict of interest.** The author declares no conflict of interest.

Received September 30, 2021. Revised December 24, 2021. Accepted December 27, 2021.

Original Russian text www.bionet.nsc.ru/vogis/

Model systems of human immunodeficiency virus (HIV-1) for *in vitro* efficacy assessment of candidate vaccines and drugs against HIV-1

N.B. Rudometova , D.N. Shcherbakov, A.P. Rudometov, A.A. Ilyichev, L.I. Karpenko

State Research Center of Virology and Biotechnology "Vector", Koltsovo, Novosibirsk Region, Russia
 nadenkaand100@mail.ru

Abstract. HIV infection still remains a major challenge for healthcare systems of the world. There are several aspects on counteracting the HIV/AIDS epidemic. The first aspect covers preventive measures including educational campaigns on HIV/AIDS and promotion of a healthy lifestyle, protected sex, and pre-exposure prophylaxis of vulnerable groups. The second aspect is timely HIV testing and the use of antiretroviral therapy when test results come back positive. The third aspect is the scientific research associated with discovering new pharmaceutical agents and developing HIV-1 vaccines. Selecting an adequate tool for quick and accurate *in vitro* efficacy assessment is the key aspect for efficacy assessment of vaccines and chemotherapy drugs. The classical method of virology, which makes it possible to evaluate the neutralizing activity of the sera of animals immunized with experimental vaccines and the efficacy of chemotherapy agents is the method of neutralization using viral isolates and infectious molecular clones, i. e. infectious viral particles obtained via cell transfection with a plasmid vector including the full-length HIV-1 genome coding structural, regulatory, and accessory proteins of the virus required for the cultivation of replication-competent viral particles in cell culture. However, neutralization assessment using viral isolates and infectious molecular clones is demanding in terms of time, effort, and biosafety measures. An alternative eliminating these disadvantages and allowing for rapid screening is the use of pseudoviruses, which are recombinant viral particles, for the analysis of neutralizing activity. Pseudotyped viruses have defective genomes restricting their replication to a single cycle, which renders them harmless compared to infectious viruses. The present review focuses on describing viral model systems for *in vitro* efficacy assessment of vaccines and drugs against HIV-1, which include primary HIV-1 isolates, laboratory-adapted strains, infectious molecular clones, and *env*-pseudoviruses. A brief comparison of the listed models is presented. The HIV-1 *env*-pseudoviruses approach is described in more detail.

Key words: HIV-1; primary isolates; infectious molecular clones; *env*-pseudoviruses; virus neutralization assay.

For citation: Rudometova N.B., Shcherbakov D.N., Rudometov A.P., Ilyichev A.A., Karpenko L.I. Model systems of human immunodeficiency virus (HIV-1) for *in vitro* efficacy assessment of candidate vaccines and drugs against HIV-1. *Vavilovskii Zhurnal Genetiki i Selekcii* = *Vavilov Journal of Genetics and Breeding*. 2022;26(2):214-221. DOI 10.18699/VJGB-22-26

Модельные системы вируса иммунодефицита человека (ВИЧ-1), используемые для оценки эффективности кандидатных вакцин и лекарственных препаратов против ВИЧ-1 *in vitro*

Н.Б. Рудометова , Д.Н. Щербаков, А.П. Рудометов, А.А. Ильичев, Л.И. Карпенко

Государственный научный центр вирусологии и биотехнологии «Вектор» Роспотребнадзора, р.п. Кольцово, Новосибирская область, Россия
 nadenkaand100@mail.ru

Аннотация. ВИЧ-инфекция по-прежнему остается одной из глобальных проблем здравоохранения во всем мире. Борьба с инфекцией ведется по нескольким направлениям. Во-первых, это профилактические мероприятия, которые включают просвещение населения по проблеме ВИЧ/СПИДа, пропаганду здорового образа жизни, защищенные половые контакты, доконтактную профилактику уязвимых групп населения. Во-вторых, прохождение своевременного тестирования на ВИЧ и применение антиретровирусной терапии в случае его обнаружения. В-третьих, это научные исследования, связанные как с поиском новых лекарственных агентов, так и с разработкой вакцины против ВИЧ-1. Ключевой момент при определении эффективности вакцин и химиотерапевтических препаратов – выбор инструмента, позволяющего быстро и точно оценить их эффективность *in vitro*. Классическим методом вирусологии, позволяющим оценить нейтрализующую активность сывороток животных, иммунизированных экспериментальными вакцинами, и эффективность химиотерапевтических агентов, является метод нейтрализации с использованием вирусных изолятов, а также инфекционных молекулярных клонов, которые представляют собой инфекционные вирусные частицы, полученные путем

трансфекции клеток плазмидным вектором, содержащим полноразмерный геном ВИЧ-1, кодирующий структурные, регуляторные и вспомогательные белки вируса, необходимые для образования репликационно-компетентных вирусных частиц в культуре клеток. При этом метод нейтрализации с использованием вирусных изолятов и инфекционных молекулярных клонов отличается трудоемкостью, продолжительностью и требует повышенных мер биобезопасности. Альтернативным решением, устраняющим указанные недостатки и позволяющим проводить быстрый скрининг, является использование для анализа нейтрализующей активности псевдовирuсов, которые представляют собой рекомбинантные вирусные частицы. В отличие от инфекционных вирусuсов, работа с псевдовирuсами безопасна, поскольку геном псевдовирuсов нарушен для того, чтобы их инфекция ограничивалась лишь одним циклом. Данный обзор посвящен описанию модельных вирусных систем, используемых для оценки эффективности вакцин и лекарственных препаратов против ВИЧ-1 *in vitro*: первичных изолятов ВИЧ-1 и лабораторно-адаптированных штаммов, инфекционных молекулярных клонов и *env*-псевдовирuсов. Кратко представлена их сравнительная характеристика. Более подробно описана технология *env*-псевдовирuсов ВИЧ-1.

Ключевые слова: ВИЧ-1; первичные изоляты; инфекционные молекулярные клоны; *env*-псевдовирuсы; анализ нейтрализации вирусa.

Introduction

The HIV/AIDS pandemic still remains a major problem for healthcare systems of the world with about two million newly infected individuals every year¹. At present, antiretroviral therapy is the most common way to manage HIV infection, as it reduces viral loads and prolongs and improves the quality of life of HIV-infected patients. However, the currently available antiretroviral drugs also have major shortcomings, such as high costs, marked side effects, developing drug resistance, a necessity for regimen changes, and the life-long duration of the therapy (Arts, Hazuda, 2012). Above all that, we are yet to find the cure for HIV infection (Phanuphak, Gulick, 2020). As a result, the development of effective preventive vaccines against HIV/AIDS remains a top priority (Stephenson et al., 2020).

As of today, the RV144 clinical trials performed in Thailand from 2003 to 2009 are considered the most successful. The studied vaccine showed an efficacy of 60 % in 12 months after vaccination and 31.2 % – after a 3.5-year follow-up (Kim et al., 2015). Several years later the RV144 vaccine components were modified to express the antigens of the HIV strains circulating in South Africa. In January 2020, early results of clinical trials showed that the modified vaccine failed to prevent HIV-1 infection in volunteers (Gray et al., 2021). Nowadays, there are still numerous unresolved issues in HIV-1 vaccine development, yet it is clear that it is necessary to use new approaches to its design (Hsu, O'Connell, 2017), hence the intense research for the induction of the protective T and B cell immune response to HIV-1, including broadly neutralizing antibodies (bnAbs) (Shcherbakov et al., 2015; Rudometov et al., 2019b; Jones et al., 2020; Liu et al., 2020; Ng'uni et al., 2020).

Selecting an adequate tool for *in vitro* efficacy assessment is an integral part of scientific research aimed at developing vaccines and chemotherapy drugs against viral pathogens, including HIV-1. The neutralizing activity of the sera from the animals immunized with experimental vaccines and the efficacy of chemotherapy agents are conventionally assessed using viral isolates (Jackson et al., 1988). However, this process is demanding in terms of time, effort, and biosafety measures.

¹ Fact Sheet on HIV/AIDS. World Health Organization, 2020. URL: <https://www.who.int/ru/news-room/fact-sheets/detail/hiv-aids> (Accessed June 2, 2021).

An alternative method is to use infectious molecular clones, i.e. infectious viral particles obtained via cell transfection with plasmid vector including the full-length HIV-1 genome coding structural, regulatory, and accessory proteins of the virus required for the cultivation of replication-competent viral particles in cell culture (Peden et al., 1991).

In recent years, many researchers give preference to the pseudotyped virus approach, a safer method suitable for BSL-2 lab settings (Li Q. et al., 2018; Montefiori et al., 2018). Compared to viral isolates and infectious molecular clones, pseudotyped viruses are harmless, because virus replication is restricted to a single cycle due to mutations in coding regions of the genome, which is why pseudotyped viruses are often called single-cycle viruses (Cheresiz et al., 2010; Li Q. et al., 2018).

HIV-1 model systems for *in vitro* efficacy assessment of chemotherapy drugs, bnAbs, and candidate vaccines against HIV-1 will be considered in the present review.

HIV-1 isolates and laboratory-adapted strains

Historically, HIV-1 primary isolates were the first system for analyzing vaccine efficacy and neutralizing the activity of antibodies (Jackson et al., 1988). Viral isolates are obtained via cocultivation of the peripheral blood mononuclear cells (PBMC) of an HIV-positive patient and the PHA-stimulated PBMC of a healthy donor. Here, the viruses isolated from blood appear as a genetically heterogeneous population due to the quasispecies nature of HIV-1. To eliminate possible selective pressure on viral isolates and ensure optimal preservation of a viral phenotype, the virus is cultivated using primary cell culture, rather than cell lines (Voronin et al., 2007; Van't Wout et al., 2008). The presence of neutralizing antibodies in sera from vaccinated subjects or the efficacy of an antiviral agent is typically identified in a PBMC culture with an added infectious dose of the virus and serial dilutions of immune serum or tested compound. HIV-1 replication suppression is assessed using ELISA by measuring p24 content (structural component of HIV-1 capsid) in the culture medium (Zyryanova et al., 2020a).

However, the use of HIV-1 primary isolates for virus neutralization analysis has several shortcomings, including the use of primary PBMCs for pathogen replication, high biosafety requirements, low repeatability of the results, and therefore

standardization issues (Mascola et al., 1996, 2005). Thus, some HIV-1 strains (IIIB/LAV, MN, SF2) were adapted for replication in immortalized cell lines (H9, CEM) for the sake of simplicity and to ensure repeatability of the experiments in the first years of vaccine development. These were later referred to as laboratory-adapted strains or, more accurately, T cell line adapted strains. Vaccination of volunteers with recombinant trimers based on laboratory-adapted HIV-1 strains induced the antibodies neutralizing these specific laboratory strains. The additional experiments involving HIV-1 primary isolates showed the absence of neutralizing activity against primary isolates, despite intense induction of neutralizing antibodies against the laboratory-adapted strains (Mascola et al., 1996; Montefiori et al., 2018). Apparently, the neutralization analysis performed using laboratory-adapted strains could produce misleading results, and the researchers came back to primary isolates as a more adequate tool for analyzing the virus-neutralizing activity of the antibodies induced as a result of vaccination. Since the method is labor-intensive and does not allow for mass analysis, it began to be used for the concluding stages of research.

HIV-1 infectious molecular clones

Taking into account the cultivation difficulties and significant heterogeneity of HIV-1 primary isolates and laboratory-adapted strains, as well as the variability of donor PBMCs (Polonis et al., 2008), HIV-1 infectious molecular clones (IMCs) were chosen for consistent replication of viral particles. IMCs are obtained via cell transfection with a plasmid vector including a full-length HIV-1 genome to ensure the generation of replication-competent viral particles in a eukaryotic cell culture (Fig. 1). Compared to HIV-1 primary isolates, this approach makes it possible to obtain genetically homogeneous viral particles, since an HIV-1 genome is present in the plasmid vector in the form of DNA (Edmonds et al., 2010; Zyryanova et al., 2020b). To ensure standardization of neutralization analysis using IMCs, modified continuous cell lines with a cell-surface CD4 receptor and CCR5 and CXCR4 co-receptors were genetically engineered (Princen et al., 2004; González et al., 2009). Since IMCs are essentially infectious viral particles, the relevant biosafety requirements are to be fulfilled, similarly to primary isolates and laboratory-adapted strains, and the analysis itself is rather time-consuming.

At the same time, the use of IMCs makes it possible to characterize and study biological properties of genetically different HIV-1 isolates (Ochsenbauer et al., 2012; Baalwa et al., 2013; Wang et al., 2013; Chenine et al., 2018; Zyryanova et al., 2020b), investigate the development mechanisms of drug-resistant HIV-1 strains and the effect of mutations on the biological properties of the virus (Johnston et al., 2005; Pugach et al., 2007; Varghese et al., 2013), and discover new antiretroviral agents (Su et al., 2019; Wagstaff et al., 2019; Mavian et al., 2020).

HIV-1 *env*-pseudoviruses

The use of classical virological methods to work with HIV-1 faces a number of difficulties noted above. *Env*-pseudovirus technology has proved to be a potent tool for quick and adequate assessment of humoral immune response to vaccine

constructs and screening of potential chemotherapeutic agents, specifically entry inhibitors (Montefiori et al., 2018).

HIV-1 *env*-pseudoviruses are recombinant viral particles obtained via eukaryotic cell transfection with the two plasmids referred to as core and envelope. The core plasmid includes genes of structural (Gag and Pol), regulatory (Tat and Rev), and accessory (Vpu, Vpr, Vif, and Nef) HIV-1 proteins necessary for viral particle assembly, as well as sequences required for viral RNA packaging (Ψ). The envelope plasmid carries an envelope glycoprotein gene (*Env*) of certain HIV-1 subtype. As a result of transfection, viral particles with a defective genome incapable of assembling infectious daughter virions are obtained (Li M. et al., 2005; Li Q. et al., 2018). Electron microscopy studies show that the HEK293 cell line transfection with two plasmids produces viral particles morphologically identical to the HIV-1 virions (Zaitsev et al., 2019; Ladinsky et al., 2020).

The determination of the functional activity of *env*-pseudoviruses and analyses neutralization are carried out on a TZM-bl cell line, which is a continuous, genetically modified HeLa cell line with cell-surface CD4 receptors and CCR5 and CXCR4 co-receptors. In addition, firefly luciferase and β -galactosidase *E. coli* reporter genes are integrated into the TZM-bl cell line genome under transcriptional control of HIV-1 long terminal repeat. When a pseudotyped virus enters the target TZM-bl cell, synthesis of a viral Tat protein triggers luciferase reporter gene expression detectable by a luminometer. Here, high luminescence intensity indicates that pseudotyped viral particles have entered target cells, whereas suppressed luminescence indicates that the HIV-1 *env*-pseudoviruses have been neutralized (Platt et al., 1998; Wei et al., 2002). A general work technique of *env*-pseudovirus system is shown in Fig. 2.

An *env*-pseudovirus system has a number of distinct advantages. First, since TZM-bl is a stable continuous cell line, it may be used as a substitute for human primary T cells, thereby reducing the need for individual donor cells. Second, *env*-pseudoviruses are harmless compared to viral isolates and IMCs requiring higher biosafety levels, which makes experimental studies more complicated and expensive. Third, *Env* protein forms trimer structures at the surface of pseudotyped viral particles, which are identical to those of the natural virus. However, the main advantage of the pseudotyped virus technology is that it makes it possible to obtain the equivalents of the viral particles of various HIV-1 subtypes and strains, thereby providing broad coverage of HIV-1 genetic diversity (Seaman et al., 2010; Montefiori et al., 2018). In addition, the neutralization assessment method using *env*-pseudoviruses favors further optimization and standardization (Wei et al., 2002; Seaman et al., 2010; Sarzotti-Kelsoe et al., 2014). A brief comparison of HIV-1 primary isolates and laboratory-adapted strains, IMCs, and *env*-pseudoviruses is presented in the Table.

It should be noted that the protocols and recommendations for neutralization assessment using *env*-pseudoviruses are available at the website of the Los Alamos National Laboratory (<https://www.hiv.lanl.gov/content/nab-reference-strains/html/home.htm>). In addition, the HIV Reagent Program supported by the National Institute of Allergy and Infectious Diseases and curated by the National Collection of Type Cultures

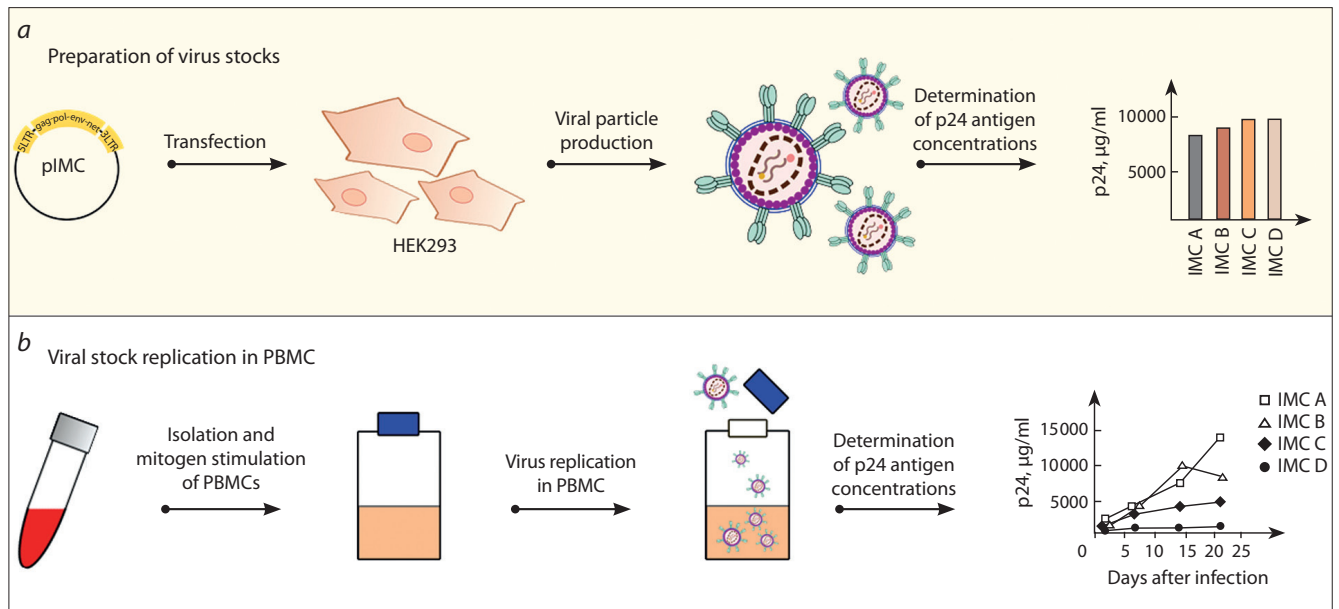


Fig. 1. HIV-1 IMC technology.

Conditionally, HIV-1 IMCs are obtained in two stages. At the first stage (a), viral particles, also referred to as virus stock, are produced via HEK293 cell line transfection. At the second stage (b), the virus stock is further replicated for several weeks using PHA-stimulated PBMCs from a healthy donor. The titers of viral particles are measured at each stage using the ELISA based on p24 antigen content in the culture medium. A replication-competent virus is produced if p24 capsid protein content becomes at least 1000 times as high as its initial content in the culture medium.

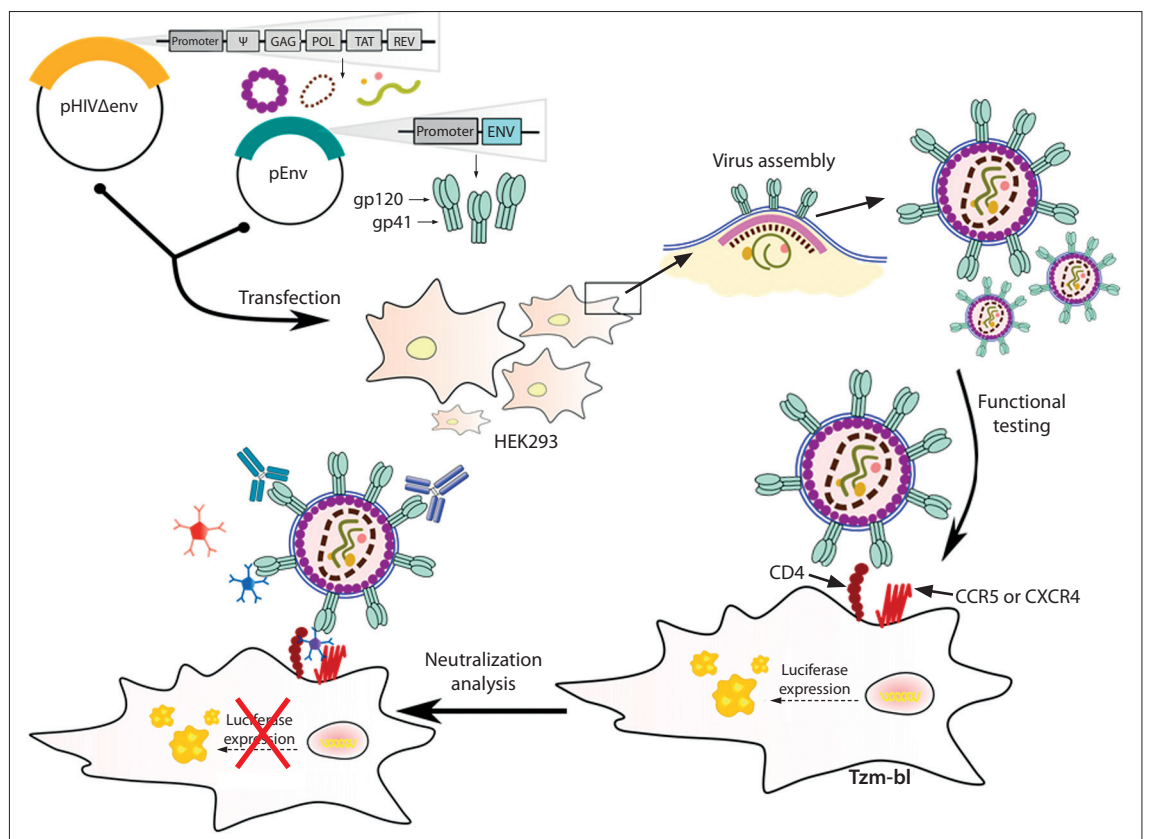


Fig. 2. HIV-1 *env*-pseudovirus technology.

Experimental study of *env*-pseudoviruses is done in several stages: Stage 1 includes viral particle assembly via HEK293 cell line transfection with two plasmids, referred to as core and envelope; at Stage 2, one measures the functional activity of pseudotyped viral particles, i.e. their ability to infect target cells and trigger firefly luciferase reporter gene expression; at Stage 3 the neutralization level is analyzed using immune sera or chemotherapeutic agents to measure their ability to block pseudotyped virus entry to target cells.

Comparison of HIV-1 model systems used for *in vitro* efficacy assessment of vaccines and drugs against HIV-1

Parameter	<i>Env</i> -pseudoviruses	Infectious molecular clones	Primary isolates and laboratory-adapted strains
Biosafety requirements (hazard level)	Low	High	High
Analysis speed	High	Low	Low
Standardization	High	High	Low
Investigation of virus properties and virus cycle	Only at the entry stage	All stages of HIV-1 life cycle	All stages of HIV-1 life cycle
Cultivation conditions	Continuous cell lines	Continuous cell lines; PBMCs	PBMCs

makes it possible to obtain all the components (cell lines, plasmids, monoclonal antibodies) required for implementing the technology.

Here are several noteworthy applications of *env*-pseudoviruses panels. Antiviral activity of clinically approved co-receptor antagonist Maraviroc was demonstrated using 160 HIV-1 subtype B *env*-pseudoviruses and 40 *env*-pseudoviruses of other HIV-1 subtypes (Dorr et al., 2005). The activity of Ibalizumab, a monoclonal antibody binding to the CD4 receptor, was demonstrated using 116 *env*-pseudoviruses of subtypes A, B, C, and CRF01_AE (Pace et al., 2013). HIV-1 *env*-pseudoviruses panels were also used to investigate the bnAbs spectrum with respect to various genetic variants of HIV-1. For instance, the neutralization breadth of 98 % for bnAb 10E8 was demonstrated using a panel of 181 *env*-pseudoviruses of subtypes A, B, C, D, G, CRF01_AE, and CRF02_AG (Huang et al., 2012); neutralization breadth of 91 % for bnAb VRC01 was demonstrated using 196 *env*-pseudoviruses (Wu X. et al., 2010); neutralization breadth of 49 % for bnAb VRC34.01 was demonstrated using 179 *env*-pseudoviruses (Kong et al., 2016). It is the introduction of pseudotyped virus panels, including a wide range of genetically diverse HIV-1 variants, that led to a breakthrough in the production and characterization of monoclonal broadly neutralizing antibodies.

Env-pseudoviruses panels are extensively used to study the humoral immune response induced by candidate vaccines against HIV-1 at a design stage and during pre-clinical and clinical trials, since the presence of virus-neutralizing antibodies in the vaccinated subjects is among the key indicators of HIV vaccine effectiveness (Rudometov et al., 2019a; Ou et al., 2020). Recent papers by Xu et al., who developed a vaccination regimen based on fusion peptide (FP) of gp41, a key structural component of HIV-1, may be cited as an example. Earlier, they identified the VRC34.01 antibody from an HIV-positive donor, which was aimed at the conservative N-terminal region of HIV-1 FP. Since FP is a short linear peptide, it has low natural immunogenicity, which is why garden snail hemocyanin widely used in biotechnology was used as a carrier protein. Immunization of laboratory animals by an FP bound to garden snail hemocyanin with subsequent boosting by a BG505 trimer resulted in induction of antibodies with neutralization breadth of 31 % demonstrated using a panel of 208 *env*-pseudoviruses of various HIV-1 subtypes (Xu et al., 2018).

In conclusion of this review, it should be mentioned that an HIV-1 pseudotyping system is tolerant to incorporation

of surface proteins of various enveloped viruses. Since most laboratory experiments and studies involving viruses are to be performed in BSL-3 or BSL-4 lab settings, the use of pseudotyped viruses instead of wild-type ones makes it possible for various research groups to study viruses of interest and design antiviral drugs and vaccines against highly dangerous viruses. For example, HIV-1 pseudotyping system was used to obtain the viral particles carrying surface glycoproteins of Ebola virus (Mohan et al., 2015), Marburg virus (Zhang L. et al., 2019), Lassa fever (Zhang X. et al., 2019), Middle East respiratory syndrome coronavirus (Zhao et al., 2013), Rabies virus (Nie et al., 2017), Chikungunya virus (Wu J. et al., 2017), and Nipah virus (Nie et al., 2019). In addition, this technology is extensively used in designing pseudotyped virus platforms for SARS-CoV-2 (Hu et al., 2020; Hyseni et al., 2020; Johnson et al., 2020).

Conclusion

All technologies considered above have their own advantages and shortcomings and most certainly complement each other in integrated studies. Despite the labor-intensity of primary isolate and IMC technologies in neutralization assessments, these models still remain valuable tools for investigating the biological properties of viruses. However, *env*-pseudovirus technology has currently become the base method for efficacy assessment of HIV-1 vaccines and antiviral agents (potential entry inhibitors). Its main advantages include safety, high repeatability of the results, standardization potential, and ability to work with virus particles exposing surface glycoproteins of multiple virus subtypes.

References

- Arts E.J., Hazuda D.J. HIV-1 antiretroviral drug therapy. *Cold Spring Harb. Perspect. Med.* 2012;2(4):1-23. DOI 10.1101/cshperspect.a007161.
- Baalwa J., Wang S., Parrish N.F., Decker J.M., Keele B.F., Learn G.H., Yue L., Ruzagira E., Ssemwanga D., Kamali A. Molecular identification, cloning and characterization of transmitted/founder HIV-1 subtype A, D and A/D infectious molecular clones. *Virology*. 2013; 436(1):33-48. DOI 10.1016/j.virol.2012.10.009.
- Chenine A.L., Merbah M., Wiczorek L., Molnar S., Mann B., Lee J., O'Sullivan A.M., Bose M., Sanders-Buell E., Kijak G.H., Herrera C., McLinden R., O'Connell R., Michael N.L., Robb M.L., Kim J.H., Polonis V.R., Tovanabuttra S. Neutralization sensitivity of a novel HIV-1 CRF01_AE panel of infectious molecular clones. *J. Acquir. Immune Defic. Syndrom.* 2018;78(3):348-355. DOI 10.1097/QAI.0000000000001675.

- Cheresiz S.V., Grigoryev I.V., Semenova E.A., Pustyl'nyak V.O., Vlasov V.V., Pokrovsky A.G. A pseudovirus system for the testing of antiviral activity of compounds in different cell lines. *Doklady Biochemistry and Biophysics*. 2010;435:295-298. DOI 10.1134/S1607672910060049.
- Dorr P., Westby M., Dobbs S., Griffin P., Irvine B., Macartney M., Mori J., Rickett G., Smith-Burchell C., Napier C., Webster R., Armour D., Price D., Stammen B., Wood A., Perros M. Maraviroc (UK-427,857), a potent, orally bioavailable, and selective small-molecule inhibitor of chemokine receptor CCR5 with broad-spectrum anti-human immunodeficiency virus type 1 activity. *Antimicrob. Agents Chemother.* 2005;49(11):4721-4732. DOI 10.1128/AAC.49.11.4721-4732.2005.
- Edmonds T.G., Ding H., Yuan X., Wei Q., Smith K.S., Conway J.A., Wiczorek L., Brown B., Polonis V., West J.T., Montefiori D.C., Kappes J.C., Ochsenaubauer Ch. Replication competent molecular clones of HIV-1 expressing *Renilla* luciferase facilitate the analysis of antibody inhibition in PBMC. *Virology*. 2010;408(1):1-13. DOI 10.1016/j.virol.2010.08.028.
- González N., Pérez-Olmeda M., Mateos E., Cascajero A., Alvarez A., Spijkers S., García-Pérez J., Sánchez-Palomino S., Ruiz-Mateos E., Leal M., Alami J. A sensitive phenotypic assay for the determination of human immunodeficiency virus type 1 tropism. *J. Antimicrob. Chemother.* 2010;65(12):2493-2501. DOI 10.1093/jac/dkq379.
- Gray G.E., Bekker L.G., Laher F., Malahleha M., Allen M., Moodie Z., Grunenberg N., Huang Yu., Grove D., Prigmore B. Vaccine efficacy of ALVAC-HIV and bivalent subtype C gp120-MF59 in adults. *New Eng. J. Med.* 2021;384(12):1089-1100. DOI 10.1056/NEJMoa2031499.
- Hsu D.C., O'Connell R.J. Progress in HIV vaccine development. *Hum. Vaccines Immunother.* 2017;13(5):1018-1030. DOI 10.1080/21645515.2016.1276138.
- Hu J., Gao Q., He C., Huang A., Tang N., Wang K. Development of cell-based pseudovirus entry assay to identify potential viral entry inhibitors and neutralizing antibodies against SARS-CoV-2. *Genes Dis.* 2020;7(4):551-557. DOI 10.1016/j.gendis.2020.07.006.
- Huang J., Ofek G., Laub L., Louder M.K., Doria-Rose N.A., Longo N.S., Imamichi H., Bailer R.T., Chakrabarti B., Sharma S.K., Munir Alam S., Wang T., Yang Y., Zhang B., Migueles S.A., Wyatt R., Haynes B.F., Kwong P.D., Mascola J.R., Connors M. Broad and potent neutralization of HIV-1 by a gp41-specific human antibody. *Nature*. 2012;491(7424):406-412. DOI 10.1038/nature11544.
- Hyseni I., Molesti E., Benincasa L., Piu P., Casa E., Temperton N.J., Manenti A., Montomoli E. Characterisation of SARS-CoV-2 lentiviral pseudotypes and correlation between pseudotype-based neutralisation assays and live virus-based micro neutralisation assays. *Viruses*. 2020;12(9):1-18. DOI 10.3390/v12091011.
- Jackson J.B., Coombs R.W., Sannerud K., Rhame F.S., Balfour H.H., Jr. Rapid and sensitive viral culture method for human immunodeficiency virus type 1. *J. Clin. Microbiol.* 1988;26(7):1416-1418. PMID 3165981.
- Johnson M.C., Lyddon T.D., Suarez R., Salcedo B., LePique M., Graham M., Ricana C.L., Robinson C.A., Ritter D.G. Optimized pseudotyping conditions for the SARS-COV-2 spike glycoprotein. *J. Virol.* 2020;94(21):1-10. DOI 10.1128/JVI.01062-20.
- Johnston E., Dupnik K.M., Gonzales M.J., Winters M.A., Rhee S.Y., Imamichi T., Shafer R.W. Panel of prototypical infectious molecular HIV-1 clones containing multiple nucleoside reverse transcriptase inhibitor resistance mutations. *AIDS*. 2005;19(7):731-733. DOI 10.1097/01.aids.0000166098.54564.0c.
- Jones L.D., Moody M.A., Thompson A.B. Innovations in HIV-1 vaccine design. *Clin. Ther.* 2020;42(3):499-514. DOI 10.1016/j.clinthera.2020.01.009.
- Kim J.H., Excler J.L., Michael N.L. Lessons from the RV144 Thai phase III HIV-1 vaccine trial and the search for correlates of protection. *Annu. Rev. Med.* 2015;66:423-437. DOI 10.1146/annurev-med-052912-123749.
- Kong R., Xu K., Zhou T., Acharya P., Lemmin T., Liu K., Ozorowski G., Soto C., Taft J., Bailer R., Cale E.M., Chen L., Choi C.W., Chuang G., Doria-Rose N.A., Druz A., Georgiev I.S., Gorman J., Huang J., Gordon Joyce M., Louder M.K., Ma X., McKee K., O'Dell S., Pancera M., Yang Y., Blanchard S.C., Mothes W., Burton D.R., Koff W.C., Connors M., Ward A.B., Kwong P.D., Mascola J.R. Fusion peptide of HIV-1 as a site of vulnerability to neutralizing antibody. *Science*. 2016;352(6287):828-833. DOI 10.1126/science.aae0474.
- Ladinsky M.S., Gnanapragasam P.N., Yang Z., West A.P., Kay M.S., Bjorkman P.J. Electron tomography visualization of HIV-1 fusion with target cells using fusion inhibitors to trap the pre-hairpin intermediate. *eLife*. 2020;9. DOI 10.7554/eLife.58411.
- Li M., Gao F., Mascola J.R., Stamatatos L., Polonis V.R., Koutsoukos M., Voss G., Goepfert P., Gilbert P., Greene K.M., Bilska M., Kothe D.L., Salazar-Gonzalez J.F., Wei X., Decker J.M., Hahn B.H., Montefiori D.C. Human immunodeficiency virus type 1 *env* clones from acute and early subtype B infections for standardized assessments of vaccine-elicited neutralizing antibodies. *J. Virol.* 2005;79(16):10108-10125. DOI 10.1128/JVI.79.16.10108-10125.2005.
- Li Q., Liu Q., Huang W., Li X., Wang Y. Current status on the development of pseudoviruses for enveloped viruses. *Rev. Med. Virol.* 2018;28(1):1-10. DOI 10.1002/rmv.1963.
- Liu Y., Cao W., Sun M., Li T. Broadly neutralizing antibodies for HIV-1: efficacies, challenges and opportunities. *Emerg. Microbes Infect.* 2020;9(1):194-206. DOI 10.1080/22221751.2020.1713707.
- Mascola J.R., Snyder S.W., Weislow O.S., Belay S.M., Belshe R.B., Schwartz D.H., Clements M.L., Dolin R., Graham B.S., Gorse G.J. Immunization with envelope subunit vaccine products elicits neutralizing antibodies against laboratory-adapted but not primary isolates of human immunodeficiency virus type 1. *J. Infect. Dis.* 1996; 173(2):340-348. DOI 10.1093/infdis/173.2.340.
- Mascola J.R., D'Souza P., Gilbert P., Hahn B.H., Haigwood N.L., Morris L., Petropoulos C.J., Polonis V.R., Sarzotti M., Montefiori D.C. Recommendations for the design and use of standard virus panels to assess neutralizing antibody responses elicited by candidate human immunodeficiency virus type 1 vaccines. *J. Virol.* 2005;79(16): 10103-10107. DOI 10.1128/JVI.79.16.10103-10107.2005.
- Mavian C., Coman R.M., Zhang X., Pomeroy S., Ostrov D.A., Dunn B.M., Sleasman J.W., Goodenow M.M. Molecular docking-based screening for novel inhibitors of the human immunodeficiency virus type 1 protease that effectively reduce the viral replication in human cells. *bioRxiv*. 2020;1-11. DOI 10.1101/2020.11.14.382895.
- Mohan G.S., Ye L., Li W., Monteiro A., Lin X., Sapkota B., Pollack B.P., Compans R.W., Yang C. Less is more: Ebola virus surface glycoprotein expression levels regulate virus production and infectivity. *J. Virol.* 2015;89(2):1205-1217. DOI 10.1128/JVI.01810-14.
- Montefiori D.C., Roederer M., Morris L., Seaman M.S. Neutralization tiers of HIV-1. *Curr. Opin. HIV AIDS*. 2018;13(2):1-9. DOI 10.1097/COH.0000000000000442.
- Ng'uni T., Chasara C., Ndhlovu Z.M. Major scientific hurdles in HIV vaccine development: historical perspective and future directions. *Front. Immun.* 2020;11:1-17. DOI 10.3389/fimmu.2020.590780.
- Nie J., Liu L., Wang Q., Chen R., Ning T., Liu Q., Huang W., Wang Y. Nipah pseudovirus system enables evaluation of vaccines *in vitro* and *in vivo* using non-BSL-4 facilities. *Emerg. Microbes Infect.* 2019;8(1):272-281. DOI 10.1080/22221751.2019.1571871.
- Nie J., Wu X., Ma J., Cao S., Huang W., Liu Q., Li X., Li Y., Wang Y. Development of *in vitro* and *in vivo* rabies virus neutralization as-

- says based on a high-titer pseudovirus system. *Sci. Rep.* 2017;7(1): 1-12. DOI 10.1038/srep42769.
- Ochsenbauer C., Edmonds T.G., Ding H., Keele B.F., Decker J., Salazar M.G., Salazar-Gonzalez J.F., Shattock R., Haynes B.F., Shaw G.M., Hahn B.H., Kappes J.C. Generation of transmitted/founder HIV-1 infectious molecular clones and characterization of their replication capacity in CD4 T lymphocytes and monocyte-derived macrophages. *J. Virol.* 2012;86(5):2715-2728. DOI 10.1128/JVI.06157-11.
- Ou L., Kong W.P., Chuang G.Y., Ghosh M., Gulla K., O'Dell S., Variale J., Barefoot N., Changela A., Chao C.W., Cheng Ch., Druz A., Kong R., McKee K., Rawi R., Sarfo E., Schön A., Shaddeau A., Tsybovsky Ya., Verardi R., Wang Sh. Preclinical development of a fusion peptide conjugate as an HIV vaccine immunogen. *Sci. Rep.* 2020;10(1):1-13. DOI 10.1038/s41598-020-59711-y.
- Pace C.S., Fordyce M.W., Franco D., Kao C.Y., Seaman M.S., Ho D.D. Anti-CD4 monoclonal antibody ibalizumab exhibits breadth and potency against HIV-1, with natural resistance mediated by the loss of a V5 glycan in envelope. *J. Acquir. Immune Defic. Syndr.* 2013;62(1):1-9. DOI 10.1097/QAI.0b013e3182732746.
- Peden K., Emerman M., Montagnier L. Changes in growth properties on passage in tissue culture of viruses derived from infectious molecular clones of HIV-1LA1, HIV-1MAL, and HIV-1ELI. *Virology.* 1991;185:661-672. DOI 10.1016/0042-6822(91)90537-L.
- Phanuphak N., Gulick R.M. HIV treatment and prevention 2019: current standards of care. *Curr. Opin. HIV AIDS.* 2020;15(1):4-12. DOI 10.1097/COH.0000000000000588.
- Platt E.J., Wehrly K., Kuhmann S.E., Chesebro B., Kabat D. Effects of CCR5 and CD4 cell surface concentrations on infections by macrophagetropic isolates of human immunodeficiency virus type 1. *J. Virol.* 1998;72:2855-2864. DOI 10.1128/JVI.72.4.2855-2864.1998.
- Polonis V.R., Brown B.K., Borges A.R., Zolla-Pazner S., Dimitrov D.S., Zhang M.Y., Barnett S.W., Ruprecht R.M., Scarlatti G., Fenyö E., Montefiori D.C., McCutchan F.E., Michael N.L. Recent advances in the characterization of HIV-1 neutralization assays for standardized evaluation of the antibody response to infection and vaccination. *Virology.* 2008;375(2):315-320. DOI 10.1016/j.virol.2008.02.007.
- Princen K., Hatse S., Vermeire K., De Clercq E., Schols D. Establishment of a novel CCR5 and CXCR4 expressing CD4+ cell line which is highly sensitive to HIV and suitable for high-throughput evaluation of CCR5 and CXCR4 antagonists. *Retrovirology.* 2004;1(1): 1-13. DOI 10.1186/1742-4690-1-2.
- Pugach P., Marozsan A.J., Ketas T.J., Landes E.L., Moore J.P., Kuhmann S.E. HIV-1 clones resistant to a small molecule CCR5 inhibitor use the inhibitor-bound form of CCR5 for entry. *Virology.* 2007;361(1):212-228. DOI 10.1016/j.virol.2006.11.004.
- Rudometov A.P., Chikae A.N., Rudometova N.B., Antonets D.V., Lomzov A.A., Kaplina O.N., Ilyichev A.A., Karpenko L.I. Artificial anti-HIV-1 immunogen comprising epitopes of broadly neutralizing antibodies 2F5, 10E8, and a peptide mimic of VRC01 discontinuous epitope. *Vaccines.* 2019a;7(3):1-18. DOI 10.3390/vaccines 7030083.
- Rudometov A.P., Rudometova N.B., Shcherbakov D.N., Lomzov A.A., Kaplina O.N., Shcherbakova N.S., Ilyichev A.A., Bakulina A.Yu., Karpenko L.I. The structural and immunological properties of chimeric proteins containing HIV-1 MPER sites. *Acta Naturae.* 2019b; 11(3):56-65. DOI 10.32607/20758251-2019-11-3-56-65.
- Sarzotti-Kelsoe M., Bailer R.T., Turk E., Lin C.L., Biliska M., Greene K.M., Gao H., Todd C.A., Ozaki D., Seaman M.S., Mascola J.R., Montefiori D.C. Optimization and validation of the TZM-bl assay for standardized assessments of neutralizing antibodies against HIV-1. *J. Immunol. Methods.* 2014;409:131-146. DOI 10.1016/j.jim.2013.11.022.
- Seaman M.S., Janes H., Hawkins N., Grandpre L.E., Devoy C., Giri A., Coffey R.T., Harris L., Wood B., Daniels M.G. Tiered categorization of a diverse panel of HIV-1 Env pseudoviruses for assessment of neutralizing antibodies. *J. Virol.* 2010;84(3):1439-1452. DOI 10.1128/JVI.02108-09.
- Shcherbakov D.N., Bakulina A.Y., Karpenko L.I., Ilyichev A.A. Broadly neutralizing antibodies against HIV-1 as a novel aspect of the immune response. *Acta Naturae.* 2015;7(4):11-21. PMID 26798488.
- Stephenson K.E., Wagh K., Korber B., Barouch D.H. Vaccines and broadly neutralizing antibodies for HIV-1 prevention. *Annu. Rev. Immunol.* 2020;38:673-703. DOI 10.1146/annurev-immunol-080219-023629.
- Su S., Rasquinha G., Du L., Wang Q., Xu W., Li W., Lu L., Jiang S. A peptide-based HIV-1 fusion inhibitor with two tail-anchors and palmitic acid exhibits substantially improved *in vitro* and *ex vivo* anti-HIV-1 activity and prolonged *in vivo* half-life. *Molecules.* 2019;24(6):1-13. DOI 10.3390/molecules24061134.
- Van't Wout A.B., Schuitemaker H., Kootstra N.A. Isolation and propagation of HIV-1 on peripheral blood mononuclear cells. *Nat. Protoc.* 2008;3(3):363-370. DOI 10.1038/nprot.2008.3.
- Varghese V., Mitsuya Y., Fessel W.J., Liu T.F., Melikian G.L., Katzenstein D.A., Schiffer C.A., Holmes S.P., Shafer R.W. Prototypical recombinant multi-protease-inhibitor-resistant infectious molecular clones of human immunodeficiency virus type 1. *Antimicrob. Agents Chemother.* 2013;57(9):4290-4299. DOI 10.1128/AAC.00614-13.
- Voronin Y., Chohan B., Emerman M., Overbaugh J. Primary isolates of human immunodeficiency virus type 1 are usually dominated by the major variants found in blood. *J. Virol.* 2007;81(19):10232-10241. DOI 10.1128/JVI.01035-07.
- Wagstaff K.M., Headey S., Telwate S., Tyssen D., Hearps A.C., Thomas D.R., Tachedjian G., Jans D.A. Molecular dissection of an inhibitor targeting the HIV integrase dependent preintegration complex nuclear import. *Cell. Microbiol.* 2019;21(1):1-13. DOI 10.1111/cmi.12953.
- Wang Z., Hong K., Zhang J., Zhang L., Li D., Ren L., Liang H., Shao Y. Construction and characterization of highly infectious full-length molecular clones of a HIV-1 CRF07_BC isolate from Xinjiang, China. *PLoS One.* 2013;8(11):1-9. DOI 10.1371/journal.pone.0079177.
- Wei X., Decker J.M., Liu H., Zhang Z., Arani R.B., Kilby J.M., Saag M.S., Wu X., Shaw G.M., Kappes J.C. Emergence of resistant human immunodeficiency virus type 1 in patients receiving fusion inhibitor (T-20) monotherapy. *Antimicrob. Agents Chemother.* 2002; 46:1896-1905. DOI 10.1128/aac.46.6.1896-1905.2002.
- Wu J., Zhao C., Liu Q., Huang W., Wang Y. Development and application of a bioluminescent imaging mouse model for Chikungunya virus based on pseudovirus system. *Vaccine.* 2017;35(47):6387-6394. DOI 10.1016/j.vaccine.2017.10.007.
- Wu X., Yang Z.Y., Li Y., Hegerkorp C.M., Schief W.R., Seaman M.S., Zhou T., Schmidt S.D., Wu L., Xu L. Rational design of envelope identifies broadly neutralizing human monoclonal antibodies to HIV-1. *Science.* 2010;329(5993):856-861. DOI 10.1126/science.1187659.
- Xu K., Acharya P., Kong R., Cheng C., Chuang G.Y., Liu K., Loulder M.K., O'Dell S., Rawi R., Sastry M. Epitope-based vaccine design yields fusion peptide-directed antibodies that neutralize diverse strains of HIV-1. *Nat. Med.* 2018;24(6):857-867. DOI 10.1038/s41591-018-0042-6.
- Zaitsev B.N., Taranov O.S., Rudometova N.B., Shcherbakova N.S., Ilyichev A.A., Karpenko L.I. An optimized method for counting viral particles using electron microscopy. *Vavilovskii Zhurnal Genetiki i Selektii = Vavilov Journal of Genetics and Breeding.* 2019;23: 337-342. DOI 10.18699/VJ19.498.

- Zhang L., Lei S., Xie H., Li Q., Liu S., Liu Q., Huang W., Xiao X., Wang Y. Screening and identification of Marburg virus entry inhibitors using approved drugs. *Virol. Sin.* 2020;35:235-239. DOI 10.1007/s12250-019-00184-3.
- Zhang X., Yan F., Tang K., Chen Q., Guo J., Zhu W., He S., Banadyga L., Qiu X., Guo Y. Identification of a clinical compound losmapimod that blocks Lassa virus entry. *Antiviral Res.* 2019;167:68-77. DOI 10.1016/j.antiviral.2019.03.014.
- Zhao G., Du L., Ma C., Li Y., Li L., Poon V.K., Wang L., Yu F., Zheng B.J., Jiang S., Zhou Y. A safe and convenient pseudovirus-based inhibition assay to detect neutralizing antibodies and screen for viral entry inhibitors against the novel human coronavirus MERS-CoV. *Virol. J.* 2013;10(1):1-8. DOI 10.1186/1743-422X-10-266.
- Zyryanova D.P., Bogacheva N.V., Totmenin A.V., Gashnikova N.M. HIV-1 CRF63_02A6 models as a tool for evaluating efficacy of developing antiretroviral drugs. *Infektsiya i Immunitet = Russian Journal of Infection and Immunity.* 2020;10(4):769-774. DOI 10.15789/2220-7619-MHC-1261. (in Russian)
- Zyryanova D.P., Totmenin A.V., Bogacheva N.V., Gashnikova N.M. Construction and characterization of infectious molecular clones of HIV-1 CRF63_02A6. *AIDS Res. Hum. Retrovir.* 2020;36(3):227-233. DOI 10.1089/aid.2019.0177.

ORCID ID

N.B. Rudometova orcid.org/0000-0002-1684-9071
D.N. Shcherbakov orcid.org/0000-0001-8023-4453
A.P. Rudometov orcid.org/0000-0003-2808-4309
A.A. Ilyichev orcid.org/0000-0001-5356-0843
L.I. Karpenko orcid.org/0000-0003-4365-8809

Acknowledgements. The reported study was funded by the grant of the President of the Russian Federation MK-583.2020.4 and RFBR and Novosibirsk region, according to the research project No. 19-44-543013, and the state assignment of FBSI SRC VB "Vector", Rospotrebnadzor.

Conflict of interest. The authors declare no conflict of interest.

Received June 10, 2021. Revised August 7, 2021. Accepted August 9, 2021.

Прием статей через электронную редакцию на сайте <http://vavilov.elpub.ru/index.php/jour>
Предварительно нужно зарегистрироваться как автору, затем в правом верхнем углу страницы выбрать «Отправить рукопись». После завершения загрузки материалов обязательно выбрать опцию «Отправить письмо», в этом случае редакция автоматически будет уведомлена о получении новой рукописи.

«Вавиловский журнал генетики и селекции»/“Vavilov Journal of Genetics and Breeding”
до 2011 г. выходил под названием «Информационный вестник ВОГиС»/
“The Herald of Vavilov Society for Geneticists and Breeding Scientists”.

Регистрационное свидетельство ПИ № ФС77-45870 выдано Федеральной службой по надзору в сфере связи, информационных технологий и массовых коммуникаций 20 июля 2011 г.

«Вавиловский журнал генетики и селекции» включен ВАК Минобрнауки России в Перечень рецензируемых научных изданий, в которых должны быть опубликованы основные результаты диссертаций на соискание ученой степени кандидата наук, на соискание ученой степени доктора наук, Российский индекс научного цитирования, ВИНТИ, базы данных Emerging Sources Citation Index (Web of Science), Zoological Record (Web of Science), Scopus, PubMed Central, Ebsco, DOAJ, Ulrich’s Periodicals Directory, Google Scholar, Russian Science Citation Index на платформе Web of Science, каталог научных ресурсов открытого доступа ROAD.

Открытый доступ к полным текстам:
на сайте ИЦиГ СО РАН – bionet.nsc.ru/vogis/
платформе Elpub – vavilov.elpub.ru/index.php/jour
платформе Научной электронной библиотеки – elibrary.ru/title_about.asp?id=32440
PubMed Central, <https://www.ncbi.nlm.nih.gov/pmc/journals/3805/>

Подписку на «Вавиловский журнал генетики и селекции» можно оформить в любом почтовом отделении России. Индекс издания 42153 по каталогу «Пресса России».

При перепечатке материалов ссылка на журнал обязательна.

✉ e-mail: vavilov_journal@bionet.nsc.ru

Издатель: Федеральное государственное бюджетное научное учреждение
«Федеральный исследовательский центр Институт цитологии и генетики
Сибирского отделения Российской академии наук»,
проспект Академика Лаврентьева, 10, Новосибирск, 630090.

Адрес редакции: проспект Академика Лаврентьева, 10, Новосибирск, 630090.

Секретарь по организационным вопросам С.В. Зубова. Тел.: (383)3634977.

Издание подготовлено информационно-издательским отделом ИЦиГ СО РАН. Тел.: (383)3634963*5218.

Начальник отдела: Т.Ф. Чалкова. Редакторы: В.Д. Ахметова, И.Ю. Ануфриева. Дизайн: А.В. Харкевич.

Компьютерная графика и верстка: Т.Б. Коняхина, О.Н. Савватеева.

Подписано в печать 22.03.2022. Выход в свет 31.03.2022. Формат 60 × 84 1/8. Усл. печ. л. 12.32.

Уч.-изд. л. 14.6. Тираж 150 экз. (1-й завод 1–45 экз.) Заказ № 143. Цена свободная.

Отпечатано в Сибирском отделении РАН, Морской проспект, 2, Новосибирск, 630090.